Proceedings of the First U.S.

WATER JET SYMPOSIUM

April 1981/Golden, Colorado

Sponsored by Colorado School of Mines

FOREWORD

It is with great pleasure that we present the Proceedings of the First U.S. Water Jet Symposium held at the Colorado School of Mines, Golden, Colorado. This meeting was particularly timely in that it coincides with the rapid growth of water jet applications in industry.

The Water Jet Symposium presented information on theoretical and experimental aspects of high pressure water jet cutting technology and its application to mining and civil engineering, as well as for industrial use. The general theme of the conference was technology transfer between research and industry.

Investigations into the theory and mechanics of water jets have been underway for several years. Excellent work has been accomplished in the area, and previous conferences have provided an effective transfer of knowledge on developing water jet technology. This First U.S. Symposium emphasized the commercial applications of water jets. This did not prove a difficult undertaking, since the number of papers on industrial and mining applications indicates the technology is rapidly gaining industry acceptance.

The application of water jets is diversified. The mining industry is already using water jets for development and production drilling in uranium, and is working on applying borehole mining to production of uranium and coal. Many improvements have come about in jet performance, equipment reliability, and applications in tanks, heat exchangers, pipes, and tubing. Industrial applications in cutting difficult materials with water jets have existed for a number of years, and are continuing to expand because of advantages in speed, minimal dust generation, reduced maintenance and sharpening, and environmental considerations in handling hazardous materials.

The achievement award was presented to Mr. Jacob N. Frank, Chief of the Physical Science Branch of the Technical Services and Research Division, of the Office of Surface Mining in Kansas City, Missouri for his leading role in establishing water jet cutting technology, both through research and support of industrial development.

In closing, we would like to thank all those who participated in the symposium, and particularly those individuals who presented papers. Also, sincere thanks to the unselfish efforts of the organizing committee, and the staff at the Colorado School of Mines for compiling these proceedings.

Fun-Den Wang
Levent Ozdemir
Russell J. Miller

Editors

SYMPOSIUM AGENDA

April 6, 1981 (Monday) - Metals Hall, Green Center

Short Courses: Chairman: Dr. George Savanick, U.S. Bureau of Mines, Twin Cities Minnesota
Co Chairman: Dr. David Summers, University of Missouri-Rolla, Rolla, Missouri

Morning -
8:00 - 8:45 Short Course Registration
8:45 - 12:00 Short Course:

Fundamentals - John Olsen, Vice President, Flow Industries, Kent, Washington
Mining - Jack Frank, Office of Surface Mining, Kansas City, Missouri
David Summers University of Missouri - Rolla, Rolla, Missouri
Civil Engineering - To; Labus, SCIRE Corporation, Fontana, Wisconsin

10:00 - 10:15 Coffee Break

12:00 - 1:30 Lunch - Friedhoff Hall, Green Center

Afternoon -
1:30 - 3:30 Short Course Continued:
Industrial Application - Dave Burns, University of Waterloo, Waterloo, Ontario, Canada
Equipment - Seymour Bortz, IIT Research Institute, Chicago Illinois

April 7, 1981 (Tuesday) - Metals Hall, Green Center

Morning - -
7:30 - 8:30 Registration
8:30 - 9:00 Opening Remarks - Dr. William Mueller, Vice President, Academic Affairs, Colorado School of Mines
10:00 - 10:15 Coffee Break
12:00 - 1:30 Lunch - Friedhoff Hall, Green Center

Afternoon - -
1:30 - 4:30 SESSION II - Experimental
Chairman: Dr. George Savanick, U.S. Bureau of Mines, Twin Cities Minnesota
3:00 - 3:15 Coffee Break
5:00 - 6:00 Social Hour - Freidhoff Hall, Green Center
Hosted by Exhibitors

APRIL 8, 1981 - (Wednesday) - Metals Hall, Green Center

Morning

8:30 - 12:00	SESSION III - Mining Chairman: Dr. Dave Summers, University of Missouri - Rolla, Rolla, Missouri
10:00 - 10:15	Coffee Break
12:00 - 1:30	Lunch, Friedhoff Hall, Green Center

Afternoon - -

1:30 - 4:30	SESSION IV - Civil Engineering Chairman: Dr. William Cooley, Terraspace, Inc., Rockville, Maryland Co-Chairman: Dr. Charles Miller, Jet Propulsion Laboratory, Pasadena, California
3:00 - 3:15	Coffee Break

Evening

6:00 - 7:00	Social Hour Friedhoff Hall Hosted by Exhibitors
7:00 - 8:30	Banquet - Friedhoff Hall Speaker: Dr. L.W. Leroy, Department of Geology, Colorado School of Mines

APRIL 9, 1981 - (Thursday - Metals Hall, Green Center)

Morning -

8:30 - 12:00	SESSION V - Industrial Application Chairman: Mr. Jack Frank, Office of Surface Mining, Kansas City, Missouri
10:00 -10:15	Coffee Break
12:00 -1:30	Lunch - CSM Student Center

***
*

ORGANIZING COMMITTEE

Fun-Den Wang (Chairman), Colorado School of Mines
Seymour Bortz, IIT Research Inst., Chicago, Illinois
John Cheung, Flow Industries, Kent, Washington
Charles Miller, Jet Propulsion Laboratory, Pasadena, California
John Olson, Flow Industries, Kent, Washington
Hamilton Reese, Bureau of Mines, Washington, D.C.
George Savanick, U.S. Bureau of Mines, Twin Cities, Minnesota
David Summers, University of Missouri - Rolla, Rolla, Missouri
Doug Uthus, Department of Energy, Germantown, Maryland

LIST OF PARTICIPANTS

Anderson, Milton N., Partek Corporation, Houston, Texas
Bergkvist, Hans R., Institut CERAC, Switzerland
Bonge, Nick, Earth Mechanics Institute, Colorado School of Mines, Golden, Colorado
Bortz, S.A., IIT Research Institute, Chicago, Illinois
Brierley, William H., National Research Council, Ottawa, Ontario, Canada
Briggs, Aubrey C., Dravo Corporation, Pittsburgh, Pennsylvania
Burns, Dave, University of Waterloo, Waterloo, Ontario, Canada
Callaghan, Thomas, Foster-Miller Associates Inc., Waltham, Maine
Collyer, Philip L., Anaconda Copper Company, Denver, Colorado
Conn, Andrew F., Hydronautics, Incorporated, Laurel, Maryland
Cooley, William C., Terraspace Inc., Rockville,Maryland
Davies, Thomas W., University of Exeter, Exeter, Devon, UK
Dean, Thomas J., University of Waterloo, Kitchener, Ontario, Canada
DeBusk, Pat J., Hydro-Services, Inc., Missouri City, Texas
Draughon, Roderick N., Flow Systems Inc., Kent, Washington
Dressel, Michael 0., Bendix Corporation, Englewood, Colorado
Dubugnon, Oliver, Institut CERAC S.A., Switzerland
Eddingfield, David L., Southern Illinois University, Carbondale, Illinois
Edlund, Hans E., Gardner-Denver, Cooper Industries, Henderson, Colorado
Eecloo, John, H.M. Aquablast Limited, Scarborough, Ontario, Canada
Evans, Robert J., U.S. D.O.E., Pittsburgh Mining Tech. Center, Pittsburgh, Pennsylvania
Evers, James, L., Southern Illinois University, Carbondale, Illinois
Farris, Nathandale, Conoco Inc., Ponca City, Oklahoma
Fine, Jacques C., Ecole des Mines de PARIS, Fontainebleau, France
Frank, Jake N., Office of Surface Mining, Kansas City, Missouri
Frederick, Harold W., Pacific Sound Industrial, Inc., Longview, Washington
Frye, J. D., Hydro-Services, Inc., Missouri City, Texas
Gilpin, Robert R., University of Alberta, Edmonton, Alberta, Canada
Giovando, Carol G., National Mine Service Company, Nashville, Illinois
Groom, Jack J., Jeffrey Mining Machinery Division, Columbus, Ohio
Grunig, James K., Anaconda Copper Co., Tucson, Arizona
Hamel, Mohamed A., Ecole des Mines, Paris, France
Haent jens, Walter D. , Barrett, HaentJens and Company, Hazleton, Pennsylvania
Hruska, Donald C., Anaconda Copper Co., Jeffrey City, Wyoming
Harzer, Johann, Bergbau AG Westfalen, West Germany
Hashish, Mohamed, Flow Industries, Inc., Kent, Washington
Jacobs, Thomas L., Reed Mining Tools, Houston, Texas
Knoke, G. Stuart, Flow Industries, Inc., Kent, Washington
Kortenbusch, Werner, Bergbau AC Westfalen, West Germany
Kubo, Arthur S., The BDM Corporation, McLeary, Virginia
Kramer, Harry W., WOMA Corporation, South Plainfield, New Jersey
Laborde, Russell G., The Oilgear Company, Milwaukee, Wisconsin
Labus, Thomas J., SCIRE Corporation, Fontana, Wisconsin
Lefin, Yves R., C.E.R.C.H.A.R., Verneuil En Halatte, France
Lievsveld, Daniel, J., G & L Granite Company, Denver, Colorado
Lindenmuth, William ., Hydronautics, Incorporated, Laurel, Maryland
Lohn, Peter D., TRW Defense & Space Systems Group, Redondo Beach, California
Lombard, David, Flow Systems Incorporated, Kent, Washington

Lugan, Phillipe M., Ecole des Mines, Paris France
Mahal, Harry S., Towler Hydraulics Incorporated, Urbana, Ohio
Mazurkiewicz, Marian, University of Missouri - Rolla, Rolla, Missouri
Meng, Guo-Qin, Earth Mechanics Institute, Colorado School of Mines, Golden, Colorado
Miglierini, Raul A., Dresser Industries, Dallas, Texas
Miller, Charles G., Jet Propulsion Laboratory, Pasadena, California
Miller, Russell, Haagmiller, Inc., Golden, Colorado
Mohaupt, Udo H., University of Waterloo, Waterloo, Ontario, Canada
Nebeker, Eugene B., Scientific Associates, Inc., Santa Monica, California
Olsen, John H., Flow Industries, Inc., Kent, Washington
Ozdemir, Levent, Earth Mechanics Institute, Colorado School of Mines, Golden, CO
Pechalat, Francois, CERCHAR, Verneuil En Halatte, France
Peters, Joseph F., Colorado Springs Granite Company, Colorado Springs, Colorado
Phipps, John E., Camsco, Incorporated, Richardson, Texas
Plum, George L., Dravo Corporation, Pittsburgh, Pennsylvania
Radtke, Robert P., Strata Bit Corporation, Houston, Texas
Raether, Roger J., Dakota Granite Company, Milbank, South Dakota
Reichman, James M., Flow Industries, Incorporated, Kent, Washington
Riordan, R.F., U.S. Steel, Salt Lake City, Utah
Roberts, Robert R., Anaconda Copper Company, Tucson, Arizona
Rockwell, Philip K., Civil Engineering Laboratory, Port Hueneme, California
Rollins, Ronald R., West Virginia University, Morgantown, West Virginia
Romell, Vigg R., Atlas Copco Mct AB, Stockholm, Sweden
Ropchan, David, Earth Mechanics Institute, Colorado School of Mines, Golden, CO
Sami, Sedat, Southern Illinois University, Carbondale, Illinois
Savanick, G. A., U.S. Bureau of Mines, Twin Cities Research Center, Minneapolis, MN
Setork, Ali, Southern Illinois University, Carbondale, Illinois
Silverstein, Joel, Partex Corporation, Houston, Texas
Simpson, Robert J., Le Groupe SNC, Montreal, Canada
Sterling, Arther M., Louisiana State University, Baton Rouge, Louisiana
Struhs, Kenneth E., Applied Engineering Products Co., Salt Lake City, Utah
Summers, David A., University of Missouri-Rolla, Rolla, Missouri
Tessner, R. Lynnard, Georgia Institute of Technology, Atlanta, Georgia
Timmerman, Marvin, Sandia National Laboratories, Albuquerque, New Mexico
Varner, Horace M., Bendix Corporation, Englewood, Colorado
Vitay, Mohan M., National Research Council of Canada, Ottawa, Ontario, Canada
Vincze, Al, Hydroblaster, Inc., Sparks, Nevada
Wang, Fun-Den, Earth Mechanics Institute, Colorado School of Mines, Golden, Colorado
Wang, Zhi-hong, Earth Mechanics Institute, Colorado School of Mines, Golden, CO
Wayment, William R., Anaconda Copper Company, Tucson, Arizona
Wolgamott, John E., Stone Age, Durango, Colorado
Yie, Gene G., Flow Technology Company, Rent, Washington
Zhang, Rong, Earth Mechanics Institute, Colorado School of Mines, Golden, Colorado
Zink, Edwin, Stone Age, Durango, Colorado
Zink, Gerald, Stone Age, Durango, Colorado

ACKNOWLEDGMENTS

The initial meeting of the organizing committee to plan for the First U.S. Water Jet Symposium began two years ago. The committee members were responsible for determining the theme and technical sessions of the conference.

The success of the symposium is due largely to the efforts of committee members, the session chairmen, authors and the contribution of the staff of the Mineral Research Center and the Earth Mechanics Institute of Colorado School of Mines.

The following organizations provided financial support:

Flow Industries, Inc.
Towler Engineering, Inc.
Denver Valve and Fitting Company
Hydroblasters, Inc.

THE EFFECT OF THE PIPING SYSTEM ON LIQUID JET MODULATION

J. L. Evers
Southern Illinois University
at Carbondale
College of Engineering & Technology
Carbondale, IL 62901

D. L. Eddingfield
Southern Illinois University
at Carbondale
College of Engineering & Technology
Carbondale, IL 62901

ABSTRACT

The interaction of a liquid jet modulator and the supply piping has been modeled utilizing the method of transfer matrices and the method of characteristics. This study has demonstrated the potentially dominant effect that the piping system can have on the resulting modulation. A comparison is made between the modulation wave shapes produced by oscillating the fluid resistance and those produced by a positive displacement volumetric oscillator.

INTRODUCTION

Investigators have found that when a continuous high speed jet is directed onto a stationary target, the highest rate of erosion occurs during the first second of impact (1). The transient pressure resulting from the impact of the leading edge of the jet and the solid surface has been found to be several times the steady state stagnation pressure (2,3,4). In order to extend the duration of this increased cutting rate, attempts have been made to interrupt the flow and cause the jet to arrive at the cutting surface in a series of liquid particles. Shuttering mechanisms have been used with some degree of success, but they tend to cause excessive disturbance to the jet (2,5). Pulsed jets or water cannons that produce a succession of single jets have been tested. However, low firing rates have been a source of dissatisfaction with these devices (1). A scheme for breaking a continuous water jet into a series of water bunches by either periodically changing a volume in the flow circuit (14) or by varying the fluid resistance (6) has been shown to produce a free liquid jet with a periodic volumetric flow. Under controlled frequencies, amplitudes and wave shapes, it is speculated that near spherical water particles can be made to form near the impact surface, producing a continuous series of water hammer impacts that will extend the higher cutting rate by its direct stress effect, by resonating internal pore spaces, or by reinforcing reflected stress waves in the solid materials.

Any form of jet modulation that periodically changes the pressure inside the supply piping is known to be significantly affected by the elasticity of the pipes and the compressibility of the flowing fluid (7). The magnitude of this effect can be graphically illustrated by driving a volumetric or resistive fluid oscillator through a wide range of frequencies and observing with a strobed light the resulting water nodes along the jet stream. For a fixed amplitude of oscillator movement, the degree of jet modulation can be seen to vary from indiscernible to that of a disc shaped water bunching that appears to explode as the frequency reaches a particular value. This jet action is consistent with that predicted by fluid piping transient analyses. This investigation utilizes two standard hydraulic transient methods, namely the method of characteristics and the method of transfer matrices, to evaluate both volumetric and fluid resistance oscillators in a variety of simple piping systems. Generalizations on the behavior of a modulator piping system have been sought that can guide in the initial stages of component selection as well as to illustrate the magnitude of the effect that supply piping can have on the resulting modulation.

METHODS OF ANALYSIS

The steady oscillatory flows considered in this study were analyzed by the transfer matrix method - a technique commonly utilized in describing the response of mechanical vibratory systems and electrical networks (9,10,11) and the method of characteristics - a standard technique (12) for converting the hyperbolic partial differential equations of continuity and momentum into ordinary differential equations that can be solved in finite difference form with a high speed computer.

Transfer Matrix Method

Whenever a periodic variation in pressure and flow rate are insured, it is possible to determine the steady state amplitude of vibration by converting the one dimensional continuity and momentum equations into equations involving the pressure and flow rate fluctuations, position along the pipe, and frequency of the fluctuation. This is done by assuming that the pressure and flow rate can be expressed as a mean quantity plus a sinusoidal deviation from the mean. The nonlinear viscous terms are either linearized or ignored and nonlinear boundary conditions are linearized by dropping higher order terms. These approximations limit the analysis to small oscillations. However, when realistic pressures and flow rates are required for larger oscillations, the transfer matrix method can be useful in obtaining the complete frequency response diagram. Then the method of characteristics, which is much less economical with respect to computer time, can be used to obtain the magnitudes of the pressures and flow rates at the critical frequencies of interest. The details of the transfer matrix method have been adequately covered in the literature and will not be repeated here.

The transfer matrix for a frictionless pipeline supplied by a positive displacement pump and modulated by an oscillating value at the end of the pipe (Figure 1) can be described by the following pair of equations expressed in matrix notation.

$$P = \begin{bmatrix} 1 & 0 & 0 \\ \dfrac{-2Ho}{Qo} & 1 & \dfrac{2HoK}{\tau_o} \\ 0 & 0 & 1 \end{bmatrix}$$

where

$$F = \begin{bmatrix} \cos\dfrac{\ell\omega}{a} & \dfrac{-jgA}{a}\sin\dfrac{\ell\omega}{a} & 0 \\ \dfrac{-jgA}{a}\sin\dfrac{\ell\omega}{a} & \cos\dfrac{\ell\omega}{a} & 0 \\ 0 & 0 & 1 \end{bmatrix}$$

and

$$P = \begin{bmatrix} 1 & 0 & 0 \\ \dfrac{-2Ho}{Qo} & 1 & \dfrac{2HoK}{\tau_o} \\ 0 & 0 & 1 \end{bmatrix}$$

The deviation in flow rate q and the deviation in pressure h are designated by an R to indicate that they are quantities to the right of points 1 and 2 in Figure 1. In these equations, l is the length of the pipe, a is the speed of sound, g is the acceleration of gravity, ω is the circular frequency of oscillation, H_o is the mean pressure head at the nozzle, Q_o is the mean flow rate, τ_o is the mean relative valve opening, and k is the amplitude of valve motion. Since the flow at point 1 is constant, q_1^R is equal to zero.

Downstream of the oscillating valve is atmospheric pressure so h_2^R is also equal to zero. This leaves two unknowns h_1^R and q_2^R to be determined from the given pair of equations. These equations are solved for a spectrum of frequencies. The resulting values presented in Figure 1 illustrate that modulation is completely attenuated at even harmonics of the piping system while full modulation is accomplished at odd harmonics. When the constant displacement pump is replaced by a constant pressure source q_1^R is no longer known. However, h_1^R is now zero, leaving two unknowns that can be determined. The frequency response of this system indicates the opposite conditions from those of the constant flow pump. The modulation is totally attenuated at odd harmonics. However, in both of these cases, as well as many other conditions analyzed in this study, the oscillating valve produces full modulation only when it is located at a pressure node. Full attenuation occurs when the valve is located at a pressure antinode. The pressure antinode building up at the valve suggests that the effect of the valve opening and the oscillating pressure are out of phase and thereby canceling the effect of the other.

For more complex systems, resonant conditions producing fully modulated and attenuated flows will not necessarily occur at exact harmonics of any of the individual pipes. However, a frequency response can be determined using the transfer matrix method to indicate the degree of modulation as a function of modulator frequency.

Various piping components such as dead end pipes, series junctions connecting pipes of different sizes, or parallel branches can be used to change the frequency response of a modulator piping system. This is of considerable interest in developing a modulator for a particular frequency or range of frequencies, where modulation attenuation is normally to be minimized at these frequencies. However, it is conceivable that control of the degree of modulation could be more easily accomplished by tuning the piping system than by changing the parameters of the oscillator.

To illustrate the effect of a parallel branch on the frequency response of a piping system, the modulation behavior of a single branch pipe of two different materials is determined and then a parallel branch is added and the responses compared. The results are presented as plots of modulation amplitude q_3^R nondimensionalized with the mean flow Q_o versus the ratio of the modulation frequency f to the theoretical natural frequency fth where the theoretical natural frequency is given by

$$fth = \frac{1}{4\sum_{i=1}^{n}\frac{\ell_i}{a_i}}$$

where l_i is the length of each pipe in the main branch and a_i: is the corresponding speed of sound in that pipe.

A single branch piping system made of two different materials and its frequency response are shown in Figure 2. One can observe that about 25 percent of the modulation is attenuated at frequencies halfway to the next lower and higher harmonics. The same system equipped with a parallel circuit having a natural frequency that is one half of the natural frequencies of the two equal pipe segments between points 1 and 2 has a modulation frequency response indicated in Figure 3. This system shows no discernable attenuation of the modulated flow even well beyond the midway points to the next harmonics. The same trend can be observed with a properly placed dead end pipe branch or a series pipe junction, although no arrangement considered in this investigation showed such a dramatic extension of unattenuated modulation as the parallel pipe system.

Pipe length in general can play a significant role in the satisfactory design of a modulator system. Recalling that the natural frequency of a piping system is inversely proportional to the pipe lengths, the longer the piping system, the closer together will be the resonance conditions. Therefore, a modulator system with pipes on the order of 100 feet (30.5m) in length would typically go from one totally attenuated resonance condition to another every 20 cycles per second. This would be particularly restrictive if the modulator was designed to operate at a few thousand cycles per second since even one percent adjustment at any properly functioning setting would produce a totally attenuated condition.

Long dead end branch pipes that have not been closed off from the main branch can also dominate the response of a modulator. This is due to the fact that odd harmonics in a dead end branch pipe fully attenuate the input modulation. Therefore, the longer the dead end pipe, the closer together will be these frequencies of ineffective modulation.

Method of Characteristics

In order to study the wave shapes of the modulated flows produced by periodic valves and positive displacement oscillators, the method of characteristics was employed. This method retained all of the nonlinear behavior of the fluid and piping components as the hyperbolic partial differential equations of continuity and momentum were transformed into four total differential equations. The resulting equations were expressed in finite difference form and the solutions obtained with a digital computer. The ability of this method to accurately model transient and periodic pipe flows has been amply demonstrated in the literature (8,13). The reason that this method was not utilized in the analysis of all the systems in this study was the relatively large amount of computer time required to obtain steady periodic conditions.

The numerical results of these calculations are presented in the form of pressure profiles along the pipe for each increment of time and another curve located in the lower half of the figure that plots flow rate at the nozzle as a function of time. The pressure plots along the pipe for all time increments are plotted on the same curve (upper half of the figure). Although this form of data presentation obscures the location and shape of a single pressure trace, it clearly shows the envelope of pressures in the pipe and illustrates the locations of pressure nodes and antinodes. The volumetric flow rates at the nozzle are plotted in the lower figures and illustrate the differences in wave shapes for various modulation techniques and flow conditions.

All of the systems analyzed by this technique were comprised of a two inch (0.051m) steel pipe with a nozzle at the end, supplied by a constant flow rate pump with a capacity of 1 ft3/sec (0.028m3/sec). The length of the pipe in each case is indicated on the figure as the horizontal scale of the pressure plots.

When a positive displacement oscillator was placed at the pump and was driven at an even harmonic of the piping system, the modulation was the same as the input fluctuation of 20 percent as illustrated in Figure 4. When the modulator was driven at one of the odd harmonics of the piping system, the modulation was attenuated by about 50 percent (Figure 5) with intermediate results for fractional harmonics. The variation in flow appears to be sinusoidal for all frequencies.

Next, the positive displacement oscillator was placed at different positions along the pipe. In Figure 6, the oscillator was placed at 3 feet (.9m) from the pump and was driven at the tenth harmonic of the pipe. The resulting flow was fully modulated. When the frequency was halved to the fifth harmonic, the modulation was attenuated (Figure 7). In the first case, the modulator was positioned at a pressure antinode and in the second, at a pressure node. An inspection of the transfer matrix for this system indicates that this will always be true for a constant flow source and a single pipe. The oscillator located at an antinode produced even harmonics on both sides of the oscillator. The arguments of the sine and cosine functions in the pipe transfer matrices were multiples of a, yielding unity matrices for both pipes. Therefore, the resulting flow modulated as if the system contained only a pump, a modulator and a nozzle - an arrangement that is expected to produce full modulation. In a similar manner, it can be shown that in a single pipe constant flow system, a modulator located at a pressure node will produce odd harmonics in the pipes on both sides of the oscillator and thereby eliminate completely the modulation at the nozzle.

The same mathematically modeled piping system supplied by the positive displacement pump was next modulated by a periodic valve that produced a sinusoidal relative valve opening. It was felt that some straightening length should be provided after the valve. Therefore, the computer program was designed to allow placement of the valve at any position along the pipe. Whenever the valve was placed so that each section of pipe was oscillated at an odd harmonic, the resulting wave shape, although no longer sinusoidal, was periodic and even symmetric. Figure 8 illustrates the pressure envelope and the nozzle flow for a piping system driven at the fifth harmonic in the longer section of pipe and the fundamental frequency in the straightening section of pipe. If a purely kinematic analysis is considered in predicting the shape of the jet stream, the additional inflection points in the modulation wave are expected to produce secondary surface irregularities within the wave length. By reducing the degree of modulation by a factor of four, the nonlinear nature of the valve was greatly suppressed and the resulting wave form shown in Figure 9 had practically constant slopes which would kinematically produce cylindrical water packages.

By changing only the frequency of the modulator from the fifth harmonic illustrated in Figure 8 to a frequency that did not produce a resonant condition in either section of pipe, the wave form illustrated in Figure 10 was obtained. The modulation wave was still periodic, but with the significant additional irregularities within the wave length that could produce secondary droplets, depending on the relative strengths of the irregularities. Any deviation from the odd harmonic condition on both sides of the valve produced deformations in the symmetric wave shape in proportion to the degree of deviation.

Figure 11 illustrates the completely attenuated condition that is produced when the valve is located at a pressure antinode or, in the case of a positive displacement pump, when even harmonics are produced in the pipe between the pump and the valve.

CONCLUSIONS

This investigation has illustrated the potentially dominant effect of the piping system on the modulation produced by a periodic valve or a positive displacement oscillator. A complete frequency response for a proposed system can be readily determined by the transfer matrix method with quantitative determinations suffering as oscillations increase in size. However, pressure and flow rate magnitudes can be calculated for large oscillations at critical points of interest by the method of characteristics.

Placement of a periodic valve in the piping system should be such that odd harmonics occur in both sections of the pipe at operating frequencies. Otherwise, the resulting wave shape could produce unwanted secondary droplets.

Finally, piping components can be used to shape the frequency response of the modulator system to fit the intended application. These components can also be employed in regulating the degree of modulation when it is not practical to provide it at the oscillator.

ACKNOWLEDGEMENT

The study described in this paper was supported by a Sabbatical year grant from the Department of Energy through Oak Ridge Associated Universities.

BIBLIOGRAPHY

1. Mohaupt, U. H., and Burns, D. J. "Design and Dynamics of a Pulse-Jet Pavement Breaker", Fourth International Symposium on Jet Cutting Technology, Paper D2, BHRA Fluid Engineering, Canterbury, England, April 1978.
2. Lichtarowicz, A., and Nuachukwu, G. "Erosion by an Interrupted Jet", Fourth International Symposium on Jet Cutting Technology, Paper B2, BHRA Fluid Engineering, Canterbury, England, April 1978.
3. Heymann, F. J. "High Speed Impact Between a Liquid Drop and a Solid Surface", J. Applied Physics, 40, 1969.
4. Hwang, J. B., and Hammitt, F. G. "Transient Distribution of the Stress Produced by the Impact Between a Liquid Drop and an Aluminum Body", Third International Symposium on Jet Cutting Technology, Paper Al, BHRA Fluid Engineering, Chicago, U.S.A., May 1976.
5. Erdmann-Jesnitzer, F., Louis, H., and Wiedemeier, J. "Material Behavior, Material Stressing, Principle Aspects in the Application of High Speed Water Jets", Fourth International Symposium on Jet Cutting Technology, Paper E3, BHRA Fluid Engineering, Canterbury, England, April 1978.
6. Nebeker, E. B., and Rodriguez, S. E. "Percussive Water Jets for Rock Cutting". Third International Symposium on Jet Cutting Technology, Paper B1, Cranfield, England, May 1976.
7. Wyle, E. B. "Pipeline Dynamics and the Pulsed Jet", First International Symposium on Jet Cutting Technology, Paper A5, BHRA Fluid Engineering, Cranfield, England, April 1972.
8. Chaudhry, M. H. Applied Hydraulic Transients, Van Nostrand Rheinhold Company, New York, 1979.
9. Pestel, E. C. and Lackie, F. A. Matrix Methods in Elastomechanics, McGraw-Hill Book Co., New York, 1963.
10. Reed, M. B. Electrical Network Synthesis, Prentice-Hall Inc., New York, 1955.
11. Chaudry, M. H. "Resonance in Pressurized Piping Systems", Journal, Hydraulics Division, American Society of Civil Engineers, Vol. 96, September 1970, pp. 1819-1839.
12. Abbott, M. B. "An Introduction to the Method of Characteristics", American Elsevier, New York, 1966.
13. Streeter, V. L. and Wylie, E. B. Hydraulic Transients, McGraw-Hill Book Company, New York, 1967.
14. Sami, S. and Evers, J. L. Unpublished Research Data, 1981.

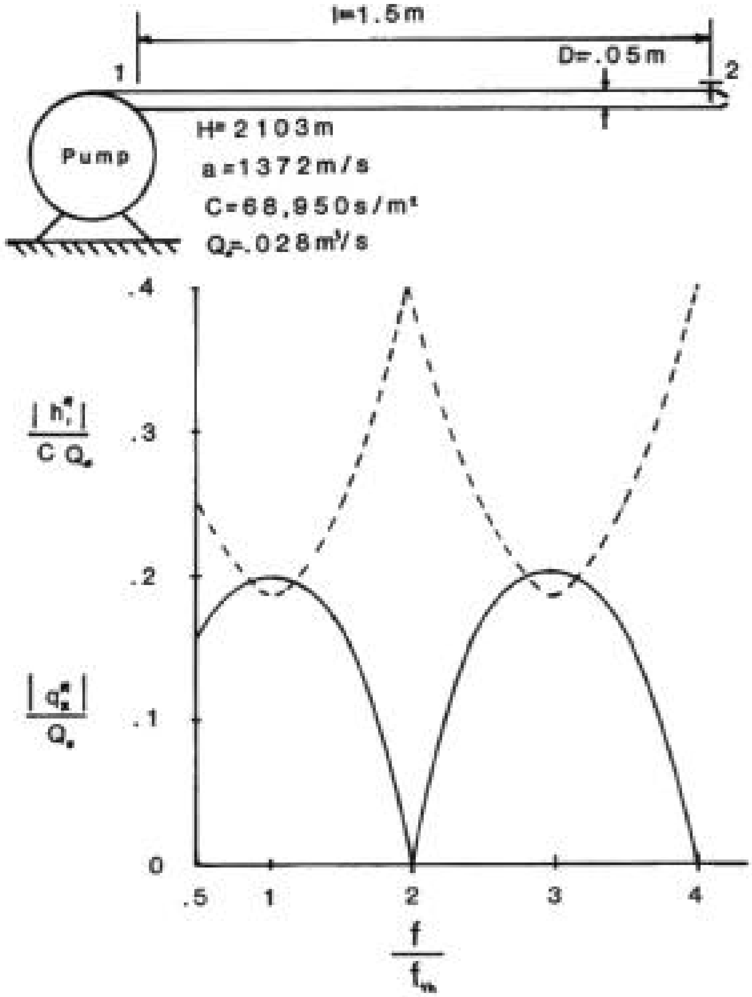

Figure 1   Control Flow Input and Frequency Response

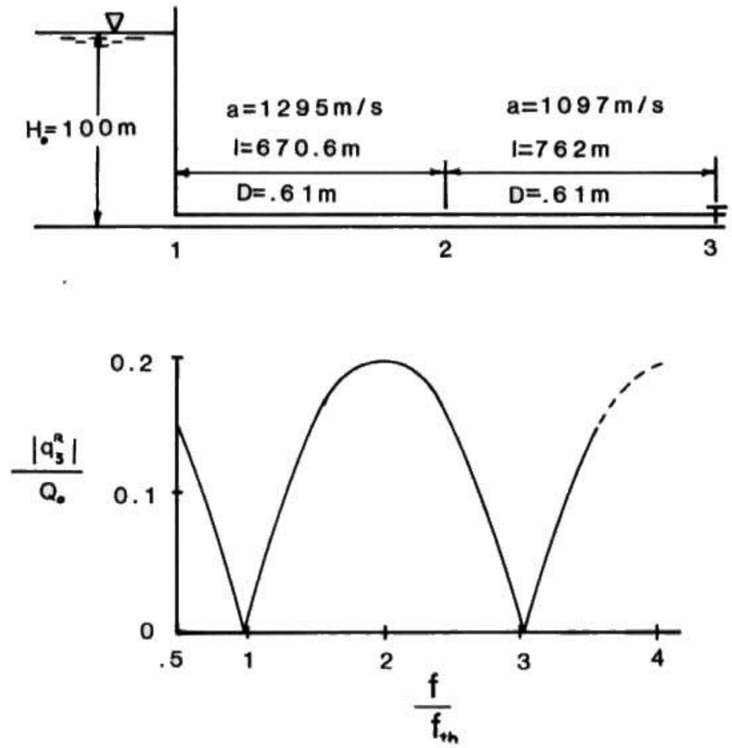

Figure 2 Modulation Frequency Response For Piping System Above

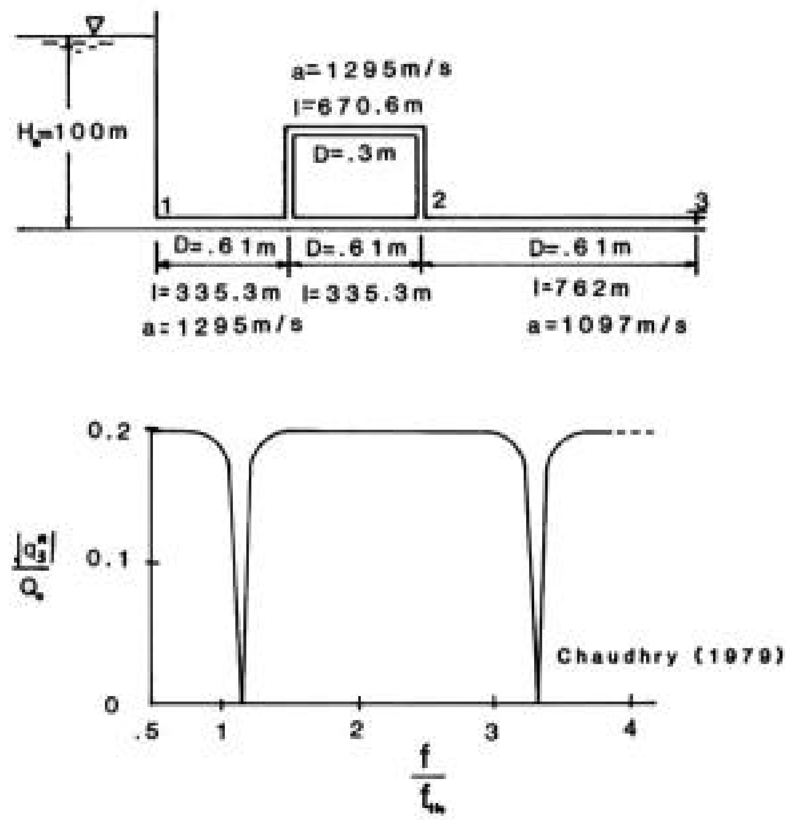

Figure 3 Modulation Frequency Response For Parallel Pipe System

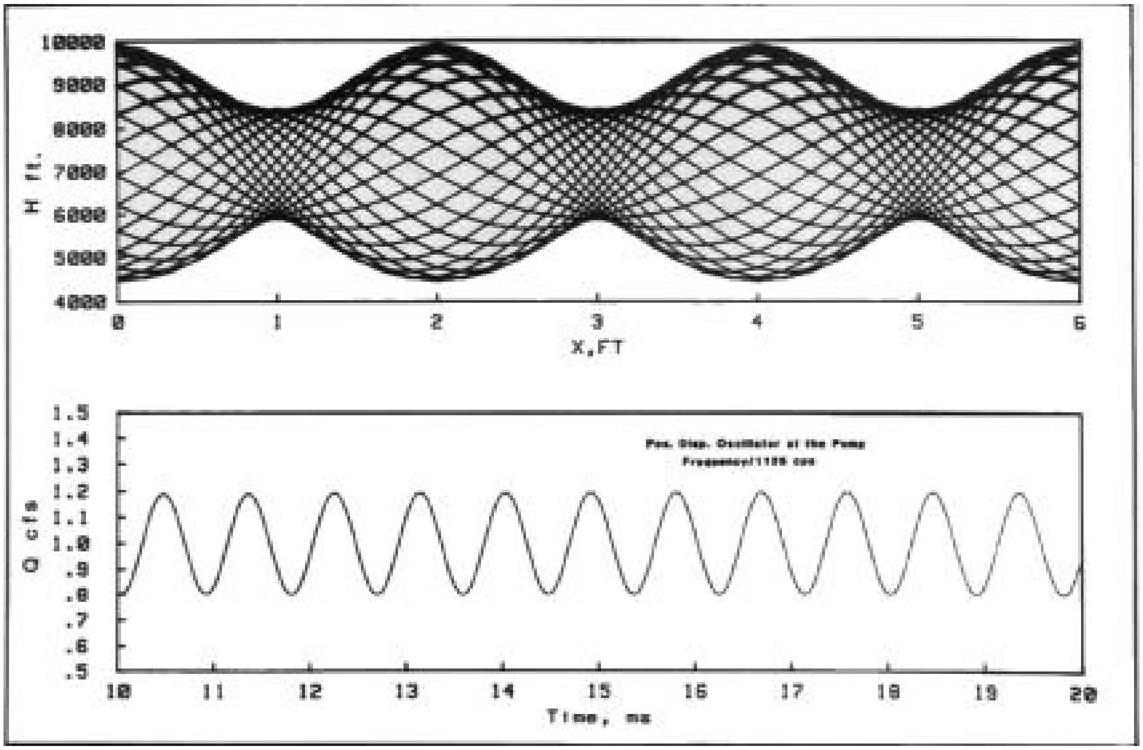

Figure 4 Pressure and Flow Rates for Oscillator at Pump

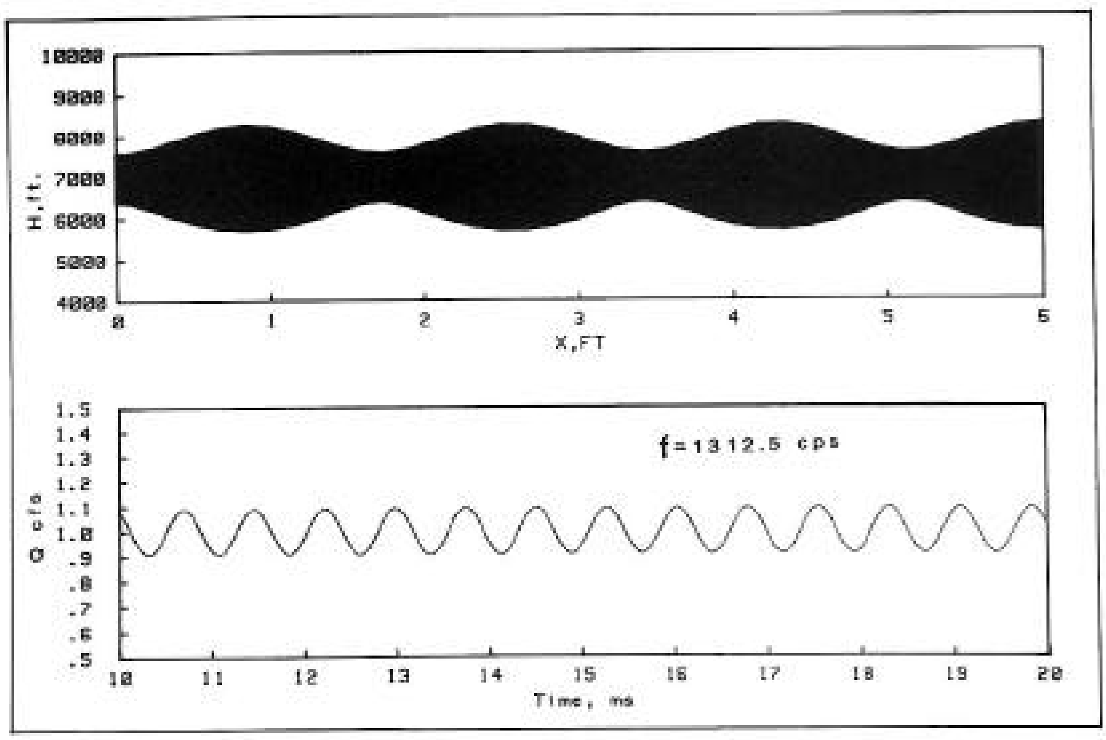

Figure 5 Pressures and Flow Rates for Oscillator at Pump

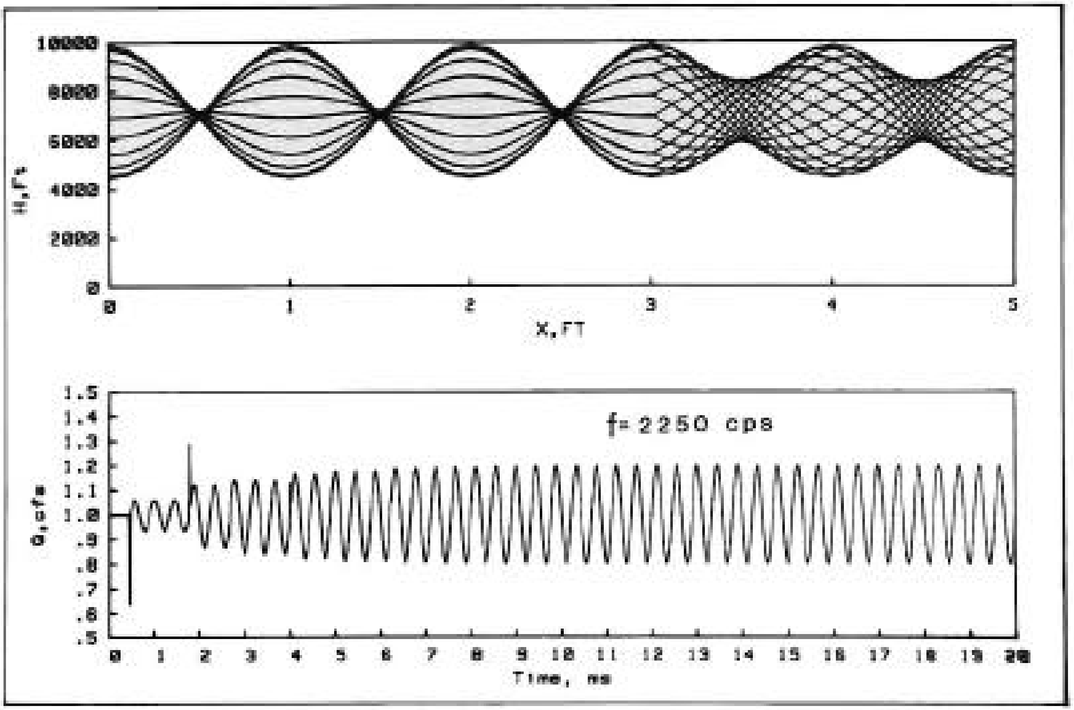

Figure 6 Pressures and Flow Rates for Oscillator at 3ft.

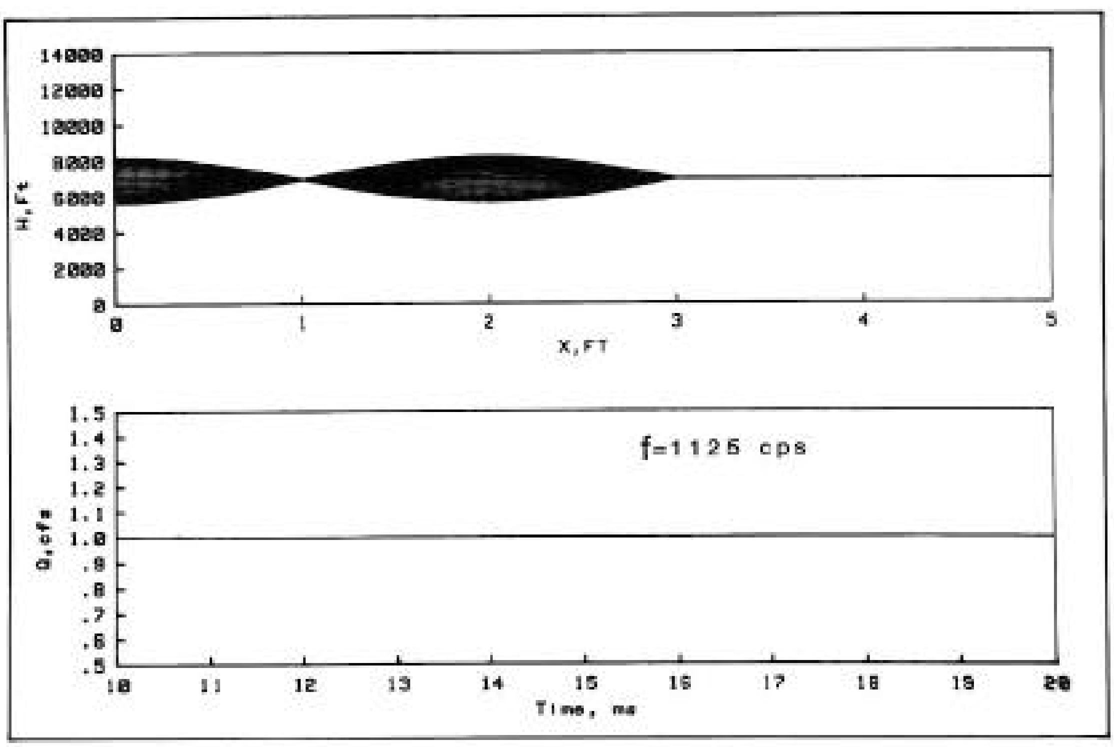

Figure 7 Pressures and Flow Rates for Oscillator at 3ft.

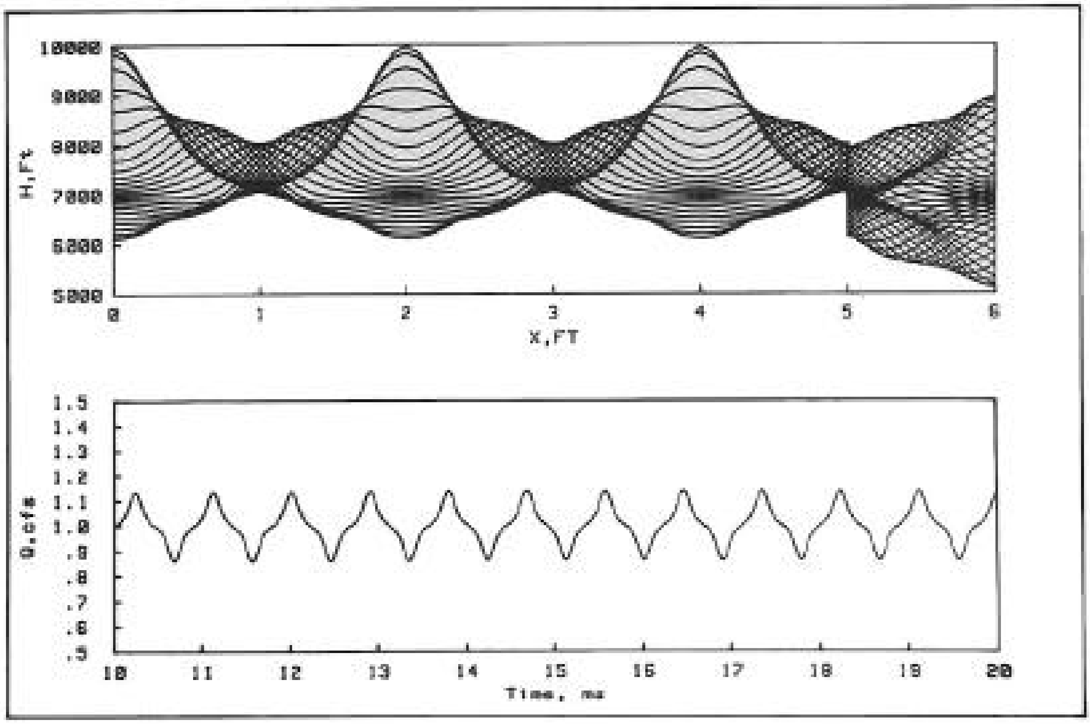

Figure 8 Periodic Valve at 5ft., f=1125 cps

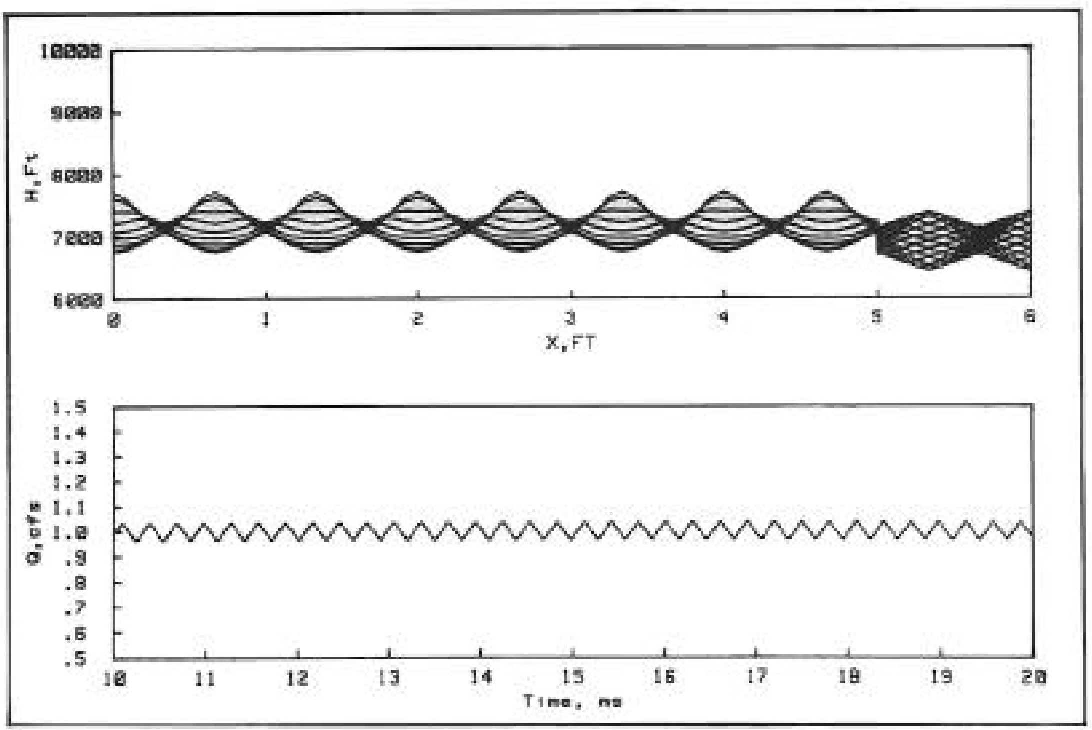

Figure 9 Periodic Valve at 5ft., f=3375 cps

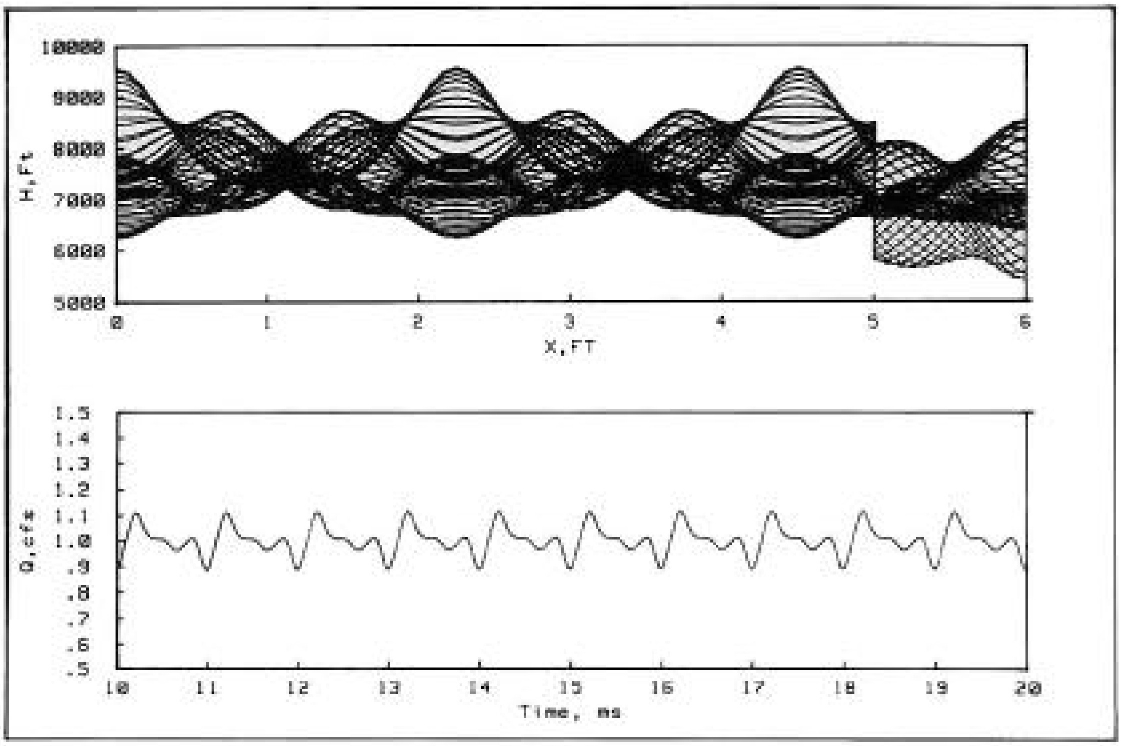

Figure 10 Periodic Valve at 5ft., f=1000 cps

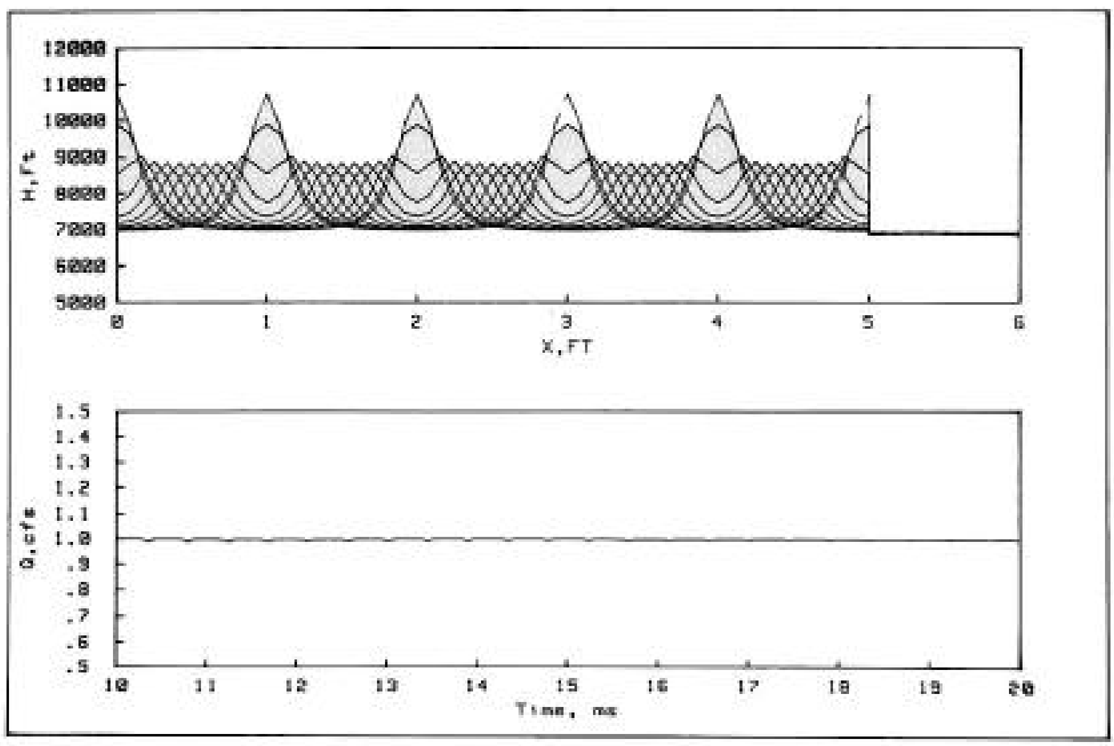

Figure 11 Periodic valve at 5ft., f=2250 cps

GOVERNING EQUATIONS IN A MODULATED LIQUID JET

Sedat Sami and Hamid Ansari
Southern Illinois University, Carbondale*

INTRODUCTION

During the last decade the conventional water jet-nozzle system has been successfully developed and used to cut, drill or fracture several target materials, including coal. The failure mechanisms contributing to such an action are considered to be (a) some granular erosion; (b) fracture under shear or tensile stress; and (c) water permeation into cracks and pores. However, it has been observed that the highest rate of erosion would occur during the initial period of impact. This observation has lead several investigators to look into the possibility of reducing the jet flow into a series of drops in order to get full advantage from the initial impact characteristics of water jets. Such a discontinuous jet is expected to be more efficient in fracturing and mining than a conventional jet of comparable energy since (a) it will have a greater ratio of impact area to water volume; (b) it would repeatedly provide initial impact effects; and (c) it will promote brittle fracture of the target material by causing cyclical unloading.

Some of the techniques investigated in the past involved the periodic interruption of the jet discharge thus resulting in the firing of bursts of steady unmodulated constant diameter-jet segments. More recently, efforts have been undertaken to develop a modulated jet-nozzle system where the flow remains continuous-no interruption-though the discharge issued from the nozzle is somewhat modulated. In such a scheme, even though the amplitude of modulation may be relatively small-five or ten percent of the average flow rate-the faster part of each cycle will eventually overtake the slower in the stream and the jet stream will become a train of separated fluid bunches. The bunching of the jet stream is analogous to the phenomenon of signal amplification so commonly referred to in Electrical Engineering as the "Klystron" effect. Any effort to develop an effective discharge-modulated water jet will, undoubtedly, require a thorough understanding of the fluid flow characteristics of the system.

LITERATURE SURVEY

Considerable literature is available on the characteristics of "submerged" jets (i.e., water into water or air into air). However, much less is known about the flow of "free" jets (i.e., water into air). Although the former, after an initial region of the flow development, is completely described by the local momentum conditions and thus amenable to simple mathematical modeling, the latter displays a total absence of "self-similarity" and is governed by parameters such as pressure, nozzle size and configuration, density, viscosity and surface tension of the jet fluid.

---

*"This project was supported by the U.S. Department of Energy Carbondale Mining Technology Center (Contract No. DE-AS22-79PC-20091) through a Special Research Agreement to the Coal Extraction and Utilization Research Center at Southern Illinois University, Carbondale, Illinois."

The breaking up of free jets has nevertheless attracted a good deal of attention. In the l9th century, Lord Rayleigh made a linearised analysis of the capillary stability of an inviscid liquid jet [Lord Rayleigh 1879a, 1879b]. His analysis has shown that asymmetric disturbances of all wavelengths are stable whereas an axisymmetric disturbance is stable or unstable depending on whether its wavelength is less or greater than the circumference of the jet. More recently, Rayleigh's work has been extended by others [Chaudhary 1980; Pimbley 1976; Lafrance 1974; Keller et al. 1973; Nayfeh 1970] to include the effects of non-linearity. However, the analysis is still inadequate in dealing with high amplitude, high frequency modulations as well as aerodynamic drag and turbulence, which are ever-present, especially when the jet flow is at a high Reynolds number and the mechanism most responsible for the bunching and eventual breakup is inertial rather than the surface tension induced.

The first account of a jet break-up due to an inertial type mechanism was reported by Crane et al. [crane et al. 1964]. Their work investigated the effects of high amplitude, high frequency mechanical vibration of an orifice on the break-up characteristics of a liquid jet emerging from the orifice into air. The results clearly indicated that under high frequency vibrations inertial effects dominate the surface tension induced displacements. In a follow-up study McCormack et al. [McCormick et al. 1965] have presented solid evidence to support their semi-quantitative theory of the "bunching" phenomenon. Fenwick and Bugler [Fenwick 1967] during their studies of the combustion instability problem have looked into the relationship between the combustion product release and the injection of the propellant at a location downstream of an injector. That there is a potential for a significant amplification was finally experimentally demonstrated by Nebeker and Rodriguez [Nebeker 1979a] who have developed a suitable flow modulation technique by causing a cyclic variation of the discharge rate by periodically varying the flow resistance upstream of the nozzle.

In what follows, the fluid dynamics of a flow system subject to a forced modulation rather than a capillary instability will be formulated, some simple predictive linear models considered and their results compared in an attempt to develop some useful parameters with which to predict the break-up length of a modulated jet.

DEFINITION OF THE PROBLEM

Consider a water jet issuing (Fig. 1) at time t from a nozzle of radius R with a velocity u(o,t) that is uniform across the exit area but periodic about a mean value U and expressed as

$$u(0,t) = U + \Delta U \sin 2\pi f t \qquad (1)$$

where U is the average exit velocity, and ΔU and f are the amplitude and frequency of the modulation respectively.

Fig. 1

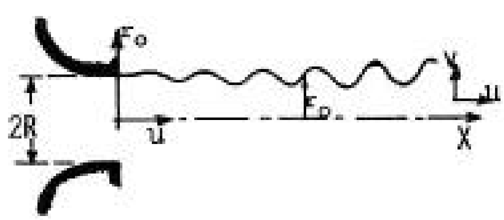

Adopting a cylindrical polar coordinate system with x representing the downstream distance from the nozzle and r the radial coordinate, one can formulate the continuity equation and the equations of motion by considering an axisymmetrical jet flow with no swirl , and by assuming the pressure and axial velocity profiles to be uniform across the jet. For the present study the problem is to determine the surface configuration of the jet (r_o (x,t)) along the jet axis at any given instant.

<u>Continuity equation:</u> Consider a control volume c.v bounded by the control surface c.s. as shown in fig. 2.

Fig. 2

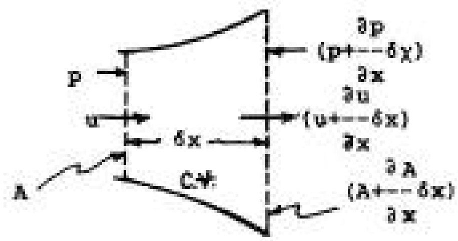

The integral form of the continuity equation can be expressed as

$$\frac{\partial}{\partial t}\int_{c.v.} p\ dV + \int_{c.s.} p\vec{V}.\vec{n}\ dA = 0 \qquad (2)$$

where the control volume c.v. is equal to (A. dx). Eq. 2 can be rewritten as:

$$\frac{\partial}{\partial t}\left(A\delta x\right) - \int_{A} u\ dA + \int_{A+\delta A} u + \frac{\partial u}{\partial t}\delta A = 0$$

For a round jet with a flat discharge velocity profile, the above expression can be rearranged, expanded and after neglecting higher order terms and dividing dx, reduce to

$$\frac{\partial r_o^2}{\partial t} + \frac{\partial}{\partial x}\left(r_o^2\right) = 0$$

Where ro(x,t) is the radius of the jet boundary given by $A=\pi r_o 2$. If one, now, expands the terms of this equation and divides by $2r_o$, one obtains the continuity equation in terms of r_o, as

$$\frac{\partial r_o}{\partial t} + u\frac{\partial r_o}{\partial x} = -\frac{r_o}{2}\left(\frac{\partial u}{\partial x}\right) \qquad (3)$$

<u>Equations of Motion</u>: The Navier-Stokes Equations for an axisymmetrical jet flow with no swirl ($v_\theta = 0$, $\partial/\partial\theta = 0$) and with viscous and gravity effects ignored, and the pressure and axial velocity profiles assumed uniform across the flow ($\frac{\partial p}{\partial r} = 0$, $\frac{\partial u}{\partial r} = 0$) are given by

$$\frac{\partial u}{\partial t} + u\frac{\partial u}{\partial x} = \frac{1}{p}\frac{\partial p}{\partial x} + \frac{\mu}{p}\left(\frac{\partial^2 u}{\partial x^2}\right) \qquad (4)$$

And

$$\frac{\partial v}{\partial t} + u\frac{\partial v}{\partial x} + v\frac{\partial v}{\partial r} = \frac{u}{p}\left(\frac{\partial^2 v}{\partial x^2} + \frac{\partial^2 v}{\partial r^2} + \frac{1}{r}\frac{\partial v}{\partial r} - \frac{v}{r^2}\right) \qquad (5)$$

Where p is the mass density, p the pressure, μ the viscosity, and u and v axial-x and radial-r components of the velocity vector.

The pressure term in Equation 4 includes the effects of surface tension. If a hydrostatic pressure distribution across the jet is assumed, all components of the pressure other than surface tension-o- can be ignored and the expression for the pressure written as

$$p = \frac{\sigma}{r_N} + \frac{\sigma}{r_T}$$

Where r_N and r_T f curvatures in the two orthogonal planes and are expressed as

$$r_N = r_o\left[1 + \left(\partial r_o / \partial x\right)^2\right]^{\frac{1}{2}}$$

And

$$r_T = -\left[1 + \left(\partial r_o / \partial x\right)^2\right]^{\frac{3}{2}} / \left[\partial^2 r_o / \partial x^2\right]$$

Assuming small amplitude modulations one can write $\partial r_o / \partial x \ll 1$ and upon simplification of the terms for r_N and t_R, they can be substituted in to the expression

$$p = \frac{\sigma}{r_N} + \frac{\sigma}{r_T} = \sigma\left[\frac{1}{r_o} - \frac{\partial^2 r_o}{\partial x^2}\right]$$

Which in turn can be used to rewrite Eq. 4 as

$$\frac{\partial u}{\partial t} + u\frac{\partial u}{\partial x} = \frac{\sigma}{p}\left[\frac{1\partial r_o}{r_0^2 \partial x} + \frac{\partial^3 r_o}{\partial x^3}\right] + \frac{\mu}{p}\left[\frac{\partial^2 u}{\partial x^2}\right] \qquad (6)$$

As stated before the problem is to solve for $r_o(x,t)$. Since the radial component v of the velocity does not appear in either Eq. 3 or Eq. 6, the problem is reduced to the simultaneous solution of Eqs. 3 and 6:

$$\frac{\partial r_o}{\partial t} + u\frac{\partial r_o}{\partial x} = -\frac{r_o}{2}\left(\frac{\partial u}{\partial x}\right) \qquad (3)$$

$$\frac{\partial u}{\partial t} + u\frac{\partial u}{\partial x} = \frac{\sigma}{\rho}\left(\frac{1\partial r_o}{r_0^2 \partial x} + \frac{\partial^3 r_o}{\partial x^3}\right) + \frac{u}{p}\frac{\partial^2 u}{\partial x^2} \qquad (6)$$

If the velocity u is now expressed in terms of a constant velocity U (unmodulated jet velocity) and a variation u' given as

U(x,t)= U+ u'(x,t)

Then, equations 3 and 6 become

$$\frac{\partial r_o}{\partial t} + u\frac{\partial r_o}{\partial x} + u'\frac{\partial r_o}{\partial x} = -\frac{r_o}{2}\left(\frac{\partial u'}{\partial x}\right) \qquad (7)$$

$$\frac{\partial u'}{\partial t} + U\frac{\partial u'}{\partial x} + u'\frac{\partial u'}{\partial x} = \frac{\sigma}{\rho}\left[\frac{\partial r_o}{r_0^2 \partial x} + \frac{\partial^3 r_o}{\partial x^3}\right] + \frac{\mu \partial^2 u'}{\rho \partial x^2} \qquad (8)$$

Next, by translating the frame of reference at the unmodulated jet velocity U, the problem can be reduced to the study of a single wavelength of the stationary stream. The introduction of the moving coordinate system can be expressed by

$$Z = x - Ut, \quad \text{where } z = z(x,t).$$

After determining the various terms ($\partial u'/\partial t$, $\partial u'/\partial x$, $\partial^2 u/\partial x^2$, $\partial r'o/\partial t$, $\partial r_o/\partial x$ and $\partial^3 r_o/\partial x^3$) in terms of z and t and upon substituting them into Eqs. 7 and 8 we obtain

$$\frac{\partial r_o}{\partial t} + u' \frac{\partial r_o}{\partial z} = -\frac{r_o}{2}\left(\frac{\partial u'}{\partial x}\right) \tag{9}$$

$$\frac{\partial u'}{\partial t} + u' \frac{\partial u}{\partial z} = \frac{\sigma}{\rho}\left(\frac{\partial r_o}{r_0^2 \partial z} + \frac{\partial^3 r_o}{\partial z^3}\right) + \frac{\mu \partial^2 u'}{\rho \partial z^2} \tag{10}$$

Equations (9) and (10) can now be non-dimensionalized by the introduction of the following dimensionless parameters:

$$\zeta = r_o / R;\ u = u'/U;\ \eta = z/\lambda;\ \tau = tU/\lambda;\ Re = \rho UR/\mu;\ We^2 = \sigma/\rho RU^2;\ St = R/\lambda \tag{11}$$

where R is the nozzle radius (or the radius of the unmodulated jet) U the unperturbed jet velocity , λ and f the wavelength and the frequency of the modulation respectively, o the surface tension of the fluid, Re, We and the St the Reynolds, Weber and Strouhal numbers of the flow respectively. Thus the Equations(9) and (10) become

$$\frac{\partial \xi}{\partial \tau} + u \frac{\partial \xi}{\partial \eta} = -\frac{\xi}{2}\left(\frac{\partial u}{\partial \eta}\right) \tag{12}$$

and

$$\frac{\partial u}{\partial \tau} + u \frac{\partial u}{\partial \eta} = We^2\left(\frac{\partial \zeta}{\zeta^2 \partial \eta} + St^2 \frac{\partial^3 \zeta}{\partial \eta^3}\right) + \frac{St \partial^2 u}{Re \partial \eta^2} \tag{13}$$

If one considers high Reynolds number flows, the last term in Eq. 13 can be neglected, and one obtains

$$\frac{\partial u}{\partial \tau} + u \frac{\partial u}{\partial \eta} = We^2\left(\frac{\partial \zeta}{\zeta^2 \partial \eta} + St^2 \frac{\partial^3 \zeta}{\partial \eta^3}\right) \tag{14}$$

Equations 12 and 14 can now be manipulated, simplified and solved simultaneously.

Method of Solution I: By assuming a small amplitude of modulation (u' << U or u << 1) one can neglect the second term of each equation (i.e., $v\partial t/\partial n$ and $v\partial v/\partial n$) and by further assuming that surface tension plays a relatively small role as compared to the role of inertia, one can ignore the right hand side of Eq. 14, and thus reduce the Equations 12 and 14 into the following [Nebeker 19761:

$$\frac{\partial \zeta}{\partial \tau} = -\frac{\zeta}{2}\left(\frac{\partial u}{\partial \eta}\right) \tag{15}$$

and

$$\frac{\partial u}{\partial \tau} = 0 \qquad (16)$$

Equation 16 is satisfied by a velocity field v which is any function of the composite dimensionless variable $n(n = z/\lambda = x/\lambda - tU/\lambda)$,

$$u = F(\eta) \qquad (17)$$

Introducing Eq. 17 into Eq. 15 yields

$$\frac{\partial \zeta}{\partial \tau} = -\frac{\zeta}{2} F(\eta) \qquad (18)$$

This equation is a quasi-linear Lagrange Equation (first order PDE) and its solution is obtained by integrating the simultaneous system of subsidiary equations. Thus one gets

$$\frac{-\zeta}{2} F'(\eta) d\tau = d\zeta$$

Upon integration, one has

$$\ln \zeta = -\frac{1}{2} F(\eta) \qquad (19)$$

The initial condition is $\zeta(0, \eta) = 1$

If a purely sinusoidal modulation is given by the function

$$F(\eta) = M \sin 2\pi\eta, \text{ where } M = \Delta U/U$$

one would get, upon substitution into Eq. 19,

$$\ln \zeta = -\pi M \tau \cos 2\pi\eta$$

or

$$\zeta = \exp[-\pi M \tau \cos 2\pi\eta] \qquad (20)$$

<u>Method of Solution II</u>: If the jet radius r_o is expressed, like the velocity, in terms of a constant radius R (the unmodulated jet radius) and a variation r'_o given by $r_o = R + r'_o$, the dimensionless parameter ζ becomes

$$\zeta = r_o / R = 1 + r'_o / R = 1 + \zeta$$

Thus, Eq. 15 can be written as

$$\frac{\partial \zeta}{\partial \tau} = -\frac{(1+\zeta')\partial u}{2\partial \eta} \qquad (21)$$

By assuming that $\zeta' << 1$, this equation can further be simplified into the form

$$\partial u/\partial \eta = -2\, \partial \zeta'/\partial \tau \qquad (22)$$

A similar transformation and simplification when applied to Eq. 14 yields

$$\frac{\partial u}{\partial \tau} = We^2\left[\frac{\partial \zeta'}{\partial \eta} + St^2\frac{\partial^3 \zeta'}{\partial \eta^3}\right] \qquad (23)$$

Equations 22 and 23 can be cross-differentiated and reduced into

$$\frac{\partial^2 \zeta'}{\partial \tau^2} + \frac{We^2 \partial^2 \zeta'}{2\partial \eta^2} + \frac{We^2}{2} St^2 \frac{\partial^4 \zeta'}{\partial \eta^4} = 0 \qquad (24)$$

When a solution of the type

$$\zeta'(\eta,\tau) = T(\tau).\ \sin k_o \eta \qquad (25)$$

where k_o is the dimensionless wave number $2r/\lambda_O$ and λ_o the dimensionless wavelength (λ_O = unity by definition), is substituted into Eq. 24, one gets, after simplification, the Rayleigh Criteria ($\lambda > 2\pi R$) for capillary instability. The solution to Equation 24 has been reported by others [Lee 1974]. However, if one were to ignore the effects of surface tension upon the bunching phenomenon, Eq. 23 reduces to Eq. 16, and the two simultaneous equations to be solved are now

$$\frac{\partial u}{\partial \eta} = -2\frac{\partial \zeta'}{\partial \tau} \qquad (22)$$

and

$$\partial u/\partial t = 0 \qquad (16)$$

For a purely sinusoidal modulation ($F(n) = M \sin 2\pi n$) the solution to the set of Equations (22) and (16) is given by

$$\zeta' = -\pi M\tau \cos 2\pi\eta \qquad (26)$$

In terms of the jet's dimensionless outer radius this gives

$$\zeta = 1 + \zeta' = 1 - \pi M\tau \cos 2\pi\eta \qquad (27)$$

Method of Solution III: Assuming no fluid particle interaction, the jet bunching phenomenon can be also investigated [Fenwick 1967] by considering the kinematics of a fluid particle P. leaving the nozzle at time t_o with a velocity u and arriving at a downstream section x at time t_l. The relationship can be expressed as

$$T_1 = t_o + x/u \qquad (28)$$

where the velocity u of the particle is given by

$$\mathbf{u} = U + u'(t_o) \qquad (29)$$

Substituting Eq. (29) into Eq. (28) gives

$$t_l = t_o + x(U + u')^{-1} \qquad (30)$$

Introducing the binomial expansion and rearranging terms Eq. 30 becomes

$$t_1 = to + x/U - xu'/u^2 \qquad (31)$$

and upon differentiation one gets

$$dt_l/dt_o = 1 - xu'/U^2 + \ldots \qquad (32)$$

where $u' = du'/dt_o$.

The law of conservation of mass requires that the flow rate (q_O) crossing the nozzle section during an interval dt_o be equal to that (q_l) crossing section x during the period dt_l:

$$q_o\, dt_o = q_l\, dt_l \qquad (33)$$

Introducing Eq. 32, one can rewrite Eq. 33 in the form

$$\frac{q1}{qo} = \left(\frac{dt_1}{dt_o}\right)^{-1} = \left(1 - \frac{xu'}{u^2}\right)^{-1} \qquad (34)$$

Since, assuming no particle interaction, any fluid particle leaving the nozzle at $t = t_o$ with a velocity u_p will retain its velocity at all times, one can write

$$u_p = \frac{q_o}{\pi R^2} = \frac{q_1}{\pi r_0^2} \qquad (35)$$

When Equation 35 is rearranged and combined with Eq. 34 one has

$$\frac{r_o}{R} = \frac{q_1}{q_o} = \left(1 - \frac{xu'}{u^2}\right)^{\frac{1}{2}}$$

which can be expanded by the introduction of the binomial theorem

$$\frac{r_o}{R} \quad 1 + \frac{1}{2}\left(\frac{xu'}{u^2}\right) + \ldots \qquad (36)$$

If now one considers a purely sinusoidal modulation given by

$$u = U + u' = U + \Delta U \sin 2\pi ft \qquad (37)$$

where ΔU and f are the amplitude and frequency of the modulation, respectively, and evaluating the term $\frac{xu'}{u^2}$ as

$$2\pi \frac{xf}{U} \frac{\Delta U}{U} \cos 2\pi ft$$

and substituting into Eq. 36, one can write

$$\frac{r_o}{R} \quad 1 + \frac{1}{2}\left(2\pi \frac{xf}{U} \frac{\Delta U}{U} \cos 2\pi ft\right) \qquad (38)$$

Introducing the dimensionless parameters

$$\zeta = \frac{r_o}{R},\ \alpha = \frac{xf}{U} = \frac{x}{\lambda},\ \tau = \frac{t}{T} = ft = \frac{tU}{\lambda},\ M = \frac{\Delta U}{U},\ St = \frac{R}{\lambda}$$

Equation 38 becomes

$$\zeta = 1 + \frac{1}{2}F \qquad (39)$$

where $F = 2\pi M\alpha \cos 2\pi\tau$.

DISCUSSION OF RESULTS

Fluid bunching will eventually lead to a discontinuity (break-up) along the jet axis. This will occur when $\zeta_b = 0$ The corresponding dimensionless break-up length (x_b/R or a_b/St) can be evaluated for each of the methods outlined above. A comparison of the various solutions is presented in Table 1.

TABLE 1

Method	ζ	x_b/R
I	$\exp[-\pi M\tau \cos 2\pi\eta]$	$\ln \zeta / \pi M\ St$
II	$1 - \pi M\tau \cos 2\pi\eta$	$1 / \pi M\ St$
III	$1 + \pi M\alpha \cos 2\pi\tau$	$1 / \pi M\ St$

It is interesting to note that Eqs. 27 (Method II) and 39 (Method III) predict identical break-up lengths. Equation 20 (Method I) leads to an exponential solution and therefore, in this case, it is necessary to define the break-up length in terms of a finite ratio between the reduced and the unperturbed jet radii. In order to permit the evaluation of such a length, a downstream distance where G = 0.20 has arbitrarily been chosen. Figure 3 presents a logarithmic plot of the predicted dimensionless break-up length xb/D against the relative amplitude of modulation M and for various values of the Strouhal number.

A word of caution is now in order: analytical predictions for the break-up length presented in Figure 3 and by Equations 20, 27 and 39 are, of course, inadequate in projecting the shape of the fluid bunches prior to disintegration, Flow visualization experiments presently carried out with 1/8" and 1/4" diameter nozzles indicate that the effects of aerodynamic drag will have to be incorporated in the analysis since the deformation sustained by the pancake shaped disks as they move forward at high velocities appears to be the main mechanism causing the eventual disintegration of the jet by tearing up the fluid at the edges of the disks.

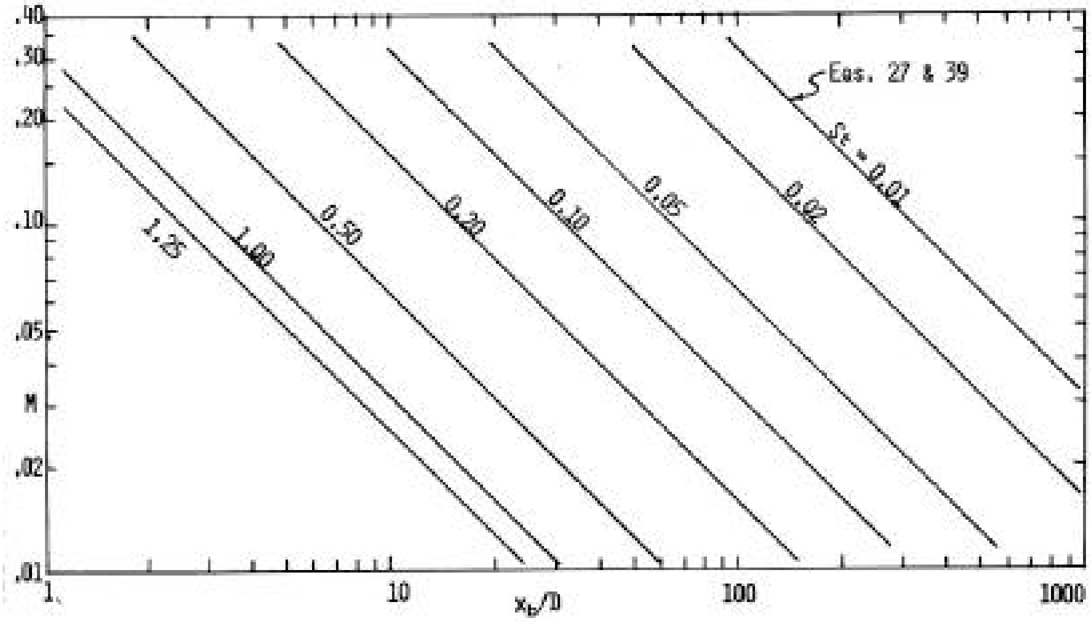

Figure 3.- Breakup Length versus the relative amplitude of modulation

REFERENCES

Chaudhary, K. C., and Redekopp, L. G., 1980, "The Nonlinear Capillary Instability of a Liquid Jet. Part 1. Theory," J. F. M., v. 96, pt. 2, pp. 257-274.

Crane, L., Birch, S., and McCormack, P. D., 1964, "The Effect of Mechanical Vibration on the Breakup of a Cylindrical Water Jet in Air," Brit. J. Appl. Phys., v. 15, pp. 743-750.

Fenwick, J. R., and Bugler, G. J., 1967, "Oscillatory Flame Front Flowrate Amplification Through Propellant Injection Ballistics (The Klystron Effect), Chem. Propulsion Info. Agency, Publ. 138, v. 1, pp. 417-427.

Keller, J. B., Rubinow, S. I., and Tu, Y. O., 1973, "Spatial Instability of a Jet," The Physics of Fluids, v. 16, No. 12, pp. 2052-2055.

Lafrance, P., 1974, "Nonlinear Breakup of a Liquid Jet," The Physics of Fluids, v. 17, No. 10, pp. 1913-14.

Lee, H. C., 1974, "Drop Formation in a Liquid Jet," IBM J. Res. Develop., v. 18, pp. 364-369.

Lord Rayleigh, 1879, "On the Instability of Jets," Proc. London Math. Soc., v. X, pp. 4-13.

Lord Rayleigh, 1879, "On the Capillary Phenomena of Jets," Proc. Royal Soc., v. XXIX, pp. 71-97.

McCormack, P. D., Crane, L., and Birch, L., 1965, "An Experimental and TheoreticalAnalysis of Cylindrical Liquid Jets Subjected to Vibration," Brit. J. Appl. Phys., v. 16, pp. 395-408.

Nayfeh, A. H., 1970, "Nonlinear Stability of a Liquid Jet," The Physics of Fluids, v. 13, No. 4, pp. 841-847.

Nebeker, E. B., and Rodriguez, S. E., 1979, "Percussive Water Jets for Rock

Cutting,"Paper B-1, Proc. 3rd Intern. Symp. Jet Cutting Technology, BHRA Fluid Engineering, Cranfield, pp. Bl-9.

Nebeker, E. B., and Rodriguez, S. E., 1979, "Development of Percussive Water Jets," Final Report, U.S. Dept. of Energy, 80 pgs.

Pimbley, W. T., 1976, "Drop Formation from a Liquid Jet: A Linear One-Dimensional Analysis Considered as a Boundary Value Problem," IBM J. Res. Develop., v. 20, pp. 148-156.

MATHEMATICAL MODELING OF HIGH VELOCITY WATER JETS

D. L. Eddingfield
Southern Illinois University at Carbondale
College of Engineering and Technology
Carbondale, IL 62901

J. L. Evers
Southern Illinois University at Carbondale
College of Engineering and Technology
Carbondale, IL 62901

Ali Setork
Southern Illinois University at Carbondale
College of Engineering and Technology
Carbondale, IL 62901

ABSTRACT

In the study of the effect of nozzle design and the mechanism of breakage in hydraulic cutting, the flow characteristics of water jets are highly desired. In this paper, the mathematical modeling of the flow field of a high velocity water jet is examined, and a review of the existing literature is presented. It is believed that a complete and an accurate flow field description is possible through a multi-component formulation of the problem. A two-dimensional axisymmetric, multi-component mathematical model is proposed which couples the three flow fields which exist in a water jet, that is, the continuous water flow field, the entrained air flow field, and the droplet flow field. A numerical procedure together with its stability and convergence criteria is proposed for the solution of such a multi-component model.

INTRODUCTION

High velocity water jets have received considerable attention because of their applications in many engineering fields. Hydraulic coal mining [1, 2, 3], cutting and grinding a wide variety of materials [4, 5] are some examples of applications as well as many other areas [6, 7]. To date an adequate model to predict the flow field of a high velocity water jet has not been developed. This is unfortunate since such a model would be useful in analytical studies of the effect of nozzle design on the flow field as well as in studies of the characteristics of the flow field itself. Researchers have found that the effectiveness of cutting and breakage is largely determined by the dynamic pressure profile at the contact surface and by the jet structure. These, in turn, are functions of the nozzle design and standoff distances. Therefore a model which accurately determines the velocity and the pressure distribution of the complete flow field of a water jet is highly desired.

In spite of the importance, there is little understanding of the detailed structure and the characteristics of high speed water jets into air. Some limited analysis can be found in three papers by Yanaida [8, 9, 10] together with his experimental measurements and those of Shavlovsky [11]. In contrast, the behavior of a submerged free jet into surroundings of similar physical properties has been investigated analytically and experimentally by many researchers [12, 13].

Submerged jets solutions cannot be used for jets of water into air mainly because of the density difference between the core water and the ambient fluid. In fact, interaction between the air flow and the water flow, and the surface tension of water will cause the generation of droplets resulting in a multi-component flow consisting of the inner core water, the surrounding air flow, and the droplet flow. The flow of each component can be characterized by a set of continuity and momentum equations which are coupled together by appropriate interaction terms.

This work presents a review of the existing literature of analytical studies in the fields of submerged jets and of jets of water issuing into the air. It is found that the existing literature is not adequate for the complete analysis of the flow field of a water jet and a multi-component formulation of the flow field is essential. A two-dimensional axisymmetric, multi-component model of a high speed water jet is presented and its numerical solution together with its stability and convergence difficulties are discussed.

THEORY OF SUBMERGED JETS

A submerged jet is the fluid flow issuing from a nozzle into a surrounding of the same fluid. In particular, a free jet is defined as a submerged jet issuing into a stagnant medium. The velocity at the nozzle exit is approximately uniform and a potential core can be observed which maintains a constant velocity, but decreases in size until finally it vanishes. A growing boundary layer appears, which is due to mixing and entrainment effects between the stream issuing from the nozzle and the surrounding fluid, see Figure 1. The flow field of a circular laminar jet can be found by solving the following system of equations for u (r, z) and v (r, z).

$(\partial u/\partial z)+(\partial v/\partial r)+v/r = 0$		(1)
$u(\partial u/\partial z)+v(\partial u/\partial r)=vr^{-1}(\partial/\partial r)(r\partial u/\partial r)$		(2)
$v(o,z)=0$	centerline symmetry	(3)
$\partial u(o,z)/\partial r=0$	zero slope at centerline	(4)
$u(\infty,z)=0$	zero velocity at x	(5)
$J_z = 2\pi\int_0^\infty \rho u^2 r dr =$	constant total z momentum	(6)

where u and v are the components of velocity in z and r directions respectively, and P and v are the fluid density and kinematic viscosity respectively. Equations 1 and 2 are the continuity and momentum equations of laminar boundary layer flow in axisymmetric coordinates respectively [14]. The flow is assumed to be incompressible, steady, with no body force, and the pressure is the same everywhere, i.e., the pressure gradient in both z and r direction is assumed zero. Further if a similarity law for the velocities is assumed [14], the two partial differential equations 1 and 2 are reduced to a second order ordinary differential equation. The boundary conditions 3 to 6 are used to solve the resulting ordinary differential equation by some further transformations [151 to get:

$$u=(3/8\pi PYZ)/(I—.25 f^2) \quad \text{for } z > O \qquad (7)$$

$$V =0.25Z^{-1}(3 J_z /P\pi)^5(f-.25f^3)(1+.25f^2)^{-2} \quad \text{for } z > 0 \qquad (8)$$

Where

$$f = (3J_z/ 16P\pi)^5 (r/YZ) \qquad (9)$$

The streamline pattern calculated from equations 7 and >3 are plotted in Figure 2. The validity of the solution is restricted to Re < 30. While such laminar jets are not of great importance, the analysis of laminar jets is very useful because it illustrates, through a simple analytical solution, some of the basic characteristics of a free jet system. Note that the solutions are not valid at z = 0. This is because of the similarity assumptions that were made for the velocity profiles.

Now consider a turbulent circular jet, issuing from a nozzle into a fluid at rest which is identical to the jet fluid. The turbulent mean flow equations for a steady, two-dimensional axisymmetric, incompressible flow with no body forces and with zero pressure gradient in both z and r directions can be written as follows:

$$(\partial u/\partial z)+(\partial v/\partial r)+v/\ r=o \qquad (10)$$

$$u(\partial u/\partial z)+V(\partial u/\partial r)=r^{-1}p(\partial/\partial r)(\mu_e\ r\partial u/\partial r) \qquad (11)$$

$$\mu_e = \mu_e + \mu \qquad \text{effective viscosity} \qquad (12)$$

$$v(o,z)= O \qquad \text{centerline symmetry} \qquad (13)$$

$$\partial u(o,z)= O \qquad \text{zero slope at centerline} \qquad (14)$$

$$U(\infty,z) = O \qquad \text{zero velocity at x} \qquad (15)$$

$$J_z \int_0^\infty 2\pi\rho u^2 r dr = \qquad \text{constant total z momentum} \qquad (16)$$

where u and v are the mean velocity components in z and r directions respectively, and p, V and pt are the fluid density, viscosity and the turbulent viscosity. Equations 10 and 11 are the continuity and momentum equations for the mean flow of a turbulent boundary layer flow in axisymmetric coordinates [15]. For turbulent jets it is generally safe to assume pt >>> It has been suggested that, because of the symmetry of the flow field in turbulent circular jets and due to the absence of solid boundaries, the prandtl mixing length model would be adequate for the representation of the turbulent viscosity [15, 16]. Thus,

$$\mu_t = \rho\ell_m^2|\partial u/\partial r| \qquad (17)$$

Spalding and Launder [17] recommended the following relationship for lm

$$\ell_m / b = 0.075 \qquad (18)$$

where b is the half width of the jet; i.e., the distance from the centerline where the fluid velocity equals 1% of the maximum velocity u_m. u_m is the centerline velocity which decays along the z axis, making b a function of z. Using this expression in equation 17 we get

$$\mu_t = \rho(0.075b(z))^2|\partial u/\partial r| \qquad (19)$$

This was originally proposed by Prandtl himself (p. 683 of Schlichting [14]). Using equation 19 in equations 10 to 16, the system of two partial differential equations can be solved numerically for u and v. Note that b (z) is not known and has to be implicitly determined. The computational procedure employed is described by Patankar and Spalding [20] who found good agreement between predictions and measurements, both for secondary fluids moving with a uniform velocity and for stagnant secondary fluids. Also note that if pt is constant, then a closed form solution is possible since the problem reduces to the laminar case.

A much simpler approximate approach can be found by an order of magnitude analysis as done by Schlichting (p. 684 of [14]) which leads to

$$b(z)= K \bullet Z \qquad (20)$$

$$U_m(z\ ) = K' \bullet Z^{-1}(J_z/p)^5 \qquad (21)$$

where K and K' are constants.

Tollmien [18] used equation 21 together with the assumption that

$$\mu_t = \alpha' \bullet \rho b(z) Um(z \qquad (22)$$

where α' is a constant, and derived the first analytical, closed form solution for a turbulent submerged jet in 1945 by using the method of similarity profiles [19]. The three equations, 20, 21, and 22, are equivalent to suggesting that μ_t is constant throughout the jet system. Tollmien's solutions, which reflect that the value of a' in equation 22 is empirically determined, are as follows:

$$U=(3/8\pi^{\mu}{}_0 z) \bullet K \bullet (I+.25n^2\ )^{-2} \qquad (23)$$

$$V=.25Z^{-1}(3K/\pi)^5(n-.25n^3)(1.25n^2)^{-2} \qquad (24)$$

$$W = 0.404(\ J_z \bullet p)^5 Z \qquad (25)$$

where $\eta = .25\left(3K/\pi\right)^{.5}\left(r/^{\mu}_{o} z\right)$, K = J/p = kinematic momentum, μ_o is the virtual kinematic viscosity, and w is the mass rate of entrainment. The streamline patterns corresponding to the above solution of a turbulent submerged jet are shown in Figure 3. Note that the solutions for u (r, z) and v (r, z) becomes infinite at z = 0, this is because the similarity profile assumption is not valid in the near flow field, therefore the solutions are good only after some distance (z_c) from the exit of the nozzle. Wang [13] considers this limitation and numerically solves the boundary layer conservation equations for steady, axisymmetric, compressible, turbulent and laminar free jet, and obtains valid solutions near the nozzle exit.

To summarize, turbulent free jets are numerically solvable, by assuming a mixing length model for the turbulent viscosity. However, a turbulent jet of water into stagnant air requires special attention due to air resistance and droplet generation.

FLOW CHARACTERISTICS OF HIGH SPEED WATER JETS INTO THE AIR

Although a turbulent free jet is at least solvable by means of a numerical method as seen in the previous section, the characteristics of a turbulent jet of water into air have not been analytically determined except for a very restrictive set of assumptions. In addition, most of the existing results are mainly experimental and are for particular configurations. Most authors have divided the structure of a water jet into two parts: initial region and main region, as shown in Figure 4. Note that for a turbulent free jet, as discussed previously and found on page 686 of [14], the jet spread b is proportional to the axial distance x, and the axial velocity on the centerline u_m is inversely proportioned to the axial distance x. In the rest of the section, correlations for axial and radial dynamic pressure, initial core length x_c, and the jet spread b (x) are presented for a water jet. Here (r, x) is taken for coordinate variables.

A. Initial Length X_C

Shovlovsky [11] has the following equation, where Re = $(D_o D_u)/v$ is the Reynolds number.

$$X_C/D_O = A - 68 \bullet 10^{-6} Re \tag{26}$$

A= 85 to 112 depending on type of nozzle (27)

Yanida [8] gives the expression,

$$X_c = O.97(D_o/0.237)^2 \tag{28}$$

B. Jet Spread b (x)

Shovlovsky [11] gives the following equation for b (x):

$$b/D_o = (\mu/K_o)^{.5} (P_o / P)^{.25} \tag{29}$$

where µ = nozzle discharge coefficient which varies from .93 to .98 and

$$K_o = (9.12 D_o)/x \quad .7 \tag{30}$$

P = average specific dynamic pressure found from $\dfrac{P}{P_o} = \dfrac{D_o}{x}.07$

Note the formula is given for all x > O.

Yanida [8] through an analytical and experimental analysis gives

$$b/D_o = K (X/D_o)^{.5} \tag{31}$$

where K = .168

C. Axial Dynamic Pressure

$$P_m / P_o (X_c / X)^{\{U(X/X_c - 1)[.27 + 0.075(X/X_c)^2 ...} \tag{32}$$

where U is unit step function and XC is the length of initial region. Equation 32 is given by Shovlovsky [11].

Yanida [8] has analytically found the following result

$$P_m / P_o = X_c / X \qquad (33)$$

D. Dynamic Pressure Profile

Yanida [8] experimentally found that

$$P / P_o = f(\eta_c) = (1 - \eta_c^{1.5})^2 \qquad \text{for initial region.} \qquad (34)$$

$$P / P_m f(\eta) = (1 - \eta^{1.5})^2 \qquad \text{for the main region.} \qquad (35)$$

where n = Y/b and $n_c = (Y - Y_c)/b_c$

Shovlovsky [11] has found that:

$$P / P_m = EXP[-\phi(r/b)] \qquad \text{for } x>x_c \qquad (36)$$

where $\phi = 0.009\ (X / D_o) + 1.3 \qquad \text{for } x > x_c \qquad (37)$

and λ can be found using a normal distribution to be close to 4.

MULTI-COMPONENT FORMULATION

The previous works which have been reviewed in this paper form a broad basis for a better understanding of the characteristics of a high speed water jet. However, collectively they possess the following shortcomings:

1. Air entrainment, droplet formation and flow, and air resistance have not been considered together.
2. All existing solutions for the water jet assume some similarity profile for the flow variables.
3. Almost no rigorous analytical solutions exist, even for the case of a highly simplified jet of water into air.
4. There is no two-dimensional solution for the flow field of a water jet into air except those for the submerged case (i.e., water jet into water).

The only paper which considers the droplet region of a high velocity water jet is given by Yanida and Ohashi in 1978 [9]. They assume the jet is divided into three regions: continuous region, droplet region, and diffused region. They then assumed that the flow field is known in the continuous region from their 1974 paper [8]. Further they assumed that the fluid is inviscid and air-droplet mixture is a pseudo fluid with a non-uniform density p = Pa (1 + k) where k is the weight concentration of the mixture and P_a is the density of air. Momentum balance equation was then written, and through the use of some empirical formulae determined the breakup length, x_b is given by $x_b = 3.55\ x_c$ where XC is the length of initial region.

In the multi-component formulation the flow field of the water jet consists of three different flow fields, namely, the flow of the water core, the surrounding air flow, and the droplet flow as shown in Figure 5. The flow of each component is governed by a set of continuity and momentum equations, which are coupled together by appropriate interaction terms. This formulation is supported by an extensive literature found in the area of two-phase or multi-phase flows. The term "multi-component" flow is applied to the water jet formulation because the water jet flow field is considered to be made up of three distinct components, i.e., water, air, and droplets. The field equations for multi-phase or multi-component flow have been derived by many investigators, usually by means of applying the conservation equations for mass, momentum and energy to a control volume containing more than one component. According to the "two fluid model" of Ishii [21], the field equations corresponding to Figure 5 for the case of steady, two-dimensional, isothermal flow of a water jet with no body forces can be written as follows:

$$(\alpha_\ell \rho_\ell V_\ell) = -J_d \qquad \text{liquid continuity} \qquad (38)$$

$$(\alpha_g V_g P_g) = 0 \qquad \text{gas continuity} \qquad (39)$$

$$(\alpha_d \rho_d V_d) = J_d \qquad \text{droplet continuity} \qquad (40)$$

$$(\alpha_\ell P_\ell V_\ell V_\ell) = -\alpha_\ell \quad \rho_\ell + \quad (\alpha_\ell \sigma_\ell) - \alpha_g F_\ell - J_d V_\ell \qquad \text{liquid momentum} \qquad (41)$$

$$(\alpha_g \rho_g V_g V_g) = -\alpha_g \quad P_g + \quad (\alpha_g \sigma_g) + \alpha_g F_\ell + \alpha_d G_g \qquad \text{gas momentum} \qquad (42)$$

$$(\alpha_d \rho_d V_d V_d) = -\alpha_d \quad P_d + \quad (\alpha_d \sigma_d) - \alpha_d G_d + J_d V_\ell \qquad \text{droplet momentum} \qquad (43)$$

where liquid and gas refer to water core and surrounding air respectively. Subscripts 1, g, d are used for liquid, gas, and droplet flow variables respectively. α_i is the void fraction of the ith component, which satisfies the condition $\alpha_l + \alpha_g + \alpha_d = 1$, called the axiom of continuity [21, 26].

These equations include the effect of mass and momentum transfer due to phase change, i.e., droplet generation, and due to interfacial friction on momentum transfer between liquid and gas, between gas and droplet and between liquid and droplet. The exchange functions J_d F_1, G_g depend in general, upon the flow field and are usually given in terms of flow variables by empirical formulae. Boure and Reocreux [22] in 1972, and Boure [23] in 1973 have shown that contradictions are induced by constitutive equations that involve only the main dependent variables but not their derivatives. Although certain elements of the highly complex microphysics of the exchange processes are neglected [21], the solutions of these equations have described two-phase flow phenomena realistically in a variety of applications [24, 25].

The continuity and the momentum equations of each componentate expanded in axisymmetric coordinates (r, z). The liquid pressure P_1 is assumed to be a function of z only, and is determined by the gas pressure P_g at any z, in other words P_1 (z, r) = P_1 (z) only = P_g (z, ri) where (z, ri) are the coordinates of the interface between liquid and gas. It is further assumed that μ_1, μ_g, ρ_1 ρ_d are constant, and pressure and viscous terms are neglected within the droplet flows. Using the nozzle diameter D and the nozzle exit velocity U_O as the characteristic length and velocity respectively, and for all three components, and $P_{g,o}$ as the characteristic density for the gas phase, the following four dimensionless quantities are defined:

$(Re)_\ell = (P_\ell U_o D_o)\mu_\ell$	Liquid Reynolds number	(44)
$(Re)g = (Pg,oUoDo)/\mu_g$	gas Reynolds number	(45)
$(Eu)_\ell = (Pg,o(RT))/(\ell P U_0^2)$	liquid Euler number	(46)
$(Eu)g = RT / U_0^2$	gas Euler number	(47)

where R is the ideal gas constant for air. The conservation equations for the three components can be written in the following non-dimensional form:

$$(\partial/\partial r)[r\alpha\ell v\ell] + (\partial/\partial z)[r\alpha\ell u\ell] = -(P\ell Uo)^{-1} Jd \quad (48)$$

$$(\partial/\partial r)[rP_g\alpha_g v_g] + (\partial/\partial z)[rP_g\alpha_g u_g] = 0 \quad (49)$$

$$(\partial/\partial r)[r\alpha_d v_d] + (\partial/\partial z)[r\alpha_d u_d] = (PdUo)^{-1} J_d \quad (50)$$

$$\alpha_\ell\left(u_\ell\frac{\partial u_\ell}{\partial z} + v_\ell\frac{\partial u_\ell}{\partial r}\right) = -\alpha_\ell (Eu)_\ell\left(\frac{\partial\rho_g}{\partial z}\right) + \left[(R_e)_\ell r\right]^{-1}\left(\frac{\partial}{\partial r}\right)\left(\alpha_\ell r\frac{\partial u_\ell}{\partial r}\right) - Const(F_{z\ell}\alpha_\ell) - Const(J_d u_\ell)$$

(51)

$$\alpha\ell(u\ell.\partial v\ell/\partial z + v\ell.\partial v\ell/\partial r) = -(Do\alpha\ell / P\ell U_0^2)F_r\ell - (P_\ell U_o)^{-1}.D_o.J_D.V_\ell$$

(52)

$$\alpha_g P_g(Ug.\partial u_g / dz + Vg.\partial u_g / dr) = -(Eu)g\alpha_g(\partial P_g / dz) +$$
$$[(Re)gr]^{-1}(\partial/\partial r)(\alpha gr.\partial u g / dr) + Const.(\alpha_{\ell Fz\ell} + \alpha_d G_{gz})$$

(53)

$$\alpha_g P_g(u_g.\partial v g / dz + vg.dvg/\partial r) = -\alpha g(Eu)g(\partial Pg/\partial r) + Const.(\alpha\ell F_{r\ell} + \alpha_d G_{gr})$$

(54)

$$\alpha_d(U_d \quad u\partial_d / dz + vd \quad d\partial_d/\partial r) = -(P_d V_0^2)^{-1} D_o\alpha_d G_{gz} +$$
$$(P_d Uo)^{-1} DoJd \quad u\ell \quad (55)$$

$$\alpha_d(u_d \quad d\partial_d / dz + Vd \quad d\partial d/\partial r) = -(P_d U_0^2)^{-1} Do\alpha_d G_{gz} +$$
$$(P_d Uo)^{-1} DoJd \quad V\ell \quad (56)$$

The above set of equations, constitute a system of nine equations for the nine unknowns (p_g α_1, α_d, u_l, v_l, u_g, v_g, ad, v_d). The advantage of this model compared to other multi-component models is its comprehensiveness. However, the potential of this model rests on a good knowledge of the three interfacial relationships; namely, the three correlations needed for J_d , F_1, G_g. There is a great deal of demand for adequate correlation for such transfer conditions in the general field of multi-phase flow [27]. In particular, the work of Rowe [28] and Richardson [29] and Shih [30] suggest a reasonable expression for the drag force G_g exerted by gas on the droplets per unit volume of droplets.

$$G_{dz} = 3C_{Dgz}P_g(4d_d)^{-1} \ (u_g - u_d)^2 \alpha_g^{-2.65} \quad (57)$$

$$G_{gr} = 3C_{Dgr}Pg(4d_d)^{-1} \ (v_g - v_d)^2 \ \alpha_g^{-2.65} \quad (58)$$

The above correlation for the drag force is valid for spherical droplets where d_d is the droplet diameter and c_{Dgz} and c_{Dgr} are the drag coefficients in the z and r directions, respectively. The drag coefficients can be related to the Reynolds number [28] by means of the relations

$$C_{Dgz} = 24 \ (Re)_{gz}^{-1}[1 + 0.15(Re)_{gz}^{.687}] \quad \text{for}(Re)_{gz} \leq 1000 \quad (59)$$

$$C_{Dgr} = 24 \ (Re)_{gr}^{-1}[1 + 0.15(Re)_{gr}^{.687}] \quad \text{for}(Re)_{gr} \leq 1000 \quad (60)$$

$$C_{Dgz} = 0.44 \quad \text{for } (Re)_{gz} > 1000 \quad (61)$$

$$C_{Dgr} = 0.44 \quad \text{for } (Re)_{gr} > 1000 \quad (62)$$

where

$$(Re)_{gz} = \alpha_g \rho_g d_d (u_g - u_d) \mu_g^{-1} \quad (63)$$

$$(Re)_{gr} = \alpha_g \rho_g d_d (v_g - v_d) \mu_g^{-1} \quad (64)$$

For J_D and F_1, no correlations currently exist for the particular case of a water jet. Experimental measurements are needed in this area. However, some candidate expressions for Jd and F1 exist in the work of Wallis on annual flows [31] and in other papers [9, 32].

ANALYSIS OF NUMERICAL SOLUTION

The three continuity equations, 48 to 50, together with the six momentum equations, 51 to 56, are a set of six non-linear partial differential equations. A fully implicit numerical solution of such a system of equations is practically impossible, although highly desirable, since they are at least locally, unconditionally stable in terms of the increments Δz and Δr. Explicit iterative numerical solutions are practical, but they require a careful analysis of stability and convergence. In this section a numerical procedure for the solution of the system of nine equations is proposed and its stability and convergence criteria are examined.

In the two fluid model approach, if the constitutive equations are linear in terms of the derivatives of the flow variables then the set of partial differential conservation equations can be reduced to a quasi-linear system of equations of the following form [27]:

$$A(u,r,z)(\partial u/\partial z) + B(u,r,z)(\partial u/\partial r) = c(u,r,z \qquad (65)$$

where A and B are square matrices, and U and C are column vectors. Since the viscous stress terms are not linear in terms of $\partial u/\partial z$ and $\partial u/\partial r$ two more variables

$$(\partial u_\ell / \partial r) = u'_\ell \qquad (66)$$

$$(\partial u_g / \partial r) = u'_g \qquad (67)$$

are introduced and an eleven by eleven quasi-linear system of equations is derived;

$$A(\partial u/\partial z) + B(\partial u/\partial r) = C \qquad (68)$$

where U = $[P_g.\ \alpha_1,\ \alpha_d,\ u_l,\ v_l,\ u_g,\ v_g,\ u_d,\ v_d,\ u'_1,\ u'_g\ ]^T$

and C is a column vector of order eleven, and A and B are eleven by eleven matrices in the following form:

$$A = \begin{pmatrix}
o & x & o & x & o & o & o & o & o & o & o \\
x & x & x & o & o & x & o & o & o & o & o \\
o & o & x & o & o & o & o & x & o & o & o \\
x & o & o & x & o & o & o & o & o & o & o \\
o & o & o & o & x & o & o & o & o & o & o \\
x & o & o & o & o & x & o & o & o & o & o \\
o & o & o & o & o & o & x & o & o & o & o \\
o & o & o & o & o & o & o & x & o & o & o \\
o & o & o & o & o & o & o & o & x & o & o \\
o & o & o & o & o & o & o & o & o & o & o \\
o & o & o & o & o & o & o & o & o & o & o
\end{pmatrix}$$

$$B = \begin{pmatrix}
o & x & o & o & x & o & o & o & o & o & o \\
x & x & x & o & o & o & x & o & o & o & o \\
o & o & x & o & o & o & o & o & x & o & o \\
o & x & o & x & o & o & o & o & o & x & o \\
o & o & o & o & x & o & o & o & o & o & o \\
o & x & x & o & o & x & o & o & o & o & x \\
x & o & o & o & o & o & x & o & o & o & o \\
o & o & o & o & o & o & o & x & o & o & o \\
o & o & o & o & o & o & o & o & x & o & o \\
o & o & o & x & o & o & o & o & o & o & o \\
o & o & o & o & o & x & o & o & o & o & o
\end{pmatrix}$$

where "x" represents any non-zero element. The value of each "x" can be found using the corresponding differential equation. If A is non-singular, the system of equations may be written as

$$(\partial u / \partial z) + \grave{B}(\partial u / \partial r) = \grave{C} \qquad (69)$$

where

$$\grave{B} = A^{-1}B \qquad (70)$$

$$\grave{C} = A^{-1}C \qquad (71)$$

In equation 69 the term $\frac{\partial u}{\partial r}$ can be expanded by a finite difference approximation in the r direction. Equation 69, by such an expansion, will be reduced to an initial value problem in terms of z. The nodal values of U can be found by marching in the z direction using a Runge-Kutta type of method. The question is now will such a numerical method work correctly?

According to the Lax's theorems [33, 34, 35, 36] for the system of equation 69, it is impossible to find a numerically stable finite difference scheme to solve the equations as an initial value problem, if the characteristic of the equations are complex. Real characteristics are a necessary condition for a well posed set of equations. The characteristics of equation 69 are roots of the following generalized Eigen value problem [36].

$$\det.[A\lambda + B] = 0 \qquad (72)$$

If A or B is non-singular, then the above generalized Eigen value problem can be reduced to a regular Eigen value problem of the form:

$$\det.[K - \lambda I] = 0 \qquad (73)$$

where k = -A ^{1}B. Equations 72 and 73 have the same Eigen values, that is, the values for λ, which are found from equation 73, are in fact the Eigen values of the generalized Eigen value problem, given in equation 72. A computer program is written which uses the EISPACK package [37] to find the Eigen values of the problem. Promising results have been obtained for typical values of the flow parameters. This indicates that it is reasonable to expect that the stability requirement of the numerical solution can be met. Satisfying the stability requirement insures the convergence of the numerical method, according to Lax equivalence theorem [34].

CONCLUSION

A model of water jet issuing into air which treats the flow field as a multicomponent one, is the only model which is capable of handling the interaction of the water jet with air. This involves consideration of the coupling between the components such as droplet generation, interfacial shearing stress, and air-droplet drag.

Preliminary results indicate the set of equations can be solved as an initial value problem. This is encouraging since this approach simplifies the numerical solution process.

Future work involves the determination of reasonable correlations for continuity and momentum transfer terms, and the development of numerical solutions.

ACKNOWLEDGMENT

This work was performed at Southern Illinois University at Carbondale under contract number DE AC 2279PD20091-06 for the U.S. Department of Energy, the Division of Surface Mining, Carbondale Mining Technology Center.

REFERENCES

[1]. du Plessis, M. P., and Hashish, M., "Experimental and Theoretical Investigation of Hydraulic Cutting of a Western Canadian Coal " Fifth International Symposium on Jet Cutting Technology, Paper E3, pp. 269, BHRA Fluid Engineering, Cranfield, Bedford, England, June (1980).

[2]. Cooley, W. C., "Survey of Water Jet Coal Mining Technology." Third International Symposium on Jet Cutting Technology, Paper D1, pp. Dl-l, Cranfield, England, May (1976).

[3]. Summers, D. A., Barker, C. R., and Keith, H. D., "Water Jet Drilling Horizontal Holes in Coal." Mining Engineering, pp. 698, June (1980).

[4]. Labus, T. J., "Cutting and Drilling of Composites Using High Pressure Water Jets." Fourth International Symposium on Jet Cutting Technology, Paper G2, pp. G2-9, BHRA Fluid Engineering, Canterbury, England, April (1978).

[5]. Eddingfield, D. L., and Trinh, V. D., "A Preliminary Study of Coal Comminution with a High Velocity Water Jet." Fifth International Symposium on Jet Cutting Technology, Paper E1, pp. 251, BHRA Fluid Engineering, Cranfield, Bedford, England, June (1980).

[6]. Leslie, E. N., "Application of the Water Jet to Automated Cutting in the Shoe Industry." Third International Symposium on Jet Cutting Technology, pp. F3-23, BHRA Fluid Engineering, Cranfield, U.K., May (1976).

[7]. Vijay, M. M., Brierley, W. H., "Drilling of Rocks by High Pressure Liquid Jets: A Review." Petroleum Division of the ASME, 80-Pet-94, (1980).

[8]. Yanaida, K., "Flow Characteristics of Water Jets." Second International Symposium on Jet Cutting Technology, pp. A2-19, BHRA Fluid Engineering, Cranfield, Bedford, England, April (1974).

[9]. Yanaida, K., Ohashi, A., "Flow Characteristics of Water Jet." Fourth International Symposium on Jet Cutting Technology, pp. A3-39, BHRA Fluid Engineering, Cranfield, Bedford, England, April (1978).

[10]. Yanaida, K., Ohashi, A., "Flow Characteristics of Water Jets in Air." Fifth International Symposium on Jet Cutting Technology, Paper A3, pp. 33, BHRA Fluid Engineering, Cranfield, Bedford, England, June (1980).

[11]. Shavlovsky, D. S., "Hydrodynamics of High Pressure Fine Continuous Jets." First International Symposium on Jet Cutting Technology, pp. A6-81, BHRA Fluid Engineering, Cranfield, England, April (1972).

[12]. Abramovich, G. N., "The Theory of Turbulent Jets." MIT Press, Cambridge, Mass. (1963).

[13]. Wang, R. L., and du Plessis, M. P., "An Explicit Numerical Method for the Solution of Jet Flows." Transaction of the ASPIE, pp. 38, March (1973).

[14]. Schlichting, H., "Boundary Layer Theory." McGraw-Hill, Sixth Edition, (1968).

[15]. Szekely, J., "Fluid Flow Phenomena in Metal Processing." Chapter 9, Academic Press, (1979).
[16]. Romiti, A., "Fluid Dynamics of Jet Amplifiers." International Center for Mechanical Sciences, Springer-Verlag, Wien-New York, (1972).
[17]. Spalding, D. B., and Laundert B. E., "Mathematical Models of Turbulence." Academic Press, New York, (1972).
[18]. Tollmien, W., Translation of 1928 German Original, NACA Tech. Note TN 1085, (1945).
[19]. Tollmien, W., Berechnug Turbulenter Ausbreitungsvorgange, ZAMM 6, pp. 468-478, 1926, NACA TM 1085, (1945).
[20]. Patankar, S. V., and Spalding, D. B., "Heat and Mass Transfer in Boundary Layers." Second Edition, Intertext Books, London, (1970).
[21]. Ishii, M., "Thermo-Fluid Dynamics Theory of Two Phase Flow." Eyrelles, Paris, (1975).
[22]. Boure, J. A., and Reocreux, M., ~8General Equations of Two-Phase Flows, Applications to Critical Flows and to Non-steady Flows." Fourth All-Union Heat-Transfer Conference, Minsk, (1972).
[23]. Boure, J. A., "Dynamique des Ecoulements Diphasiques: Propagation de Petits Perturbations, C. E. A. R-4456, (1973).
[24]. Veziroglu, T. N., editor, "Multiphase Transport: Fundamentals, Reactor Safety, Applications." 5 Vol., Hemisphere Pub. Corp., (1979).
[25]. Durst, F., Tsiklauri, G. N., and Afgan, N. H., editors, "Two Phase Momentum, Heat and Mass Transfer in Chemical, Process and Energy Engineering System." 2 Vol., Hemisphere Pub. Corp., (1979).
[26]. Wallis, G. B., "One-Dimensional Two-Phase Flow." McGraw-Hill, New York, (1969).
[27]. Boure, J. A., "Constitutive Equations for Two-Phase Flows." Chapter 9, pp. 157 of the book edited by Ginoux, J. J., Two-Phase Flow and Heat Transfer, Hemisphere Pub. Corp., (1978).
[28]. Rowe, P. N., and Henwood, G. A., "Drag Force in a Hydraulic Model of a Fluidized Bed." Trans. Institute of Chem. Engr., 39, pp. 43-54, (1961).
[29]. Richardson, J. F., and Zaki, W. N., "Sedimentation and Fluidization: Part I." Trans. Institute of Chem. Engr., 32, pp. 35-53, (1954).
[30]. Shih, Y. T., "Hydrodynamic Analysis of the Horizontal Solid Transport." Master's Thesis, Institute of Gas Technology-IIT Center, Chicago, Illinois, May (1980).
[31]. Wallis, G. B., Richter, H. J., Bharathan, D., "Air-Water Countercurrent Annular Flow in Vertical Tubes." Electric Power Research Institute (EPRI), EPRI NP-786, Project 443-2, May (1978).
[32]. Solbrig, C. W., McFaddent J. H., Lyczkowski, R. W., and Hughes, E. D., "Heat Transfer and Friction Correlations Required to Describe Steam-Water Behavior in Nuclear Safety Studies." AICHE Symposium Series, No. 174, Vol. 74, pp. 100, (1978).
[33]. Lax, P. D., "Differential Equations, Difference Equation and Matrix Theory." Comm. Pure and Appl. Math., 11, pp. 175-194, (1958).
[34]. Lax, P. D., and Richtmyert R. D., "Survey of Stability of Linear Finite Difference Equations." Comm. Pure and Appl. Math., 9, pp. 267-293, (1956).
[35]. Lax,P. D., and Courant, R., "On Non-linear Partial Differential Equations with Two Independent Variables." Comm. Pure and Appl. Math., 2, pp. 255-273, (1949).

[36]. Lyczkowski, R. W., Gidaspow, D., Solbrig, C. W., and Hughes, E. D., "Characteristics and Stability Analysis of Transient One-Dimensional Two-Phase Flow Equations and Their Finite Difference Approximations." Nuclear Science and Engineering, 66, pp. 378, (1978).

[37]. Goos, G., and Hartmanis, J., editors, "Matrix Eigensystem Routines - EISPACK Guide." Lecture notes in Computer Science, Vol. 6, Springer-Verlag, New York, (1976).

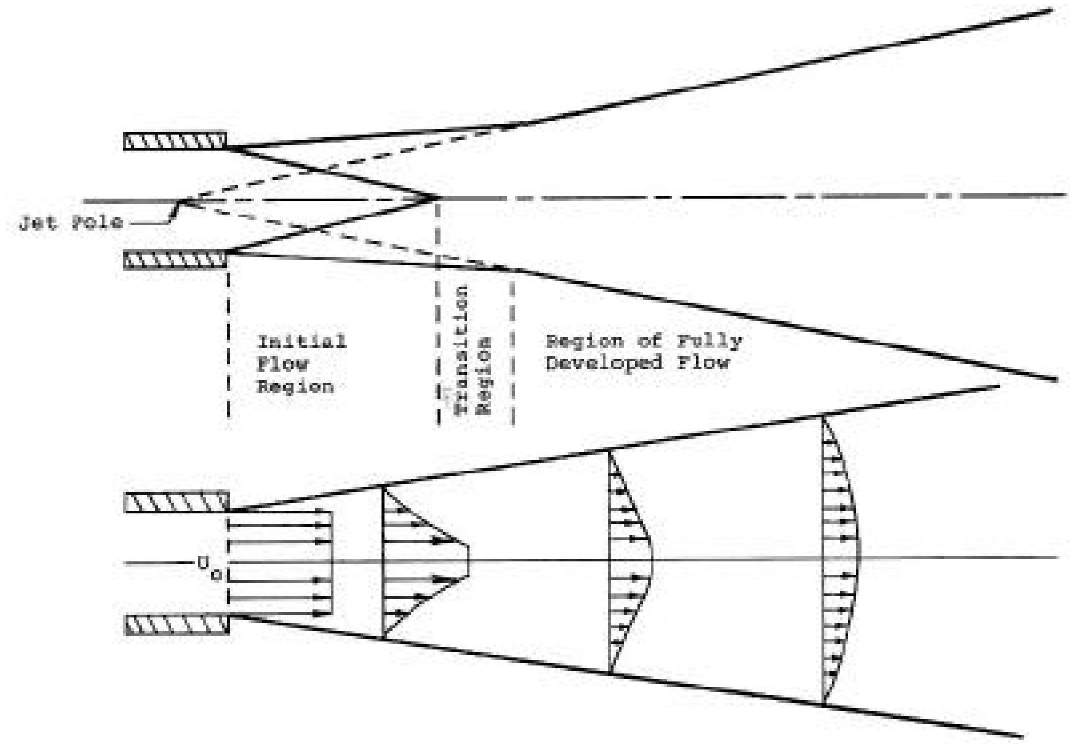

FIGURE 1. Schematic flow diagram of a free jet showing the potential core and the velocity profiles at various distances from the origin [15].

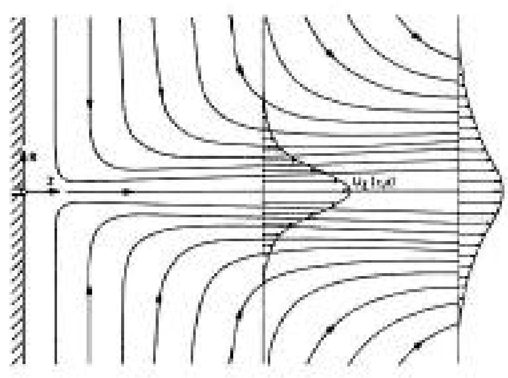

FIGURE 2. The streamline pattern and the velocity profiles produced by a circular laminar jet [15].

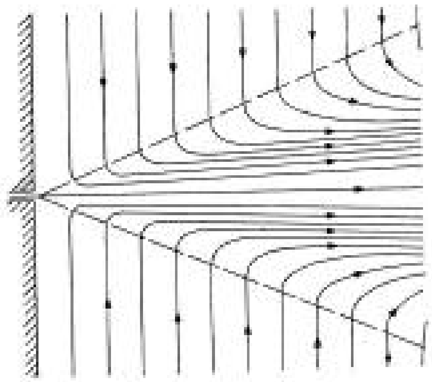

FIGURE 3. The streamline patterns for a turbulent circular free jet [15]

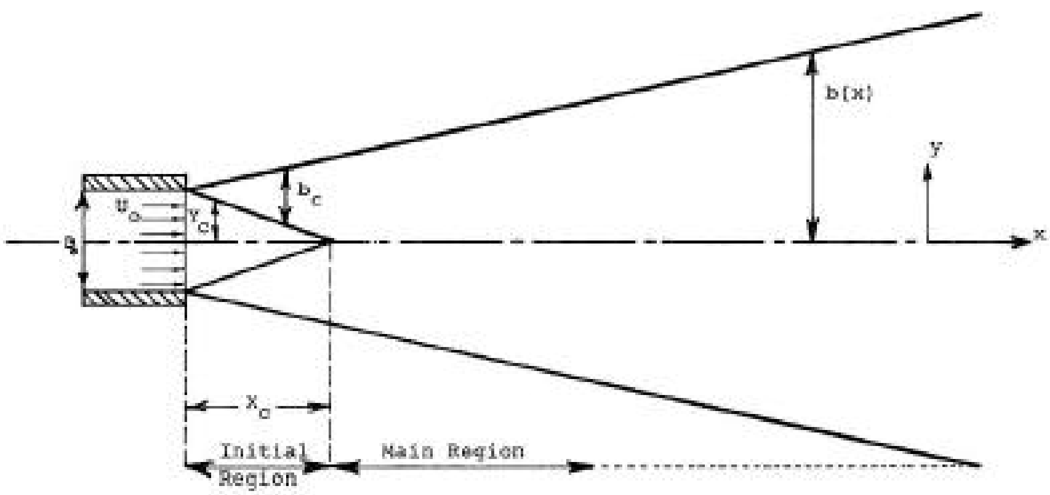

FIGURE 4. Jet structure.

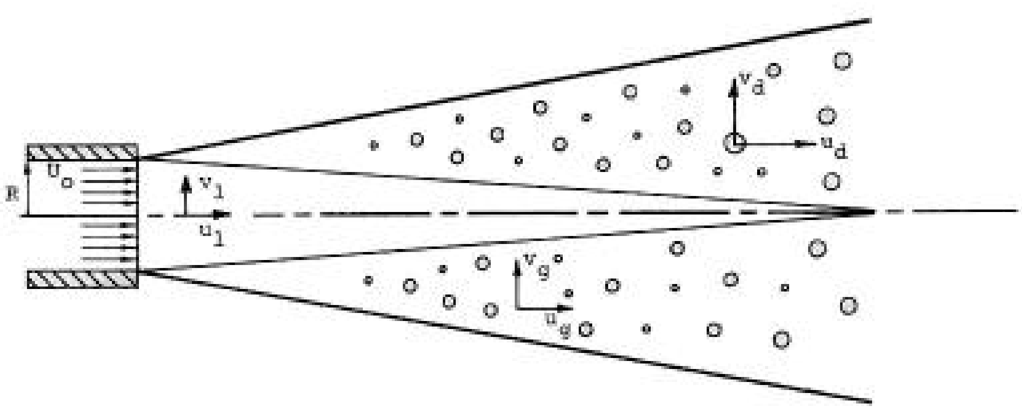

FIGURE 5. The three different fields of the flow.

MECHANISMS OF WATER JET INSTABILITY

Arthur M. Sterling
Department of Chemical Engineering
Louisiana State University
Baton Rouge, Louisiana 70803

Warren T. Abbott
Department of Chemical Engineering
Louisiana State University
Baton Rouge, Louisiana 70803

ABSTRACT

The fundamental mechanism responsible for the breakup of a liquid jet is a surface tension induced instability. Other mechanisms, however, can modify the breakup process and alter both the continuous length of the jet and the size distribution of the drops. These mechanisms include the aerodynamic forces on the jet surface, heat or mass transfer at the jet surface, and the relaxation of the velocity profile in the jet as it exists from the nozzle. We are currently investigating these mechanisms in our laboratory. Our experimental facility is described, and some results from our measurements are given.

INTRODUCTION

The well-known capillary instability that results in the breakup of a liquid jet into drops has a number of less well-known collaborators. These secondary mechanisms can either enhance or inhibit the fundamental capillary mechanism. For example, the relative motion between the jet and the surrounding air gives rise to pressure forces on the jet surface that enhance the instability. At very high relative velocities, the shearing forces at the jet surface strip away ligaments of fluid. The transfer of heat and mass between the jet and the surrounding air can either inhibit or enhance the instability if the transfer gives rise to thermal or concentration gradients which, in turn, create a surface tension driven flow within the jet. Finally, the relaxation of the parabolic velocity profile of a laminar jet issuing from a tube can enhance the capillary instability.

The ultimate effects of these secondary mechanisms is to alter the breakup characteristics from those observed when the fundamental capillary instability acts alone. Both the continuous length of the jet and the size distribution of the drops are affected. In principle, one could take advantage of these secondary mechanisms to tailor the breakup behavior for a particular application. But our understanding of these mechanisms is not sufficiently well developed to provide the necessary mathematical models. We are currently studying the effects of velocity profile relaxation on the instability of laminar liquid jets cast from long tubes. There is substantial evidence to indicate that the result of these effects are similar to the result of relative motion between the jet and its ambient gas, i.e. as the velocity is increased, the jet length reaches a maximum and then decreases as the velocity is increased further. The effect of velocity profile relaxation on the drop size distribution, however, has not yet been measured. Our goal is to obtain correlations from which both the jet length and drop size may be predicted.

EXPERIMENTAL FACILITY

A schematic diagram of our experimental facility is shown in Figure 1. The system consists of four principal parts:

- A flow system
- A detector
- A signal processor
- A mini-computer for data collection and analysis.

The flow system consists of a pressurized reservoir, a calming section, nozzles made from hypodermic tubing, and a fluid collector. The calming section, to which the nozzles are attached, is fastened to a 300-lb inertia pad. The inertia pad, in turn rests on inflated inner tubes. This arrangement isolates the nozzles from building vibrations.

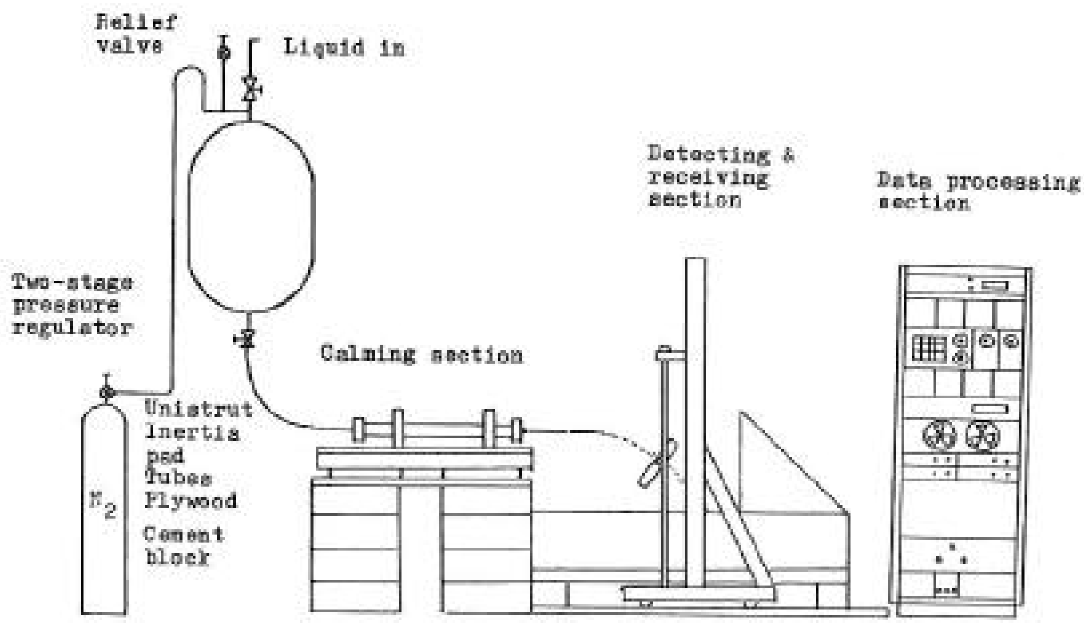

Figure 1. Schematic diagram of experimental facility.

The detector, Figure 2, consists of a light source, a collimator, two optical slits, and a photo detector. These components are fixed to a rigid aluminum frame. The two slits define a thin (0.5 mm) uniform light field that falls on a photodiode. The active area of the photodiode is 100 x 2.5 mm2. The width of the light field is limited by the 57 mm diameter lens of the collimator. When a drop passes through the light field, a shadow is cast on the detector and an electrical pulse is generated. The amplitude of the pulse is proportional to the crossing diameter of the drop.

The signal processor (Fig. 3) consists of an amplifier and a signal conditioner. A five-stage amplifier converts the current output of the diode to voltage, removes the DC offset, clamps the baseline to zero volts, filters, and amplifies the signal. The gain of the amplifier is adjusted to produce a 1.0 volt pulse when a l-cm drop passes through the light field. The signal conditioner stretches the pulses, shifts the baseline of the stretched pulses to -1.0 volts, and provides TTL pulses synchronized with the pulse peaks.

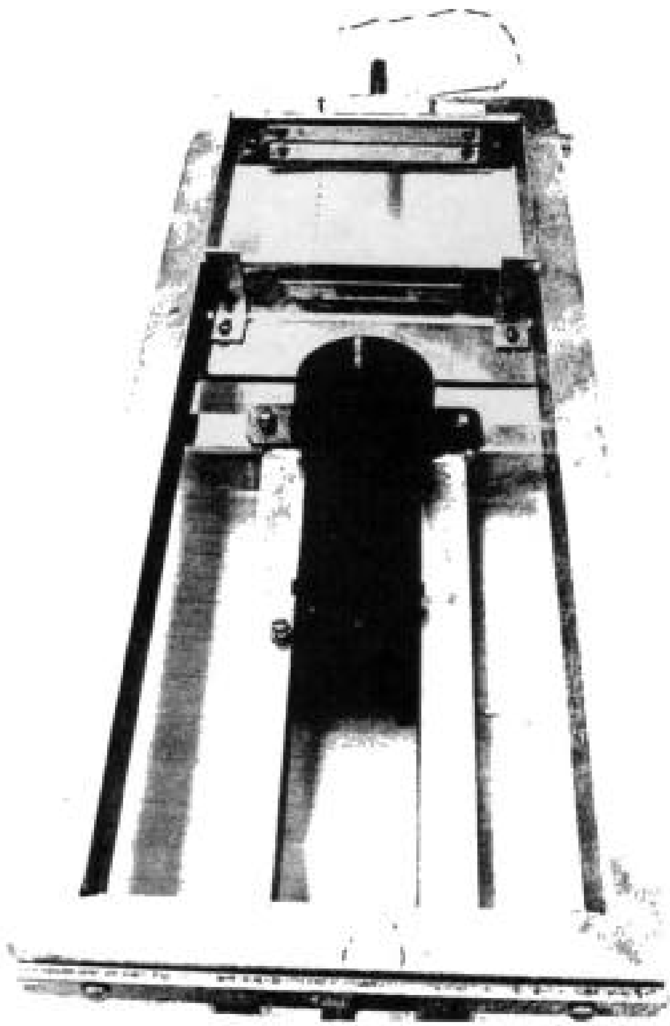

Figure 2. Photograph of electro-optical detector. The photodiode is enclosed in the frame behind the upper optical slit.

The output of the conditioner is fed to the A/D converter of a HP 2116 B computer. The TTL pulse triggers an A/D conversion of the stretched pulse. The time between pulses is obtained from a real-time clock. Thus for each drop passing through the light field, two data values are obtained and stored by the computer; the drop diameter and the time interval since the preceding drop. These data are then sorted into drop size and time interval distributions. The typical correspondence between the train of drops and a train of pulses from the amplifier is shown in Figure 4. Owing to deformation and overlapping of the drops in the light field, the correspondence between pulse height and drop diameter is not exact. However, we can calculate the average drop volume from the drop size distribution and the average drop frequency from the time interval distribution. The product of average volume and average frequency is the flow rate. Since the flow rate can be easily measured independently, the drop size distribution can be corrected for pulse distortion.

EXAMPLE

One of the early applications of this experimental method was to an investigation of turbulent jets. We wanted to determine the effect of nozzle turbulence on the drop size distribution. The study was carried out in two parts.

The first part of the study was done by R.J. Lissenburg at the Aero-and Hydrodynamics Laboratory of the Delft Technical University, under the direction of J.O. Hinze. Lissenburg measured the turbulent spectra at various distances downstream of an obstruction in a cylindrical tube. The measurements were made for air flow at a Reynolds number of 5000.

Typical results are shown in Fig. 5. These data were obtained when a square-edged orifice was placed 5, 10, and 20 diameters upstream from the exit of a 2-cm diameter tube. The turbulence measurements were made at the tube exit, 1 mm from the wall. The normalised energy spectra is shown. The solid line in Fig. 5 represents the spectra obtained when no obstruction was present in the tube. The critical frequency, f , shown in the figure is the maximum frequency for unstable disturbances (if this were a water jet rather than an air jet.)

When the obstruction was within 10 diameters of the tube exit, its effect was to shift the energy from low to high frequencies and to reduce the turbulence intensity. The shift is particularly noticeable in the frequency range below the critical frequency. Thus we would expect an obstruction of this type to alter the breakup characteristics of a liquid jet that was geometrically and dynamically similar to the air jet produced in this study.

The second part of the study was done by H. Vliem at the University of Leiden. Water jets were formed by a 4 mm ID tube; the Reynolds number of the flow was identical to the Reynolds number used by Lissenburg. Obstructions, geometrically similar to those used by Lissenburg, were placed at various distances upstream from the tube exit. The size distribution of the drops formed by the jets was measured with the optical technique described above.

Typical results are shown in Fig. 6 for conditions corresponding to the conditions that produced the energy spectra shown in Fig. 5. Despite an alteration of both the spectral distribution and the intensity of the turbulence by the obstruction, no variation in the drop size distribution could be observed. Furthermore, Vliem found that effect of the obstruction was to alter the jet length by only + 1%.

We concluded from these studies that, for a Reynolds number of about 5000, obstructions in a tube could not be detected by observing the breakup characteristics of a jet formed by that tube. Indeed, turbulent jets behaved very much like laminar jets. The jet length increased linearly with velocity and the observed drop size was within 2% of the drop size predicted by the laminar theory. Calculations showed that the amplitude of the initial disturbance was about loot times the disturbance amplitude calculated for laminar jets.

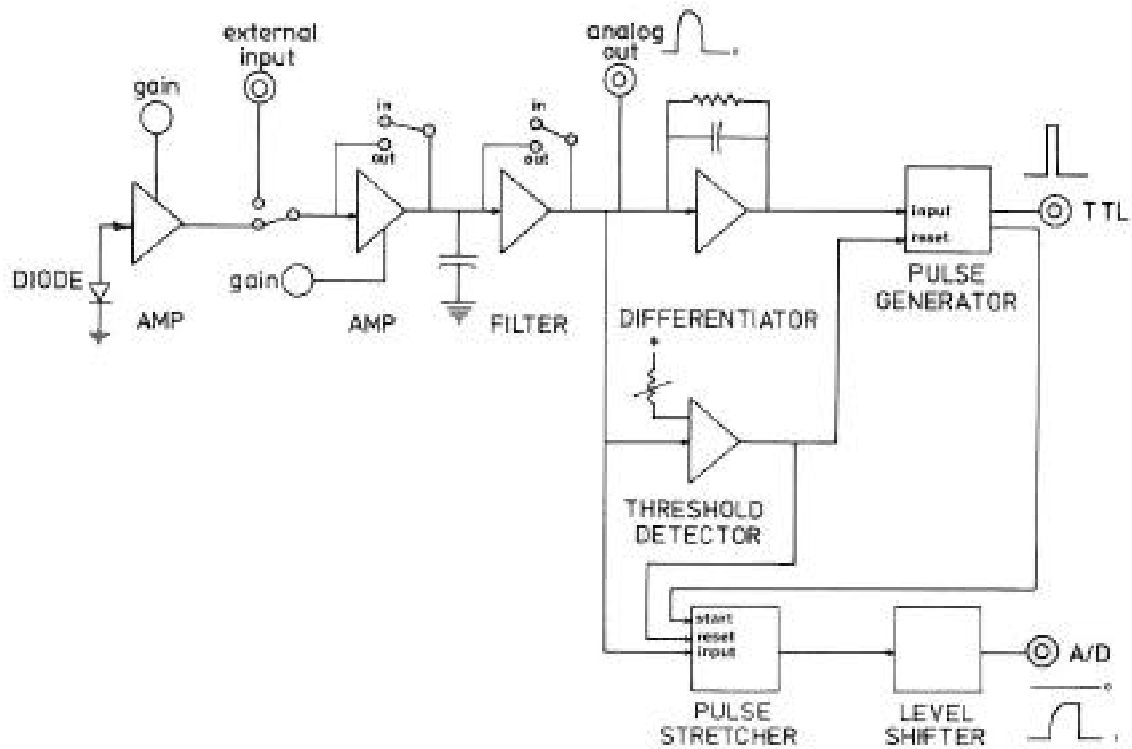

Figure 3. Schematic diagram of signal processor. The input signal can come directly from the photo diode or from an FM recorder through the external input.

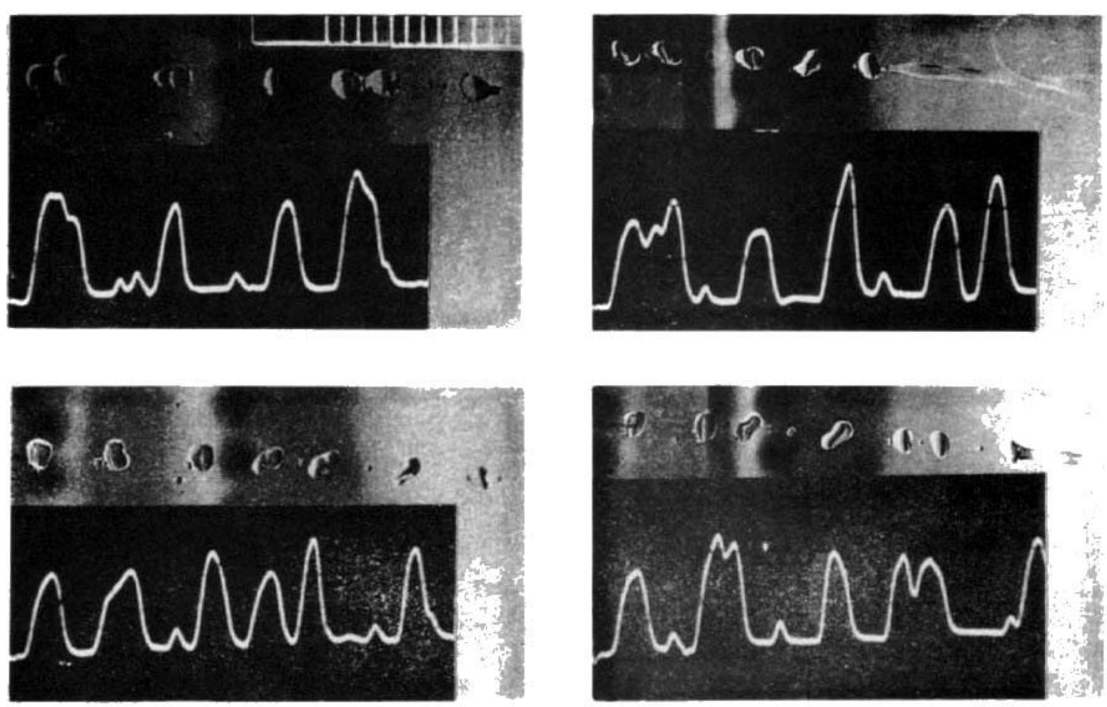

Figure 4. Correspondence of drop trains to pulse trains.

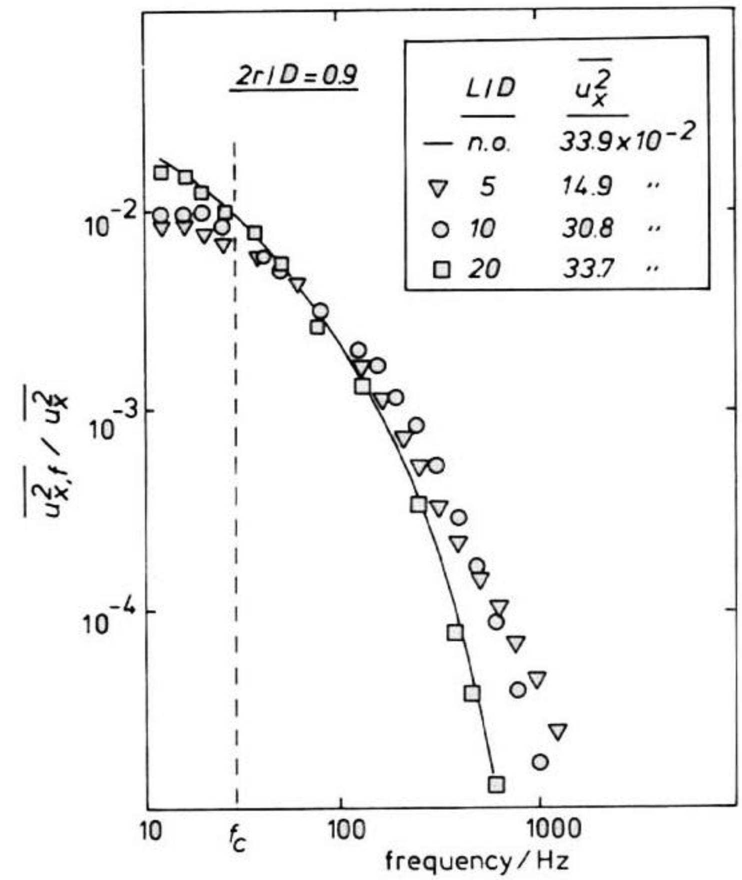

Figure 5. Turbulent energy spectra near the wall for Re - 5000.
The solid line is the spectra for an open tube. The data points show the effect of a square-edged obstruction on the spectra.

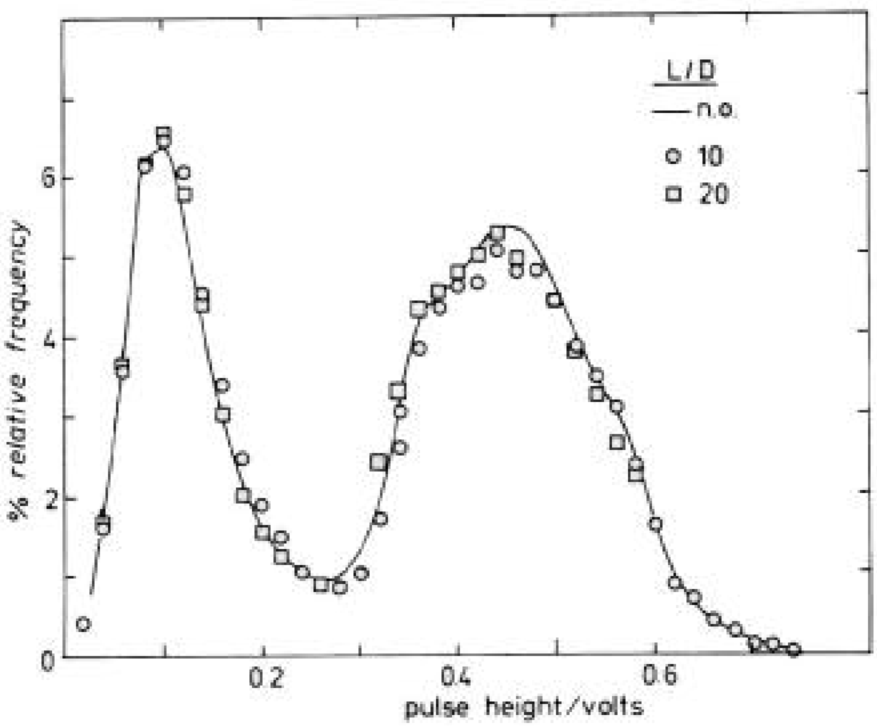

Figure 6.The drop size distribution for a turbulent water jet with Re = 5000.
The solid line is the distribution for an open tube. The data points show the effect of a square-edged obstruction. The system has dynamic and geometricsimilarity to the systemused to obtain the data in Figure 5.

CLOSURE

We have just begun to take data in our study on the effect of velocity profile relaxation on the instability of laminar liquid jets. When this study is completed, we intend to return to turbulent jets, extending the measurements described above to higher values of the Reynolds number.

I-4.6

THE FURTHER DEVELOPMENT OF A CAVITATION TEST CELL

Dr. David A. Summers
University of Missouri-Rolla
Rock Mechanics & Explosives Research Center
Rolla, Missouri 65401

Dr. Marian Mazurkiewicz
University of Missouri-Rolla
Rock Mechanics & Explosives Research Center
Rolla, Missouri 65401

ABSTRACT

Conventional cavitation testing involves the vibration of a small button-shaped specimen at a high frequency in a fluid bath. Such procedure cannot be used for rock testing. A high fluid velocity, cavitation cell has been developed by Dr. Lichtarowicz at Nottingham University which does, however allow the testing for rock samples. This equipment has been used to review the basic mechanisms of erosion and establish relative levels of erosion resistance for a suite of rocks. It does not, however, allow testing of some ancilliary parameters of erosion such as the effect of traverse rate or multiple nozzle orientation on the erosion of materials. A new test unit has therefore been designed to incorporate features which will allow the effect of such test parameters to be determined. The design of this test frame is described and the results of some preliminary testing, evaluating the effect of traverse rate on the cavitation erosion resistance, is described and discussed.

INTRODUCTION

The major interest in cavitation erosion has arisen, because of the damage which is incurred in pumps and marine equipment when cavitation occurs. For this reason the majority of the techniques developed to examine cavitation behavior, and material resistance, have been developed for metals. The most common test procedure has been developed by the ASTM through their Committee on Erosion and Wear, Committee G2. The result of their endeavor has been the development of a standard where small button shaped samples of material are prepared, such that they can be threaded on the end of a specially shaped horn. This is attached to an ultrasonic driver. Detailed specifications are then mandated (Ref. 1) wherein the test sample must be placed in a container of a known size, at a known depth of submersion, in distilled water and the ultrasonic drive excited such that the specimen vibrates at a frequency of 20 Kilohertz.

Several problems exist with such a procedure in regard to the testing of rock. It is difficult to machine rock samples to the small size required to fit the commercially available test equipment. It is impossible to machine threads onto the rock such that they can be screwed into the ultrasonic horn. Further it is impossible to maintain an integrity of samples in many instances, under the high vibration frequency due to tensile failures within the rock samples.

The need to develop a cavitation erosion test procedure for rock was based on two initial requirements. The first is that this would provide a relatively simple and potentially readily reproducible method of testing the water jet erosion resistance of a rock. This property is now required, due to the advent of water jet cutting as a commercially viable proposition in the mining industry. Secondly it has been shown that the use of cavitation in high pressure water jet flow allows effective excavation of the rock at a lower pressure than is otherwise the case. Further, the development of a proper test cell would allow a more detailed study of the mechanism by which cavitation erosion of rock occurs and this in turn may bring a greater insight into the phenomenon of high pressure water jet erosion of rock.

INITIAL TESTING

At the time that the research work was being initiated, the G2 Committee of ASTM formed a task force to look at the use of other methods of cavitation testing. The one most seriously considered at that time was known as the stationary specimen test. In this procedure, a sample is prepared and located in a fixed holder, underneath the vibrating horn, on the end of which a hardened dummy button is attached (Fig. 1,2). In this way cavitation bubbles created by the vibrating horn impinge upon the underlying rock surface. This procedure had been examined by a number of investigators elsewhere including Hobbs (Ref. 2), Preece (Ref. 3), and others and would provide a basic method of comparison, where rocks could be evaluated using a pre-existing method of test, and this data compared with the results of any future method we develop. Accordingly, a suite of rocks was tested in this manner (Ref. 4).

The test procedure followed closely that recommended by the ASTM panel. Tests were first carried out, using metal specimens, and then a suite of rocks comprising; three granites, three marbles, two sandstones, and one dolomite were tested in this program. Tests were carried out over a period typically on the order of 7 hours with the sample being removed at 1/2 hour increments to determine the weight loss. Typically, over the course of the test, the calculated cumulative depth of erosion over the surface of the sample was on the order of 500 pm, or less (Fig. 3). The test procedures using this method illustrated some interesting aspects of the cavitation erosion of materials. For example it was found that the cavitation erosion differentially attacked the weakness planes around crystal boundaries (Fig. 4). In this manner the grains, in time, become liberated from the rock matrix leading to relatively large steps in the erosion rate plotted with time. This phenomenon of preferential attack by cavitation bubbles on pre-existing cracks has been described earlier by Brunton (Ref. 5). Problems with this test, as currently practiced, were the relatively slow rate at which it was conducted; the relatively small amounts of mass loss which occurred and therefore the sensitivity of the results to individual crystal removal; and that the wear of the dummy specimen changed the surface over the test and may affect the result.

Because of these problems, we were interested to read of the development of cavitation test cell by Dr. Lichtarowicz at the University of Nottingham (Ref. 6) and therefore developed a cell of our own based on the design which he had created.

LICHTAROWICZ CELL

The principle of operation of this cell is that cavitation is caused, when a fluid at high velocity is exhausted, through a nozzle, into a test chamber filled with fluid at a low but positive pressure. This cavitation cloud is formed around the jet created and, by positioning the sample within the cloud, erosion ensues.

The procedure adopted for testing was to prepare samples 2.5 cm in diameter and place these in a specimen holder in front of the fluid nozzle, within the cell, which was then sealed (Fig. 5). The high pressure pump supplying the nozzle with fluid was then started. The cell was first filled with fluid, then the exit valve was set so that, as the pump was brought up to pressure, the cell pressure would be maintained at the correct level (on the order of 0.4 MPa).

Unfortunately, in many instances, with the original cell, the stresses induced in the rock sample was sufficient to cause it to fail catastrophically into several pieces. A similar result had been seen in another program, which had led to use of a 5 cm diameter, 2.5 cm thick sample, which was sufficiently large as to contain the energy of impact without failure. Such a specimen however would not fit within the dimensions of the original cell and accordingly a larger cell was made.

With this larger cell, it was possible to test the suite of rocks originally examined, and this was carried out. The test procedure was close to that suggested by Dr. Lichtarowicz, namely that the sample was located in the holder, at the opposite side of the cell to the jet nozzle, the fluid jet was brought up to pressure and the flow of fluid of the cell restricted to develop the required back pressure within the cell.

The result of the work with this cell was extremely promising. Test results were obtained in a matter of minutes rather than hours and the specimens were eroded at a much more rapid rate. This overcame most of the disadvantages of the ASTM method of test. Mass loss, for example, was at a much greater level than that of the conventional cavitation testing, such that the failure of individual crystals or grains of the rock had a much smaller influence on the total erosion resistance of the material. From these tests, it was possible to identify a basic test procedure for evaluating the erosion resistance of materials to cavitation attack. However this was not the only purpose of the test program. As discussed earlier, the ability of cavitation erosion to enhance the cutting ability of a water jet implies a substantial benefit if it can be used in the field. Under field conditions, however, the jet would be moved relative to the rock surface and there is also a potential of more than one nozzle being applied and further the jet would impact at different angles to the rock surface. Such a range of parameters could not be tested with the existing test cell. We have therefore moved to the third generation.

TEST EQUIPMENT

Because of the nationality of most of the investigators who have worked on this program, we are designating this as the "Polish Cavitation Cell". The primary requirement of this cell is that it allow the specimen to traverse under the cavitation nozzle. For this reason, a rectangular rather than circular cell was required. Based on the test procedures developed with the second cell, the standoff distance required will be on the order of 2.5 cm. The cell was made of sufficient size that it would allow testing of rock samples prepared from NX core, a standard size used in core recovery. Further, two windows were also incorporated into the current cell structure. In order to simplify the method of feed of the sample across the jet path, a cylindrical drive shaft was taken out through one wall of the cell which was carved from a single block of aluminum. This shaft was in turn connected to a sliding block drive along a guide channel by a threaded rod (Fig. 6b). The speed of rotation of the rod was controlled, through a reduction gear, from a variable speed, 1 hp dc motor. The specimen holder was designed such that the samples could be sized to fit with the line of impact of the cavitating jet occurring 2.5 cm from the nozzle face.

Each test would be started with the cavitation jet directed onto one end of the specimen holder until it had been raised to the required pressure. At this time, the drain valve would be closed, the cell filled with fluid. The valve was then opened to the point that the cell pressure would reach the required level. The test is carried out by traversing the 5 cm long sample underneath the jet, and ending the test with the jet impacting on the sample holder at the other end. In order to guard against severe erosion of the sample holder, small replaceable plates were fixed to the top of the holder at both ends (Fig. 6a).

INITIAL TEST RESULTS

For the initial test program, samples of dolomite were used since dolomite is a local rock, is relatively homogeneous, and easy to prepare and it has been shown, particularly susceptible to cavitation erosion attack, thus allowing a clear monitoring of the effect of the parameters under investigation.

In the initial test program, it was decided to operate with a cavitation number of approximately .01. Under these conditions, the jet would be delivered into the cell at a pressure of 50 MPa while cell pressure would be held to a value of .5 MPa. Transmission oil was used as the jet fluid during this test. The reason for this has nothing to do with the optimization of jet cavitation, but rather deals with the practicality of operating high pressure water equipment during the winter months. (The results from the earlier test program has indicated water is a much more severe cavitation fluid than this particular oil.) The oil was pressurized by a Kobe size 4 pump, and fed through a 14.3 mm O.D., 4.75 mm I.D., high pressure line to the cavitation chamber, and thence, through the 0.33 mm diameter sapphire nozzle. The nozzle face was located 2.5 cm above the rock samples.

For the initial test program, the tests were designed to observe the effect of traverse velocity on erosion damage. The velocity of traverse was set so that it took either 1, 2, 3, 4, 5, or 10 minutes for the 5 cm long sample to pass under the jet.

The results of the test program were somewhat different to that anticipated, and reference is made to Figs. 7, 8, 9, and 10 which illustrate the results achieved. These figures show samples traversed under the jets at periods of 1, 2, 4, and 5 minutes, respectively. In the 1 minute test (Fig. 7) the jet path can clearly be discerned over the target surface, for a distance of approximately 0.5 cm on the either side of the jet track, the surface is mildly pitted. Where the traverse velocity is halved (Fig. 8) it can be seen that at one or two points, erosion is more severe, although the depth of the jet cut itself is relatively unchanged at about 3 mm. The zone of cavitation damage is, however, much more clearly defined. Nevertheless, material removal is still relatively small. Where the jet traverse velocity is halved again (1.25 cm/min) much more severe damage can be observed (Fig. 9). There has still been very little depth penetration of the sample (now about 5 mm), apart from at the left hand end, which was close to the point where the jet was brought up to pressure. However, the character of the surface has changed, quite dramatically. It can be seen that while, after the 2 min. test one or two flaws and cracks had been exploited, at approximately half this traverse velocity, major flaws are being developed by cavitation erosion. It can be seen that the surface no longer retains its original characteristic, although as yet, substantial surface penetration has not taken place. In contrast where one studies the sample which took 5 min. to traverse (Fig. 10 a, b), substantial penetration, to a depth of approximately 1.2 cm has occurred. Major crack development has occurred throughout the sample surface, leading to the removal of relatively large fragments of the rock surface.

The sharp change in erosion rate, with a small change in the traverse velocity, from 2.5 cm/min to 2 cm/min, indicates a substantial change in the erosion process. This, however, should not have been unexpected if one reviews the data from the standard cavitation erosion testing of metals, where an incubation period is quite commonly found prior to major erosion occurring.

One can equate the very slow initial stages of rock removal with the incubation period of the normal metal test. During this period the cavitation erosion is developing the cracks within the rock surface to the point where major material removal can be achieved by growth of those particular crack systems.

It is interesting to note that where one slows the advance rate to 1 cm/sec, very little increase in the depth of cut is achieved. The likely reason for this is that the cavitation jet is of a finite length and the actual erosion itself, once it is initiated, occurs relatively rapidly until the zone of cavitation bubble collapse has been passed through, at which point the water jet stops eroding.

This experimental data is as yet very premature and data has only been collected for samples cut from one individual piece of dolomite. It is perhaps pertinent however, to point out that the tests have shown that a very marketed sensitivity of the rock erosion resistance exists to parameters which are not as yet identified. To be more specific, there is very little difference in the strength between two samples of dolomite collected from the school mine, one of which was used in the test described above. In order to gain more data points, a second block of dolomite, from an adjacent site, was also tested. The results from a single 1 min traverse across the sample (traverse velocity of 5 cm/sec) is shown in Fig. 11. It can be seen that the sample has been eroded to a depth of over 2 cm over its entire length and for approximately 3/4 of its width within this time frame. The specific difference between the two samples of dolomite are not immediately discernable apart from one of color and slight textural differences which can be perhaps seen in the photographs.

Several simple mechanical problems have arise with the cell at the present time which will lead to slight further modification in the near future, to cope with problems which have arisen in holding the sample and coping with fragments broken off during testing. However, these are relatively small details and we look forward in the near future to reporting in more detail on the progress we have made with a more precise set of results on the effectiveness of cavitation in improving the cutting ability of water jets and also in allowing us a better understanding of the mechanisms of cavitation erosion and hopefully thereby the mechanism of water jet erosion in rock.

ACKNOWLEDGEMENTS

This work is being funded in part by the Office of Surface Mining of the Department of Interior under contract #USDI G5105035. We are grateful acknowledge this support, without which, the work could not have reached its current stage. We also are grateful to Mr. Hale, Mr. Tyler, Mr. Robison, and Mr. Blaine of the Rock Mechanics staff and Mr. Mike Scully, our undergraduate assistant, who have assisted in constructing this equipment and helped with the preparation for these tests.

REFERENCES

1. A.S.T.M., "Standard Method of Vibratory Cavitation Erosion Test," Designation G 32-72, under jurisdiction of ASTM Committee G2 on Erosion and Wear, published July 1972.
2. Hobbs, J.M. and Rachman, D., "Environmentally Controlled Cavitation Test (Improvements in a Cavitating Film Erosion Test)," Characterization and Determination of Erosion Resistance, ASTM STP 474, 1970, pp 29-47.
3. Preece, C.M., Personal discussion and letters to D.A. Summers, April 1978.
4. Summers, D.A. and Sebastian, Z., "The Reaming Out of Geothermal Excavations," Final Report to Sandia Labs on Contract 13-3246, University of Missouri-Rolla, April 1980.
5. Brunton, J.H., "Cavitation Damage', Paper 7.1, Proc. 3rd Int. Conf. Rain Erosion and Associated Phenomena, Elvetham Hall, U.K., August 1970, pp 821-843.
6. Lichtarowicz, A., "Cavitation Jet Apparatus for Cavitation Erosion Testing," presented at ASTM Symp. On Erosion, Prevention and Useful Applications, October 24-26, 1977, Vail, Colorado.

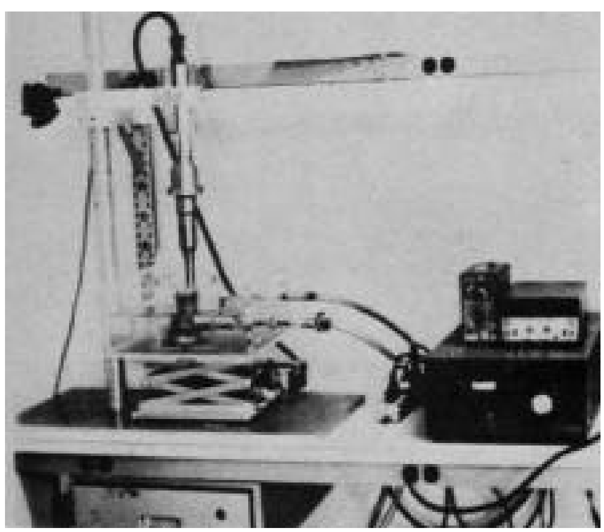

Fig. 1. "Stationary Sample" cavitation test equipment.

Fig. 2. Sample position beneath the vibrating horn in the "stationary specimen" test.

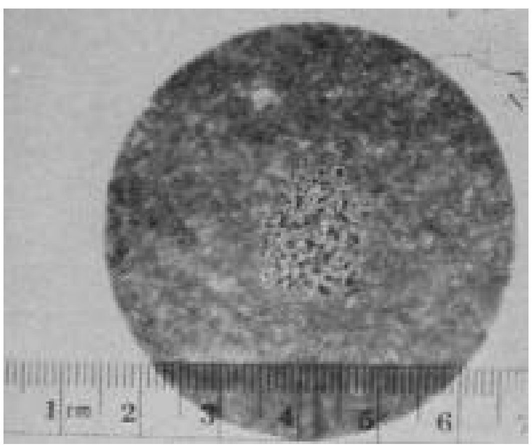

Fig. 3. Results after a 7-hour test on a marble sample.

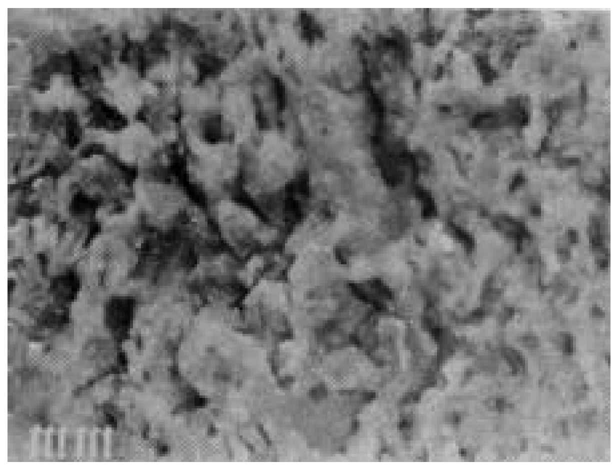

Fig. 4. Surface of marble after test showing erosion around grains.

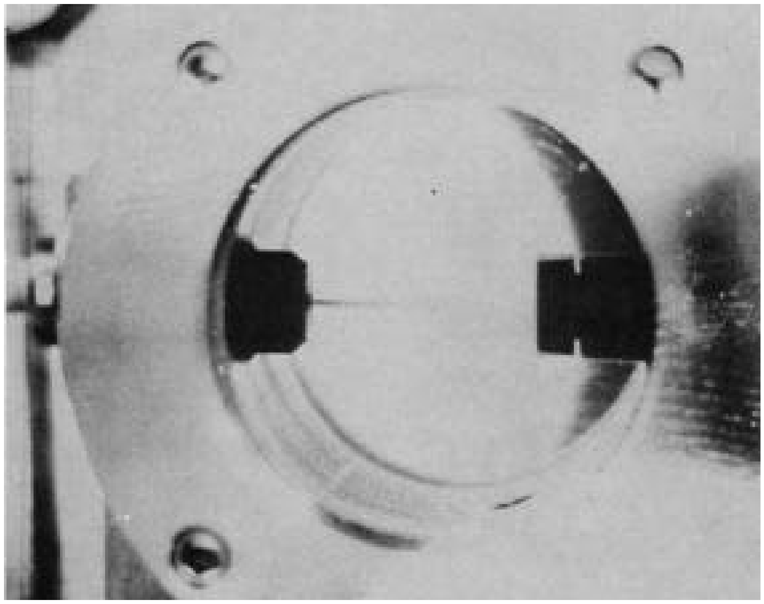

Fig. 5. Lichtarowicz Cell showing the location of the nozzle, cavitating jet, and sample, within the Cell.

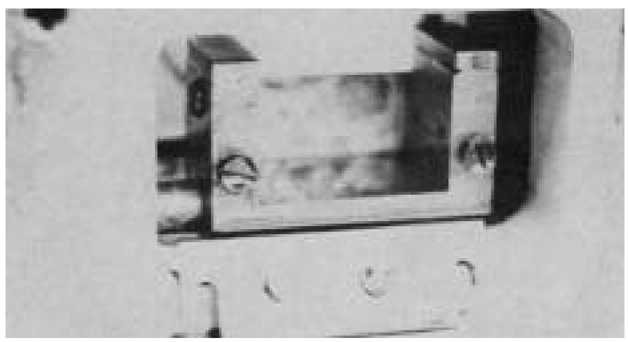

Fig. 6(a). Detail of the Polish Cell showing the sample carriage.

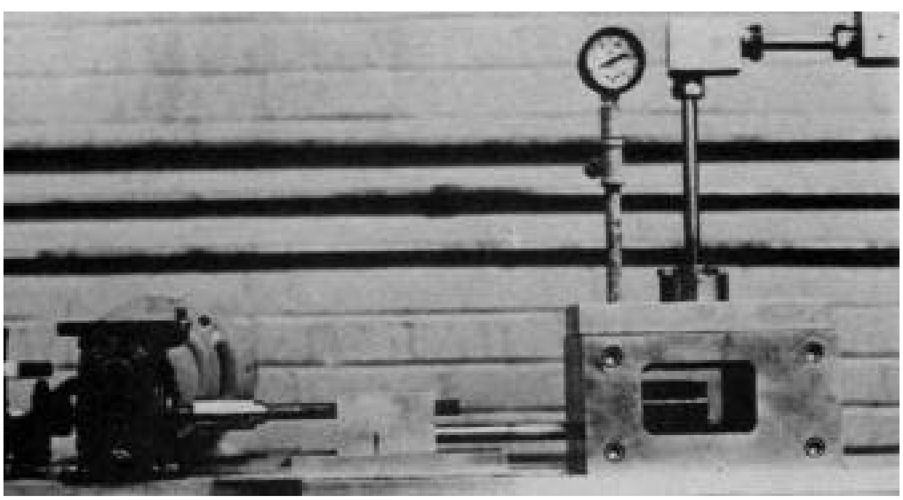

Fig. 6(b). Polish Cavitation Cell showing the method of drive for the sample carriage.

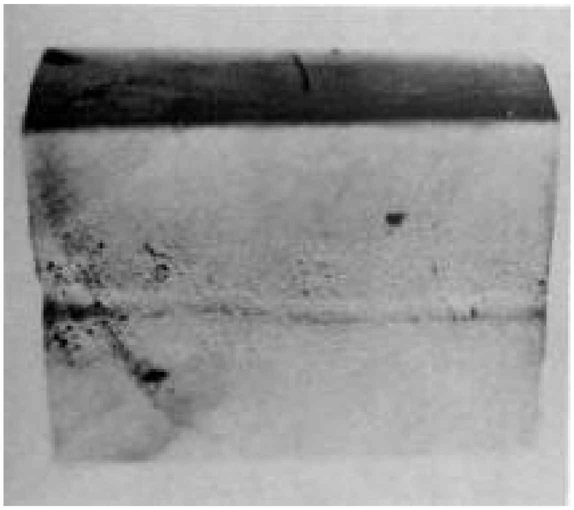

Fig. 7. Sample cut at a traverse velocity of 5cm/min.

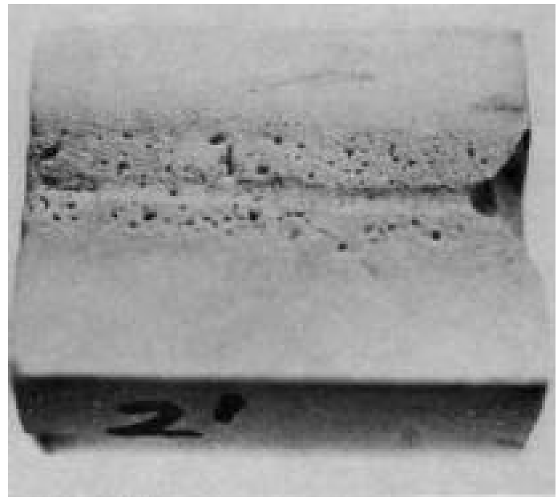

Fig. 8. Sample cut at a traverse velocity of 2.5 cm/min.

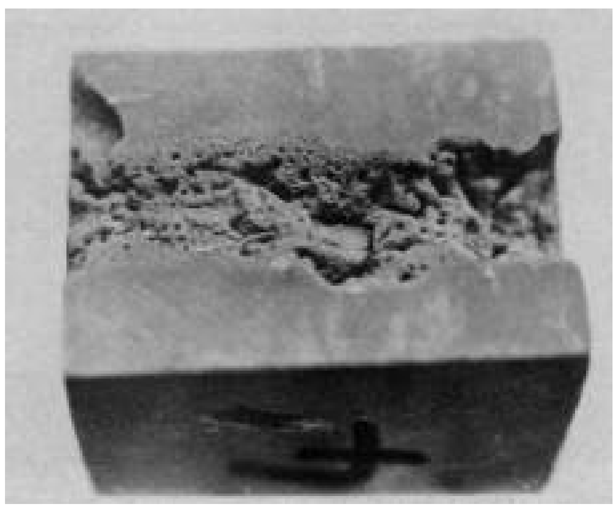

Fig. 9. Sample cut at a traverse velocity of 1.25 cm/min.

Fig. lOa. Sample cut at a traverse velocity of l cm/min.
(top view)

Fig. 10b. Sample cut at a traverse velocity of l cm/min.
(side view)

Fig. ll. Sample of grey dolomite eroded at a traverse velocity of 5 cm/min.

TECHNIQUES FOR THE MEASUREMENT OF THE AIR-WATER DISTRIBUTION IN THE FLOWFIELD OF A HIGH VELOCITY WATER JET

D. L. Eddingfield
Southern Illinois University at Carbondale
College of Engineering and Technology
Carbondale, IL 62901

J. L. Evers
Southern Illinois University at Carbondale
College of Engineering and Technology
Carbondale, IL 62901

ABSTRACT

Beyond a relatively short distance downstream of the nozzle, a high velocity water jet invariably produces a flowfield which consists of a water core, an annular air-water droplet region and an induced external air flow region. The study of the air-water droplet region is essential to a more complete understanding of high velocity water jet flows. Existing experimental techniques employed to measure the phase or component distributions are discussed. In addition, a technique is suggested for use for measurements in a high velocity water jet.

INTRODUCTION

When a high velocity water jet issues from a nozzle into ambient air, a complex multi-component flowfield develops. Beyond a relatively short distance downstream of the nozzle exit, the flowfield consists of essentially three regions as shown in Figure 1. These are a water core region, an annular air-water droplet region and an induced external air flow region.

Previous research has been concentrated on the analysis and study of the water core region. This emphasis is to be expected since it is of primary importance in water jet flows, especially in the near flowfield of the jet. However, at larger distances downstream of the nozzle, the air-water droplet region and the induced air flow region become increasingly more important. The consideration of these flow regions is pertinent to the study of water jets which are to be employed at large stand-off distances; for example, in borehole mining applications.

The existence of these two regions is evidence of the deterioration of the quality of the water jet; that is, a radial spreading of the momentum and kinetic energy of the jet. Jet turbulence and aerodynamic interaction might initiate this process and in turn lead to mass, momentum, and energy loss of the water core by the production of droplets. Experimental characterization of the air-water droplet region should contribute to a better understanding of high velocity water jets. In addition, this type of experimental measurement is important for the development of a viable computer model for the study of water jets.

PHASE OR COMPONENT DISTRIBUTION CHARACTERIZATION

Phase or component distribution characterization can be done in several different ways. An air-water droplet flow is a two-phase, two-component system. However, just the phrase, two-phase flow, will be employed to denote the fluid system.

One approach to characterizing the distribution of phases, especially in pipe flows, is to define the variation of the volume of one phase per unit total volume. For example $\alpha = \frac{\ _G}{}$ is known as the void fraction, that is, the fraction of a given volume

that is occupied by the gas phase. Equivalently (1 - a) is the volume occupied by the liquid phase since $_G + \ _L = $. The void fraction can be determined for small sample volumes at various locations in the cross-section of a flow giving a spatial distribution.

A bulk density of each phase (ρ') can be defined as

$$\rho'_G = \frac{\ _G}{}\rho_G = \alpha\rho_G$$

$$\rho'_G = \frac{\ _L}{}\rho_G = (1-\alpha)\rho_L$$

where ρ_G and ρ_L are the densities of the gas and liquid phase respectively.

The loading, z, is defined in terms of the bulk densities of the two-phase as

$$z = \frac{\rho'_L}{\rho'_G}$$

Consequently if the void fraction distribution is known the loading factor, z, is also known.

If not only the volumetric distribution is desired but also characterization with respect to size, a number frequency distribution can be used as illustrated in Figure 2. In the figure, FN(D) is the number of particles of size D. Two typical characterizations of the number frequency distribution are the number mean and the number variance, given by

Number Mean, $\mu_N = DF_N(D)dD$
Number Variance, $\sigma_N^2 = (D-\mu_N)^2F_N(D)dD$

Similarly a characterization of size distribution with respect to mass can be made. If F_M is the mass of particles of size D,

Mass Mean, $\mu_M = D\,F_M(D)dD$

Mass Variance, $\sigma_M{}^2 = (D - \mu_M)^2 F_M(D)dD$

Finally, a mass cumulative distribution can be determined as illustrated in Figure 3.

$C_M = F_M(\eta)d\eta$

where $C_M(D)$ is the fraction of mass associated with component of size D or less. The mass median diameter is the diameter corresponding to $C_M = 0.5$.

REVIEW OF MEASUREMENT METHODS

There is an extensive field of literature on measurement methods in two-phase flows. Reviews of measurement techniques are given by [1, 2, 3, 4, S] and an index to two-phase flow literature is given by [6].The measurement techniques fall into two broad categories; those which determine an overall mean value of phase content and those which determine a spatial distribution of phase content. Hewitt [1] denotes the former as a primary factor and the latter as a second order parameter.

Mean Phase Content Measurements

Radioactive Absorption and Scattering Techniques

One of the most common methods for measuring the average value of the phase content; e.g., the void fraction a, at a given section is by radioactive absorption and scattering techniques. Hewitt [1] indicates that the technique most widely employed for two-phase flows in a conduit is the measurement of the attentuation of a beam of gamma rays by the flow. This technique has been utilized for many years and is used to calibrate other measuring devices. A brief introduction to the use of radiation attentuation in two-phase void fraction measurements is given by [7]. A chordial average can be obtained by passing beams through the cross-section at different angles as shown in Figure 4. The calibration of such a device without use of expensive spectrometry is accomplished by measuring the intensity of the beam at the detector with the sample area occupied by the gas phase only and occupied by the liquid phase only. The average void fraction α is given by

$$\alpha = \frac{\ln I - \ln I_L}{\ln I_G - \ln I_L}$$

where I_L is the intensity for liquid only, I_G is the intensity for gas only and I is the measured two-phase intensity.

Other related techniques are β ray absorption, and neutron absorption and scattering. Hewitt [1] gives a brief discussion and references for these methods.

Impedance Measurements

Impedance methods are commonly employed for average void fraction determination of a two-phase flow. These methods are based on the measurement of the electrical impedance since the conductance and capacitance of a two-phase flow is related to the concentration of the phases. Merilo et al. [7] provides a good discussion of this technique. The average void fraction is given by the expression

$$\alpha = 1 - \frac{(A\varepsilon_L - A_C\varepsilon_G)}{(A\varepsilon_L + 2A_c\varepsilon_G)}\frac{(\varepsilon_L + 2\varepsilon_G)}{(\varepsilon_L - \varepsilon_G)}$$

where

A is the admittance (reciprocal of impedance) of the two-phase mixture,

A_C is the admittance of the gauge when immersed in the liquid phase only and ε_G and ε_L are the gas phase and liquid phase dielectric constants respectively.

Local Phase Content Measurements

Considerably more insight into the details of the two-phase flow is provided by the determination of the distribution of the phase content across the flow field. This involves measuring the phase content in a small sample volume or area at various radial locations in the flow. A variety of techniques are discussed in this section.

Photographic Methods

Photographic methods have been employed extensively to give size and distribution of phase content in two-phase flows. Azzopardi [5] gives an overview of the techniques available.

For photographic methods to be applicable, the flowfield must be illuminated. Two important considerations should be kept in mind when selecting the means of illumination; namely, the illumination intensity/particle,size/velocity relationships and the angular variation of scattered light. Azzopardi [5] points out that if the minimum amount of light to produce an image on the developed photographic plate is provided, then the dependence of the incident light intensity on the particle size and velocity are

$$I_o \quad dp^{-3}$$

$$I_o \quad V_p$$

where
I_o is the incident illumination
and d_p and V_p are the particle diameter and velocity respectively.

These relationships indicate that the smaller and faster the particle, the more illumination required. In addition the illumination should be as parallel to the observing direction as possible.

Another related method involves replacing the camera with photodetector arrays and processing the photodetector signals by a computer. Also holography has been employed in particle size measurements [9].

Electrical Methods

A needle bridging method developed by Wicks and Dukler [10] employs two needles in line with each other with their tips a small distance apart in a circuit with a resistance and a battery. When a drop large enough to bridge the distance between the tips of the needles occurs, an electrical pulse is generated. The spacing between the needle tips is varied and mean count rates are obtained. This method has some difficulty in the interpretation of the data.

Other electrical methods which may be applicable are the local impedance probes [4] and charge removal devices [5].

Optical Methods

A number of optical methods based on light scattering methods are discussed by [5]. He points out that these methods rely on the principle that the intensity of light scattered by a particle depends on the intensity of the illuminating radiation, the diameter and refractive index of the particles, the wavelength and polarization of the light and the direction of illumination. These methods will not be discussed here.

However, most of the devices depend on the flow containing a low concentration of the liquid phase.

Several investigators have developed fiber optic probes to measure the local void fraction. A commercial system by DISA employs a probe containing an optical fiber bent at the tip to form a U shaped sensor. The presence of a phase at the tip can be detected by the dependence of light transmission through the fiber on the refractive index of the phase present at the probe tip. The void fraction is defined as

$$\alpha = \frac{t_G}{t_G + t_L} = \frac{t_G}{T}$$

where
t_G is the time the gas phase is present at the probe tip
and t_L is the time there is liquid present.
T is the total measurement time.

The probe tip is about 100 pm in diameter. Most applications have been in bubble flow and very little application in gas-droplet flows.

Miscellaneous Methods

In two-phase pipe flows, isokinetic probes have been employed. An isokinetic probe is a sampling tube which collects or withdraws a sample of the flow in a manner so that the velocities of the two phases at the mouth of the probe are equal to that which they would have been in the absence of the probe. This is achieved by adjusting the sample rate until the gas static pressure in the probe is equal to the static pressure in the undisturbed flow. Schraub [11] provides an analysis of the isokinetic probe and gives details of a probe design. However, the high velocities which occur in a water jet pose difficult problems in the use of an isokinetic probe. Another approach is to freeze the droplets and perform a size analysis on the frozen droplets. This might be accomplished by diverting a portion of the spray over a liquid nitrogen bath.

WATER JET DROPLET CHARACTERIZATIONS

The size, distribution and speed of the droplets produced by a high velocity water jet are not known. However, an estimate of the expected size and velocity of droplets is desirable so that an appropriate measurement method can be selected.

One possible mechanism of droplet formation in a high velocity water jet is a wave-like disturbance initiated by the combined effects of turbulence, aerodynamic interaction and surface tension. The wave structure grows and is rapidly deformed and stretched into an elongated filament or ligament of fluid which is broken in droplets which can be subjected to subsequent breakup. The stability of a droplet moving through a gaseous atmosphere depends mainly on the ratio of aerodynamic pressure forces trying to deform it and surface tension forces trying to make its shape spherical.

This is characterized by the Weber number

$$We = \frac{\rho_G V_R^2 d}{\sigma}$$

where

ρ_G is the gas phase density,
V_R is the relative velocity of the droplet to the gas velocity,
σ is the surface tension and d is the droplet diameter.

The critical minimum value of the Weber number required for droplet breakup to occur varies from a value of 10 reported by [12] to a value of 20 reported by [3]. For We = 20, property values for air and water, and a relative velocity of 150 m/s (50% of a jet velocity of 300 m/s), the maximum stable drop diameter is

$$d_{crit} \quad 500\mu m$$

A droplet with a diameter greater than approximately 500 pm will be subjected to secondary breakup. Note, however, that the relative velocity is squared which makes the calculation sensitive to this value. Crowe [12] indicates the time of breakup is of the order,

$$\Delta t_b = (0.3 - 1)\frac{\pi}{4}\frac{d^3\rho_L}{\sigma}$$

For a water droplet diameter of 500 µm, this yields

$$4.5x10^{-4}\,s \le \Delta t_b \le 1.5x10^{-3}\,s$$

The time required for the droplet to assume the local gas velocity is characterized by the aerodynamic response time [12] given by

$$\tau_A = \frac{\rho_L D^2}{18\mu_G}$$

For a water droplet in air,

$$\tau_A = 0.7s$$

These very approximate calculations indicate the water droplets in the two-phase flow, a reasonable distance from the water core, should be less than 500 µm in diameter. Also since the aerodynamic response time is much longer than the breakup time, the droplet breakup is governed mainly by the initial relative velocity. In other words, the droplet cannot move to a region where the lower relative velocity would allow a larger diameter before it is broken up. The distance traveled during the breakup time is on the order of 0.2 m based on a droplet average axial velocity of 150 m/sec. This means that any measuring device positioned near the water core will encounter a large number of droplets that are in the process of breaking up into smaller droplets.

A PROPOSED MEASUREMENT TECHNIQUE

In relation to the development of a model of a water jet which incorporates the generation and flow of an air-water droplet region, the most important considerations are (1) the amount of droplet generation per unit length and (2) the size and spatial distribution of the droplets. Also any measurement device must be able to operate in the environment of high velocity air-water droplet flows.

A proposed design as shown in Figure 4 has been developed, and based on this design a device will be built and tested. The device consists mainly of a flexible fiber optic bundle placed in an airfoil-shaped support approximately 15 cm long and 5 cm wide. The optical fiber bundle terminates at a viewport approximately 6 mm in diameter. For protection, the optical fiber is covered by a sapphire window. The optical fiber bundle is segregated so that a portion of the fibers are used to transmit light for illumination and the rest are employed for observation. The latter are connected to a camera equipped with a telephoto lens. The use of an optical fiber bundle allows the camera to be located outside of the spray but yet give an optical image as if the camera lens was at the viewport. In addition the optical fiber provides a means of illuminating the plane of focus. Photographs will be taken at various radial and axial positions in the air-droplet flow region and analyzed to yield the size and distribution of the water droplets. The appropriate illumination technique is still being investigated. A method which will give a high intensity, short duration pulse is required.

SUMMARY

A variety of methods are available to measure the distribution of phases in an air-droplet flow. Rough estimates suggest that the air-droplet region of a high velocity water jet will contain stable droplets for droplet diameters less than 500 µm. In addition, near the water core a considerable number of droplets in the process of secondary breakup will be encountered. It is suggested that a photographic technique utilizing fiber optics is a relatively simple but perhaps tedious technique which would give the greatest insight into the characteristics of the two-phase flow field.

ACKNOWLEDGEMENTS

This work was performed at Southern Illinois University at Carbondale under contract number DE AC 2279PC20091-06 for the U.S. Department of Energy, the Division of Surface Mining, Carbondale Mining Technology Center.

REFERENCES

[1]. Hewitt, G. F., Measurement of Two-Phase Flow Parameters, Academic Press, New York, N.Y., 1978.

[2]. Soo, S. L., Fluid Dynamics of Multiphase Systems, Blaisdell Publishing Company, Waltham, MA, 1967.

[3]. Moore, M. J., and Sieverding, C. H., Two-Phase Steam Flow in Turbines and Separators, Hemisphere Publishing Corporation, Washington, D.C., 1976.

[4]. Lahey, R. T., "A Review of Selected Void Fraction and Phase Velocity Measurement Techniques," Fluid Dynamic Institute Short Course Notes, Dartmouth College, Hanover, N.H., August 1978.

[5]. Azzopardi, B. J., "Measurement of Drop Sizes," Int. J. Heat Mass Transfer, Vol. 22, p. 1245, 1979.

[6]. Gouse, S. W., An Index to the Two-Phase Gas-Liquid Flow Literature, The M.I.T. Press, Massachusetts Institute of Technology, Cambridge, MA, 1966.

[7]. Schrock, V. E., "Radiation Attentuation Techniques in Two-Phase Flows Measurement," 11th Nat. ASME/AICHE Heat Transfer Conference, Minneapolis, Minn., August 1969.

[8]. Merilo, M., Dechene, R. L., and Cichowlas, W. M., "Void Fraction Measurement with a Rotating Electric Field Conductance Gauge," J. Heat Transfer, Vol. 99, 1977.
[9]. Webster, J. M., "A technique for the Size and Velocity Analysis of High Velocity Droplets and Particles," Br. J. Photography, Vol. 34, p. 752, 1971.
[10]. Wilks, M., and Dukler, A. E., "In Situ Measurements of Drop Size Distribution in Two-Phase Flow - A New Method for Electrically Conducting Liquids," 3rd Int. Heat Transfer Conference, Chicago, IL, Vol. 5, p. 39, 1969.
[11]. Schraub, F. A., "Isokinetic Sampling Probe Technique Applied to Two-Component, Two-Phase Flow," Winter Annual Meeting ASME, November 1967.
[12]. Crowe, C. T., "Numerical Modeling of Gas-Particle Flows," Workshop Notes, ASME Century 2 ETC Conference, San Francisco, CA, August 1980.

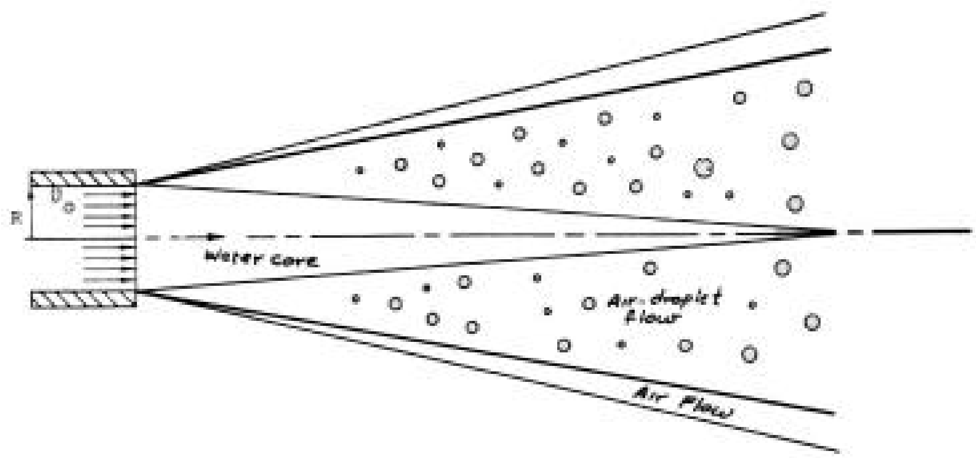

FIGURE 1. The three different regions of the flow.

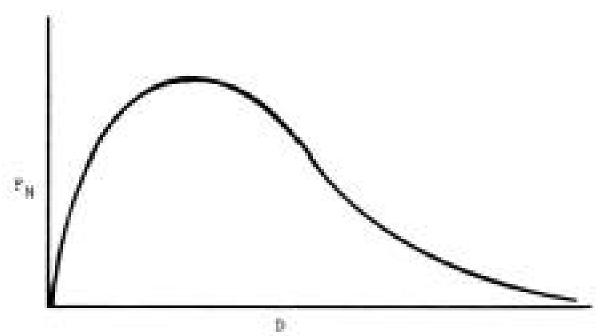

FIGURE 2. Number frequency distribution.

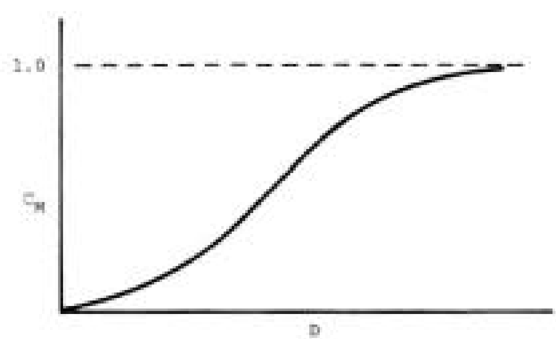

FIGURE 3. Cumulative mass distribution.

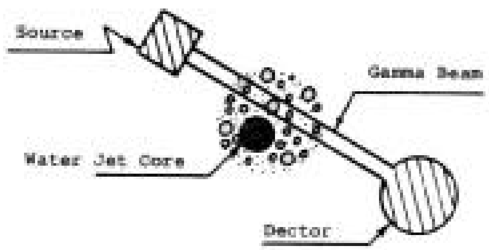

FIGURE 4. Gamma ray attentuation device.

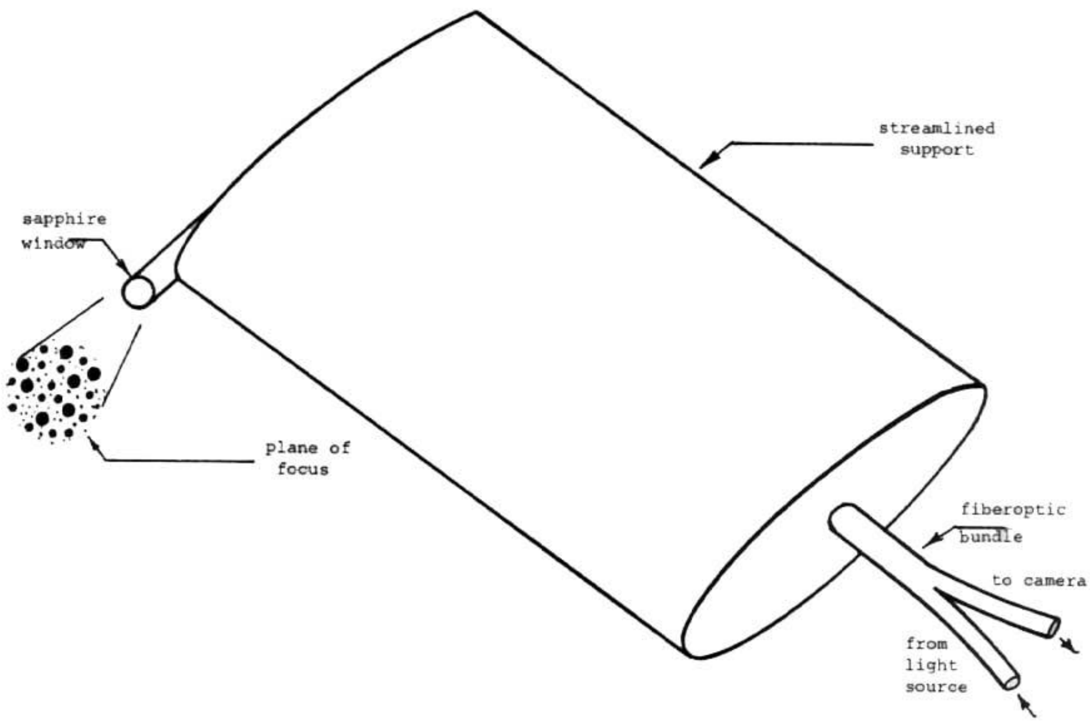

FIGURE 5. Proposed probe design.

CRITICAL AND OPTIMUM TRAVERSE RATES IN JET CUTTING

M. Hashish, Ph.D.
Flow Industries, Inc.
21414 - 68th Avenue South
Kent, Washington 98031

Notation

C_f	hydrodynamic coefficient of friction
$C_\ell C_e C_\rho$	speed of wave propagation in liquid, elastic and plastic speed of wave propagation in solids
d_n	nozzle diameter
E	energy
h, h_c,h_i	depth of cut, cumulative depth of cut, initial penetration rate
M, M_c	Mach number, critical Mach number
N	number of passes
n	number of nozzles
P	jet pressure
P_c	critical pressure
P_m	minimum pressure resulting in maximum depth of cut at u
P_{th}	hydrodynamic penetration threshold pressure
R	ratio of xc/dn
r	ratio of h/y
SE	specific energy
s	specific gravity of solid
t	time of exposure
U	traverse rate
u_1,u_2,u_3,u_4	critical traverse rate
v_e,v_c	elastic and critical solid particle velocities
x	standoff distance
x_c	length of jet initial region
y	kerf spacing
z_e,z_ρ,z_ℓ	elastic, plastic, and liquid impedences
Δv	volume removal rate
η	damping coefficient
σ_c,σ_y	material strength, compressive and yield
p_l,p_s	densities, liquid and solid
φ	jet angle

1. Introduction

General waterjet cutting equations ([1], [2]) have been developed to predict depth of cut, width of cut, volume removal, and specific energy. These cutting results were expressed in terms of jet parameters, cutting parameters, and material properties. Jet parameters include nozzle diameter, pressure, spreading coefficients, and nozzle frictional losses. Cutting parameters include standoff distance, traverse rate, and number of passes. Material properties related to the jet cutting phenomena in the moderate range of traverse rates were found to be the compressive strength, yield strength, material Theological property (expressed as damping coefficient), and the hydrodynamic coefficient of friction between the jet and the solid target.

The concept of the effect of traverse rate on the cutting mechanism was introduced [3]. A different set of material properties were found to relate to the jet and cutting parameters at very high or very low traverse rates.

This paper presents an effort made towards identifying critical and optimum traverse rates. Critical traverse rates are those which distinguish among different cutting mechanisms. The cutting equations in a range of traverse rates can be simplified to include only the most dominant material properties in a relatively simple functional relationship with jet and cutting parameters. Optimum traverse rates, on the other hand, are those that result in maximum or minimum cutting results. The existence of optimum traverse rates is associated with some cutting strategies. Among those strategies that will be treated here are:

A. Spaced cutting for simultaneous material removal between two parallel kerfs. Minimum specific energy is required in this case.
B. Multipass cutting, i.e., the optimum combination of traverse rate and number of passes required to achieve maximum depth of cut.

The jet cutting equation that will be used in determining the optimum traverse rates is presented in Section 2. This equation covers a wide range of practical cutting traverse rates. The shift in the cutting mechanism due to traverse rate will be neglected in the portion of optimum traverse rates analysis.

2. Jet Cutting Equations

The nondimensional jet cutting equation for depth of cut prediction when the standoff distance x is less than the length of jet initial region X_C is given by [4]

$$\frac{hc_f}{d_n} = \frac{\sqrt{\pi}}{2}\left(1 - \frac{\sigma_y}{2P}\right)\left(1 - e^{-\frac{4}{\sqrt{\pi}}\frac{C_f P}{\eta U}}\right) \qquad (1)$$

This equation is based on a control volume analysis to determine the hydrodynamic forces acting on the solid boundaries of the cutting slot. A Bingham model is used to describe the time-dependent stress/strain relationship of the solid material as it flows under the high normal stress of the jet.

The effect of standoff distance on depth of cut is determined by using the jet-spreading characteristics [4]. The derived equation in a nondimensional form is

$$\frac{hc_f}{d_n} = 0.297\sqrt{\frac{Rx}{x_c}}\,\psi^{2/3}\left(1 - \frac{\sigma_y}{2P\beta}\right)\left(1 - e^{-\frac{4}{\sqrt{\pi}}\frac{C_f P\beta}{\eta u}}\right) \qquad (2)$$

where

$$\psi = 1 - \sqrt{\left(\frac{\sigma_c}{2P}\right)\left(\frac{x}{x_c}\right)}$$

$$\beta = 2\left(\frac{x_c}{x}\right)\left(0.5 - 0.57\psi + 0.2\psi^2\right)$$

Equations (1) and (2) are valid within a range of traverse rates (as will be seen) and based on the impingement effect of the jet hydrodynamic force. At very high traverse rates, the waterhammer effect that occurs at the initial period of impact results in the depth given in [3] and rearranged here to appear in the nondimensional form

$$\frac{h}{d_h} = \frac{M - s\left(\frac{V_e}{C_\ell}\right)\left(\frac{C_e}{C_\ell}\right)}{1 + s\left(\frac{V_c}{C_\ell} - \frac{V_e}{C_\ell}\right)} \qquad (3)$$

when

$$V_e = \frac{\sigma_y}{z_e}$$

$$V_c = \frac{\sigma_c}{z_p} + \sigma_y\left(\frac{1}{z_e} - \frac{1}{z_p}\right)$$

for brittle materials, Equation (3) will take the simple form

$$\frac{h}{d_h} = \frac{M}{1 + s\left(\frac{V_e}{C_\ell}\right)} \qquad (4)$$

Equations (3) and (4) are only applicable when the jet Mach number M is equal to or greater than an M_c given by

$$\left.\begin{array}{l} M_c = M_1\left(\frac{C_\ell}{C_p} + s\right) + M_2\left(\frac{C_\ell}{C_e} - \frac{C_\ell}{C_p}\right) \text{for equation (3)} \\ \hline M_c = M_2\left(\frac{C_\ell}{C_e} + s\right) \text{ for equation (4)} \end{array}\right\} \qquad (5)$$

where

$$M_1 = \frac{\sigma_c}{s\rho_\ell c_\ell^{\,2}}, \quad M_2 = \frac{\sigma_y}{s\rho_\ell c_\ell^{\,2}}$$

This shows that cutting at high traverse rate introduced a new set of properties related to wave propagation, i.e., elastic and plastic speed of wave propagation in solids (C_e, C_p), speed of wave propagation in liquid (C_l) and dynamic strength properties. As will be shown, these equations will be used to identify critical and optimum traverse rates; also, simplified versions will be derived.

3. <u>Critical Traverse Rates</u>

The following critical traverse rates will be determined:

A. First critical traverse rate u_1. This is the lowest traverse rate that results in maximum possible depth of cut in single-pass linear cutting.

B. Second critical traverse rate u_2. Above this traverse rate, the penetration equation can be simplified by dropping the less effective properties in Equation (1).

C. Third critical traverse rate u_3. This critical rate signals the necessity for including the waterhammer phenomena with the hydrodynamic effect.

D. Fourth critical traverse rate u_4. Above this rate, the cutting mechanism is controlled by erosion and wave propagation similar to erosion by drop impact.

3.1 <u>First Critical Traverse Rate u_1</u>

The maximum possible depth of cut in a single pass is reached when the jet normal stress on the step shown in Figure 1 is no higher than the material resistance. In this case, the wall friction force balances the jet input momentum and material resistance in the control volume shown on Figure 1. The momentum equation for this "statically" balanced situation gives

$$\frac{h_O c_f}{d_n} = \frac{\sqrt{\pi}}{4}\left(2 - \frac{\sigma_c}{p}\right) \qquad (6)$$

This equation has experimental significance in determining both C_f and σ_c. The above hydrodynamic coefficient of friction will be the slope of line representing the data of h_O/d_n versus $\sqrt{\pi}\,(2 - \sigma_c/P)$ when the traverse rate is very slow ($U < u_l$). If only one nozzle diameter at a certain specified pressure is used, then only one data point is required. The threshold pressure that will result in no depth of cut at a very slow traverse rate represents half the compressive strength as suggested by Equation (6) and supported by many published data ([5], [6]). The slower first critical traverse rate u_l is determined by substituting h_o in Equation (6) for h in Equation (1). The result is

$$u_1 = \frac{4}{\sqrt{\pi}} \frac{C_f P}{\eta} / \log\left(\frac{2P - \sigma_y}{\sigma_c - \sigma_y}\right) \qquad (7)$$

The yield strength σ_y is a dynamic property that expresses material resistance to flow when the strain rates are high. For brittle materials, when the dynamic yield strength equals approximately the compressive strength, the first critical traverse rate will be equal to zero. In that case, σ_c will replace σ_y in Equation (1) for depth of cut prediction.

The characteristic velocity C_fP/η for a given material can be used to replace the critical velocity u_1 in identifying the lowest traverse rate limit for maximum depth of cut. This characteristic velocity can also be used to identify u_2.

3.2 Second Critical Traverse Rate u_2

This critical traverse rate does not indicate a shift in the cutting mechanism, but rather identifies a beginning of a range of traverse rates where some parameters in Equation (1) are less significant.

The jet instantaneous penetration rate can be determined from Equation (1) by replacing U with d_n/t and differentiating with respect to t. The jet initial penetration rate h_i is then obtained by differentiating $(\partial h/\partial t)$ and letting t = O. The resulting expression for h_i is

$$h_i = \frac{2P - \sigma_y}{\eta} \qquad (8)$$

It is observed that the initial penetration rate is independent of the hydrodynamic coefficient of friction as there is yet no interface between the jet and the kerf. This frictional interaction can also be neglected over a certain kerf depth in some cases where the effect of material resistance to flow is much greater in magnitude than the shear force between the jet and the material. This condition can be realized when cutting medium-strength homogeneous materials such as plastics, or when the depth of cut is small for a wide range of materials. In these cases, the depth of cut can be obtained simply by multiplying the initial penetration rate by the time of exposure t = d_n/U. The resulting hyperbolic depth of cut versus traverse rate is

$$\frac{h_i}{d_n} = \frac{2P - \sigma_y}{\eta U} \qquad (9)$$

The second critical traverse rate u2 that allows both use of equation (9) rather than the more complicated exponential formula given in Equation (1) and a maximum overestimation error of 10% in depth of cut is given by

$$u_2 = \frac{K}{1.1(1 - e^{-K/u_2})} \qquad (10)$$

where

$$K = \frac{4C_fP}{\sqrt{\pi}\eta}$$

Equation (10) is obtained by putting h_i = l.lh and substituting from Equations (1) and (9) for h and h_i, respectively. Figure 2 shows such an approximation. Solution of Equation (10) gives u_2 as

$$u_2 = 0.194\frac{4}{\sqrt{\pi}}\frac{C_fP}{\eta} = 0.43\frac{C_fP}{\eta} \qquad (11)$$

This equation indicates that Equation (9) can be used to predict depth of cut with acceptable accuracy when the nondimensional number $C_f P/\eta U$ is smaller than 2.32. However, no advantage is gained by this simplification as the coefficient of friction is still needed in Equation (11) to determine whether Equation (9) can be used or not. One way to overcome this difficulty is to conduct linear experimental cuts at gradually increasing traverse rates. This is done until the damping coefficient calculated from Equation (9) and the experimental results remains unchanged with increasing traverse rates. This procedure will serve two purposes: (1) it will determine the damping coefficient required in either Equation (1) or Equation (9) and (2) it will determine which equation to use, (1) or (2), by comparing the experimentally determined critical rate u2 to the required range of traverse rates for the investigation.

The hyperbolic relationship between depth of cut and traverse rate has been observed in some investigations ([7], [8]). Traverse rates in these investigations were higher than the second critical rate as the case when $u_1 = u_2$.

It has been observed that the depth-of-cut/traverse-rate relationship for some materials is hyperbolic over a very wide range of traverse rates. In these materials, as indicated earlier, the coefficient of hydrodynamic friction is irrelevant to the cutting process. Equating u_l from Equation (7) to u_2 from Equation (11), we obtain a condition such that Equation (9) can be used over the full range of traverse rate beyond up. This condition is

$$\frac{2P - \sigma_y}{\sigma_c - \sigma_y} \geq 173 \qquad (12)$$

This condition is realized when the cutting pressure is much greater than the threshold pressure. For example, cutting a material with σ_c = 2000 psi, σ_y = 1500 psi, and P = 40,000 psi will satisfy Equation (12) while cutting such a material at P = 20,000 psi will not. In the first case, Equation (9) can be used to predict depth of cut. In the second case, Equation (1) must be used at least until $U = u_2$.

3.3 Third Critical Traverse Rate U_3

The third critical traverse rate expresses the relative effects of the hydrodynamic penetration stage and the initial stage of penetration by erosion due to the waterhammer phenomenon. The third critical traverse rate U_3 identifies the beginning of the traverse rate range where both penetration stages have to be considered. The depth of cut at traverse rates higher than U_3 will be given as the summation of both effects given by Equations (9) and (4)

$$\frac{h}{d_n} = \left(\frac{2P - \sigma_y}{\eta U}\right) + \frac{M}{1 + s\dfrac{v_c}{c_\ell}} \qquad (13)$$

Equation (13) will be the depth-of-cut prediction equation as long as the terms on the right hand side are of a comparable order of magnitude.

If the second term in Equation (13) is at least 10% of the combined value of both terms, then a traverse rate U_3 can be defined as

$$u_3 = \frac{(2P - \sigma_y)\left(1 + s\frac{v_c}{c_\ell}\right)}{9\eta M} \qquad (14)$$

For materials with low specific gravity and low hardness, the term S(VC/Cg) can be neglected relative to unity. Then

$$u_3 = \frac{(2P - \sigma_y)}{9\eta M} \qquad (15)$$

The traverse rate u_3 in Table 1 is much higher than traverse rates encountered in practical applications for cutting the materials listed. This suggests that the erosion mode of penetration does not take place in the cutting of these materials. u_3 will be within practical cutting speeds of sheet metals or high-strength composites. For example u_3 = 26 fpm at 20,000 psi for polycarbonate.

A plot for the minimum traverse rate (up) for different materials at different pressures is shown on Figure 3. Traverse rates below the plotted values will not increase depth of cut. The data on concrete cutting is from inhouse experimental results using three different nozzle sizes (0.01, 0.015, and 0.02 in.).

3.4 Fourth Critical Traverse Rate u_4

The fourth critical traverse rate u_4 at which the "waterhammer" erosion mode will prevail can be defined similarly to u_3 by bounding the error of neglecting the first term in Equation (13) to a maximum of 10%. This will yield the following expression for u_4:

$$u_4 = \frac{9(2P - \sigma_y)\left(1 + s\frac{v_c}{c_\ell}\right)}{\eta M} \qquad (16)$$

This formula is simplified for light, soft materials to

$$u_4 = \frac{9(2P - \sigma_y)}{\eta M} \qquad (17)$$

The Mach number in the previous equation should be higher than the critical Mach number given by Equation (5). This critical Mach number can be replaced by the critical pressure P_c given by

$$P_c = \frac{\sigma_{yd}^{\;2}}{2\rho_\ell c_\ell^{\;2}}\left(\frac{z_\ell}{z_e} + 1\right)^2$$

This critical pressure is not to be confused with the threshold pressure for hydrodynamic penetration $P_{th} = \sigma_c/2$. Also, the Mach number can be replaced by the pressure in Equations (14), (15), (16), and (17) as $M = (2P/P)^{1/2}/C_l$, $\partial u_l/\partial P = O$. which gives

$$1 = \left(1 - \frac{\sigma_y}{2P_m}\right) \mathrm{Log} \frac{2P_m - \sigma_y}{\sigma_c - \sigma_y}$$

where P_m is the minimum pressure required to result in maximum depth of cut at the critical traverse rate u_l.

3.5 Analytical and Experimental Results

For a given material, the critical traverse rates are functions of the pressure only as shown in Equations (7), (11), (15), and (17). Table 1 lists the different critical rates at different pressures for some materials. (The material properties are also listed in Table 1.) The damping coefficient and the hydrodynamic coefficient of friction were extracted from published cutting data for their corresponding materials. Compressive and yield strength are taken as published or calculated from experimental results. The first and second critical traverse rates are considered to be equal if $u_2 < u_l$ for all materials listed except coal, which implies that Equation (9) will predict cutting results with fair accuracy for these materials. This equation will cover a very wide range of traverse rates, e.g., from 5 to 100 fpm for white granite and almost any traverse rate beyond 19 fpm for red woolten. Additional experimental analysis is required to more accurately determine the critical traverse rates; however, Table 1 gives an order-of-magnitude approximation for these values.

Another observation is the existence of a certain minimum pressure at which the first critical traverse rate u_l will result in maximum depth of cut. This is observed in the white granite results. This observation can also be realized from Equation (7).

C. Optimum Traverse Rates

The existence of optimum traverse rates in jet cutting is associated with some applications such as multipass cutting for maximum depth of cut and parallel linear kerfing for maximum material removal. The optimum traverse rates for these cases will be determined in this section.

4.1 Multipass Cutting for Maximum Depth of Cut

Within a given period of time, there exists an optimum traverse rate and number of passes to achieve maximum depth of cut. (This has been observed by many investigators [15].) The reason for this is associated with the frictional drag imposed on the jet by the cutting kerf. The depth of cut achieved during any pass eliminates wall friction during the next pass over that depth. This is equivalent to replacing wall friction with air friction as the factor that reduces jet effectiveness as a function of the standoff distance. It will be assumed first that the jet will not be affected by air friction and remains coherent over the required cumulative depth of cut.

The relationship between traverse rate and number of passes such that any combination of them results in the same elapsed cutting time is

$$\frac{N}{U} = \text{constant } C \qquad (18)$$

The cumulative depth of cut he after N passes is

$$\frac{h_c C_f}{d_n} = \frac{N\sqrt{\pi}}{2}\left(1 - \frac{\sigma_y}{2p}\right)\left(1 - e^{\frac{-4}{\sqrt{\pi}}\frac{C_f P\beta_i}{\eta U}}\right) \qquad (19)$$

Substituting for N in Equation (18) for that in Equation (19), differentiating h_c with respect to U. and equating the result to zero gives an optimum traverse rate of infinity. For all practical purposes, this means that both the traverse rate and number of passes should be as high as possible. However, as the traverse rate becomes very high, the mechanism of penetration changes from the hydrodynamic mode to the erosion mode, which results in very small depth (pit) of cut. In order to maintain the dominance of the hydrodynamic mode of penetration without it being affected by wall friction, the traverse rate should be kept between the second and third critical traverse rates.

The cumulative depth of cut required will determine the ratio N/U. Any selected value for U between u_2 and u_3 will consequently yield the number of passes as expressed by

$$N = \frac{h_c}{d_n}\frac{\eta U}{2P - \sigma_y} \qquad (20)$$

The transition in the cutting mode must be considered in a computer program in order to more accurately determine the optimum traverse rate and number of passes for this case.

This is avoided here since a simple equation, such as Equation (20), with reasonable supporting logical argument, provides sufficient accuracy and can be easily used. When the depth of cut required is beyond the jet coherent range, the effect of standoff distance on depth of cut as given by Equation (2) must be considered. In this case, no explicit forms for the optimum traverse rate and number of passes can be given. If the initial standoff distance is x_l and the depth of cut after the i^{th} pass is h_i, then the standoff distance after N passes is $x_{N=l}$ where

$$x_{N+1} = x_1 + \sum_{i=1}^{i=N}\frac{h_i}{x_c} \qquad (21)$$

This equation is normalized for convenience by dividing by x_C

$$\left(\frac{x}{x_c}\right)_{N+1} = \frac{x_1}{x_c} - \sum_{i=1}^{i=N}\frac{h_i}{x_c} \qquad (22)$$

The depth of ratio hi/xc can be expressed by using Equation (2) as

$$\frac{h_i}{x_c} = \frac{0.297}{c_f\sqrt{R}}\sqrt{\left(\frac{x}{x_c}\right)_i}\,\psi_i^{2/3}\left(1-\frac{\sigma_y}{2P\beta_i}\right)\left(1-e^{\frac{-4}{\sqrt{\pi}}\frac{c_f P\beta_i}{\eta u}}\right) \qquad (23)$$

The cumulative depth of cut after N passes is given by

$$\frac{h_c}{x_c} = \left(\frac{x}{x_c}\right)_{N=1} - \left(\frac{x}{x_c}\right)_1 \qquad (24)$$

A computer program was written for the recurrence relationship Equations (22), (23), and (24) to predict the cumulative depth of cut h_c. A sample of the predicted, theoretical, and experimental results for poplar cutting is shown on Figure 4 along with the cutting parameters used. Each dotted line represents an equal elapsed cutting time. The dotted curve on the top represents more cutting time than the curves below. The following observations are emphasized:

A. No optimum for the U/N curve is observed for small cumulative depth of cut. The jet in this case is still coherent over the total depth of cut. As discussed earlier, the cumulative depth of cut achieved within a given period of time remains constant for any combination of U and N as shown by the lowest dotted line.

B. The existence of an optimum U and optimum N is observed for more exposure time and consequently more cumulative depth of cut. However, increasing both U and N beyond the optimum does not significantly change depth of cut. This is due to the less pronounced effect of wall friction and the shift of traverse rate into the region between u_2 and

C. The cumulative depth of cut achieved at eight passes and a traverse rate of 0.396 cm/sec is about 40% greater than that achieved at two passes and a O.O99-cm/sec traverse rate.

Both cases represent an equal exposure time. This case is represented by the top dotted line, which also shows a decreasing tendency beyond the optimum as the range of traverse rates still below u_2.

4.2 <u>Parallel Kerfing for Maximum Volume Removal Rate</u>

It has been observed ([5], [16], [17]) that the material between two parallel kerfs is either automatically removed or can be removed with very little additional power expenditure when the ratio of the depth of cut h to kerf spacing y has a minimum value r. Mathematically, this is expressed as

$$h/y \geq r \qquad (25)$$

The ratio r depends on the material and the angle of the jet Φ as shown on Figure 5. In this analysis, a single-pass cut is assumed with Φ = 90°. The rate of volume removal equals

$$\Delta v = h \;\; y \;\; U = \frac{h^2}{r} U \qquad (26)$$

Expressing h in Equation (1) as

$$h = k_1\left(1 - e^{-K/U}\right) \qquad (27)$$

where

$$K_1 = \frac{2}{\sqrt{\pi}} \frac{d_n}{C_f} \left(1 - \frac{\sigma_y}{2P}\right)$$

$$K = \frac{4}{\sqrt{\pi}} \frac{C_f P}{\eta}$$

Substituting from Equation (27) into Equation (26), the result is

$$\Delta v = \frac{k_1^2 u}{r} \left(1 - e^{-K/U}\right)^2 \qquad (28)$$

This equation has a maximum value when U is given by

$$U = 1.797 \frac{C_f P}{\eta} \qquad (29)$$

This optimum traverse rate is independent of the r ratio and is a function of the pressure only for a given material. It is also observed that this traverse rate is greater than the second critical traverse rate given by Equation (11). Therefore, it is expected that the depth of cut and kerf spacing will be small for medium-strength rocks. Accordingly, the advantage gained by cutting at the optimum rate will be better realized in cleaning applications where only a thin layer of material is to be removed. For deep kerfing, combined multipass-spaced cutting will be desirable. An example of such a procedure is given in the literature [15] for coal cutting. In that procedure, Equations (22), (23), (24), and (26) are used in a computer program to obtain the critical traverse rate which can not be expressed explicitly.

The specific energy, defined as the energy required to remove the unit volume, has a minimum value at the defined optimum critical speed. This minimum specific energy can be further reduced by operating at the optimum pressure. In order to determine that optimum pressure, the rate of volume removal is expressed first by substituting from Equations (29) and (11) into Equation (26)

$$\Delta v = 0.556 \frac{\left(2P - \sigma_y\right)^2 d_n^2}{\eta C_f \, Pr} \qquad (30)$$

The energy E required to drive n jets at pressure P to remove (N-1) Δv is given by

$$E = \frac{n\pi}{2\sqrt{2\rho}} d_n^2 P^{3/2}$$

The specific energy SE is then expressed as

$$SE = K_3 \frac{N}{N-1} \frac{P^{5/2}}{(2P - \sigma_y)^2} \qquad (31)$$

where

$$K_3 \quad \frac{2}{\sqrt{\rho}} C_f \eta r$$

Differential calculus on Equation (31) yields the optimum pressure as

$$p = \frac{5}{2} \sigma_y \qquad (32)$$

The minimum possible specific energy at the optimum pressure and traverse rate is

$$SE_{min} = 8.784 C_f \eta r \frac{N}{N-1} \sqrt{\frac{\sigma_y}{\rho}} \qquad (33)$$

Again, the minimum specific energy obtained from Equation (33) can be reduced by multipass cutting.

D. Experimental Observations

Experimental observations on the spaced cutting of coal have been reported earlier [18]. The minimum specific energy observed using two parallel jets spaced 7 cm apart, 15,000-psi pressure, and 0.3-mm nozzle diameters was 58 J/cm^3 for a single pass, l-cm/sec traverse rate. This value agrees with the predicted 11% underestimation obtained using Equation (31). The minimum possible specific energy as given by Equation (33) is listed in Table 2 for some materials assuming that r=l, N=2, and the material between the two parallel kerfs will be removed simultaneously. The minimum possible specific energy for western Canadian coal is 31 J/cm^3 [18]. This value is approximately half the observed value mentioned earlier. Full optimization around pressure, nozzle spacing, number of passes, and traverse rate is possible using the equations developed in this analysis.

6. Conclusions

A. Critical traverse rates have been identified to select the relevant cutting equation in terms of the cutting mechanism or the dominant material properties.

B. If $U < u_l$ use Equation (6) to predict depth of cut
If $u_l < U < u_2$ use Equation (1) to predict depth of cut

If $u_2 < U < u_3$ use Equation (9) to predict depth of cut
If $u_3 < U > u_4$ use Equation (13) to predict depth of cut
If $U > u_4$ use Equation (3) to predict depth of cut

C. A scheme to determine the optimum traverse rate is presented for the case of multipass cutting.

D. The optimum traverse rate for parallel spaced cutting is determined for minimum specific energy application.

E. The observed critical and optimum traverse rate phenomena agree with experimental data; however, limited experimental results are used for comparison.

7. References

[1] Hashish, M., "Theoretical and Experimental Investigation of High Velocity Waterjet Cutting," Ph.D. Thesis, Concordia University, Montreal, Canada, 1977.

[2] Hashish, M., and duPlessis, M. P., "Theoretical and Experimental Investigation of Continuous Jet Penetration of Solids," ASME Paper No. 77-WA/PROD-38, November 1977.

[3] Hashish, M., and Reichman, J., "Analysis of Waterjet Cutting at High Traverse Rates," Fifth Int. Symp. on Jet Cutting, BHRA, June 1980.

[4] Hashish, M. and duPlessis, M. P., "Prediction Equations Relating High Velocity Jet Cutting Performance to Standoff Distance and Multipasses," ASME Paper No. 78-WA/PROD-ll, December 1978.

[5] Hamada, H., et al., "Basic Study of Concrete Cutting by High Pressure Continuous Jets," Second Int. Symp. on Jet Cutting, BHRA, April 1974.

[6] Cooley, C., "Rock Breakage by Pulsed High Pressure Waterjets," First Int. Symp. on Jet Cutting, BHRA, April 1972.

[7] Reichman, J. and Cheung, J., "Research and Development of a High Pressure Coring Device for Geothermal Exploration and Drilling," Fifth Int. Symp. on Jet Cutting, BHRA, June 1980.

[8] Hashish, M., "Experimental Results of Wood Cutting Using High Energy Waterjets," Report FC-0074, Concordia University, Montreal, Canada, August 1974.

[9] Summers, D. A. and Peters, J. F., "Preliminary Experimentation on Coal Cutting in the Pressure Range 35 to 200 MN/m2," Second Int. Symp. on Jet Cutting, BHRA, Cambridge, England, April 1974.

[10] Moodie, K. and Arlingstall, G., "Some Experiments on the Application of High Pressure Waterjets for Mineral Excavation," First Int. Symp. on Jet Cutting, BHRA, Coventry, England, April 1972.

[11] Mohaupt, U. H. and Burns, D. J., "Machining Unreinforced Polymers with High Velocity Waterjets," Experimental Mechanics, Vol. 14, No. 3, pp. 152-157, April 1974.

[12] Hurlburt, G. H., Crow, S. C. and Lade, P. V., "Experiments in Hydraulioc Rock Cutting," Int. Journal Rock Mech. Min. Sci. & Geomech. Abstr., Vol. 12, pp. 203-212, 1975.

[13] Labus, T. J., "Energy Requirements for Rock Penetration by Waterjets," Third Int. Symp. on Jet Cutting, BHRA, Chicago, May 1976.
[14] Harris, H. E. and Mellor, M., "Penetration of Rocks by Continuous Waterjets," Second Int. Symp. on Jet Cutting, BHRA, Cambridge, England, April 1974.
[15] Summers, D. A., "The Effect of Change in Energy and Momentum Levels on the Rock Removal Rate in Indiana Limestone," First Int. Symp. on Jet Cutting, BHRA, April 1972.
[16] Frank, L. and Lohn P. D., "Fragmentation of Native Copper Ore with Hydraulic Jets," Second Int. Symp. on Jet Cutting, BHRA, April 1974.
[17] Nikonov, P. G. and Goldin, A. Y., "Coal and Rock Penetration by Fine, Continuous High Pressure Waterjets," First Int. Symp. on Jet Cutting, BHRA, Coventry, England, April 1972.
[18] DuPlessis, M. P. and Hashish, M., "Experimental and Theoretical Investigation of Hydraulic Cutting of a Western Canadian Coal," Fifth Int. Symp. on Jet Cutting, BHRA, 1980.

Material	Ref.	P = 20,000 psi				P = 40,000 psi				P = 50,000 psi			
		u_1	u_2	u_3	u_4	u_1	u_2	u_3	u_4	u_1	u_2	u_3	u_4
Coal	9	3.66	5.4	800	very large	6.31	10.81	1138	very large	7.56	13.51	1274	very large
Red Woolen	10	19.19	19.19	2000	very large	29	29	2970	very large	33	35	3300	very large
Polycarbonate	11	0.38	0.38	26	2000	0.51	0.4	39	3200	0.58	0.5	44	3600
White Granite	12					5.23	5.23	143	very large	5.65	5.65	160	
Wilkenson Sandstone	12	11.2	11.2	52.5		15.8	15.8	749		18	18	83	
Limestone	13	0.19	0.19	22	1790	0.27	0.27	31	2500	0.31	0.31	35	large
Indiana Limestone	14	1.13	1.13	168		1.73	1.73	240		2	2.14	269	

U in fpm

Table 1. Critical Traverse Rates in ft/min. for Different Materials at Different Pressures

Material	Reference	Minimum Specific Energy, J/cm^3
Coal	[9]	70
Coal	[18]	31
Indiana Limestone	[14]	275
Red Woolten	[10]	34

Table 2. Minimum Specific Energy Values for Single-Pass Cutting Using Two Spaced Nozzles

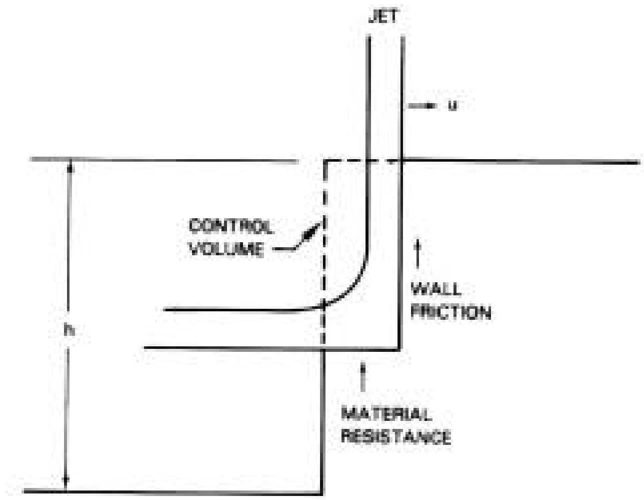

Figure 1. Control Volume of Jet Penetration

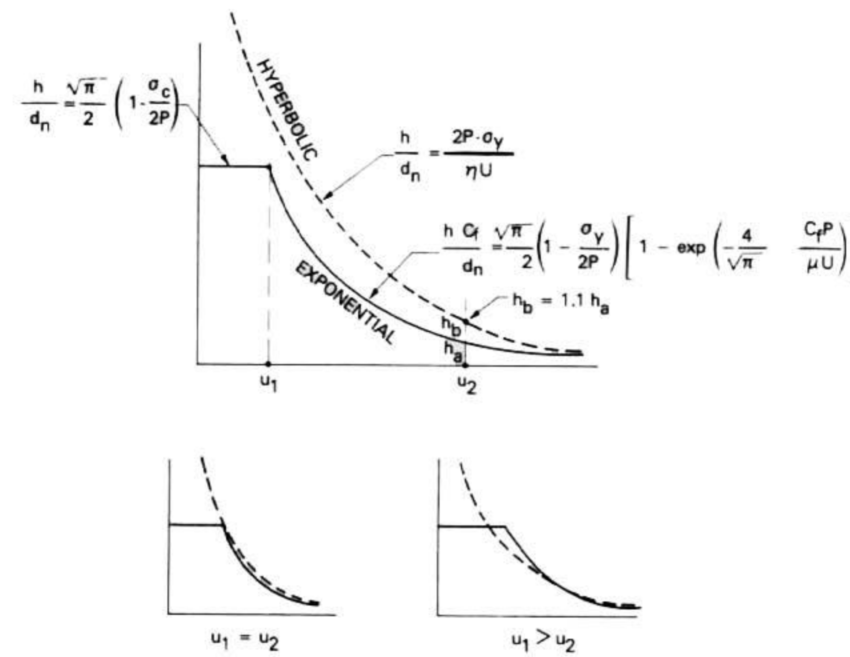

Figure 2. First and Second Critical Traverse Rates

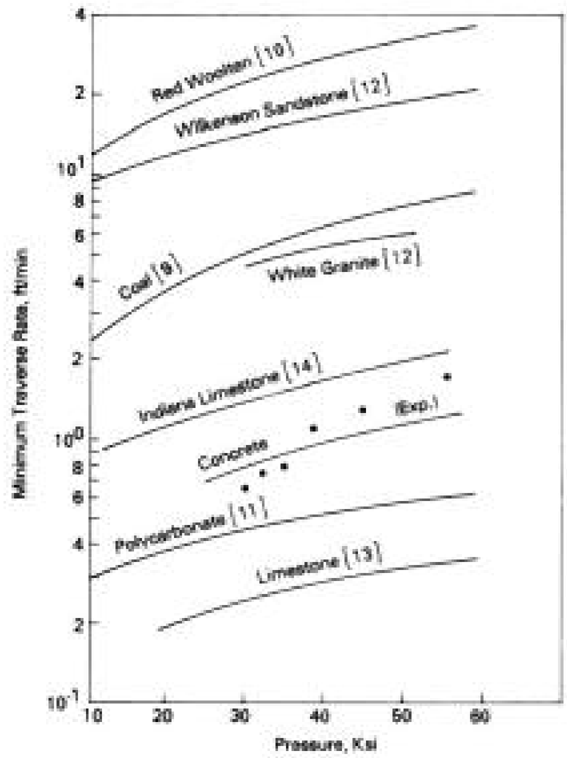

Figure 3. First Critical Traverse Rate for Some Materials

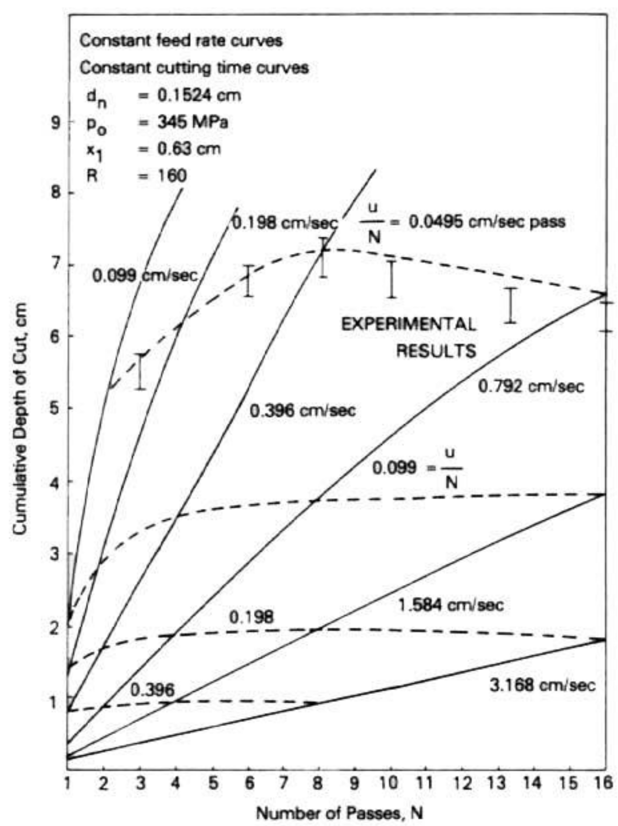

Figure 4. Effect of Multipasses and Traverse Rate

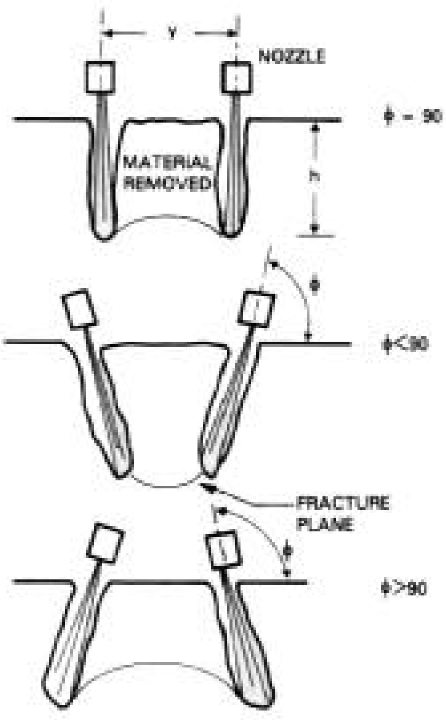

Figure 5. Different Nozzle Arrangements on Depth of Cut for Poplar for Parallel Kerfing

AN EXPERIMENTAL STUDY OF WATER ASSISTED DRAG BIT CUTTING OF ROCKS

O. Dubugnon, M.D.
Institut CERAC SA.
1024 Ecublens
Switzerland

ABSTRACT

It has been known for some time that water jets of moderate pressure (below 100 MPa) are effective in assisting drag bit cutting of rocks. Provided that they are directed onto a rock region close to the tool tip, the water jets lead to a substantial reduction of the tool forces. The actual physical process underlying this effect is still poorly understood, so that the technique has not yet been optimized.

In order to better understand the action of such water jets, an experimental investigation was made in the laboratory. A linear cutter capable of a cutting force of 10 tons was used to cut 50 x 50 cm blocks of granite, sandstone and limestone. The drag bit cutter was installed on a biaxial dynamometer in order to measure the cutting and thrust forces, calculate their average and peak values and deduce the influence of the water jets. Two nozzles were installed such that the jets were alternatively directed to the side or in front of the tool. The water was supplied by a commercially available 25 kW pump, generating pressures up to 100 MPa.

It was found that the power ratio between the jets and the tool and the rock type play a dominant role in the process, while the tool geometry and the jet arrangement are less important. The fact that rather low pressures can still reduce the tool forces and the observation of the rock surface after tests made at higher pressures, suggest that several distinct phenomena occur: one of them is the erosion of the crushed material situated between the tool and the rock, already at low pressure. At a higher pressure the water is injected into the cracks driven by the tool, producing a hydraulic fracturing effect. In addition, the rock surrounding the tool tip is highly stressed so that inelastic dilatancy generates a large increase of pore volume. The pressurization of this porosity by the water undoubtedly reduces the rock strength.

INTRODUCTION

There are two basic limitations to a generalized application of the present mechanical rock excavation techniques. One is the rock hardness and abrasively, the other is the resulting inflexibility of the machines designed to excavate hard rocks. Relatively light and flexible machines, like Roadheaders, can be used in soft rock formations. Their drag bit cutter tools, however, are very sensitive to the rock hardness and abrasivity. In hard rock formations, it is necessary to use roller disc cutters which require, in that case, a heavy and inflexible frame able to feed the large thrust force needed to maintain the penetration. Such TBMs, although very effective are cumbersome and difficult to install, so that they can only be used economically for rather long tunnel projects.

There is, however, a great need for light and flexible machines able to excavate hard rocks for short tunnels and particularly in mines, where down-the-hole installations are often required for a large number of utility tunnels. There are at present no indications that a new material, such as synthetic diamonds, could replace advantageously the hard metal bits on the Roadheaders tools, so that they could cut harder formations. There is also no expected new method of excavation that could replace successfully the actual TBMs in the near future. In that respect, the only technology that could be envisaged at the moment to improve the performance and reduce the weight of the existing machines is the assistance with high pressure water jets. Both laboratory and field experiments have been carried out since 1974 and have demonstrated the feasibility of such a technique.

There are two distinct approaches that have been considered in the past : initially studied in USA (1), (2), then in Germany (3), the first approach consists of a separate action of a water jet and a cutter tool. The latter takes advantage of a slot previously kerfed by the high pressure water jet (up to 4 kb), which results in a substantial reduction of the thrust force. The second approach was realized first in South Africa (4) and more recently in USA (5) and consisted in a combined action of a drag bit tool and a water jet of a moderate pressure (below 1 kb).

In view of the important benefit on forces and penetration that was observed with water jets of moderate pressure, it was decided to investigate this method further and to evaluate its potential application to drag bit cutting machines.

The present study consists of laboratory testing of water assisted drag bit cutters. It is concentrated on the low cutting speed concept, that is known to allow the use of a drag bit cutter in harder rock formations than an normally be excavated by the Roadheaders machines (6).The complexity of the water assistance mechanism, in which there are involved two distinct processes, requires that one consider a large number of parameters in the study. In order to maintain the experimental effort at a moderate level, it is necessary to restrict the parameter variations to a minimum. This in turn, generates an inevitable loss of precision, which must be taken into account during the interpretation of the results.

LABORATORY EXPERIMENTS

All the experiments were performed on a linear cutting facility built from an ancient metal shaping machine, able to produce up to 10 tons (~ 100 kN) of thrust and cutting force. Blocks of rock 50 x 50 cm were placed onto an hydraulically powered table moving linearly below a fixed cutting tool. The tool was installed onto a biaxial dynamometer that allowed measurements of thrust and cutting components of the force exerted by the rock on the tool. The corresponding relative displacement, i.e. the movement of the table, was measured by a rotating transducer installed beside the table.

The data were recorded on a digital transient recorder, a Biomation 800, using two channels for the thrust and the cutting forces. The memory, which consists of 2000 words of 8 bits, was directly driven by the displacement transducer, so that the records were reproducible in the form of forces versus cutting distance. Several types of tool and nozzle arrangements were tested. As shown schematically in fig. 1, all the tools were machined with a clearance angle of about 10° and a rake angle of 20°. These angles are dictated by the optimal shape determined for hard rock cutting with TBS. It is, however, possible that other values could be found in the future to be more appropriate to the water assisted cutting. The tool shown on fig. 1A was made of high speed steel (HSS) while the two others shown in fig. 1B and C included a hard metal (HM) inserts. Although only the HM can be considered in practice as a material for drag bit cutters, HSS tools can be used at low speeds (below 10 cm/s) and for short distances during laboratory experiments in which the wear is not considered. As can be seen in fig. 1B and C, the HM tools were machined with a V-shape, which again corresponds to a practical requirement of the application to actual TBMs. Two different tool widths of 14 mm and 35 mm have been tested. The typical wear, although varying during the experiment with HSS tools, corresponded to a wear flat of about 2 mm of width.

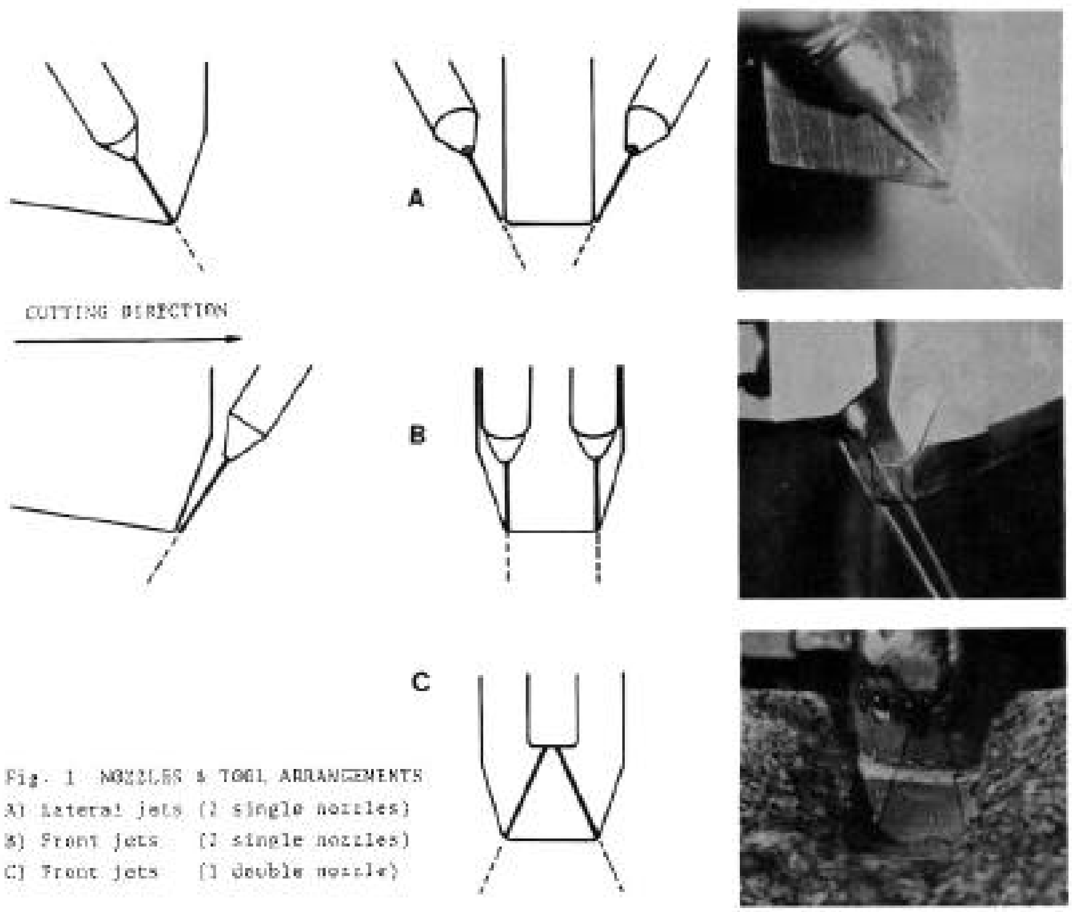

Fig. 1 NOZZLES & TOOL ARRANGEMENTS
A) Lateral jets (2 single nozzles)
B) Front jets (2 single nozzles)
C) Front jets (1 double nozzle)

Because of differences in wear flat between experiments, cuts without water jet were systematically made before each test with water jets, so that the influence of the latter could be well estimated.

The nozzles used to produce the water jets were of two types: the single jet nozzle (SJ), of which the arrangements are shown in fig. 1A and B. was made of steel, with a conical entrance of 13° and a cylindrical output of length equal to 2 to 4 times the output diameter. In order to be able to vary independently pressure and flow in the water jets, a series of 7 pairs of single nozzles were machined with output diameters ranging from 0.4 to 1.6 mm. The second type of nozzle was the double jet nozzle (DJ) of which the arrangement is illustrated in fig. 1C. This nozzle is made with a unique convergent cone of 16° at the entrance and two cylindrical outputs oriented at 30° to each other. It was designed in view of being applied to deep slot cutting, for which the hydraulic system (nozzle and connectors) must not be wider than the tool body. Since it replaces two single nozzles, the double jet nozzle is naturally easier to install in a limited space, as illustrated in fig. 1C (photo of a tool and a double jet nozzle engaged in a deep slot).

Figure 1 also indicates how the different nozzles have been arranged so that the water jets are oriented toward the corner of the tool tip, in a configuration which has been shown by (4) to be the most effective for 2-jets. Two main arrangements were considered: the lateral jets, illustrated in fig. 1A, can be used for cutting the rock surface, as in the case of a Roadheader. The jets, being oriented in the direction of cutting, are in the optimum position to assist the fracturing action of the tool. Due to the large overbreaking of the rock around the tool, the jets have constantly a free access to the region close to the tool tip.

The front jets, on the other hand, are oriented backward as indicated in fig. B and C. Although they might be somewhat less effective than the lateral jets in regard to the chipping action of the tool, their configuration is optimum when the interaction with the tool tip and the crushed zone is considered.

The pressurized water was supplied by a Hammelmann volumetric pump able to produce a flow rate of ~ 25 l/min at pressures ranging from zero up to 1000 b (100 MPa).

Three hard rocks were chosen for testing with regard to their typical mechanical properties:

1) The Hohensyburg sandstone (Germany) is a fine grain, tough, abrasive and porous rock (compressive strength 1.3 to 1.7 kb, porosity 3.5%)
2) The Bohus granite (Sweden) is a medium grain rock, fairly similar to the well-known Westerly granite, regular and homogenous (compressive strength _ 2 kb, porosity 0.6%, grain size 1-2 mm)
3) The Balmholz limestone (Switzerland) is a very tough, silicious limestone, with a very fine grain structure, rather inhomogenous and irregular (compressive strength _ 2.5 kb).

The major portion of the experiments was performed on Bohus granite. The influence of the rock's characteristics was investigated in specific tests with the two other rocks. The experiments were divided into two distinct series. The first one included the main variation of the parameters, with a fixed tool width of 14 mm and corresponds to the results presented in fig. 2 to 8. Except for the test at variable penetration, the cutting depth was fixed to 6 mm, and except for the tests in deep slots implying successive cuts, the experiments of this first series were all made on fresh, intact rock surfaces. The cutting speed, which was observed to have only a small influence on the process, in the range of the values tested here, was varied from 3 to 20 cm/s.

The second series of tests was restricted to a few specific experiments with an actual TBM tool of 35 mm width. In that case the cutting speed was fixed at 15 cm/s, which is the value commonly used in hard rock drag bit cutting with such tools (6).

The measured data are the cutting and the thrust force denoted by Fc and FT, presented in peak and average values directly estimated from the force-displacement records. In fig. 3 to 8 (except fig. 7) and in table 1, the forces are set in terms of relative values, i.e., the ratio in percentage of the force measured with water jets to the force without water jets. The whole program included the following variation of parameters:

6) Cutting depth (with and without water jets):
7) 2 - 8 mm 2) Water pressure: 0 to 850 b
8) Water flow: 0 - 27 l/min
9) Initial depth (deep slot cutting): 0 - 30 mm
10) Nozzle arrangement: A, B and C (fig. 1)
11) Jet tool distance: 0 - 4 mm
12) Tool width: 14 and 3s mm
13) Rock nature: granite, sandstone, limestone

RESULTS OF THE EXPERIMENTS

1) <u>Influence of the cutting depth</u>

In order to measure the effect of the water jets, the forces were first measured without any assistance of water jets at various cutting depths into the Bohus granite. The results presented in fig. 2 indicate how the forces increase with the cutting depth and those of fig. 3 indicate the relative amplitude of the forces when low pressure water jets are used (100 to 180 b). With increasing cutting depth, the benefit on the thrust force increases while the cutting force benefit remains approximately constant.

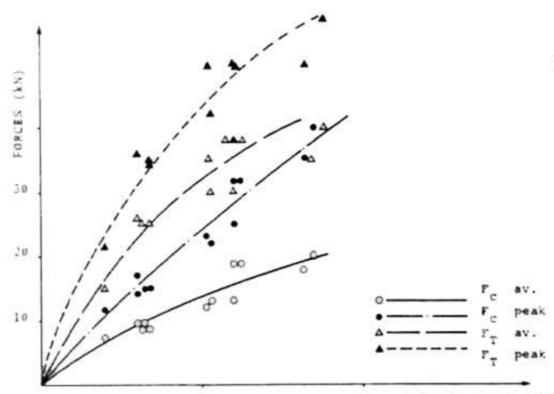

Fig. 2 FORCES VERSUS CUTTING DEPTH, Bohus Granite, dry cutting

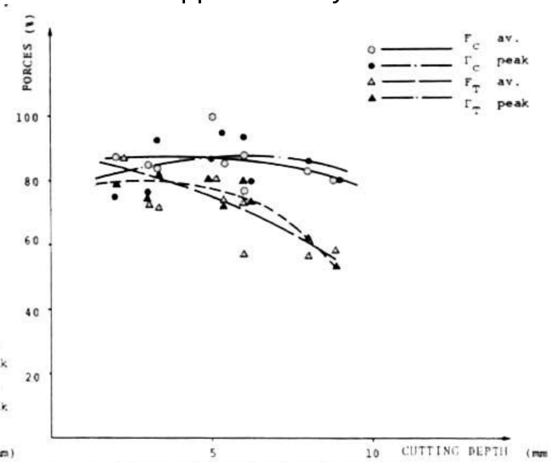

Fig. 3 FORCES VERSUS CUTTING DEPTH (% of dry value) pressure = 100-180 b, flow = 25 l/min, front jets

2) <u>Influence of the pressure</u>

In order to identify clearly the influence of the pressure, the nozzle diameter was chosen, for each value of pressure, in such a way that the flow remained constant (~25 l/min) in all the pressure range. Fig. 4 illustrates the influence of the pressure in the Hohensyburg sandstone, for lateral and front jets (arrangements A and B of fig. 1). It is seen in fig. 4 that both arrangements produce a similar benefit on the forces which turns out to be a progressive reduction of force down to ~ 35% of the dry value at 650 b of pressure. Here, the peak cutting force is less sensitive to water jets and is only reduced to 60% of the dry value.

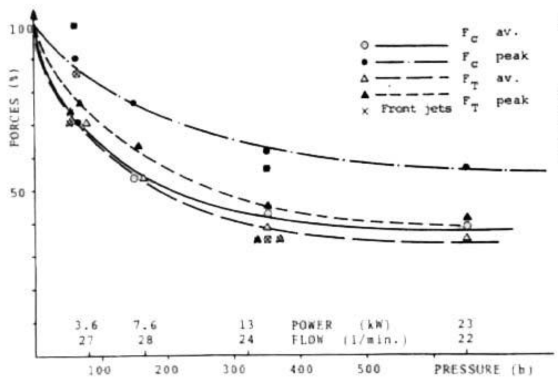

Fig. 4 FORCES VERSUS PRESSURE (% of the dry value), Hohensyburg Sandstone, lateral and front jets, constant flow ~25 l/min.

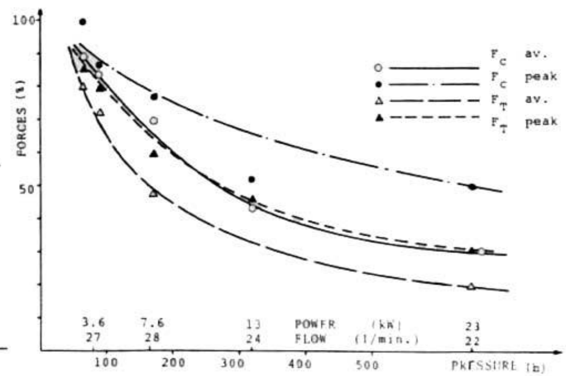

Fig. 5 FORCES VERSUS PRESSURE (% of the dry cut value), Bohus granite, lateral jets, constant flow ~25 l/min

The results of a similar test performed on Bohus granite is shown in fig. 5. Although the initial forces, or dry values, are 1.5 times higher in the granite than in the sandstone, the granite appears to be more sensitive to water jets than the sandstone, and the average thrust force is reduced to 208 of the dry value at a pressure of 650 b. As for the sandstone, the peak cutting force is reduced less than the other forces. It is also observed that in the granite the average cutting force is not reduced in the same way as in the sandstone.

3) <u>Influence of the flow</u>

As for the variation of pressure, it was interesting to separate well the relative influence of the flow by keeping the pressure constant. Figure 6 shows the effect of the flow on the forces for the three nozzle diameters at a constant pressure of 700b, in the granite. Here the two nozzle arrangements A & B of fig. 1 were used. The main information obtained here is that a reduced flow is still able to generate a substantial reduction of force, the thrust force being again the most reduced, down to 40% of its dry value with a flow of only 6 1/min.

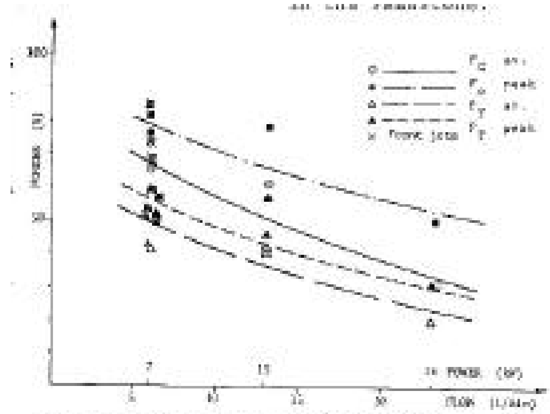

Fig. 6 FORCES VERSUS FLOW (% of the dry cut value), Bohus granite, lateral and front jets, constant pressure ~700 b

4) <u>Influence of the water jets in deep slot cutting</u>

These tests consisted of cutting several times in the same groove, with a constant penetration. These successive cuts are obviously not made onto a fresh, intact surface of rock, so that cumulative damage takes place. Its effect can be measured as a progressive reduction of the relative amplitude of force with the increasing total cutting depth. It can be seen in fig. 7, which corresponds to successive cuts made without water jets, that the forces increase and stabilize when the initial depth (i.e. the total depth of the previous cut) is larger than 10 mm. As a consequence, the increasing benefit on forces observed in fig. 8, which corresponds to the same test made with 850 b water jets through 0.4 mm nozzles, can be interpreted as an effect of the cumulative damage.

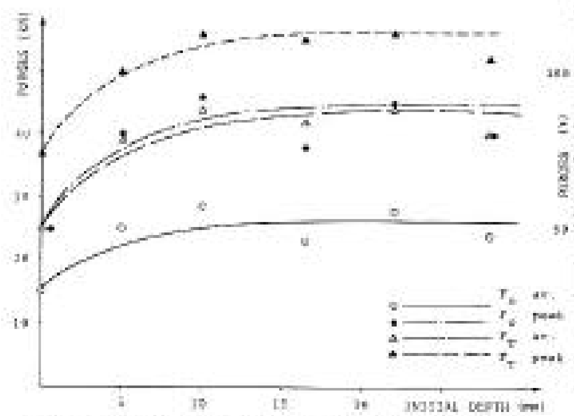

Fig. 7 FORCES VERSUS INITIAL CUTTING DEPTH (successive cuts) ... granite, dry cutting, cutting depth ... mm

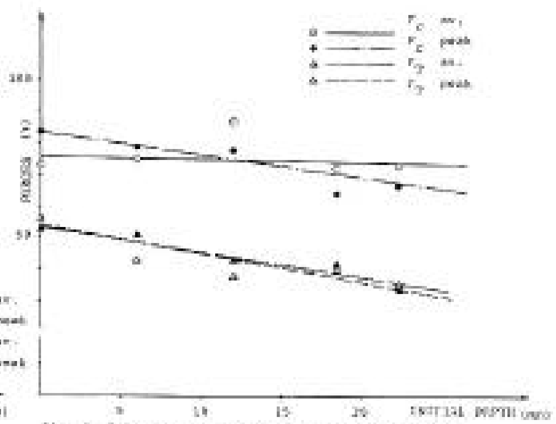

Fig. 8 FORCES VERSUS INITIAL DEPTH WITH WATER JETS (% of the dry value), same other parameters as fig. 7, except pressure 850 b, nozzle diameter 0.4 mm, front jets

This important result indicates that the measurements made on a fresh surface would be pessimistic if a mechanized excavation technique is considered, because, in that case, the rock is constantly submitted to successive cuts. These tests also indicate that the deep slot cutting technique, i.e. the undercutting principle described by (6), is as well suited to be assisted with water jets as the surface cutting technique.

5) <u>Influence of the nozzle arrangement</u>

Considering the three types of nozzle arrangement A, B and C of fig. 1, it has been observed that lateral jets A are slightly more effective than the front jets B. However, they can be used only in surface cutting and are, in general, more difficult to install than the front jets. In addition the front jets C (the double jet nozzle) have proved to be more efficient than the front jets B in deep slot cutting, as indicated in table 1. These differences might be more related to the nozzle efficiency and the jet quality than to the actual jet orientation, so that a definite conclusion cannot be drawn at present. In any case, the jet orientation is not found to have a large influence on the performance of water assisted cutters in the range of pressure and flow considered here.

1) <u>Influence of the jet-tool distance</u>

The results presented in table 1 for the limestone indicate the measured forces in dry cuts and the relative amplitude of the forces measured with the water jets for jet-tool distances ranging from 0 to 4 mm. As already observed by (4) and (5), the optimum position is about 2 mm. Below 4 mm, the jet-tool distance has only a moderate influence on the water jet assistance.

7) Influence of the tool width

The results of table 1 with the granite and the wide tool of 35 mm width, must be compared with those presented in fig. 7 and 8 for the tool of 14 mm width. Both of those tests were made into deep slots and include cumulative damage effects.

Considering, in table 1, the cut into granite with the 2 single jet nozzles (2 x SJ) at 600 b of pressure, the corresponding hydraulic power is about 20 kW. With the narrow tool of fig. 8, 850 b of pressure were used in smaller diameter nozzles, so that the power is here only 8 kW. In both cases, the thrust force is reduced to about 40t of its dry value, so that it can be concluded that the tool width has an influence on the water assistance which is of the same order as the hydraulic power. Because the other parameters such as penetration, cutting speed, water pressure, and tool shape are not perfectly identical between the two cases, this comparison is only approximate. It, however, indicates that the nozzles and the hydraulic system must be designed with regard to the dimension of the tool and the cutting process.

8) Influence of the rock's nature

The rock's nature is one of the most influential parameters. Comparing fig. 4 and 5, it is observed that the granite is more sensitive to the water assistance than the sandstone. A comparison between granite and limestone, from table 1, indicates even a larger difference. Clearly, the limestone is much less sensitive than the granite. This difference is, however, selective: in the limestone the benefit is about the same on both thrust and cutting forces. In the granite the benefit is the largest on the thrust force. Comparing the reduction of forces between the two rocks for the same pressure of 600 b, the 60t reduction of the thrust force in granite is 3 times larger than 205 observed in limestone. This result indicates that the grain structure as well as the failing modes of the rock submitted to a combined action of a drag bit tool and a water jet has a dominant effect on the benefit that can be expected with this technique.

Rock Type	Cutting depth mm	Jet pressure b	Nozzle diameter mm	Nozzle type	Jet-tool distance mm	Fc av/peak kN	Fc rel. av/peak %	Ft av/peak kN	Ft rel. av/peak %
Balmholz									-
Limestone	5	-	-	-	-	44/67	-	40/65	-
"	5.5	-	-	-	-	42/68	-	45/67	-
"	6	-	-	-	-	59/79	-	53/70	-
"	5.5-6.5	800	0.6	DJ	0-1	36/51	61/65	36/50	68/71
"	6.5	800	0.6	DJ	2	35/58	59/73	36/55	68/79
"	5.5-6	800	0.6	DJ	4	38/54	75/73	38/55	78/80
"	5.5-6	600	0.8	DJ	1-2	37/57	73/78	38/55	74/80
"	8.5	800	0.6	DJ	0.1	57/82	-	44/69	-
Bohus									
Granite	4-5	-	-	-	-	54/73	-	72/97	-
"	4-5	600	0.8	DJ	1-2	33/39	61/53	29/37	40/38
"	4-5	600	0.8	2xSJ	0-1	36/42	67/58	30/41	42/43

DISCUSSION OF THE RESULTS

TABLE 1 CUTTING AND THRUST FORCES (abs. value and relative value to dry cutting) for water assisted cutting in Bohus granite and Balmholz limestone. Tool width 35 mm. Initial depth > 20 mm (deep slot cutting). Cutting speed 15 cm/s. DJ = double jet nozzle, SJ = single jet nozzle.

DISCUSSION OF THE RESULTS

1) Basic aspects

The present results contain some information about the mechanism of interaction between rock, tool and water jets. Figure 9 illustrates the cutting process many times observed under dry conditions (7). Due to the brittleness of the rock, a compressive failure occurring in the contact region of rock and tool, produces a fine powder by means of a confined crushing process. This pressurized crushed zone is extended by the propagation of a number of small cracks which either coalesce so as to produce further crushing, or extend suddenly to the free surface, removing a large chip. The propagation of this single crack is to be analyzed by fracture mechanics and is a process significantly different from the initial crushing, which can be treated as a continuum, as long as the numerous cracks are small compare to the tool dimensions.

The action of the water jets, directed as close as possible to the tool tip, is of a multiple nature. Although there is no distinct frontier between them, three main mechanisms can be schematically identified: the erosion of the crushed zone, the hydraulic fracturing, and the dilatant pore pressurization.

The erosion of the crushed zone is made possible by the overbreaking of small chips, that is always present around the tool tip. This is clearly seen during dry cutting, a continuos powder ejection in front of and beside the tool. Since the movement of the tool is parallel to the bottom contact surface of the tip, the thrust force is strongly influenced by the presence or the absence of that cushion of crushed powder. Removing this powder with the water jets as soon as it is formed eliminates a large part of the thrust force. This assumption is strongly supported by the observation that very low pressure water jets (~100 b) can already substantially influence the thrust force, and that a relatively moderate pressure of 800 b eliminates 80t of that same force, especially into granite.

On the other hand, the water injection into the single crack producing the chipping action requires relatively higher pressures to become effective. This hydraulic fracturing is expected to produce an effect on the cutting force, since the latter is mainly produced by the horizontal movement which forces the chip formation. This assumption is well supported by the fact that the peak cutting force is much less influenced by low pressure than the thrust force. It has been also observed that a real hydraulic fracture takes place at the highest pressure in Sandstone, which is the weakest rock of the three tested. In that case, the cutting force, as suggested by the above model of hydraulic fracturing, is almost vanishing.

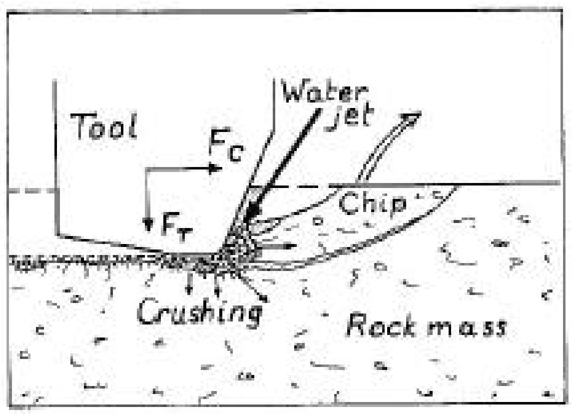

Fig. 9 TYPICAL MECHANISM OF CUTTING, involving crushing failure and fracture propagation, illustrating how the water jet may interact with powder and fracture.

There is a third mechanism which is thought to play a role in the large difference of behavior observed between granite and limestone. The poor benefit observed with the latter must be explained by other considerations than hydraulic fracture, because the fracture toughness of the limestone is, in general, lower than that of the granite. It is well known (8) that the rocks submitted to compressive stresses exhibit a large inelastic dilatation, called dilatancy, which corresponds to a large increase of porosity. This occurs already at only a fraction (less than 50%) of the ultimate fracture strength. It is also known (9) that the pressurization of the porosity directly affects the compressive strength of rocks. In the case of the granite, this dilatancy must occur all around the crushed zone, in a kind of intermediate region between failed and intact material. The dilatancy, due to the opening of microcracks, favors the pressurization of the porosity below the impact of the water jet and consequently can significantly reduce the thrust force required to break the rock further.

This mechanism is of a particular interest in explaining why the limestone is less sensitive to water assistance than the granite. Although the limestone is known to dilate as well as granite under an unconfined compression, it behaves completely differently under a confined state of stress as it exists below a cutting tool. In the limestone, the dilatancy disappears totally when the confining pressure exceeds a transition pressure above which the rock fails in a purely ductile fashion. This plasticity, closing any porosity or microcracking, cannot be directly observed because the final rock breakage relaxes the confinement, allowing a brittle failure accompanied with crushing to occur. Such conditions, however, are met locally below the tool tip so that neither the porosity nor the dilatancy remains open to the water, preventing that a pore pressurization could take place and contribute to the compressive failure. This assumption is supported by the fact that, in the limestone, the thrust force is much less reduced than in granite, while the reduction of the cutting force, more dependent on the hydraulic fracturing effect, is about the same for the two rocks.

Although the relative influences of the three mechanisms described above would be difficult to calculate with an analytical model, it can be already assumed that the erosion and the pore pressurization processes require relatively low pressure (less than 1 kb) to be effective. On the other hand the hydraulic fracturing effect strongly depends on the fracture toughness of the rock. Since, in principle, the cutting tools require water assistance only for cutting tough rocks, it can be expected that a large reduction of cutting force in such rocks will require water jets of higher pressures than 1 kb.

2) Technical aspects

One of the most important factors to be considered in the application of water jets to assist cutting tools is the power which must be added to the cutting system in order to obtain a substantial reduction of force. Using the results obtained in granite (see table 1) as an example, the dry cutting power, at 15 cm/s of cutting speed, would be about 8 kW. The use of 600 b water jets through a double jet nozzle of 0.8 mm output diameter would correspond to an additional power of 20 kW, and a cutting power reduced to about 5 kW. The reduction of thrust force down to 40% of the dry value would then be "paid" by a power equal to 3 times the dry cutting power.

The corresponding specific energy of the rock removal process is dependent on the cutting method. For the undercutting technique used for hard rock drag bit cutting (6), the bench is about 3 times the tool width so that the use of the water assistance described in the above example would correspond to a total specific energy of 300 J/cm^3, which corresponds to 83 kWh/m^3.

It can be expected that the water jets assisted cutting can be optimized and that the required power ratio might be greatly reduced in the future, especially if higher cutting speeds can be used. It is, however, still not clear if it could reach an economical level, because the investment required for a more sophisticated technology as well as the installed power supplies are important in tunneling operation, and also because the energy price of the excavated cubic meter is not negligible.

Another unknown is the applicability of water jets to Roadheaders types of machines, on which the cutting speed is more than 1 m/s. Since our experiments, as well as the previous works (4) and (5), were carried out at cutting speed of an order of magnitude lower, it would be hazardous to simply extrapolate the present results to the application of water jets to such machines. The success of applying water assistance to fast drag bit cutters depends on the sensitivity of the various mechanisms involved to the cutting speed. If a similar benefit as what is observed at low cutting speed could be obtained at more than 1.5 m/s, the contribution of the water power to the specific energy would be divided by ten. In such conditions, the method would not be more costly in energy than the dry cutting itself and would become very attractive.

REFERENCES

1) Wang, F.D., Robbins, R. and Olsen, J. "Feasibility study of hydraulic jet kerfing to improve the efficiency of mechanical disc cutting", Report No. DOT-TST-75-66, Excavation engineering and earth mechanics Institute, Colorado school of Mines, Golden, Colorado, sept. 1974

2) Wang, F.D., Robbins, R. and Olsen, J. "Water jet assisted tunnel boring" Proc. 3rd Int. Symp. on jet cutting Technology, Chicago, may 1976

3) Henneke, J. and Baumann, L. "Jet assisted tunnel boring in coal-measure strata". Proc. 4th Int. Symp. on Jet cutting Technology, Chicago, may 1978

4) Hood, M. "Water jet assisted drag-bit cutting of hard rock", Research Review Chamber of Mines of S. Africa, 1975-76

5) Wang, F.D., Apl. and Wolgamott, J. "Application of water jet assisted pick cutter for rock fragmentation", Proc. 4th Int. Symp. on Jet cutting Technology, Chicago, may 1978

6) Barendsen, P. and Cadden, R.G., "Machine-bored small-size tunnels in rock, with some case studies", Proc. Tunnelling 76, The Institution of Mining and Metallurgy, London, 1976

7) Gehring, K. "About principles of chip formation from rock treatment with cutting tools" 3rd Int. Congress on Fracture, Munich, 1-3 Apr. 1973

8) Brace, W.F., Paulding, W.B. and Scholz, C. "Dilatancy in the fracture of crystalline rocks" J. Geophys. Res., 71(16), 3939-3953, Aug. 1966

9) Nur. A., and Byerlee. J.D. "An exact effective stress law for elastic deformation of rock with fluids. J. Geophys. Res., 76, 6414-6419, 1971

HYDRAULIC FRAGMENTATION IN THE U.S.A.

Jacob N. Frank[1]
Office of Surface Mining
818 Grand Avenue
Kansas City, Missouri 64106

ABSTRACT

In the United States, hydraulic mining or "hydraulicking" was first developed in California in 1852 to excavate gold bearing gravel banks by streams of pressurized water from giants or monitors. Modern hydraulic mining of consolidated minerals in underground mines in the United States was started by the American Gilsonite Company at Bonanza, Utah, in 1949. Extensive research is being carried out throughout the United States on the disintegration of rock, mineral, and coal by water jets. Universities, institutes and government agencies are engaged in hydraulic fragmentation programs.

The U. S. Bureau of Mines has conducted research in hydraulic mining and fragmentation since 1958. This research has covered the spectrum of low pressure-high volume to high pressure-low volume and includes various commodities such as coal, uranium-bearing sandstones, phosphates, tar sands, and other rocks and minerals. Currently, the Bureau is involved in research directed at determining the feasibility of using water jets for mining phosphates. Other federal agencies: the Department of Energy, the National Aeronautics and Space Administration, the National Science Foundation, and the Office of Surface Mining are active in hydraulic fragmentation projects.

INTRODUCTION

We can observe in nature, water as a means of extracting minerals from the earth. The presence of gold in stream beds, uranium as roll front deposits in ancient stream beds, and the decomposing and pulverizing of rock into soil indicate that the effect of water upon rock is one of the most effective long-term erosion agents. Some of the most impressive phenomena of this erosion are the Grand Canyon, the wind and water erosion in the Badlands of South Dakota, Wyoming, Colorado, Utah, and Arizona.

The first recorded use of water in the mining industry dates back to 4,000 B.C. when the Ancient Egyptians used water for the separation of gold (41). Pliny, an Ancient Roman, describes how the Romans transported water great distance, stored it in 100,000 cubic meter reservoirs, then released it so that it was discharged down the slopes washing valuable minerals with it into valleys where the minerals could be separated and treated (24). Little change in this concept took place for hundreds of years. This method of storing and releasing of water was used in the gold fields of California to wash soil and gold down slopes where the specific gravity of different materials segregated the gold from the rest of the material. This was known as

[1] Formerly of the U. S. Bureau of Mines. Disclaimer: The views and conclusions contained in this document are those of the author and should not be interpreted as necessarily representing the official policies of recommendations of the Interior Department's Bureau of Mines, the Office of Surface Mining, or of the U.S. Government.

"booming," from the noise the water made as it was released and traveled down the slopes.

In the sixteenth century, Agricola (1) spoke of hydraulic mining being used in mining small alluvial deposits. This method was used in mining the clay deposits of Cornwall, England, where it is used to this day. Mechanically powered hydraulic mining began in 1852 at Gold Bluff, California, where it was used to excavate gravel banks. Streams of pressurized water from "giants" or "monitors" were used to wash down the gold-bearing gravel banks (3). In Central Prussia, mechanically powered stream of water were used to flush peat into iron flumes and to transport the peat by hydraulic current. In 1867, hydraulicking was used to mine the placer mines of Lake Baykal in Russia and in 1891 it was used in New Zealand to mine coal. The early use of hydraulicking in the United States, Russia, and New Zealand was confined to surface mining and it is still being used in open pit and overburden removal in some areas of the world. One of the most recent examples is the use of large water jets to remove the overburden at a large open pit copper mine in Bougainville of the Solomons Islands in the South Pacific.

Modern jet cutting techniques contribute to the solution of problems, not only in the fields of mining and quarrying, but also an extensive and increasing range of cutting operations in other industrial processes where the requirement is to cut accurately, quickly, cleanly, and with minimal wastage.

In 1928, droplets of water were observed causing erosion of the blades in steam turbines. By the 1940's and 50's, a considerable amount of research had been conducted and pursued in the 60's on the erosion and damage to steam turbine blades by water droplets, and this work was carried on into erosion and damage to high speed aircraft and missiles, and laboratory techniques were developed to produce water droplets and to prove the effectiveness of protective covering for aircraft and spacecraft.

Hydraulic mining and water jet cutting has been used in almost every area of the world.

U. S. BUREAU OF MINES

The Bureau of Mines has conducted research in hydraulic mining since 1958 (4). After a literature survey and visits by Bureau personnel to observe the National Coal Board's experimental program in England and the Gilsonite operation in Utah, the Bureau began investigations to determine the equipment, environmental conditions, and the parameters for hydraulic mining of coal beds varying in dip, thickness, and hardness (5, 39). Eight hydraulic coal mining research programs were completed; six in bituminous coal beds and two in anthracite coal beds. The hydraulic coal mining experiments were conducted at the following locations:

1. West Lebanon, Pennsylvania (12)
2. Roslyn No. 9 Mine, Washington (22)
3. Roslyn No. 10 Mine, Washington (25)
4. Thomson Creek Mine, Carbondale, Colorado (23)
5. Sugar Notch Mine, Pennsylvania (5, 20)

In addition, hydraulic cutting work has been carried out on concrete (14) at Sugar Notch, Pennsylvania; frozen gravels at Sugar Notch and at the Army Cold Regions Research and Engineering Laboratory Tunnel, Fox, Alaska; cemented gravels at Badger Hill, California; cutting of native copper at the Twin Cities Mining Research Center (16), thermohydraulic work at White Pine Copper Company, Michigan, dust generated during the cutting of coal with water Jets (19), augmented hydraulic-mechanical cutters at the Bruceton Experimental Mine, Bruceton, Pennsylvania rotating water jet experiments in a borehole (30), determining the force exerted by jet impact at different standoff distances at the Twin Cities Mining Research Center (29), and water jet perforation of well casings for uranium leaching wells in Wyoming and Texas (28).

In connection with the above work, a contract program has also been conducted. A partial list of those contracts are:

1. Hydronautics, Inc., Laurel, Maryland: Develop a coal cutter using cavitating water jets (7, 8).
2. University of Missouri-Rolla, Rolla, Missouri: Develop and field test a longwall water-jet mining machine and evaluate and analyze test results (35).
3. Scientific Associates, Inc., Santa Monica, California: Develop and test a practical percussive water jet.
4. Ingersoll-Rand Research Corp., Princeton, New Jersey: Study of water-jet continuous mining system (37).
5. Colorado School of Mines, Golden, Colorado: Design, fabricate and test four high-pressure, high-flow intensifiers (10).
6. FMC Corporation, San Jose, California: Develop a concept for a chock mounted jet miner, provide an economic analysis for the system, and develop a cost estimate for a working model (11).
7. TRW Systems, Inc., Redondo Beach, California: Develop a nozzle design which will maximize the distance at which jet issuing from the borehole mining tool can fracture rock (18).
8. Flow Research, Inc., Kent, Washington: Field test a hydraulic borehole mining apparatus for remote extraction of coal (6).
9. Terraspace, Inc., Rockville, Maryland: Survey of world hydraulic mining technology (9).

Other work that has recently been performed for the Bureau of Mines involves hydrominers, the hydraulic jet drilling of rock bolt holes, and borehole mining.

The Hydrominer, a longwall water jet mining machine, has been developed at the University of Missouri-Rolla. Hydrominer One was tested in an open pit coal mine to determine the feasibility of the concept. A second version of the hydrominer was then built and partially tested in artificial coal (32, 34, 35).

OTHER FEDERAL AGENCIES' WORK

U. S. Energy Research and Development Administration

Several techniques for using water jets to cut deep-kerfs in rocks were tested. Rotating, oscillating, and linear cutting experiments were performed. A physical model was developed for an oscillating or rotating deep-kerf device (26).

A water jet drilling system was developed and tested that would allow for the more rapid development of geothermal sources. Three tentative conclusions were determined: (1) the presence of a stress field on a rock will reduce the ability of the water jet to cut the rock; (2) drilling rate and advance rate must be closely coordinated; and (3) the stress field under the jet must be considered in the orientation of the jets so that rock response to the jet action can be exploited (32, 33, 36).

National Science Foundation

The application of jet cutting to a highway maintenance program was examined. Laboratory and field tests were conducted and performance curves were determined for concrete, reinforced concrete, and asphalt overlays. Comparisons were made for jet cutting versus diamond/carbide sawing operations and full depth joint cutting (17).

Sandia Laboratories

A water jet was developed that can be lowered down a vertical well, turned through a 90 degree angle and then advanced horizontally through a coal seam. Surface trials were conducted to demonstrate the feasibility of the concept. Using dual orifice nozzle co-figuration, a hole 15 m long was drilled in less than one hour (31, 33)

National Aeronautics and Space Administration

A water jet cutting device is being developed that will be used to determine the location of the interface between the coal seam and the roof rock. Using a pressure of 70MPa, a 5 cm hole was drilled, the coal core dropped out and the roof rock, containing kerfs, was left in place. An automatic focusing device now can be used to determine the depth of the hole (34).

Department of Energy

Under a contract, abrasive jets were tested to determine the potential benefit of introducing sand to water jets to improve the penetration rate in granite. Improvements in performance were achieved. However, when pressures were increased it was determined that cavitating the jet flow was a more effective means of improving jet cutting ability (32).

Presently, the Department of Energy has three contracts involving hydraulic mining and fragmentation. Two contracts, one with Gulf Resources and Chemical Corporation and one with British Columbia Coal (formerly Kaiser Resources, Ltd.) involve the hydraulic mining of coal. Both contractors are evaluating suitable sites for their research and demonstration projects.

The third contract with Scientific Associates is to demonstrate the feasibility of a scaled up nozzle (0.5 inches in diameter) to produce pulses of water capable of fragmenting coal and rock.

Office of Surface Mining

The Office awarded a grant with the Missouri Mineral Institute at the University of Missouri-Rolla, on determining if the application of the destructive power cavitation erosion can be useful in breaking rock. A new test chamber has been designed and fabricated and testing of multiple nozzles is now being done to determine the parameters of angle of impact and traverse velocity.

CONCLUSIONS

In the 70's, a great amount of research was conducted regarding hydraulic fragmentation and mining. In the 80's, this work should begin to be fruitful in that practical applications will begin to emerge. For those who wish to explore the work done in the 70's, there are two papers (13, 15) and a contract report (9) that cover most of the first half of the decade. A recently published book (21) contains chapters that cover, in excellent detail, abrasive jet drills, cavitating jet drills, high-pressure jet drills (continuous) high-pressure jet drills (pulsed), high-pressure jet assisted mechanical drills, and high-pressure jet borehole mining.

A water jet drill has been developed for the drilling of rock bolt holes. The parameters were determined and the water jet drilling system was tested in the laboratory. It was concluded that a good predictive model for water jet drilling can provide an understanding of drilling behavior (33, 38).

The application of water jet assisted pick cutters was determined by the Colorado School of Mines on coal measure rocks. A reduction of mechanical cutting forces was obtained using water pressures less than the threshold kerfing pressure of the coal measure rocks and a theoretical explanation was developed. The process of the water jet assisted cutting was determined to be a hydrofracturing process instead of a process of cutting the rock directly (40).

An inlet-nozzle device has been designed and laboratory parametric studies of cavitating jets have demonstrated the advantages of cavitating jets over noncavitating jets in cutting coal by Hydronautics Inc. Comparable slot depths in coal have been produced at one-fifth of the operating pressures and at one-half of its specific energy using cavitating jets (8).

An inlet-nozzle device has been designed and tested for the Bureau by TRW Systems and Energy, Inc. for use in the Bureau's borehole mining program. Nozzle designs and sharp-flow turn designs were developed and tested at production and near productive flow conditions (18).

The variation of force extended by jet impact as a function of nozzle design, the concentration of chemicals in the jetting water, and changing jet diameter have been determined at standoff distances from 0.46 to 3.66 meters. The tests resulted in an optimized nozzle design, demonstrated optimum concentration levels for a series of guarand polyacrylic-based additives, and showed that large diameter jets retain a higher portion of their energy than do small diameter jets at a given standoff distance (29).

The technical feasibility of hydraulic borehole coal mining has been demonstrated in work performed for the Bureau by Flow Industries, Inc. (6). The method consists of inserting a hydraulic mining device into a vertical borehole that has penetrated the coal seam. The borehole mining device used a high pressure water jet (28MPa and 760 l/min) to break the coal. A slurry of coal and water was then pumped to the surface. This device was field tested and it was able to mine 32 tons of coal from a depth of 75 feet for a mining rate of 3 tons per hour (27).

The borehole device was next used to mine uranium-ore-bearing sandstone in Wyoming (2). Cutting water jet pressures of 10MPa and flow rates of 5700 l/min were used. A new nozzle and turning vanes developed by TRW Systems and Energy, Inc. were used. During the testing program, ore was cut at horizontal distances out to 25 feet and an average rate of 8 tons per hour. A total of 350 tons of uraniferous ore was mined from a 10-foot-thick seam at depths of 75 to 100 feet (27).

The Bureau has also conducted two other research programs using the borehole mining device. The first was in the oil sands in California. Using a pressure of 10MPa and a flow rate of 1500 l/min, a mining rate of 50 tons per hour was obtained from a depth of 130 feet.

The second program carried out was in-the phosphates of Florida. Using a pressure of 10MPa and a flow rate of 1500 l/min, a mining rate of 40 tons per hour was obtained from a depth of 250 feet.

In-house studies by the Bureau have successfully demonstrated water jet perforation of 40 PCV (polyvinyl chloride) well casing for use in the in situ leaching of uranium. A three nozzle assembly was developed and field tested in 74 applications. Different hole patterns were cut in the casing and well screens of old wells used in leaching were perforated (28).

Recently, the Bureau has completed a program involving the underground hydraulic mining of foundry sands in Iowa. Using a pressure of 6.2 MPa and a flow rate of 1500 l/min, a mining rate of 50 tons per hour was obtained.

The Bureau, at the present time, has an ongoing contract with Terraspace, Inc., to determine if and what metal and nonmetal ores are amenable to underground hydraulic mining.

REFERENCES

1. Agrisola, G., DeRe Metallica, Book 8, 1555
2. Archibald, W.R., Field Test of Hydraulic Borehole Mining Systems in Shallow Uranium Sands. BuMines Contract No. H0272010, Flow Industries, Inc., September 1978, 215 pp.
3. Baker, J.H., Mining by Hydraulic Jet. Min. Cong. J., v. 45, No. 5, May 1959, pp. 45-46, 52.
4. Boyd, W. T., Mining and Transporting Coal Underground by Hydraulic Methods: A Literature Survey. BuMines Info. Circ. 7887, 1959, 33 pp.
5. Buch, J.W., Hydraulic Mining of Anthracite: Engineering Development Studies. BuMines Rept. of Inv. 6610, 1964, 24 pp.
6. Cheung, J.B., et. al. Application of a Hydraulic Borehole Mining Apparatus to the Remote Extraction of Coal. BuMines Contract No. H0252007, Flow Industries, Inc., September 1976, 95 pp.

7. Conn, A.F., and S. L. Rudy. Conservation and Extraction of Energy with the Cavijet. Proc. Fourth Intern. Symp. on Jet Cutting Tech., Caterbury, England, April 12-14, 1978, pp. n2-19 - H2-38.
8. Connt A.F., and S. L. Rudy. Parametric Study of Coal Cutting with the Cavijet Cavitating Water Jet Method. BuMines Contract No. H0252025, Hydronautics Inc., September 1976, 156 pp.
9. Cooleyt W.C., Survey of Underground Hydraulic Coal Mining Technology, BuMines Contract No. H0242031, Terraspace, Inc., 4 volumes, October 31, 1975.
10. Engineering News Record. Jet Mole Team Seeks Tunneling Breakthrough. January 27, 1970, p. 48.
11. FMC Corporation. Water Jet Chock Mounted Miner Feasibility Study. BuMines Contract No. J0155036, September 1975.
12. Fowkes, R.S., and J. J. Wallace. Hydraulic Coal Mining Research: Assessment of Parameters Affecting the Cutting Rate of Bituminous Coal. BuMines Rept. of Inv. 8090, 1968, 23 pp.
13. Frank, J.N. Hydraulic Fragmentation Research in the U.S.A. 46th Annual Meeting of the Minnesota Section of AIME and 34th Mining Symp. of the University of Minnesota, Duluth, Minnesota, January 15-17, 1973, pp. 129-142.
14. Frank, J.N., and J. W. Chester. Fragmentation of Concrete with Hydraulic Jets. BuMines Rept. of Inv. 7572, 1971, 32 pp.
15. Frank, J.N. et al. Hydraulic Mining in the U.S.A. Proc. First Internat. Symp. of Jet Cutting Technology. University of Warwick, Coventry, England, April 5-7, 1972, pp. E4-45-E4-46.
16. Frank, J.N., and P.D. Lohn. Fragmentation of Native Copper Ores with Hydraulic Jets. Proc. Second Internat. Symp. on Jet Cutting Technology. University of Cambridge, Gambridge, England, April 2-4, 1974, pp. H3-29-H3-38.
17. Hilaris, J.A., and T.H. Habus. Highway Maintenance Application of Jet Cutting Technology. Proc. Fourth Internat. Sym. on Jet Cutting Tech., Caterbury, England, April 12-14, 1978, pp. 61-1-61-8.
18. Lohn, P.D. and D.A. Brent. Design and Test of an Inlet-Nozzle Device Proc. Fourth Internat. Symp. on Jet Cutting Tech., Canterbury, England, April 12-14, 1978, pp. Dl-l-Dl-16.
19. Lohn, P.D., and J.N. Frank. Airborne Respirable Dust Generated During Cutting of Coal with Water Jets. BuMines Rept. of Inv. 8014, 1975, 19 pp.
20. Malenka, W.T. Hydraulic Mining of Anthracite: Analysis of Operating Variables. BuMines Rept. of Inv. 7120, 1969, 19 pp.
21. Maurer, W.C. Advanced Drilling Techniques. Petroleum Publishing Co., Tulsa, Oklahoma, 1980, 698 pp.
22. Nasiatka, T.M., and F. Badda. Hydraulic Coal Mining Research: Tests in a Steeply Pitching Coalbed, Roslyn Wash. BuMines Rept. of Inv. 6276, 1963, 16 pp.
23. Palowitch, E.R., and W.T. Malenka. Hydraulic Mining Research, A Progress Report. Min. Cong. J., v. 50, No. 9, September 1964, pp. 63-73.
24. Pliny. Natural History. Book XXXIII, 42, p. 21.
25. Price, G.C., and F. Badda. Hydraulic Coal Mining Research: Development Mining in a Steeply Pitching Coalbed, Roslyn, Wash. BuMines Rept. of Inv. 6685, 1965, 16 pp.

26. Reichman, J.M., and Cheung, J. B. Waterjet Cutting of Deep-Kerfs. Proc. Fourth Internat. Symp. on Jet Cutting Tech., Canterbury, England, April 12-14, 1978, pp. E2-1-E2-28.
27. Savanick, G.A. Boreholes (Slurry) Mining of Coal and Uraniferous Sandstone. AIME Annual Meeting, New Orleans, Louisiana, February 18-22, 1979, 11 pp.
28. Savanick, G.A. Water Jet Perforator for Uranium Leaching Wells. Uranium Mining Tech. Conf., U. of Nevada, Reno, Nevada, April 25-29, 1977, 36 pp.
29. Savanick, G.A., and J.N. Frank. Force Exerted by Water Jet Impact on Long Standoff Distances. Proc. Third Internat. Symp. on Jet Cutting Tech., Chicago, Illinois, May 11-13, 1976, pp. B5-59-B5-67.
30. Savanick, G.A., T.E. Ricketts, P.D. Lohn, and J.N. Frank. Cutting Experiments Using a Rotating Water Jet in a Borehole. BuMines Rept. of Inv. 8095, 1975, 34 pp.
31. Summers, D.A. Potential Advantages to Water Jet Drilling for Use in In-Site Coal Gasification Process, ASME Energy Tech. Conf. and Exhibition, New Orleans, Louisiana, February 3-7, 1980, 7 pp.
32. Summers, D.A. Practical Applications of Erosion Processes. Treatise on Materials Science and Technology, Volume 16,Bell Telephone Laboratories, Inc., 1979, pp. 395-411.
33. Summers, D.A. Recent Advances in Water Jet Coal Mining. Colliery Guardian, September 1978, pp. 538-541.
34. Summers, D.A. The Use of High Pressure Water Jets in the Mining Industry. Colliery Guardian, October 1978, pp. 40-48.
35. Summers, D.A., and C. R. Banker. Surface Trials of the Hydrominer. Proc. Fourth Symp. on Jet Cutting Tech., Caterbury, England, April 12-14, 1978, pp. J2-13 - J2-22.
36. Summers, D.A. and T. F. Lehnoff. The Development of a Water Jet Drilling System and Preliminary Evaluation of its Performances in a Stress Situation Underground. Proc. Fourth Internat. Symp. on Jet Cutting Tech., Caterbury, England, April 12-14s1978, pp. C4-41-C4-50.
37. G. duToit, P.J., et al. Study of a Water Jet Continuous Coal Mining System. BuMines Contract No. J1055138, Ingersall-Rand Research, Inc., March 1977. 450 pp.
38. Veckiuzen, S.D., J.B. Cheung, and J. Hill. Water Jet Drilling of Small Diameter Holes. Proc. Fourth Symp. On Jet Cutting Tech., Canterbury, England, April 12-14,1978, pp. C3-29-C3-40.
39. Wallace, J.J., G.C. Price and M.S. Ackerman. Hydraulic Coal Mining Research: Equipment and Preliminary Tests. BuMines Rept. of Inv. 5915, 1961, 25 pp.
40. Wang, F.D. and J. Wolgamott. Application of Water Jet Assisted Pick Cutter for Rock Fragmentation. Proc. Fourth Symp. on Jet Cutting Tech., Canterbury, England, April 12-14, 1978, pp. Cl-l-Cl-6.
41. Wilkinson, A. The Ancient Egyptians. 1874, p. 137.

WATER JET DRILLING OF LONG HORIZONTAL HOLES IN COAL BEDS

C.R. Barker
University of Missouri-Rolla
Rolla, MO 65401

K.M. Timmerman
Sandia National Laboratories
Albuquerque, NM 87185

ABSTRACT

Holes drilled horizontally into coal beds from a vertical hole can be used to drain methane from gassy coal prior to mining and to link vertical wells for in situ gasification. A device which uses water jets to drill these holes is being developed jointly by the University of Missouri-Rolla and the Sandia National Laboratories. Earlier papers have described the first generation equipment which was capable of drilling a horizontal hole 50 feet in length from a vertical borehole.

This paper will describe the second generation equipment which is intended to drill horizontal holes of lengths up to 200 feet with greatly improved control of system performance. Instruments in the drill string will provide hole pitch and azimuth data to the driller on the surface. An additional system is being developed to locate the drilling head relative to the roof and floor of the coal seam. A pitch control on the drilling head will enable the driller to use this information to control drilling direction and guide the drill through the coal seam.

INTRODUCTION

The methane which occurs naturally in many coal beds can become an impediment to safely mining the coal. At the same time that removing large portions of the methane would improve safety, the methane itself has commercial value [l]. In situ gasification techniques also involve moving gas through coal beds [2].

Hence the original interest in the development of a water jet coal drill was generated by the need for methane drainage and in situ gasification. This interest resulted in a research project at the Rock Mechanics and Explosives Research Center of the University of Missouri-Rolla sponsored by the Sandia National Laboratories. In 1975, staff of RMERC were successful in drilling a 50 foot long horizontal hole from a simulated 16 inch vertical wellbore [3]. This first demonstration generated considerable interest in the equipment which could turn the drilling head through a 90~ angle in a very short turning radius. The first generation equipment did not however address questions regarding the control of the size of the hole produced in the coal, the chip size produced, drill guidance, or operating data to assist the driller in monitoring hole progress. Consequently, further development of the system was undertaken by Sandia Laboratories with the University of Missouri serving as a subcontractor. This work has been reported in earlier publications [4,5,6] and will not be repeated here. Instead, a description of the second generation drilling head will be presented and field performance of this unit described.

DRILLING HEAD DESIGN

Because of the requirement to rotate the drilling head from a vertical position into the horizontal before advancing into the coal seam, the space limitations imposed on the drilling head are very severe. For example, if the vertical wellbore is 16 inches (41 cm) inside diameter, the drilling head can be no larger than 5 x 4 x 19 inches (12.7 x 10 x 48 cm). In this space must be located the high pressure hose to supply the cutting fluid, a rotating high pressure coupling, a device to cause the coupling rotation, a pressure transducer, an electronics package, and the Jet cutting nozzles. In attempting to position the various components in the available space, it became obvious that the optimum space utilization would only be possible if custom designed components were manufactured for many of the required elements.

An additional complication was the very poor performance record of the high pressure coupling chosen for the early test work. This device required frequent seal changes and on several occasions the thrust bearings failed in less than 10 hours of operation at 10,000 psi (69 MPa). Before the head design could be finalized, it was necessary to evaluate several commercially available couplings with a minimum goal for coupling performance established as a life of 10 hrs at 10,000 psi (69 MPa) while the coupling was rotated at 100 rpm.

The test stand shown in Figure l was used to evaluate the couplings. The high pressure water was supplied through a flexible hose to the coupling which was allowed to float on its own internal bearings. A torque arm attached to the coupling case was used to measure the torque required to prevent the case from turning when the supply pipe to the nozzle was rotating at 100 rpm. The high pressure water was supplied at a flow rate of 12 gpm (0.045 m^3/min) and the water was not recirculated. Tests were run on six different couplings with slight modifications to some of the six basic designs so that a total of 12 endurance runs were made. Only three of the twelve runs lasted the full ten hours. Premature terminations were caused by excessive leakage, total seal failure, bearing failure, or excessively high torque.

The coupling supplied by Partek Corporation was by far the best in performance. This coupling did not leak, required a low torque to operate, and was in perfect condition at the end of ten hours of operation. The coupling was reassembled and run for an additional forty hours with the same excellent result. Since only one unit of each coupling was available for testing, the results can not be regarded as conclusive. However,the Partek coupling performance was so flawless that it was selected for use in the drilling head.

The endurance test showed that the torque required to turn the coupling selected was very low. This permitted using a DC electric motor to generate the nozzle rotational motion. The advantage of using the electric motor was the ease with which power could be supplied to it, and the small space required by the power cable. Previously a hydraulic motor had been used and it was difficult to make the supply and return line connections to the motor. The need for both a supply and return hydraulic hose also required a large amount of the available space.

The drilling head layout shown in Figure 2 was therefore selected. An interesting feature of this design is the stationary supply pipe which serves an as axle about which the coupling case, seal holder, and nozzle holder are rotated. This permitted bolting the nozzle holder to the rotating case so that different nozzle configurations could easily be evaluated. Figure 3 shows the DC electric motor and the 24 tooth spur gear. Figure 4 shows the coupling case, the 32 tooth spur gear, and the large bearings in which the coupling case rotates. Figure 5 shows the seal holder on the left, the high pressure seal in the center, and the supply pipe and internal coupling bearings on the right side of the photograph.

After the seal holder and high pressure seal were in position, different nozzle holders could be bolted to the coupling case. An O-ring was used as a static seal to prevent leakage between the seal holder and the nozzle holder. Figure 6 shows a typical nozzle holder which in this case had six possible locations for the tungsten carbide inserts used as the jet cutting nozzles. The size of the hole produced in the coal was a function of the number of nozzles used, the location and angle of inclination of the nozzles, the exit diameter, and the effective cutting range of each nozzle. With this many parameters, a great many combinations would be possible that could produce the desired result of cutting a 6 to 8 inch (15.2 to 20.3 cm) diameter hole in the coal.

NOZZLE ARRANGEMENT

Since the effective cutting range of a given nozzle has a finite limit, the hole size produced can be controlled passively by knowing approximately how far from the nozzle the target material can be cut. For example Figure 7 illustrates one of the nozzle arrangements which produced a satisfactory result in the field testing. In this case three carbide inserts were used in the nozzle holder shown in Figure 6 with inserts located at positions l, 2, and 4. Locations 3, 5, and 6 were plugged. In Figure 7 a 0.041 in. (l mm) diameter jet was inclined out at an 18° angle from location l. A 0.047 in. (1.2 mm) jet was angled out at a 30° angle and a .062 in. (1.6 mm) jet was angled out at a 10° angle from locations 2 and 4 respectively.

With this arrangement the hole size was maintained in the range of 6 to 8 in. dia (15.2 to 20.3 cm) with the drilling head advancing at a rate of l to 2 ft/min (30 to 60 cm/min) and cutting in clean coal. In cases where impurities were present in the coal, the hole size tended to fall below the lower limit, and it was necessary to backup the drilling head to cut forward again to enlarge the hole size. More sophisticated methods of actively controlling the hole gauge were developed, but were not tested because of the difficulty in fabricating the equipment so that it could pass through the corner turning mechanism.

FIELD EQUIPMENT

The drilling head described was connected to a drill string composed of 3 x 5 inch (7.6 x 12.7 cm) rectangular structural tubing hinged at spacings of 17 inches (43.2 cm) as shown in Figure 8. The holes located on the top surface of the drill string were used to move the string in and out of the horizontal hole by means of a pair of pin gears located above the drill string. Power to the pin gears was supplied from a hydraulic motor and roller chain and sprocket arrangement. The interior of the rectangular tubing was used to house a high pressure and low pressure water hose, three hydraulic hoses, and two electrical cables. The water hoses supplied cutting water at l0,000 psi and 26 gpm (68.9 MPa and 0.098 m^3 /min) and flushing water at 300 psi and 40 gpm (2 MPa and 0.15 m^3/min). The three hydraulic hoses were used to activate hydraulic cylinders two of which were located in the first box immediately behind the head while the third cylinder was located in the fourth box. The two cylinders behind the head pushed against it to define stop positions so that the head could be positioned relative to the drill string at 2° up, aligned, and 2° down. The third hydraulic cylinder was used to apply a compressive load to the head and the first four boxes so that a "stiff" length of drill string of 7 feet (2.16 m) could be achieved.

The two electrical cables were used to supply power to the DC electric motor used to rotate the nozzle holder, and to provide drilling instrumentation. The instrumentation provided cutting water pressure at the head, rotation rate of the nozzle holder, axial load on the drilling head, head pitch, and drill string pitch. The cutting water pressure was taken just before the nozzle holder to insure that no leaks were present between the high pressure supply pump and the drilling head. Accurate readings were taken at the pump and at the drilling head to measure the pressure loss with 112 and 212 foot lengths (34.2 and 64.7 m) of 0.5 inch I.D. (1.29 cm) water hose. These readings were taken because the supply hose length will be a critical factor as the distance from the drilling head to the pump increases. Figure 8 shows the pressure loss reached values of 494 and 818 psi (3.4 and 5.64 MPa) respectively for the two hose lengths with the pump bypass valve completely closed. The other pressure readings shown in Figure 8 were taken with the bypass value partially open to generate pump pressures at specified values.

The axial load exerted on the drilling head was taken to inform the drill operator when the head was encountering an obstruction. Unfortunately the system used to measure this load was affected by spurious inputs and did not provide any useful information.

The data from the head and drill string pitch sensors were processed along with an operator supplied distance increment to provide a record of the hole elevations. The technique used shows promise for providing useful data to the drill operator. However, in this series of tests the accuracy of the output information was not satisfactory. The accelerometers used to measure the pitch values were affected by pressure pulsations in the high pressure hose, and mechanical noise from the head environment.

Although the entire test series was plagued by instrumentation problems, a total of 236 feet (72 m) of hole was drilled horizontally into the coal. The longest hole was 102 feet (31.l m) in length and was drilled at a rate of approximately 2 ft/min (0.61 m/min). It was possible to remove the cuttings from this hole and to move the drill string in and out of the hole as desired.

CONCLUSIONS

The latest series of tests have clearly demonstrated the need for an extremely high level of reliability in the electronics package. Since the drilling head and drill string will be virtually inaccessible from the surface, any service needed by the down hole equipment will be costly. The environment includes water and fine coal cuttings which combine to infiltrate into every available crack and opening in the equipment. The water surrounding the drilling head may be pressurized slightly under certain conditions which aggravates the problem.

The electrical compartments and connectors were not satisfactorily sealed and consequently a great deal of test time was lost in servicing the equipment. The drill string itself was not immune from being packed with chips and fine coal cuttings. The volume of material inside the drill string was sufficient to prevent the string from passing through the corner turning equipment on the way out of the hole.

Another problem with the present equipment is the tendency for the hole to climb. Since the drill string is hinged on the top surface, any debris which gets under the lower surface of the boxes causes the string to pitch up. With the head and first four boxes stiffened, the tendency to climb is reduced somewhat. However, it was not possible to stop the hole from gradually increasing in elevation. Even with the head pitched down 2°relative to the drill string, the hole rise was recorded as about 3 ft per lOO ft (0.92 m per 30.5 m) of horizontal length.

Another operating problem can occur if the hole diameter necks down to a size just large enough for the drilling head to pass. In this case a built-in trap to prevent the chips and cuttings from flowing back along the drill string can cause the entire volume between the drilling head and trap to fill with water. When this happens, the pressure of the water surrounding the drilling head and drill string can rise which aggravates the sealing problems.

The equipment tested was capable of drilling a hole lOO ft (30.5 m) horizontally into the coal seam, and removing the cuttings from this length of hole. The drive system did not appear to be straining to move the drill string back and forth in this length of hole. Therefore, the overall system performance merits further development efforts to fully determine the limits of the round the corner drilling concept.

ACKNOWLEDGEMENTS

This research program was funded by the Department of Energy, Morgantown Energy Technology Center with Dr. H.D. Shoemaker serving as Project Officer. Sandia personnel assisting with the project were: D.J. Cooper, D.N. Harstad, S.M. Kohler, and A.E. Giddings. UMR personnel were: L.J. Tyler, J.G. Blaine, and R.G. Robison. The assistance of all these individuals is gratefully acknowledged by the authors.

REFERENCES

l. Deul, M, "The USBM Program for Methane Drainage to Reduce Safety Hazards in Coal Mines," 2nd Symposium on Methane Recovery from Coal Beds, April 1979.
2. DOE/ET-OlOO, "Underground Coal Conversion Program Description," June 1979.
3. Summers, D.A., C.R. Barker, and H.D. Keith, "Water Jet Drilling of Horizontal Holes in Coal," 1979 AIME Annual Meeting, New Orleans, Louisiana, Feb. 18-22, 1979.
4. Barker, C.R., D.A. Summers, and H.D. Keith, "The Development of a Round-the-Corner Drill," 10th U.S. Symposium on Rock Mechanics, Austin, Texas, June 3-6, 1979.
5. Summers, D.A. and C.R. Barker, "Potential Advantages to Water Jet Drilling of In situ Coal Gasification," Energy Sources Technology Conference and Exhibition, New Orleans, Louisiana, Feb. 3-7, 1980.
6. Barker, C.R. and H.D. Keith, "Design and Development of a Mechanical Drive System for Drilling Horizontal Holes in Coal from a Vertical Borehole," 6th

Oklahoma State University Applied Mechanisms Conference, Denver, Colorado, Oct. 1-3, 1979.

LIST OF FIGURES

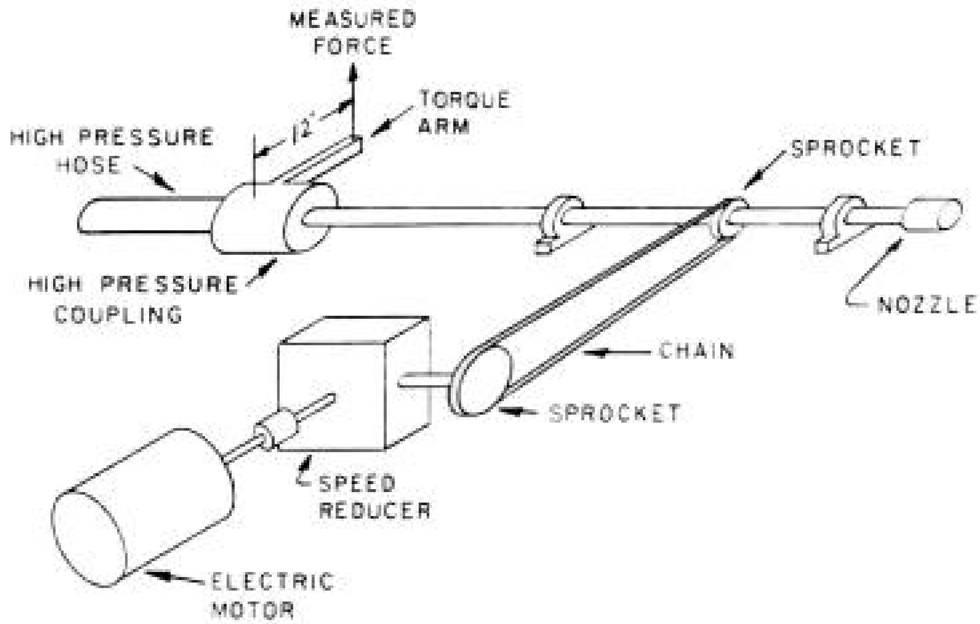

Figure l. Test Stand for Rotating Coupling Evaluation

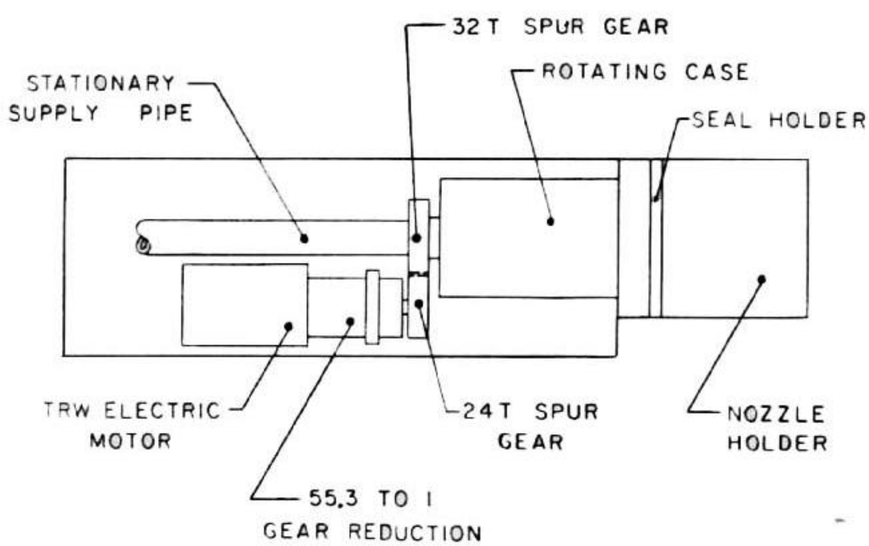

Figure 2. General Drilling Head Layout

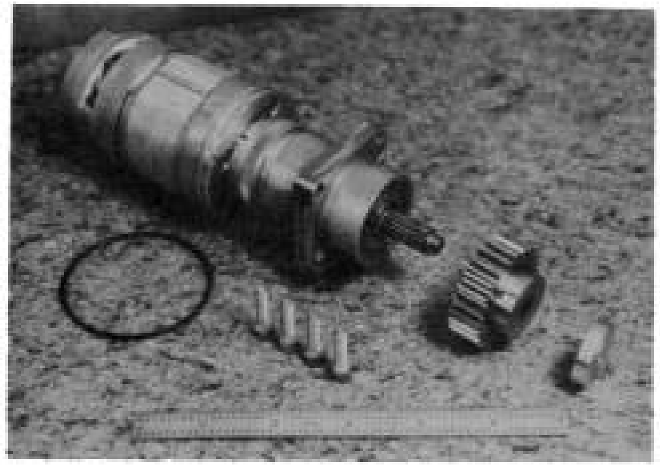

Figure 3. Electric Motor Drive Train

Figure 4. Coupling Case and Bearings

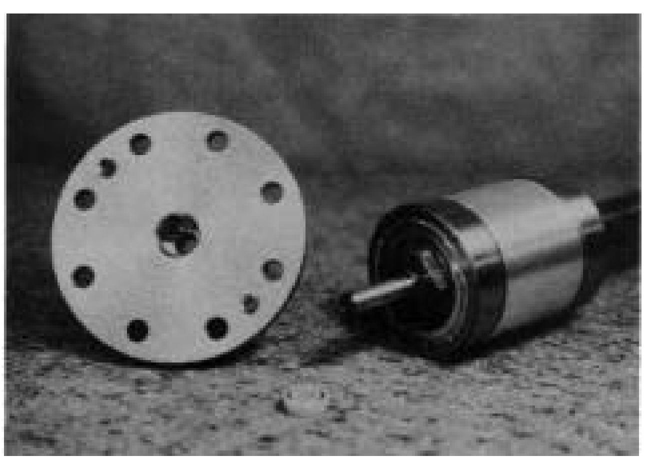

Figure 5. Rotating Coupling Components

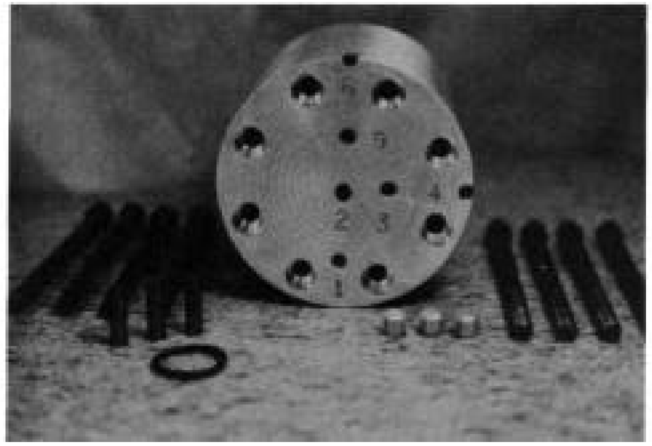

Figure 6. Nozzle Holder and Components

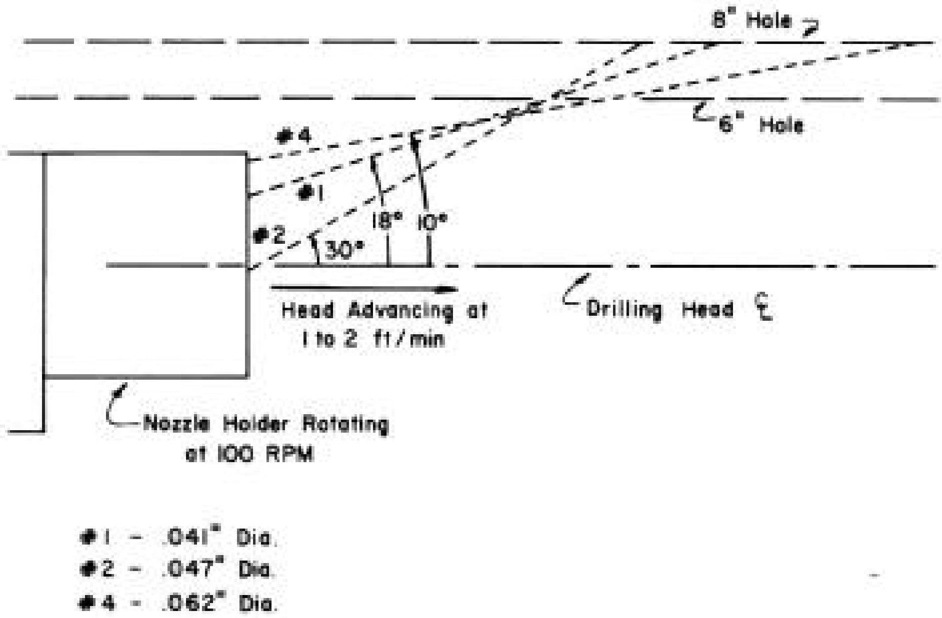

Figure 7. Jet Locations

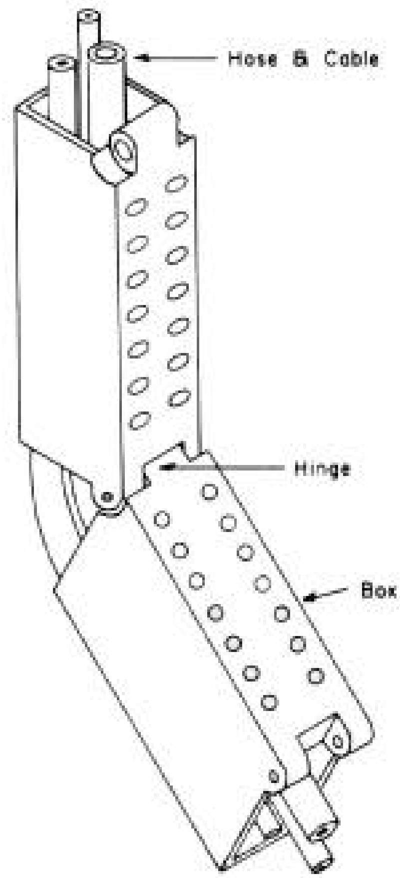

8. Drill String Arrangement

ADVANCED APPLICATION OF WATER JETS TO SMALL HOLE DRILLING

N. J. Bonge and F. D. Wang
Colorado School of Mines
Excavation Engineering and
Earth Mechanics Institute
Golden, Colorado 80401

ABSTRACT

Critical parameters influencing the interaction of water jet and mechanical fracture mechanisms were studied for the purpose of developing a superior small hole drill bit. Two StratapaxR man-made diamond cutters were assisted by three high pressure water jets in the design of a 7/8-in. diameter rotary bit. Jet power distribution trajectory and bit rotational speed were found to significantly influence penetration rate, wear rate, and penetration forces. The rake angle of the cutters was found to determine bit stability. A significant increase in penetration rate was achieved over rotary-mechanical bits and early WATER JET MECHANICAL bits accompanied by an even more profound improvement in bit life. A model was developed to assist engineers in the optimization of water jet mechanical bit design.

INTRODUCTION

In response to efforts by the U.S. Bureau of Mines and U.S. Department of Energy to improve coal mine safety and productivity, Colorado School of Mines has conducted extensive research in the development of a small hole WATER JET MECHANICAL drilling system. The action of high pressure water jets combined with a rotary-mechanical drill bit effectively "softens" the rock ahead of the bit so that torque and thrust forces are dramatically reduced. Consequently, hole diameter may be reduced since it is no longer dictated by the column strength of the drill steel. Bit life and penetration rate are greatly increased, and the range of rock types over which rotary-mechanical drilling is effective is expanded. Even very hard rocks which previously could be drilled only by percussive methods can be effectively drilled by a water jet mechanical bit. Because this drilling method requires the jets to remove only a small volume of rock, specific energy levels are far lower than those encountered in pure water jet drilling and power requirements are easily manageable.

This paper summarizes a small part of the research which sought to combine the best available mechanical drilling technology with the most advanced state-of-the-art water jet rock cutting techniques. It is presented for the purpose of making available the design methods which were found to be successful in the development of a superior, small hole drill bit in the interest of the advancement of mining technology.

WATER JET MECHANICAL DRILLING THEORY

When water jets are directed to kerf rock ahead of a rotary-mechanical drill bit, a system of concentric rock rings is formed at the hole bottom. The theory developed by the authors in reference 1 states that two primary factors work together in the reduction of penetration forces. They are the absence of side cutting and center crushing in a properly designed water jet mechanical drill bit and the unequal distribution of stress over the cutting area dictated by the geometry of the rings. The bit splits each ring into two segments. Thrust and torque supplied to the bit is distributed unequally according to the mechanics of a parallel force system. This leads to a concentration of both torsional and axial stresses in the most rigid ring segment in contact with the bit. As in purely mechanical drilling, the penetration forces exhibit rapid fluctuations which rise to a maximum just prior to the formation of a major chip. Since stresses are maximum in the most rigid ring segment, it will be the first to experience fracture. Forces on this segment then fall to zero and a greater stress is concentrated in the next most rigid ring segment. Fracture of this segment immediately follows with less total input force than in the previous case. The cycle continues in this manner and the ring segments experience fracture one at a time. The maximum input forces required in drilling are then those which would distribute sufficient stress to the most rigid ring to cause it to fracture when the bit is in contact with all the ring segments.

From Mechanics of Materials, the torque distributed to any particular ring segment is given by

$$T_i = T_o \frac{k_i}{\sum_{j=1}^{m} k_j} \qquad (1)$$

where T_i is the torque distributed to any ith ring segment
T_o is the total input torque
k_i is the angular spring rate of any ith ring
m is the total number of ring segments

The thrust distributed to any particular ring segment is given similarly by

$$F_{T_i} = F_{T_o} \frac{K_i}{\sum_{j=1}^{m} k_j} \qquad (2)$$

where F_{Ti} is the thrust force distributed to any ith ring segment
F_{To} is the total input thrust
K_i is the axial spring rate of any ith ring segment

The angular (torsional) and axial spring rates of equations (1) and (2) are a function of the jet trajectories and depths of kerf.

Assuming that fracture follows the Coulomb-Mohr criterion, the cutting force relationships derived by Nishimatsu[5] may be applied to the ring segments individually and an expression for the maximum input torque required in drilling may be derived as

$$T_o = \frac{\sum_{j=1}^{m} k_j}{k_i} r'_j \frac{2A_i \tau_o}{N+1} \frac{\cos\varphi \cos(\beta-\alpha)}{1-\sin(\varphi+\beta-\alpha)} \qquad (3)$$

where	r'_j	is the distance from the axis of rotation to the point where a horizontal cutting force may be assumed to act on the ith ring segment to produce the torque T_i from equation (1)
	A_i	is the cross sectional area of the ith ring
	τ_o	is the cohesive strength of the rock
	φ	is the angle of internal friction of the rock
	β	is the angle of friction between the normal to the cutting face and the direction of the resultant cutting force
	α	is the bit rake angle
	N	is a stress distribution factor related to the rake angle

The maximum required thrust force is derived in similar fashion as

$$F_{T_o} = \frac{\sum_{j=1}^{m} K_j}{K_i} \frac{2A_i\tau_o}{N+1} \frac{\cos\varphi\sin(\beta-\alpha)}{1-\sin(\varphi+\beta-\alpha)} \qquad (4)$$

Average torque and thrust values will be much lower as the cutter would rarely be in contact with all the rings at any given time.

MECHANICAL DESIGN

Primary mechanical design considerations include the basic bit type, cutter shape and material, rake and clearance angles, and mechanical strength. The spade-type bit has the disadvantage of crushing rock at the hole center due to the effective clearance angle being less than zero in the center region. This reduces overall cutting efficiency. In order to overcome this problem, a jet must be directed to strike very near the axis of rotation. Because jet traverse velocity is very low toward the hole center, jet cutting is least efficient in this area. Therefore, the spade-type bit is not considered favorable by the authors as a basic bit type. Although, augmenting this type of bit with water jets will certainly improve its performance.

The dual-cutter core-gap bit type is preferable for several reasons. Separation of the cutters provides space for the jet exists, and optimum jet trajectories may be more easily achieved. The jet closest to the bit center may be directed to perform more work (remove more rock) per unit input energy by striking further from the axis of rotation and removing the center core along its path. Jet energy is thereby used more efficiently to reduce penetration forces and bit wear.

Stratapax^R drill blanks were chosen for the cutter material. These are drill bit inserts composed of a man-made polycrystalline diamond layer bonded to a tungsten carbide substrate. Current research indicates that the wear life of the Stratapax drill blanks is far superior to both tungsten carbide and natural diamond cutters. Available shapes of the drill blanks, although limited at this time, are conducive to the dual-cutter bit design. Three-eighths-inch square inserts were selected for design simplicity. V-shape cutters would have, perhaps, been preferable from the standpoint of bit stability; however, Stratapax blanks of this shape are not currently manufactured.

According to Merchant's theory of mechanical cutting, forces on the cutters, for a given depth of cut, decrease with increasing positive rake angles. However, Fairhurst[8], Fish[7] and Cheatham and Daniels[3] have shown that positive rake angles can produce clogging ahead of the cutters, which can actually increase the overall stress on the cutters. For this reason, the optimal rake angle for the rock type used in the research was determined experimentally. Water jet mechanical bits with identical jet trajectories were tested under identical conditions. Rake angles of 0°, -5°, and -10° were used. In softer sandstones and shale, there was no notable difference in performance. In very hard sandstone, however, significant flaking of the diamond layer occurred with the neutral and -5° rake angles and was most pronounced with the neutral rake. The -10° rake bit experienced only a very slight amount of flaking along the leading edge of the cutter, giving indication that in hard rock, negative rake angles improve bit stability. No significant difference in penetration forces could be detected in any of the rock types tested which are discussed later in this paper. The -10° rake angle provides for a greater amount of material supporting the cutters increasing bit strength. It also provides for an acceptable bit clearance angle without the necessity of grinding the drill blanks. On this basis, the -10° rake angle was used for the majority of the testing and is recommended for hard rock drilling with water jet/stratapax bits. Rake angles more negative than -10° were found impractical to produce. In soft and medium rocks, a neutral rake may be preferable as it is the simplest to manufacture. The final mechanical design developed is illustrated in Figure 1.

NOZZLE DESIGN

For a multi-jet nozzle, the amount of flow turbulence present at the jet exit is a result of the shape of the orifice itself and the upstream contour of the nozzle (orifice holder). Several techniques including laser and electric discharge machining were used to produce orifices of the shape described by Leach and Walker[9] in which a l3° included entrance angle is employed followed by a cylindrical throat with a length-to-diameter ratio of 2 to 3. However, the jet coherency achieved with a simple sapphire orifice insert far surpassed that produced by the more elaborate techniques.

Numerous nozzles of different upstream contours were tested in kerfing experiments with the most superior shape determined purely by experiment. The optimal contour was achieved by generating a curve in which each tangent line at the point of intersection with a jet center line is perpendicular to the center line. This is depicted in two dimensions in Figure 3b.

It should be noted that the shape is actually a smooth, three-dimensional curve. The orifices inserts are placed such that the flat of the insert protrudes slightly upstream from the curve.

Figure 3a, for comparison, depicts the flat nozzle contour which proved to induce the most turbulence of any shape tested. Penetration rates in Indiana limestone using the nozzle of Figure 3b were an average of approximately 8% greater than those achieved with the nozzle of Figure 3a. Supporting data may be found in reference 1.

WATER JET MECHANICAL DRILLING MODEL

The principal-author has developed the water jet mechanical drilling model presented in Figure 2 for the purpose of defining critical design parameters. The jet farthest from the axis of rotation is termed the GAGE JET. The jet closest to the axis is termed the CENTER JET, and the jet which strikes between the two is termed the INTERMEDIATE JET. As the hole is drilled the cutters together follow a double helical path, while the path formed by each jet is that of a single helix. The minimum depth of kerf parallel to the axis of rotation for each jet is then twice the depth of cut taken by a single cutter and equal to the total depth of cut per revolution . Therefore the kerf which lies ahead of the FOLLOWING CUTTER is twice as deep as the one ahead of the LEADING CUTTER. The model requires that for maximum jet cutting efficiency, the parallel kerf depths be no greater than d.

Each jet is rotated ahead of the following cutter through an OFFSET ANGLE ψ_i as shown in Figure 4. The angle between the jet and the axis of rotation is termed the JET ANGLE φ_i fit shown in Figures 2 and 4. The jet trajectory is defined in terms of the offset angle, jet angle and the KINEMATIC TARGET λ_i, which is the distance from the axis of rotation to the point where the leading edge of the following cutter intersects the center line of the kerf.

Between the time that the kerf is formed and intersected by the following cutter, the cutter must rotate through ψ_i and penetrate a distance d' where

$$d' = d\,\frac{\psi_i}{2\pi} \tag{5}$$

Therefore, the position of the kerf relative to the cutter, and consequently the value of λ_i, varies with the depth of cut per revolution. The position of the jet relative to the cutter is constant and defined in terms of the DESIGN TARGET Xi, which is the distance from the axis of rotation to the point where the jet intersects a reference plane perpendicular to the axis of rotation and tangent to the leading edge of the cutters as shown in Figure 4. The relationship between the position of the jet and that of the kerf is given by

$$\lambda_i = x_i + d\,\frac{\psi_i}{2\pi}\tan\varphi_i \tag{6}$$

GAGE JET CONSIDERATIONS

Proper placement and sizing of the gage jet is of the utmost importance since it is this jet which controls the penetration rate and the major factors affecting bit life. Optimal work is performed by the gage jet when it is directed to fully penetrate to the bit diameter with a minimum of overcutting. If the gage jet is not given sufficient power and undercuts the hole diameter, side cutting is required of the bit, resulting in significantly higher mechanical forces and increased bit wear. If the jet is given too much power and overcuts the hole diameter, there will be no increase in penetration rate and energy is wasted to unnecessary cutting. The maximum depth of cut per revolution for optimal bit life may then be derived from Figure 2 as

$$d = w_n \csc \varphi_n \tag{7}$$

where d is the total depth of cut per revolution
w_n is the width of kerf cut by the gage jet
φ_n is the angle the gage jet makes with the axis of revolution as defined in Figure 1

This is also the depth required to optimize gage jet energy as it is the depth which allows the jet to fully cut to the hole diameter without overlapping its path. It may be noted that equation (7). agrees with the model of pure jet drilling developed by Vennhuizen and Chung .However, the length of kerf required to achieve this depth may be made far shorter for the water jet mechanical drill since the jet is only required to cut the circumference of the hole. Removing of rock toward the hole center is done by the cutters and is not required of the gage jet. This results in a significant reduction in the overall specific energy of drilling.

The length of kerf h_n required by the gage jet may be derived from Figure 2 as

$$h_n = d \sec \varphi_n + (r_{bit} - \lambda_n) \csc \varphi_n \quad (8)$$

where c_w is a constant of the particular rock type.

The kerf width of any jet is fairly constant for any orifice diameter and may be expressed

$$w_i = c_w d_{Oi} \quad (9)$$

The minimum length of kerf which will satisfy the gage jet criteria is achieved when $\lambda_n = r_{bit}$ and is given by

$$h_{Nmin} = 2 c_w d_{On} \csc 2\varphi_n \quad (10)$$

and the optimal design target,minimum kerf length, and maximum jet efficiency is given by

$$x_{n_{opt}} = r_{bit} - \frac{\psi i}{2\pi} c_w d_{o_n} \sec\varphi \quad (11)$$

CENTER JET CONSIDERATIONS

The criteria for an effective center jet trajectory are quite different than those for the gage jet. For the dual-cutter bit wear rate is reduced by eliminating side cutting at the minor radius of the cutter. The minimum kinematic target of the center jet, which produces the minimum length of kerf while satisfying this condition, is defined in Figure 2 and given by

$$\lambda_o = r_g - \tfrac{1}{2} w_o \sec\varphi_o - \tfrac{1}{2} d \sin\varphi_o \quad (12)$$

where λ_o is the kinematic target of the center jet
rg is the radius of the core gap which is the minor radius of the cutter
φ_o is the angle the center jet makes with the axis of rotation.

If for efficient jet cutting the center jet is not to overlap its own path, the minimum Center jet diameter is given by

$$d_{o_o} = d_{o_n} \csc\varphi_n \sin\varphi_o \qquad (13)$$

However, within practical design constraints, this condition typically cannot be satisfied and some overlapping will occur. As the depth of jet kerf parallel to the axis of rotation is increased below the depth of cut per revolution d, more mechanical forces will be directed to the other rings. However, the small reduction of mechanical forces which results is typically not worth the great expense of additional jet energy. Therefore, the optimum parallel depth of kerf for all jets is taken to be the depth of cut per revolution d. The minimum length of kerf of the center jet (taking into account the jet overlapping) may be derived from Figure 2 as

$$h_{o_{min}} = \lambda_o \csc\varphi_o + d(\cos\varphi_o - \tfrac{1}{2}\sec\varphi_o + \frac{3}{4}) + w_o(\tan\varphi_o - \tfrac{1}{2}\csc 2\varphi_o) \qquad (14)$$

where h_o is the length of kerf formed by the center jet
λ_O is the kinematic target of the center jet
φ_O is the angle the center jet makes with the axis of rotation
w_O is the width of kerf formed by the center jet

The minimum center jet design target which will achieve this value of h_o is found by combining equations (6), (9), and (12), yielding

$$x_{o_{min}} = r_g - \tfrac{1}{2} d_{o_o} c_w \sec\varphi_o - d(\tfrac{1}{2}\sin\varphi_o + \frac{\psi_o}{2\pi}\tan\varphi_o) \qquad (15)$$

INTERMEDIATE JET CONSIDERATIONS

The addition of an intermediate serves to reduce penetration forces as described by equations (3) and (4). Increasing the number of intermediate jets will further serve to reduce mechanical forces; however, as the number of jets is increased and more volume of rock is removed by jet cutting, the specific energy of drilling will rapidly increase, resulting in diminishing returns with respect to power input per unit force reduction. For the 7/8-in. diameter bit developed in this investigation, a single intermediate jet was sufficient to significantly reduce mechanical forces, while maintaining easily manageable power levels. The number of intermediate jets is also limited by space constraints of the bit.

It is possible to optimize the intermediate jet trajectory by making suitable approximations for the spring rates of equations (3) and (4) in terms of the ring segment radii of Figure 2. The kinematic target which results in the lowest mechanical forces may then be determined. Such analysis, however, is extremely complex. Reference 1 describes experimental studies which show that for the single intermediate jet utilized in this investigation, deviations of the intermediate jet kinematic target had little effect on penetration forces so long as reasonable distances were maintained from the other jets. Elimination of the intermediate jet, however, resulted in a two-fold increase in forces. Moving the jet toward the bit center decreases its traverse velocity and although the cutting efficiency also decreases, the total energy (orifice diameter) spent in achieving the required kerf depth may be reduced. Alternately, bit wear is more pronounced to ward the outer diameter of the bit. Moving the intermediate jet in this direction will increase bit life. Considering both factors, the optimum intermediate jet kinematic target is taken by the authors to be the midpoint between the center and gage jet targets expressed as

$$\lambda_I = 1/2(\lambda_o + \lambda_n) \qquad (16)$$

The minimum required kerf depth of the intermediate jet is easily determined from Figure 1 as

$$h_1 = \left(d_{o_1} \sin\varphi_1 + d_{o_n} \csc\varphi_n\right) c_w \sec\varphi_1 \qquad (17)$$

ENERGY REQUIREMENTS AND PENETRATION RATE

In order to maximize the penetration rate by the foregoing criteria, the characteristics of water jet cutting in the rock type to be drilled must be known. Figure 5 describes the results of kerfing tests in the rock type used for the majority of the drilling study. The rate of surface area generation, which is the product of kerf depth and velocity (h_{Vt}) is plotted against traverse velocity and normalized for d_{On}. From equation (10), a relationship n between the traverse velocity of the gage jet and the rate of area generation may be derived as

$$\left(\frac{h_{V_t}}{d_o}\right)\min = 2c_w \csc 2\varphi_n V_{t_n} \qquad (18)$$

This shows that for a given rotational speed, there is a minimum value of $\left(\frac{h_{V_t}}{d_o}\right)$ which must be achieved in drilling. When equation (l8) is plotted with the actual kerfing data in Figure 5, it may be noted that for any given traverse velocity (rotational speed), there is a specific value of pressure which must be supplied in order to satisfy the optimal drilling criteria of the model. If the water jet pressure used in drilling is less than the indicated values the gage jet will not fully penetrate to the bit diameter and will undercut the hole giving rise to greatly increased penetration forces and bit wear. The insufficient pressure cannot be compensated by increasing the orifice diameter because, although the kerf length of the jet will be increased the required length of the kerf will proportionately increase and the undercutting effect remains.

The analysis shows that the gage jet orifice diameter has no effect upon the hole diameter swept by the jet. Once the indicated pressure for a given rotational speed has been attained, the orifice diameter may be sized for any desired penetration rate given the ultimate restrictions of available power.

If the jet pressure is raised above the indicated level for the given rotational speed, the hole diameter is overcut and the additional power is wasted. It is advisable, however, to operate at pressures slightly above the indicated range to ensure minimum bit wear.

The penetration rate for any drill bit is given by

$$P_r = \omega d \qquad (19)$$

where ω is the bit rotational speed and may be expressed

$$\omega = \frac{V_{t_n}}{2\pi r_{bit}} \tag{20}$$

Combining equations (7), (9), and (l9) yields

$$P_r = \omega c_w d_{o_n} \csc \varphi_n \tag{21}$$

which is the penetration rate achieved for jet pressures at or above the indicated optimum. When jet pressure is properly matched to rotational speed, the maximum penetration rate for the power level result which, is given by

$$P_{r_{max}} = \frac{\left(h_{V_t}\right)_n \cos \Phi_n}{2\pi r_{bit}} \tag{22}$$

The relationship of ($\frac{h_{V_t}}{d_o}$) to traverse velocity and jet pressure in most coal measure rocks generally follows the shape of the curves shown in Figure 5. This relationship coupled with the fact that the value of $(h/do)n$ is constant for the gage jet indicates that specific energy decreases with increasing pressure provided that the corresponding increases in bit rotational speed are made.

DRILLING TESTS

A series of drilling tests were undertaken to finalize bit optimization. The vast majority of the testing was done in rock samples obtained from the Geneva coal mine near east Carbon, Utah. This is an extremely hard and abrasive rock type and is among the least drilling able of coal measure rocks from the standpoint of both water jet and mechanical cutting. Limited testing was also performed in Dakota sandstone, Wilkeson sandstone, Berea sandstone, and Indiana limestone.

Testing apparatus included the CSM water jet mechanical drilling system described in reference 1 powered by a 50-hp dual-reciprocating intensifier system. An analog instrument monitoring system, also described in reference 1, was used to record water jet pressure, flow rate, bit rotating speed, torque, thrust, and penetration rate.

Figure 6 plots the average penetration rate in Indiana limestone as a function of thrust for two different rotational speeds. Thrust was increased so that the penetration rate in both cases exceeded the maximum value established by equation (21). The dashed lines represent these values for each speed. The change in slope, which occurs near these limits, is probably due to the formation of a ridge of rock along the circumference of the hole which must be broken by the bit. In the softer Dakota and Berea sandstones, no such change in slope occurred.

The effect of the gage jet undercutting the hole due to excessive rotating speed is quite pronounced in Figure 7, where the dashed line indicates the maximum allowable bit speed derived from Figure 5. This effect was also seen to be less striking in the softer rock types.

The data of Figure 8 is interesting in that when all other parameters were made identical for bits containing different power distributions, faster penetration rates were obtained in Geneva sandstone with a smaller gage jet. This is not the case of the softer rock types. It may be noted that in Geneva sandstone, the penetration rate predicted by equation (21) has not been achieved. Indicating the need for higher mechanical forces, at the force levels used, much of the gage jet energy is wasted as the jet overlaps it previous path. Penetration forces and penetration rate may be increased by directing the otherwise useless energy to remove more volume of rock toward the hole center.

Typical penetration rates for the rock types tested are given in Figure 9. Figure 10 compares the final optimized bit performance to that of an early water jet mechanical bit and to the actual underground performance of a conventional bit. As may be seen, a seventy-five fold increase in bit life was achieved in Geneva sandstone with a 6 to 1 decrease in thrust. Penetration rates in the softer rock types may be seen to be approximately 2 to 3 times faster than what is typically achieved with conventional bits. More complete drilling data for this bit is available in reference 1.

CONCLUSIONS

Optimization of water jet mechanical drill bits, according to the model presented, results in the more efficient utilization of jet energy to increase penetration rate and reduce mechanical forces on the bit. The addition of Stratapax cutters adds a new dimension to the already superior wear life of the bit. A lengthy testing program would be required to determine the ultimate life of the bit in medium and soft rocks, which is likely to be at least an order of magnitude greater than the seventy-five fold increase achieved in the extremely hard sandstone used in this investigation. The combination of long life and high penetration rate coupled with the small hole capability of the bit is already beginning to exert a strong positive impact on the mining industry.

With the conclusion of this research and that of the greater program of which it was a part, water jet mechanical drilling need no longer be considered novel drilling technique, but a practical and viable means of increasing mine safety, productivity, and reducing production costs.

REFERENCES

1. Bonge, N. J. and Wang, F. D. (1981), "Development of a System for High Speed Drilling of Small Diameter Roof Bolt Holes," CSM, U.S. Department of Energy Contract No. ET-76-C-O19107.
2. Bonge, N.J. and Wang, F. D. (1979), "Improved Methods of Mechanical Rock Drilling Assisted by Water Jets," CSM, South African Chamber of Mines.
3. Cheatham, J. B., Jr. and Daniels, W. H. (1978), "A Study of Factors Influencing the Drill ability of Shales: Single Cutter Experiments with StratapaxR Drill Blanks," ASME Conference and Exhibition, November 5-9, Houston, Texas.
4. Leach, S. J. and Walker, G. L. (1966), "Some Aspects of Rock Cutting by High-Speed Water Jets," Phi. Trans. R. Soc. A260, 295-308.

5. Fairhurst, C. (1955), "Some Possibilities and Limitations of Rotary Drilling in Hard Rocks," Transactions of the Institution of Mining Engineers, Vol. 115.
6. Fish, B. G., "The Design of Rotary Drilling Tools," National Coal Board, Mining Research Establishment, Islewort, November 1957.
7. Maurer, W. C., (1980), "Advanced Drilling Techniques," Maurer Engineering, Inc., Houston, Texas.
8. Nicnmatsu, Y. (1964), "The Mechanics of Rock Cutting," International Journal of Rock Mechanics and Mining Science, Vol. 1.
9. Veehuizen, S. D., Kirby, M. J., Cheung, J. B., and Summers, D. A., (1976), "Development of a System for High Speed Drilling of Small Diameter Roof Bolt Holes, Phase I Report, - Flow Research, Inc., U. S. Bureau of Mines Contract No. H0282036.

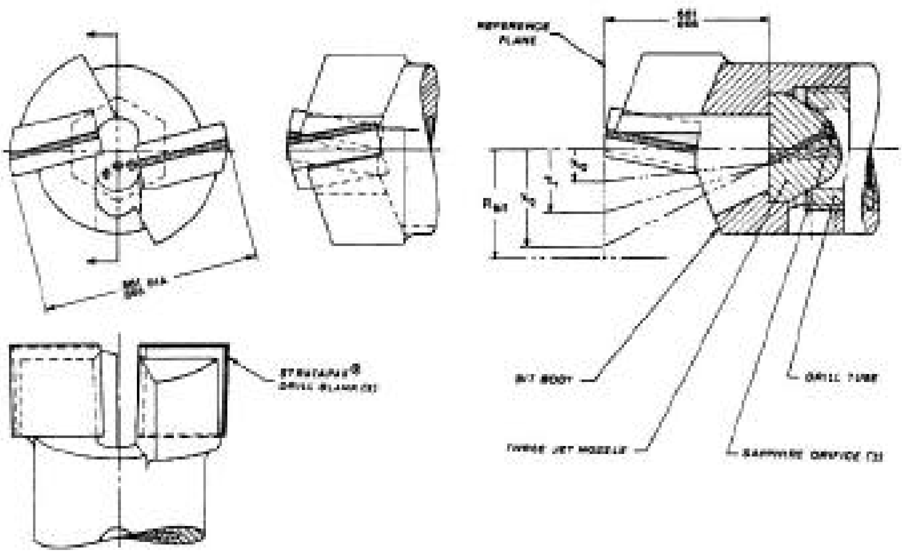

Figure 1. Mechanical Bit Design.

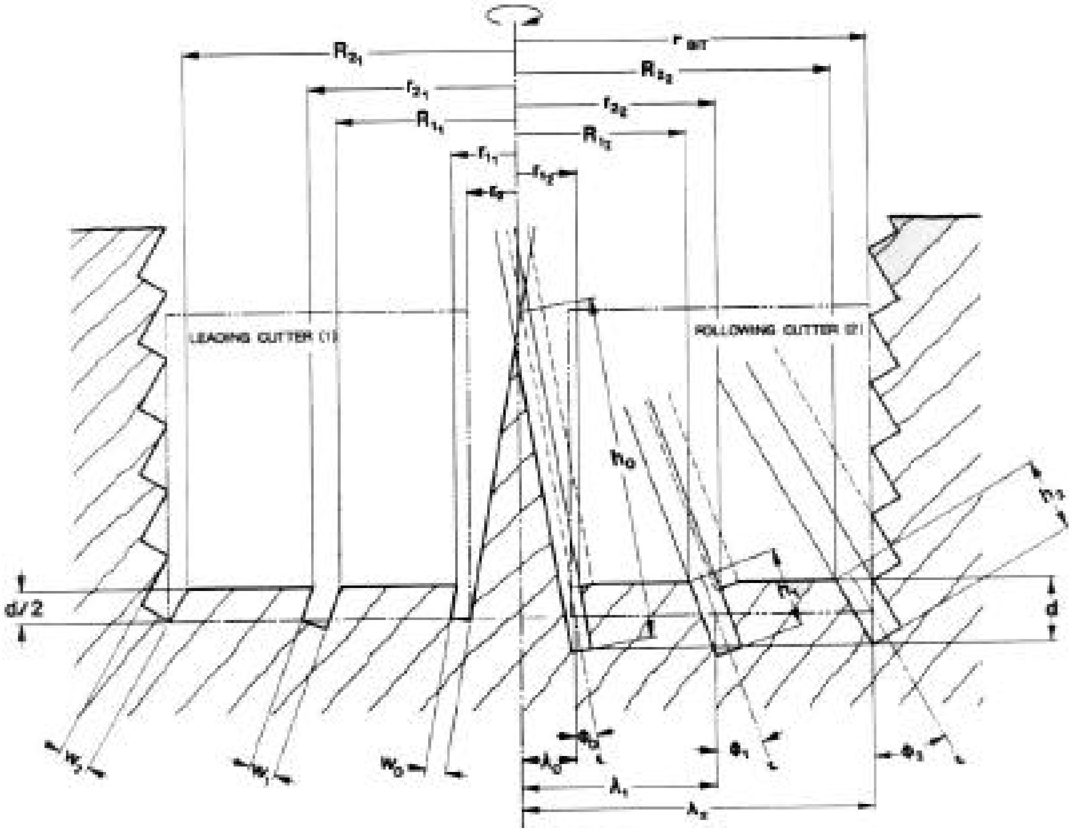

Figure 2. Water Jet Mechanical Drill Models

(a) Turbulant Nozzle

(b) Optimum Nozzle Design

Figure 3

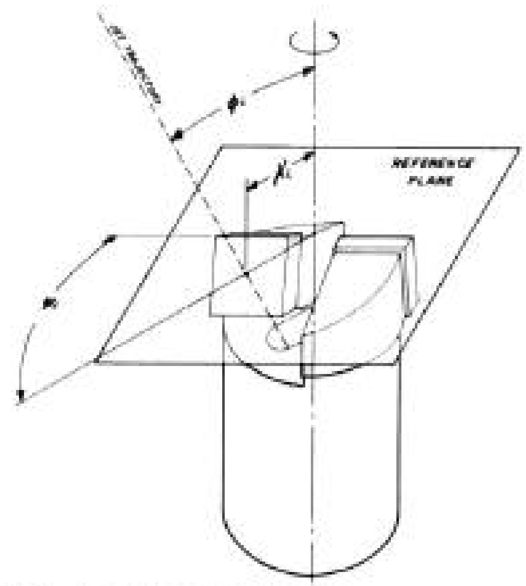

Figure 4. Definition of Jet Angles

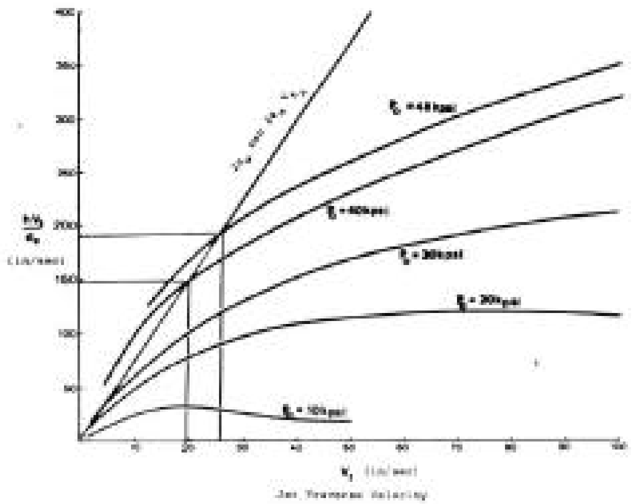

Figure 5. Jet Cutting Characteristics of Geneva Sandstone.

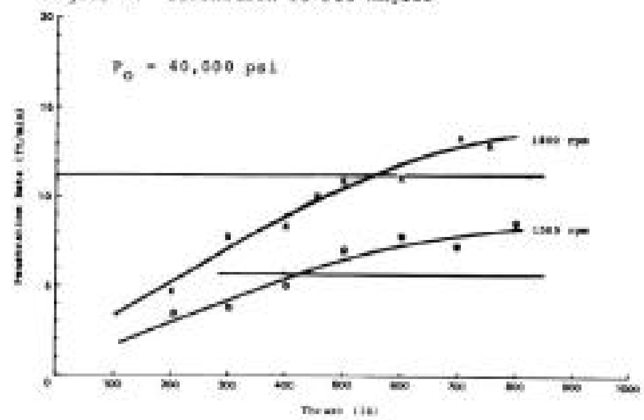

Figure 6. Effect of Rotational Speed.

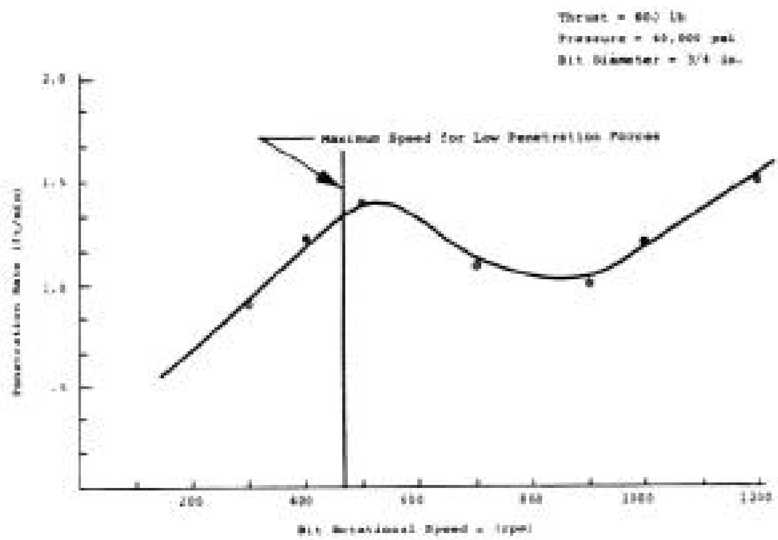

Figure 7. Effect of Gage Jet Undercutting.

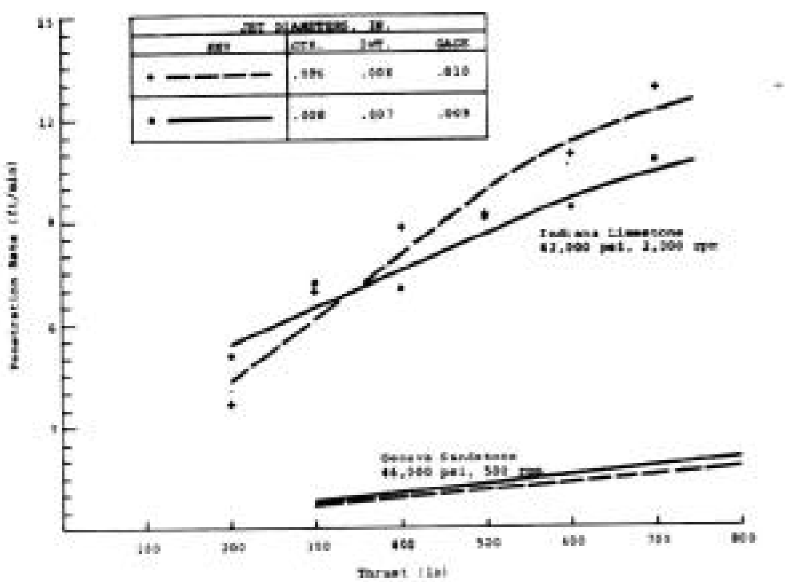

Figure 8. Effect of Jet Power Distribution in Different Rock Types.

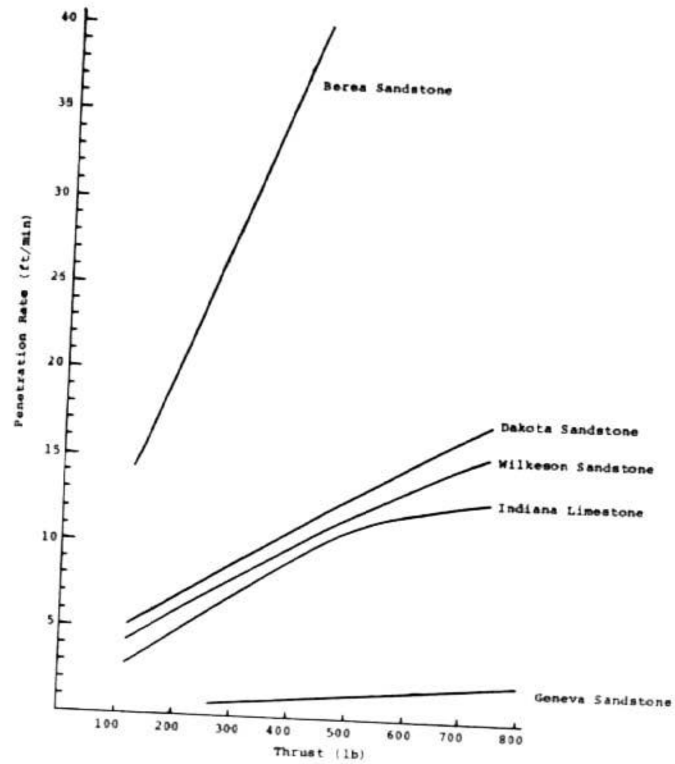

Figure 9. Penetration Rates in Various Rock Types.

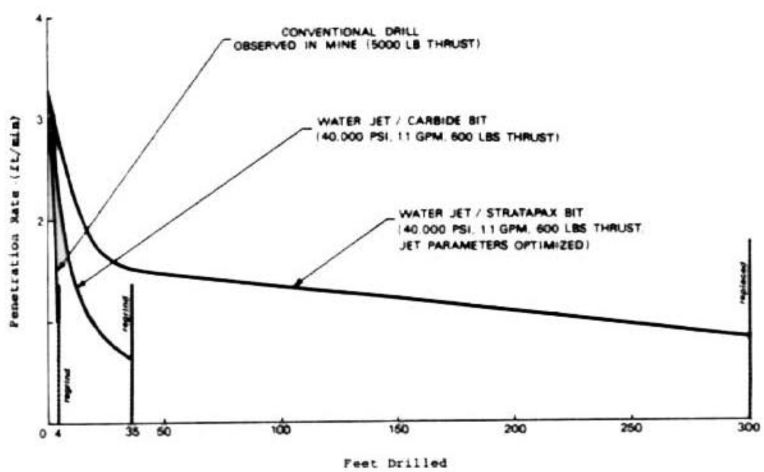

Figure 10. Comparison of Bit Life.

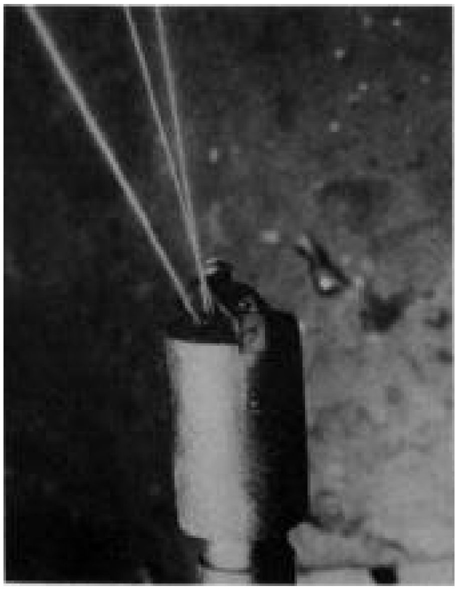
Figure 11. Early Carbide Bit.

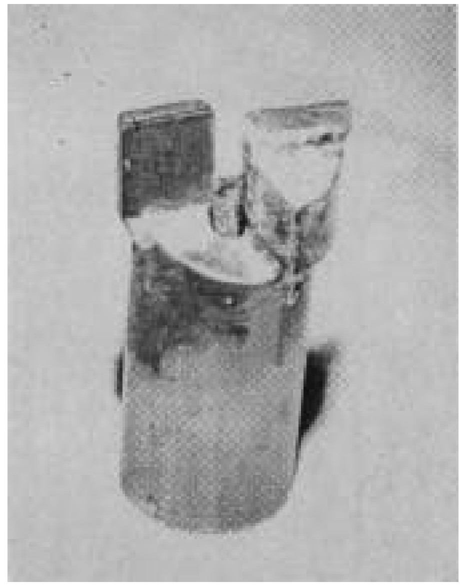
Figure 12. Stratapax Bit.

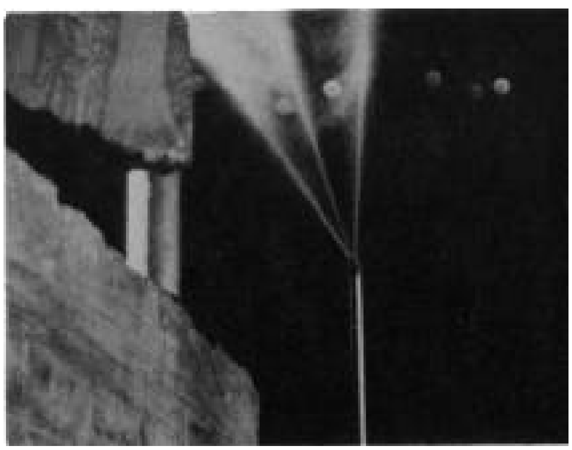
Figure 13. Water Jets.

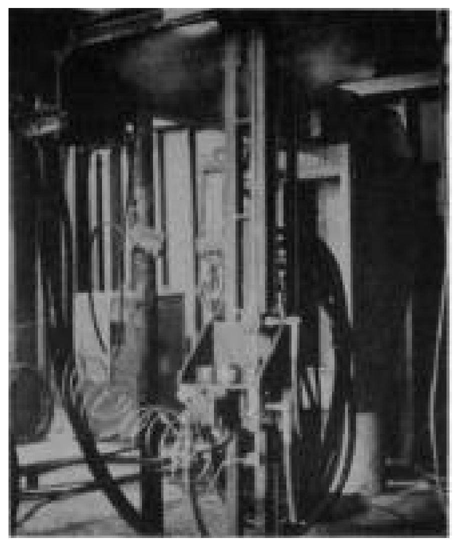
Figure 14. Small Hole Water Jet Drill.

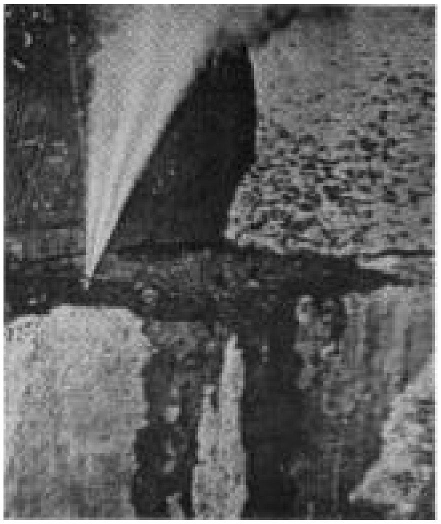

Figure 15. Drilling a Hole.

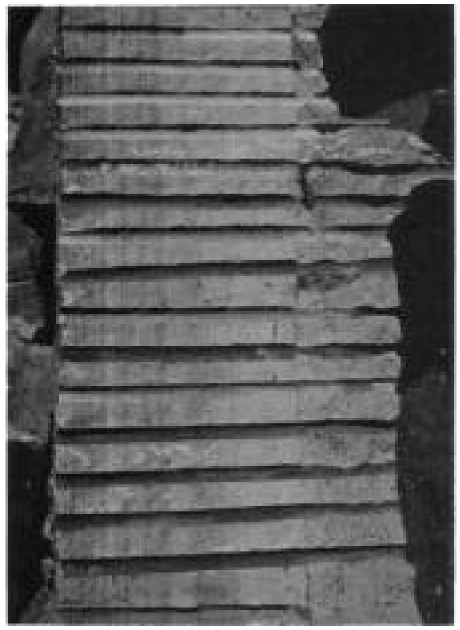

Figure 16. Hole Characteristics.

OPTIMUM CONDITIONS FOR THE HYDRAULIC MINING OF CHINA CLAY

T. W. Davies, Ph.D. M.K. Jackson, B.Sc.

Department of Chemical Engineering,
University of Exeter,
Exeter, Devon, U.K.

ABSTRACT

This paper discusses some preliminary results obtained from an experimental study of the hydraulic mining of china clay from deposits in the St Austell area of Cornwall. The ultimate objective of the study is to establish the relative importance and optimum operating values of nozzle flow rate-head, nozzle contraction shape and standoff distance for a given range of stope conditions.

The results indicate that in order to minimize specific energy consumption and establish the optimum values of mining parameters, there is a need for the reduction of standoff distance and the use of a variable area nozzle to match frequent changes in pit operating conditions.

1. INTRODUCTION

Large scale water jets are used to mine china clay hydraulically from the St Austell area of Cornwall. Monitors are used to produce and direct the water jets which remove, disaggregate and subsequently slurry stope material. The slurry is then pumped downstream, where separation, chemical treatment and dewatering operations take place.

Figure 1 indicates the hardware and production parameters defining the existing mining system. Table l indicates the parameter range in which current operations are conducted.

It is the objective of a research program, currently being conducted by the University of Exeter and English Clays Lovering Pochin & Co Ltd (St Austell), to determine the optimum combination of values of such hydraulic mining parameters and to highlight innovation in equipment design and operations which such a combination of values advocates.

The optimum combination of values of hydraulic mining parameters is that which maximizes mining efficiency. Mining efficiency is characterized by specific energy of mining, E_s, defined as the amount of energy required to remove a unit volume of stope material; hence maximum mining efficiency corresponds to minimum specific energy consumption. In general this requires a move towards a minimum primary hydraulic power requirement and a maximum wash density, ρ_s (i.e. mass of stope material <u>slurried</u> per unit volume of water projected at the stope).

Previous work has indicated that within the range of standoff currently employed, jet dynamic pressure decays to a relatively small fraction of the nozzle pressure (Ref l), that nozzle contraction shape has a considerable effect on the degree of pressure decay (Ref 2) and that rates of material removal are impact pressure dependent (Ref 3). In view of this the parameters considered currently to dominate hydraulic mining efficiency are dimensionless standoff distance (x/d_o) and nozzle contraction shape.

Optimum nozzle design is one which, given nozzle contraction ratio, C_R,and nozzle exit diameter, d_o, produces a jet exhibiting minimum axial dynamic pressure decay.

A preliminary nozzle design study (Ref 2) was conducted, the results of which implied a range of possible optimum contraction shapes. Particular examples from the range have now been manufactured, one of which has been used to obtain the pressure decay measurements presented in this paper.

From a series of velocity and pressure decay measurements conducted using a range of nozzle designs, nozzle pressures and diameters, mechanisms of velocity and pressure decay may be formulated and optimum nozzle contraction shape and standoff distance inferred.

Preliminary results presented here enable characteristic impact pressures to be estimated for present operations and a future operational standoff range to be suggested. The results are simply analyzed in terms of the observed effects: axial jet dynamic pressure and axial velocity decay; and the causes: jet breakup, aerodynamic drag and air entrainment.

Optimum nozzle pressure must be determined by both hydrodynamic and material excavation considerations. A recent study (Ref 4) of the effects of nozzle pressure on wash density for both "hard" and "soft" stopes has highlighted possible effects of impact pressures on rates of material removal. Such effects are dependent upon stope condition. In addition to the variation in relative hardness of stope material, the stope may be:

(i) blasted,
(ii) dozed,
(iii) virgin (neither blasted nor dozed).

Stopes containing large percentages of stent are initially excavated using high explosive charges (i.e. blasted) and are washed in conjunction with stent removal plant. Very soft stopes containing little stent are often ripped and dozed to reduce the strength of the matrix in order that higher production rates be achieved. Virgin stope, sometimes left exposed for a period of time to "weather" or "age", is washed only occasionally under present operating conditions.

Some results of recent pit trials are presented in this paper and analyzed in terms of a simple model of material removal.

Together, jet and material removal characteristics are used to infer a requirement for a reduction in standoff distance and greater flexibility of nozzle flow head characteristics.

2. EXPERIMENTAL

Figure 2 indicates the experimental rig in operation. A jet produced by the nozzle design shown in Figure 3 at a nozzle pressure of 758-5 kPa is illustrated.

The jet is projected onto an instrumented target plate held normal to the flow. Water is recirculated via a $12m^3$ us tank, above which the target plate, enclosed by a surrounding canopy, is situated. The pumper trucks used to pressurize the water draw suction from the recirculation tank and discharge to the monitor via flexible hosing. Standoff distance is varied by moving the bogie on which the monitor is mounted, along a railway track extending some 25 m from the recirculation tank in a direction normal to the target plate.

2.1 Pressure Measurements

Impact pressures were measured using an array of 20 transducers flush mounted in a perspex target plate as shown in Figure 6. The jet was centered on the array by moving the barrel by means of hydraulic rams and noting that the signal levels from the four transducers on each spatial contour were equal. The signal from each of the five spatial contours of transducers was subsequently recorded on a four-channel FM tape recorder and replayed to a PDP 12 computer for analysis.

Pressure measurements were performed using nozzle design 1 (Figure 3) at a nozzle pressure of 551-6 kPa and at standoffs of 4, 8, 12 and 14 m. In addition results are presented from measurements using nozzle designs 2 (Figure 4) and 3 (Figure 5) at a nozzle pressure of 689-5 kPa and a standoff of 13-5 m.

2.2 Jet Diameter Measurements

Jet diameter measurements were made from photographs taken using the shadowgraph technique. A GenRad 1540 strobolume unit giving flash durations of 10 µs was positioned 2-33 m behind a diffusion screen measuring 1-76 m x 1-30 m, itself 0-66 m behind the jet. Eight screen stations were used to cover the jet trajectory from nozzle to impact. An ordinary 35 mm camera was used with Ilford HPS 400 ASA film to take the photographs. Jets from nozzle designs 2 and 3 were used, operating at nozzle pressures of 689-5 kPa.

2.3 Velocity Measurements

Velocity measurements were made using movie films. A Hycam high speed camera was synchronized to the strobe at 70 frames per second to produce the movie films. The jet from nozzle design 3, operating at a nozzle pressure of 689-5 kPa, was used.

2.4 Material Removal Measurements

Pit trials were conducted at "Rocks" pit and "Treviscoe" pit, since they represented examples of relatively soft and hard stopes respectively. Trials were conducted using nozzle designs similar to those of design 2. Nozzle diameters used were 38-1 mm at Treviscoe and 44-45 mm at Rocks. Trials conducted on blasted stope were performed for a range of nozzle pressures between 900 and 2000 kPa and a range of standoff between 10 and 27 m. Trials conducted on virgin stope were performed for a range of nozzle pressures between 689-5 kPa and 2068-5 kPa. Standoffs were 20 m at Rocks and 25 m at Treviscoe.

Material removal rates were measured via wash density measurements, accomplished by dipping a bucket into the wash stream and retaining a sample into which a hydrometer was placed. The specific gravity was then recorded after 15 seconds. This precise timing of measurement was necessary at Treviscoe since the particle size distribution of the slurried stope material resulted in rapid sedimentation, causing a change in density with time. At Rocks this difficulty was not experienced. Sampling frequency was most commonly per minute and varied from once per 20 seconds to once per 5 minutes. Rapid sampling was necessary due to fluctuations in wash density caused by the nature of the operation and inhomogeneity of stope material. The wash stream was sampled as close to the stope face as practically possible and sampling points ranged from 15 to 65 m from the stope face.

3. ANALYSIS OF RESULTS

3.1 Pressure Measurements

Twenty five seconds of data from each transducer were analyzed. The time average pressure was recorded as a density distribution, from which the mean was calculated. Radial distributions of time average pressure were obtained by taking the mean of the four transducer signals for each of the five spatial contours.

The radial distributions of impact pressure are plotted in dimensionless form as Figure 7. Impact pressure is normalized with respect to maximum impact pressure (i.e. centerline pressure) and impact radius is normalized with respect to maximum impact radius (i.e. where $P_i = 0$)

Maximum or centerline stagnation impact pressure is chosen to characterize impact at various standoffs, since this will be identical to jet centerline dynamic pressure.

Maximum impact pressure, $P_{i\,max}$ is plotted against dimensionless standoff distance (x/d_o) in Figure 8. Figure 9 indicates the same data on log-log coordinates.

3.2 Jet Diameter Measurements

From shadowgraph photographs the core of the jet in which 99% of the water is contained can clearly be seen (Ref 1). Measurements of core diameter have been made from a number of photographs at each chosen standoff. The mean dimensionless jet core diameter (d_j/d_o) is plotted against dimensionless standoff (x/d_o) in Figure 10.

3.3 Velocity Measurements

Jet axial velocity decay from the nozzle to impact was determined by measuring the relative displacement of a unique distinguishing portion of the jet between subsequent movie film frames. The results obtained are plotted in non-dimensionalised form in Figure 11.

3.4 Material Removal Measurements

A trace of wash density as a function of time was recorded for a given set of operating conditions and averaged over a time period of half an hour to obtain mean wash densities.

Table 2 summarizes the effects of nozzle pressure on wash density when mining blasted stope. Figure 12 indicates the effects of nozzle pressure on wash density when mining virgin stope.

4. DISCUSSION

4.1 Jet Characteristics

4.1.1 Radial impact pressure distribution

In recent work other researchers (Ref 5) have indicated that the Schlichting formula for dynamic pressure profile may be applied to liquid jets:

$$P/P_{max} = f(\eta) = (1 - \eta^{3/2})^n, \; n = 2 \qquad (1)$$

It is assumed that a function of similar form represents the radial distribution of jet impact pressure. The above equation with n = 2 is plotted as curve A on Figure 8; however, curve B indicates the form of the function which best fits the data and has n = 1-5. Integration of the latter expression gives the ratio of mean to maximum pressure, p $P_m / P_{max} \approx 0\ 32$.

4.1.2 Axial jet dynamic pressure decay

Considering data obtained using nozzle design 1, Figure 9 suggests a simple model of axial jet dynamic pressure decay, namely that minimal pressure decay occurs in the first 100 d_o followed by a power law decay thereafter. Some pressure decay does occur within the first 100 d_o and the dotted line indicates a more realistic model in this region. Figure 8 indicates the best fit curve through the data obtained using nozzle design 1.

The equation of the curve is valid for $(x/d_o) > 100$ and is given by:

$$\frac{P_i \max}{P_o} = c\left(\frac{x}{d_o}\right)^k \qquad (2)$$

where c = 0.01 and k = - 0.74.

An estimate of the pressure decay curve for nozzle design 2 may be made by forcing a function of similar form to equation (2) through the single data point. This is accomplished with c = 0.01 and k = - 1.20.

Before the implications of pressure decay can be considered in terms of jet breakup and air entrainment, it is necessary to consider axial velocity decay and jet coherence.

4.1.3 Jet axial velocity decay

In Figure ll, data obtained using nozzle design 3 indicate that negligible velocity decay occurs until approximately 300 d_o. Subsequent velocity decay appears to be linear and amounts to only 6% over 380 d_o.

4.1.4 Radial spread of jet core

From Figure 10 it may be seen that within the first 150 d_o the jet produced from nozzle design 3 expands very rapidly, after which point only very gradual further expansion occurs. The jet produced from nozzle design 2, however, expands less rapidly during the first 125 d_o and linearly thereafter. Within the first 380 d_o the diameter of the jet core produced from nozzle design 2 is less than that produced from nozzle design 3 and the jet is said to be more coherent.

4.1.5 Relationship between observed jet characteristics and jet breakup

Previous work (Refs 1, 3) has shown that jets produced by all three nozzle designs breakup into discrete slugs or packets of fluid. Such packets contain considerable quantities of air and are not well defined; interpacket spacing consists of a diffuse air-water mixture.

Disturbances initially generated upstream in the monitor and nozzle are amplified in the jet and cause a wave disturbance to propagate on the surface of the jet. The amplitude of the disturbance increases with axial distance downstream of the nozzle and eventually reaches the center of the jet. When the center of the jet is broken for 50% of the time, the jet is said to be fully broken. Previous work (Ref 1) indicates that this point is reached at approximately 300 do downstream for each nozzle design.

As the water jet becomes broken due to instability, air is transferred from a boundary layer covering the water surface to the core of the jet (Figure 12). As air becomes entrained in the jet, conservation of mass requires that the jet expand. The result of air entering the jet is that the effective time average density is considerably reduced and therefore the time average jet dynamic pressure is also reduced in spite of the fact that negligible jet deceleration may have occurred.

An air boundary layer develops on the surface of the jet as a result of aerodynamic drag forces caused by the relative motion of the water surface and surrounding atmosphere.

The jet velocity profile at the nozzle exit is very nearly uniform. The effect of the drag forces is to retard gradually the surface motion of the jet as momentum is transferred from the water jet to the air boundary layer. As the velocity profile is transformed or relaxed, so the jet centerline velocity begins to decay. Within the first 300 d_o drag is considerably enhanced by the rough nature of the jet surface. The surface roughness is caused by eddies generated in the nozzle, which overcome the weak forces of surface tension at the jet surface and result in surface protrusion. The larger eddies have associated with them a smaller radial turbulent velocity and therefore take longer to travel from the jet core to the surface. Surface roughness, therefore, tends to increase with axial distance downstream of the nozzle.

Negligible velocity decay occurs within the first 300 d_o due to the finite time required for the velocity profile relaxation process described above and due to the fact that little air is entrained initially. Once a significant quantity of air is entrained, the time average jet momentum flux is greatly reduced and momentum losses due to surface drag become relatively significant, causing more rapid jet deceleration. From Figure 11 this point appears to be coincident with the defined breakup point.

4.1.6 Calculation of air entrainment

From the velocity decay and jet core diameter data available for nozzle design 3, the quantity of air entrained may be calculated.

Assuming the average jet velocity to be given by Figure 11 and the jet diameter to be given by Figure 10, the jet volumetric flow rate at any point may be calculated from:-

$$Q_j = \frac{\pi dj^2}{4} u_j \qquad (3)$$

Assuming negligible water mass loss the volumetric flow rate of air in the jet at any point is given by:-

$$Q_{ja} = 0.25\pi(d_j^{\partial} u_j - c_d d_o^{\partial} u_o) \qquad (4)$$

Using the volume fraction of water:-

$$x_{vw} = \frac{Q_o}{Q_j} = \frac{C_d d_o^2 u_o}{d_j^2 u_j} \qquad (5)$$

as an indication of the amount of air entrained, the calculated results are presented in Figure 13. The coefficient of discharge, C_d, is taken to be 0.65. From this figure it can be seen that virtually all the air is entrained between 60 d_o and 125 d_o and that negligible further air entrainment occurs downstream.

The region downstream of x = 125 d_o corresponds to the region of very gradualjet expansion in Figure 10. Effectively a large scale water jet acts as an air pump and the total amount of air entrained is given by the sum of the air entrained within the core of the jet itself and that entrained in the air boundary layer which develops on the jet surface. Presently the authors are engaged in drag modeling using boundary layer analysis in order to quantify total air entrainment and to model jet velocity decay.

From air entrainment measurements the axial pressure decay profile for nozzle design 3 may be estimated. Jet dynamic pressure is given by:

$$P_{max} = \frac{1}{2}\rho_e u_j^2 \qquad (6)$$

It is assumed that jet velocity profiles are approximately linear and therefore that ρ_e is defined as an effective fluid density assuming that the jet fluid, consisting of an air-water mixture, may be represented as a homogeneous fluid of intermediate density.

$$\rho_e = x_{vw}\rho_w + (1-x_{vw})\rho_a \qquad (7)$$

Hence,

$$P_{max} = \frac{1}{2}\left[x_{vw}\left(\rho_w - \rho_a\right) + \rho_a\right]U_j^2 \qquad (8)$$

The estimated pressure decay profile is plotted in Figure 8. Fluid properties for air and water are evaluated at a temperature of 15°C. Equation (2) is used to best fit the data with c = 0.01 and k = - 2.27 (curve C).

The calculated results are in agreement with the single data point obtained. Considering the form of the pressure decay profile (Figure 8) and the core air entrainment profile (Figure 13), it may be deduced that air entrainment is primarily responsible for the observed pressure decay.

4.1.7 Effect of nozzle design

From Figure 8 it can be seen that nozzle design has a profound effect on axial jetdynamic pressure decay and air entrainment. From Figure 10 it may be inferred that nozzle designs producing jets which are more coherent are likely to exhibit superior pressure decay characteristics since air is entrained more slowly. Evidently the way in which fluid is accelerated in the nozzle, and the disturbance generated thereby, are directly related to jet breakup and air entrainment.

A range of nozzle designs similar to design 1 have been constructed and are currently being used to determine the relationship between nozzle design parameters and axial pressure decay.

4.2 Material Removal Characteristics

4.2.1 Blasted stope

Within the range of impact pressures studied, impact pressure was seen to have a negligible effect on pit wash density. Table 2 indicates the impact pressure range over which the wash density remained constant. Impact pressures are estimated using curve B, Figure 8.

It is likely that, as impact pressure is reduced, a point where wash density begins to decrease, i.e. a threshold impact pressure, will be reached. It is thought that when mining blasted stope little stope erosion takes place but that disaggregation and slurrying of material previously excavated occurs.

Further trials over a wider range of stope impact pressures are required to evaluate thresholds which may be a function of stope hardness.

4.2.2 Dozed stope

Similar trends were observed when mining dozed stope; however, all impact pressures used resulted in the removal of large "balls" of stope material in addition to a slurry of high density. Such pieces of matrix were carried downstream of the monitor with the slurry flow and subsequently deposited on the pit floor, thus escaping the disaggregating force of the jet This practice represents lost production and wastage of pumping power consumption, and implies that lower threshold impact pressures may be required when mining dozed stopes.

4.2.3 Virgin stope

Figure 14 indicates the effect of impact pressure on wash density, suggesting a range of densities resulting from the limits of relative stope hardness encountered in present operations.

From these results dry clay material removal rates may be calculated from the following equation:-

$$M_c = 3600 Q_d \rho_c \frac{\rho_s - \rho_w}{\rho_c - \rho_w} \qquad (9)$$

Coefficients of discharge for nozzle design 2 were taken as $C_d = 0.85$. Dry clay material removal rates are plotted against maximum impact pressure in Figure 15. Dry clay material removal rates are linearly dependent on impact pressure and a particular threshold stope impact pressure is required before material removal occurs.

The relationship may be described by the following equation:-

$$M_c = k_1 \, (p_{i\,max} - c_1) \qquad (10)$$

Since impact pressures are estimated from a single data point, little significance may be attached to absolute values of material removal rates. However, k_1 and c_1 are certainly functions of relative stope hardness. For stopes mined in St Austell the limits within which k_1 and c_1 lie may be estimated from Figure 15.

$$0.04 \le k_1 \le 0.16 \text{ (tonnes/hr/kPa)}$$
$$58 \le c_1 \le 103 \text{ (kPa)}$$

Reference 6 suggests that, as the depth of cut and hence rate of material removal approach zero, the pressure required to remove material approaches a minimum given by a material strength parameter a. For materials studied in reference 6, a approached the material compressive strength.

Strength properties of china clay are difficult to measure, since clay matrix exhibits a very small strain to failure. This means that any attempt to sample the stope matrix almost certainly leads to sample failure, invalidating subsequent property measurements. An extensive series of pit trials on virgin stope could therefore provide a method by which relatively accurate measurements of a characteristic strength parameter c_l could be made.

4.3 Implications for Equipment Design

Axial pressure decay profiles indicate that a substantial reduction in operating standoff distance would permit either:

(i) reduction in nozzle pressure required to produce specified impact pressure levels, or
(ii) the use of higher impact pressures to obtain higher wash densities in some cases.

Combinations of the above alternatives lead to a reduction in the specific energy of mining and hence an increase in mining efficiency. A suggested future operational standoff range is $0 < x/d_o < 100$, which advocates the requirement for a remotely controlled mobile monitor to ensure safe and efficient practice.

Where standoff distances are required in excess of 100 d_o a nozzle design producing a maximum coherence jet exhibiting minimum pressure decay is required. Results indicate that nozzle design 1 meets these requirements.

Pit trials indicate that a range of impact pressure levels are likely to be required in order to ensure maximum mining efficiency, given the range of stope conditions encountered. It is therefore necessary that nozzle pressure be variable. If nozzle flow rate is to be maintained at a required level, then nozzle diameter must be varied. This advocates the requirement for a variable area nozzle, the diameter of which may be varied remotely in order to avoid frequent nozzle changes.

The authors are at present testing annular designs, similar to those currently used in some fire fighting operations. A suitable variable area nozzle design must produce a jet exhibiting minimal axial pressure decay within the first 100 d_o if the advantages gained by standoff distance reduction are not to be lost.

5. CONCLUSIONS

5.1 Air entrainment is primarily responsible for jet axial pressure decay.

5.2 Axial pressure decay is undesirable in hydraulic mining operations, since it reduces jet energy transmission efficiency and increases the specific energy requirement of mining.

5.3 Nozzle design has a profound effect on jet axial pressure decay. Best nozzle designs produce jets of maximum coherence with associated minimum air entrainment and axial pressure decay. The best design tested to date is that designated nozzle design 1.

5.4 A range of stope impact pressures, dictated by stope conditions, is required to mine china clay optimally.

5.5 Future operational standoff distance should lie within the range $0 \leq x/d_o \leq 100$.

5.6 Future equipment requirement is for a mobile monitor equipped with a remote controlled variable area nozzle operated in conjunction with water pressure pump discharge control. This is required in order to maintain optimal flow head characteristics when frequent changes in stope and pit conditions are encountered.

6. REFERENCES

1. "The Anatomy and Impact Characteristics of Large Scale Water Jets", T.W. Davies, R.A. Metcalfe and M.K. Jackson, Paper A2, 5th Int. Symp. Jet Cutting Technology, Hanover, June 1980.
2. "Optimum Nozzle Design Characteristics", M.K. Jackson, Dept. of Chem. Eng., Univ. of Exeter, U.K., June 1980.
3. "Second Progress Report on Small Scale Erosion Studies", G.J.W. Pettinger, Dept. of Chem. Eng., Univ. of Exeter, U.K., July 1980.
4. "Report on Wash Density Studies at Treviscoe and Rocks", G.J.W. Pettinger, Dept. of Chem. Eng., Univ. of Exeter, U.K., December 1980.
5. "Flow Characteristics of Water Jets in Air", K. Yanaida and A. Ohashi, Paper A3, 4th Int. Symp. Jet Cutting Technology, Canterbury, April 1978.
6. "Experimental and Theoretical Investigation of Hydraulic Cutting of a Western Canadian Coal", M.P. du Plessis and M. Hashish, Paper E3, 5th Int. Symp. Jet Cutting Technology, Hanover, June 1980.

7. ACKNOWLEDGMENTS

The authors wish to thank the SRC and English Clays Lovering Pochin & Co Ltd for their financial support of the project.

GLOSSARY

D barrel diameter (mm)

d_o nozzle diameter (mm)

$C_R = \left[\frac{D}{d_o}\right]^2$ Contraction ratio

C_d coefficient of discharge

E_s specific energy of mining (kJ/m^3)

M material removal rate (tonnes/hr)

P pressure (kPa)

P_O nozzle pressure (kPa)

Q volumetric flow rate (m^3/s)

Q_O nozzle exit volumetric flow rate (m^3/s)

r radial distance (m)

R_{max} jet impact radius at which Pi = 0 (m)

ρ density (kg/m3)

σ material strength parameter (kPa)

u velocity (m/s)

u_O nozzle exit velocity (m/s)

x standoff distance

x/d_o dimensionless standoff distance (d_o in m)

xv volume fraction

$\eta = r/R_{max}$ dimensionless jet impact radius

Subscripts

a	air	j	jet
c	dry clay	m	mean
e	effective	s	slurry
i	impact	w	water

PARAMETER	RANGE
Standoff distance, x	13 - 27 m
Nozzle pressure, P_o	686 - 2410 kPa (100 - 350 psi)
Nozzle flow rate, Q	0·126 - 0·252 m^3/s (2000 - 4000 gpm (UK))
Nozzle diameter, d_o	25·4 - 50·8 mm
Dimensionless standoff distance, $\frac{x}{d_o}$	260 - 600

TABLE 1 - OPERATIONAL PARAMETER RANGE

		Parameter Range within which ρ_s Constant				
Pit	Constant average producing wash density ρ_s (kg/m^3)	P_o (kPa)	d_o (mm)	x (m)	$P_{i\ max}/P_o$	Minimum $P_{i\ max}$ (kPa)
Treviscoe	1017	896 - 1517	38·10	10 - 17	0·48 - 0·16	145 - 241
Rocks	1050	1310 - 2000	44·45	10 - 27	0·58 - 0·1	131 - 200

TABLE 2 - EFFECT OF NOZZLE PRESSURE ON WASH DENSITY (BLASTED STORE)

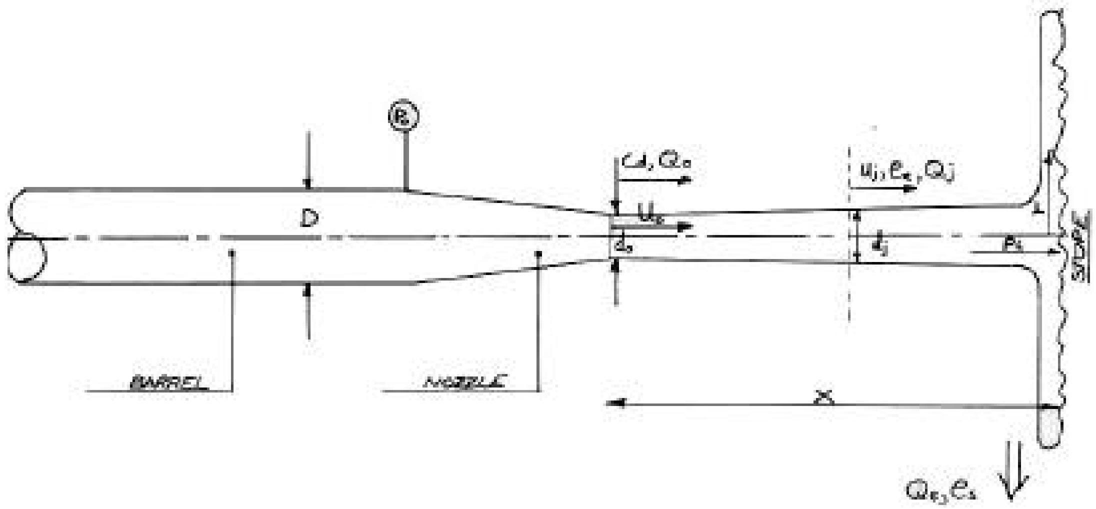

FIGURE 1 DEFINITION OF MINING SYSTEM PARAMETERS

FIGURE 2 EXPERIMENTAL RIG IN OPERATION

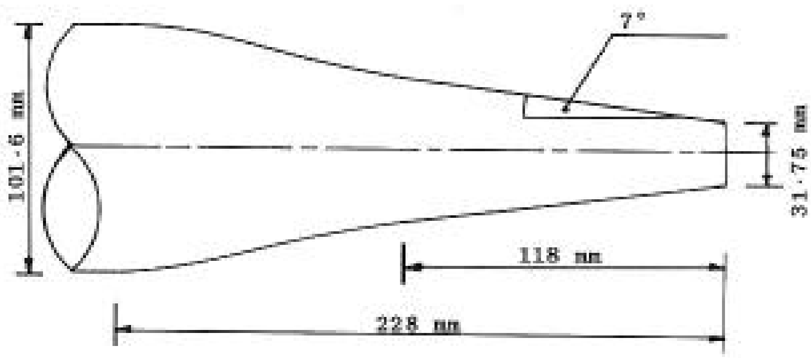

FIGURE 3 NOZZLE DESIGN 1

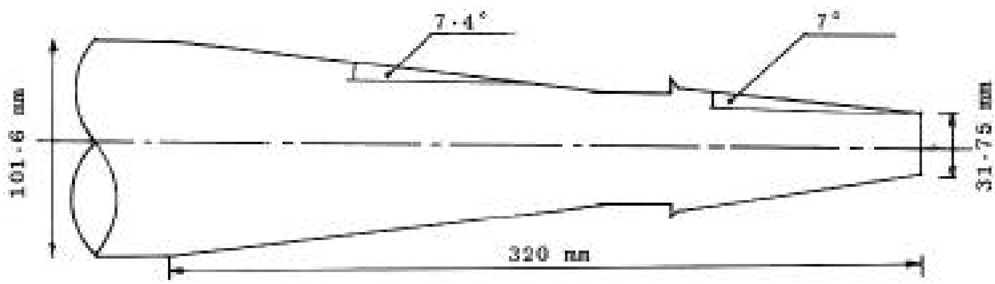

FIGURE 4 NOZZLE DESIGN 2

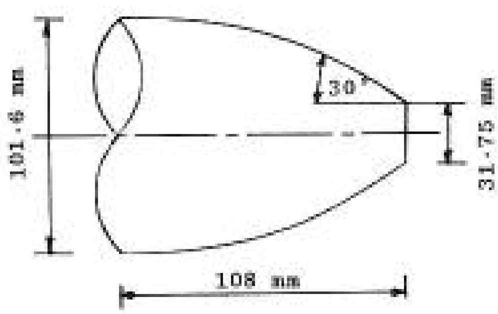

FIGURE 5 NOZZLE DESIGN 3

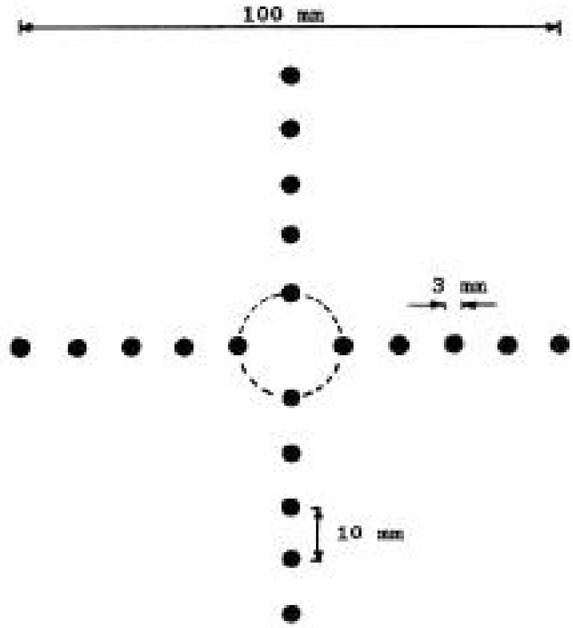

FIGURE 6 TRANSDUCER ARRAY

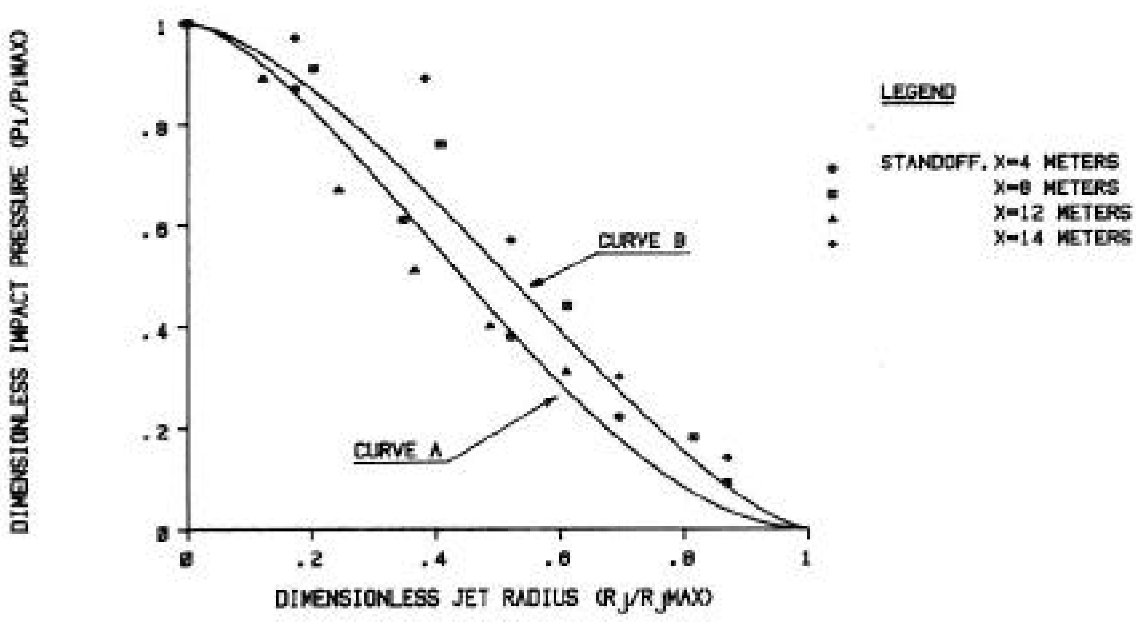

FIGURE 7 RADIAL IMPACT JESSIE DISTRIBUTION

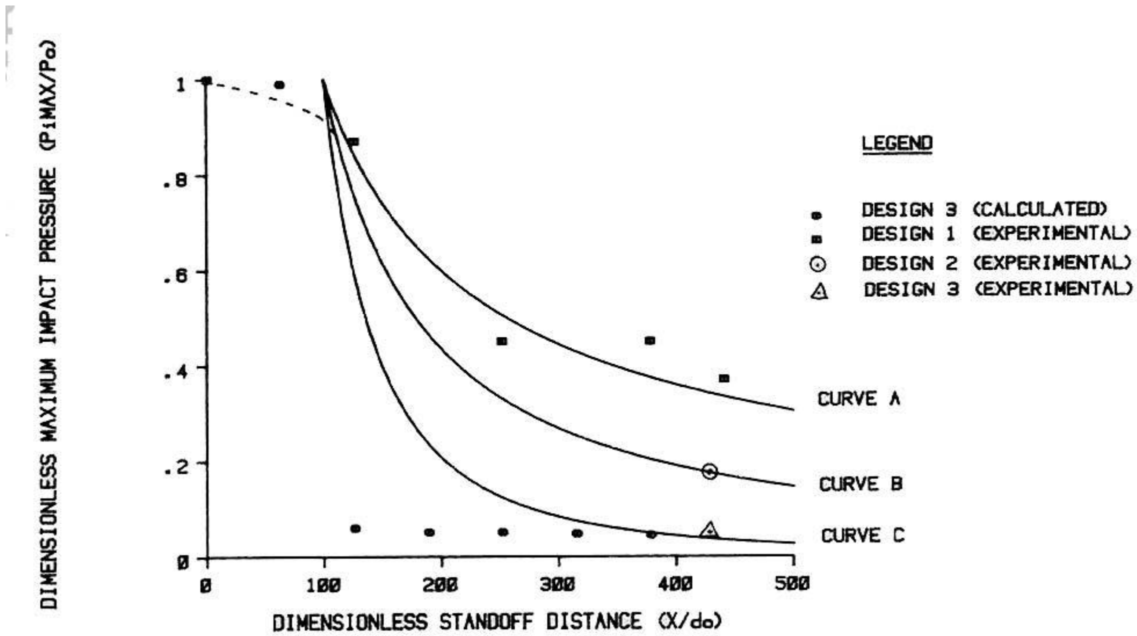

FIGURE 8 AXIAL JET DYNAMIC PRESSURE DECAY

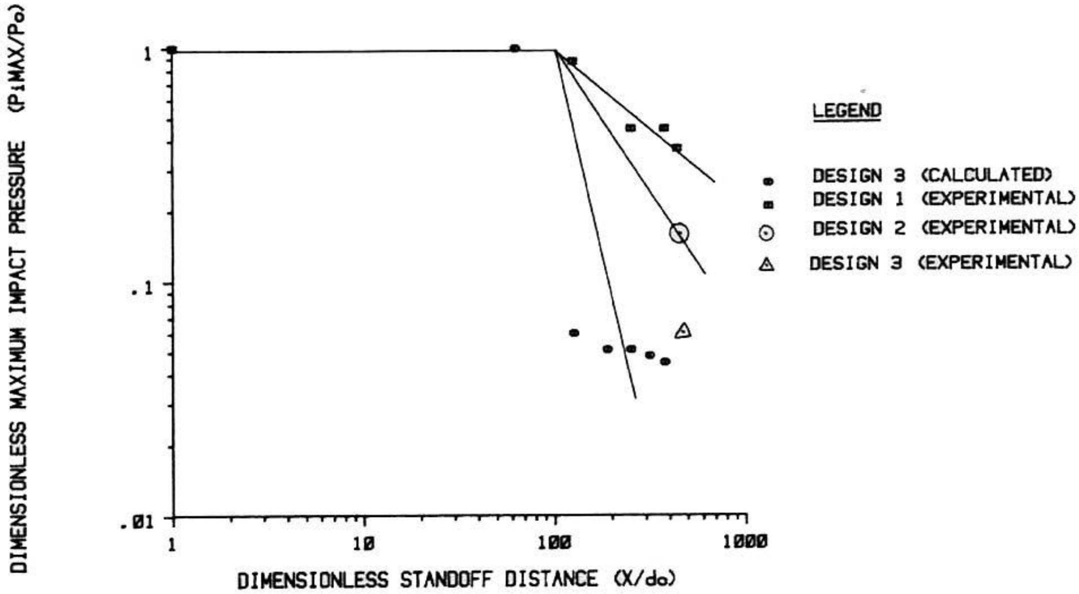

FIGURE 9 AXIAL JET DYNAMIC PRESSURE DECAY (LOG-LOG PLOT)

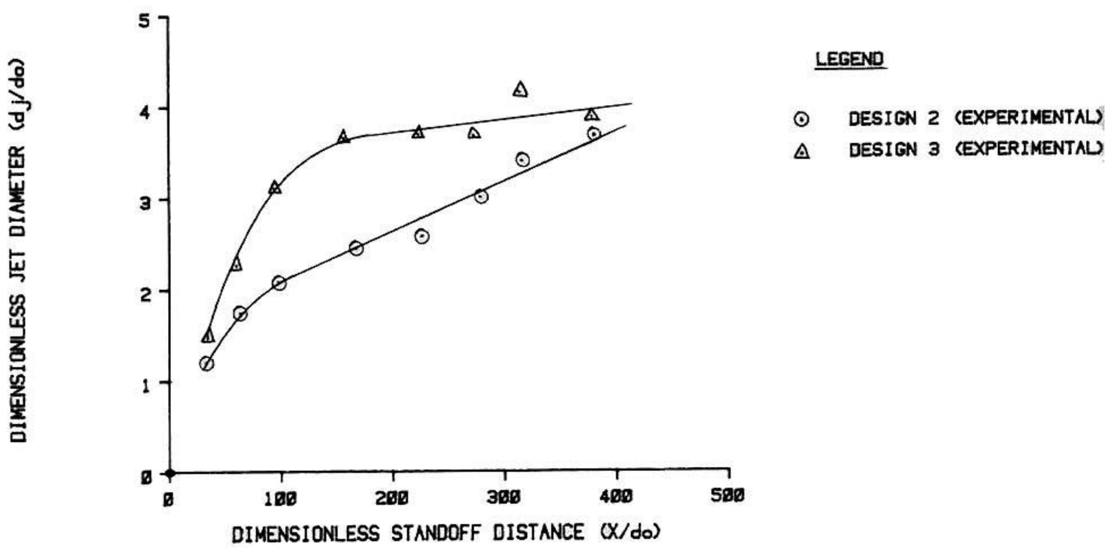

FI GURE 10 JET CORE DIAMETER

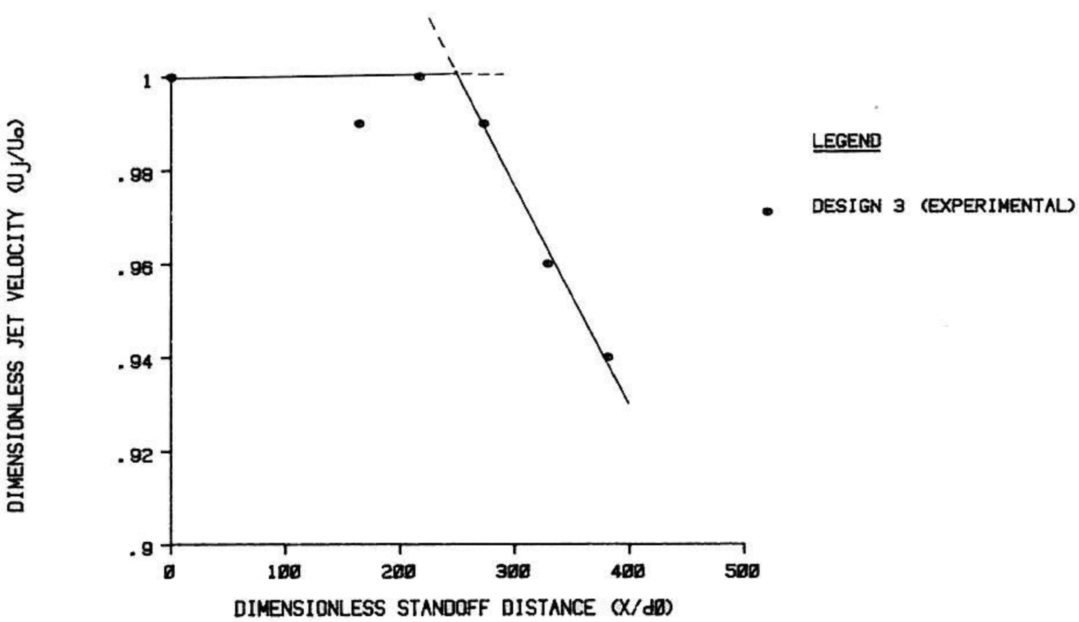

FIGURE 11 AXIAL JET VELOCITY DECAY

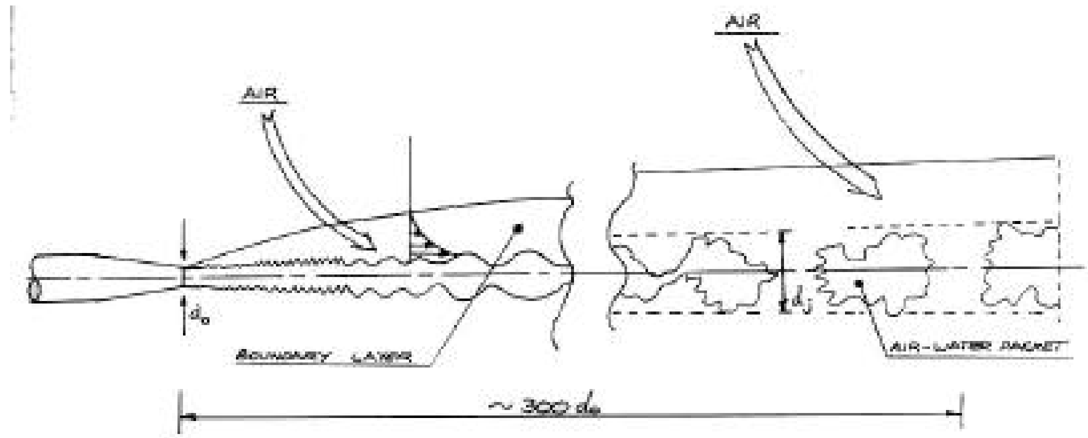

FIGURE 12 JET BREAKUP AND AIR ENTRAINMENT

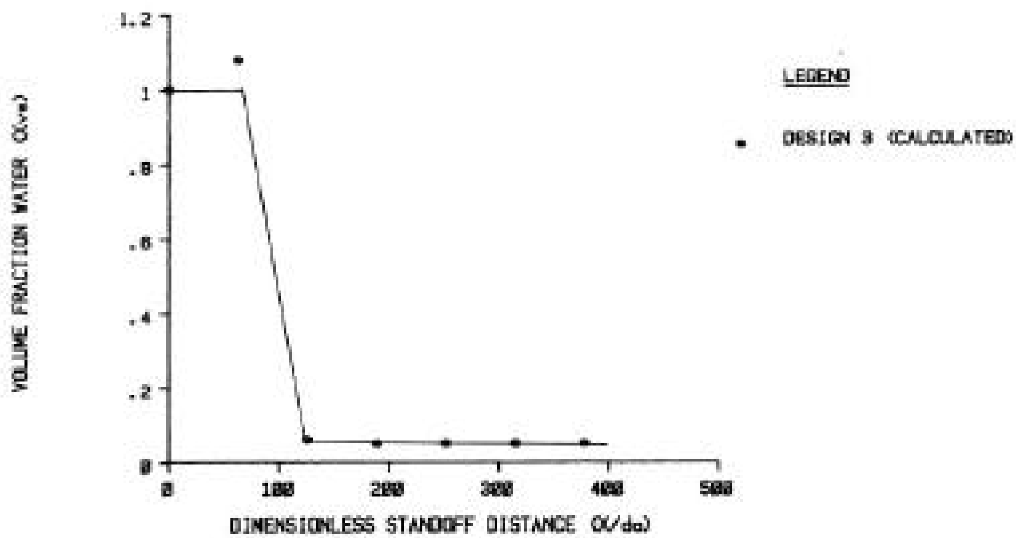

FIGURE 13 CALCULATED AIR ENTRAINMENT

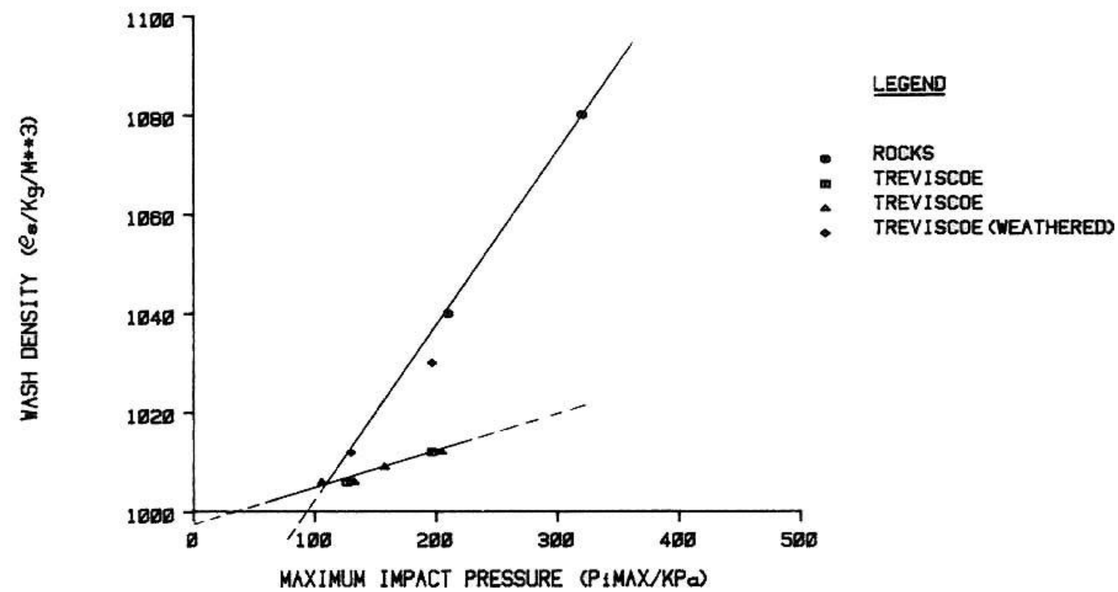

FIGURE 14 EFFECT OF IMPACT PRESSURE ON WASH DENSITY (VIRGIN STOPE)

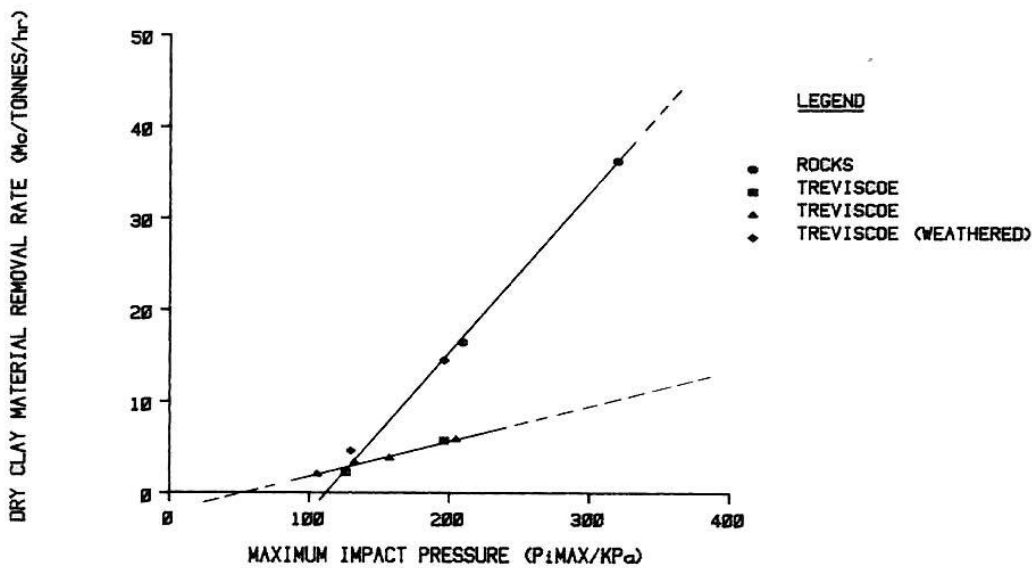

FIGURE 15 EFFECT OF IMPACT PRESSURE ON MATERIAL REMOVAL RATE (VIRGIN STOPE)

IN-SEAM TRIALS WITH THE "HYDROHOBEL"

by
E.H. Henkel
Bergbau-Forschung GmbH
Franz-Fischer-Weg 61
4300 Essen
West-Germany

by
Th. Kramer
Bergbau-Forschung GmbH
Franz-Fischer-Weg 61
4300 Essen
West-Germany

ABSTRACT

Feasibility trials relative to the combination of coal-plough picks and high-pressure water jets were run by Bergbau-Forschung GmbH. The efficiency of the Hydrohobel was tested on mock-up coal faces. For the first experimental operation of the Hydrohobel (high-pressure waterjet assisted coal plough) an experimental coal face was prepared and comparative trials of conventional coal ploughs and high-pressure waterjet assisted coal ploughs were run. The results are displayed and a performance balance is set up.

INTRODUCTION

For effective support of the mechanical cutting into hard coal by high-pressure cutting jets needs motion of the high-pressure water jet relative to the surface of the mineral to be mined. One possibility of generating this transverse movement is separate drive of the nozzle mechanism. Tests and test results of such oscillating water jet systems were described in previous papers (1) (2). Apart from this possibility to move the water jet independently another method exists, a technically simpler one, i.e. to induce transverse movement of the water jet exclusively by the forward travel of the whole machine body. In this case the transverse movement of the water jet corresponds to the travelling speed of the whole coal-winning machine.

For testing this method, a Gleithobel plough supplied by the largest coal-plough manufacturer, Messrs. Westfalia Lunen, was converted and tested as "Hydrohobel". Before the trials with life-size coal ploughs, individual trials were run with the specially designed cutting tools, and the best-suited parameters for nozzle diameter, nozzle array, nozzle spacing, and water pressure were determined. Furthermore the influence of the transverse speed on cutting efficiency was investigated. After these tests, trials with complete "Hydrohobel"-systems could be run on mock-up coal faces. Subsequently such a system was experimentally run underground on Lohberg colliery where the results could be compared directly with those of a conventional coal plough.

THEORETICAL ASPECTS

The trials here-described were run with a cutting method using continuous high-pressure water jets with pressures of max. $p = 75\ MN/m^2$. These water jets assisted mechanical cutting work of coal-plough picks. The high-pressure water jet hits the coal-face surface at an 15° angle and cuts a slot in line with the face. The coal-plough picks follow this slot. Thus the mechanical efforts for chipping off the mineral can be reduced drastically. This reduction of necessary efforts can be made use of either by reducing the power pick-up of the coalplough drive or by increasing the web and thus the overall-winning performance - Fig.1-.

Coal ploughs normally are run at a travelling speed ranging between 1.3 - 1.8 m/s. For the "Hydrohobel", however, a speed of 0.65 m/s was chosen in order to obtain sufficiently intensified water-jet action on the coal face.

On a coal plough approximately 20 picks are in action in either travel. In view of sufficient assist, therefore, a maximum of these picks should be equipped with high pressure water nozzles. Since flow and power requirements for the pump drives need to be kept within certain limits, only small nozzle diameters can be chosen. The "Hydrohobel"-version under test was equipped with 16 nozzle-equipped picks - Fig. 2 - . The nozzle diameters range between 0.8 and 1.0 mm. The total flow was of 180 l/min at a water pressure of 75 MN/m^2. This required a pump-driving performance of 265 kW. Since for conversion of conventional coal ploughs as little modification should be made as possible, the high-pressure water was supplied to the plough by a stationary pump via trailing hoses.

FEASIBILITY TRIALS

On a special test rig for determination of the cutting forces where the forces acting in three dimensions could be recorded (1), sets of four high-pressure waterjet assisted picks each were tested. The following parameters were varied throughout the tests:

- -Nozzle diameter
- -Compressive strength of the mock-up coal
- -Transverse speed
- -Water pressure
- -Web.

The initial tests already showed that with nozzle diameters of 0.8 mm and a pressure of 75 MN/m^2 no significant reduction of the mechanical chipping efforts could be recorded. All further trials therefore were run with 1.0 mm dia.nozzles - Fig. 3 - . The influence of mock-up coal strength on the cutting force of the pick sets is shown on Fig. 4 with the cutting web as parameter. At a travelling speed of 0.32 m/s, a disproportionate cutting force increase with increasing compressive strength of the mock-up coal was recorded.

In the next test series the travelling speed was increased to 0.65 m/s. The cutting forces are shown was web versus compressive strength of the mineral - Fig. 5 - . At higher travelling speed the progressive cutting-force increase was even more pronounced. The travelling speed of 0.65 m/s seems to be a limit value for the nozzle diameters and the mineral strengths investigated. This limit value probably should not be exceeded. Furthermore tests were run with and without high-pressure waterjet assist. The results of these comparative tests are shown on Fig. 6. Here, it was found that at a web of 12 cm the high-pressure waterjet assist enabled a cutting-force reduction of approximately 30% of the merely mechanical chipping efforts. These results, however, are only valid for the softer mock-up coal.

SURFACE TRIALS WITH THE "HYDROHOBEL"

The tests of the full-size "Hydrohobel" were run on a mock-up coal face of 20 m of length, 1.5 m of height, and with a compressive strength of σ_D = 4.5 N/mm². The results of the feasibility trials could be confirmed as to their trend. A 10% reduction of the normal forces was obtained. However, since it was known from previous trials that mockup coal withstands penetration of high-pressure water jets more than real coal, the underground trials were prepared in spite of this - Fig. 7 and Fig. 8 - .

IN-SEAM TRIALS WITH "HYDROHOBEL"

In an experimental face of Lohberg colliery trials were run with the "Hydrohobel" and compared with performance of a conventional Gleithobel plough. The high-pressure pumps were installed stationary in the gateroad of the experimental face. The "Hydrohobel" was supplied with high-pressure water via a 50 m trailing hose - Fig. 9 - . For recording of the normal forces an intrinsically safe measuring set developed by Bergbau-Forschung GmbH was used on the plough - Fig. 10 - .

The plough system was equipped as follows:

Travel motors: 2 x 45 kW
Plough speed: 0.65 m/s
Pump drive: 265 kW
Nozzles: 11 x 0.8 mm
Water pressure: 75 MN/m2
Flow: 180 l/min - Fig. 11 - .

The most significant results are shown on Fig. 12 . Here the power pick-up of the motors is plotted against cutting performance (web in m times travelling speed in m/min) for the "Hydrohobel" and for a Gleithobel plough. It was found that the "Hydrohobel" recorded an increase of cutting performance from 4.45 m²/min to 5.48 m²/min. Of course the additional power-pick up of the pump drives needs to be considered as well.

Throughout the trials a considerably less dust load and a higher portion of large particle sizes was stated. The high-pressure water supply via trailing hoses was practicable for experimental operation, however, needs to be replaced by another supply system for the production versions.

SUMMARY

On the one hand the hydro plough recorded underground an improved coal-winning efficiency with less dust load and better particle-size distribution of the run-of-mine coal. On the other hand, however, the overall-energy balance at present speaks against this method. A great number of nozzles with small diameters run at high travelling speed do not yield the required increasing effect on coal-winning performance. Systems with larger nozzle diameters and separate nozzle-oscillation mechanisms yielded up to present better results in experimental operations within German coal mining.

ACKNOWLEDGEMENTS

The investigations here described were sponsored by the Bundesminister fur Forschung und Technologie (Federal German ministry for research and technology). The project was carried out in cooperation of Bergbau-Forschung GmbH and Gewerkschaft Eisenhutte Westfalia Lunen.

REFERENCES:

1. Kramer, Th.
Investigations of High Pressure Water Jet Cutting Techniques for Coal Winning
Fifth International Symposium on Jet Cutting Technology Hanover, 1980

2. Henkel, E.H.
Aims for High Pressure Water Jet Assisted Coal Winning System
Fifth International Symposium on Jet Cutting Technology Hanover, 1980

LEGEND OF FORMULAE

F :	Cutting force	kN
s :	Web	cm
v :	Travelling speed	m/s
d :	Nozzle diameter	mm
p :	Water pressure	MN/m^2
V :	Flow	l/min
G_D :	Compressive strength of coal	daN/cm^2
p :	Power pick-up (drive)	kW
A :	Cutting performance	m^2/min

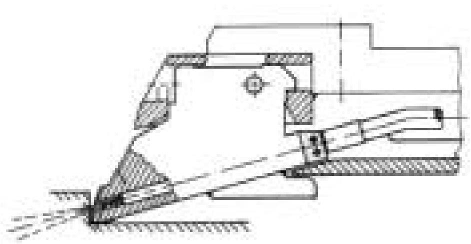

Fig. 1 Plough pick with high-pressure

Fig. 2 Hydrohobel (high-pressure waterjet assisted coal plough)

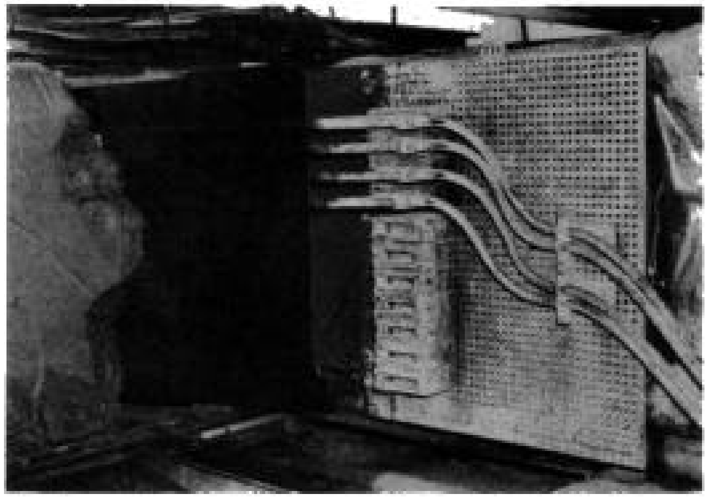

Fig. 3 Pick array on the test rig

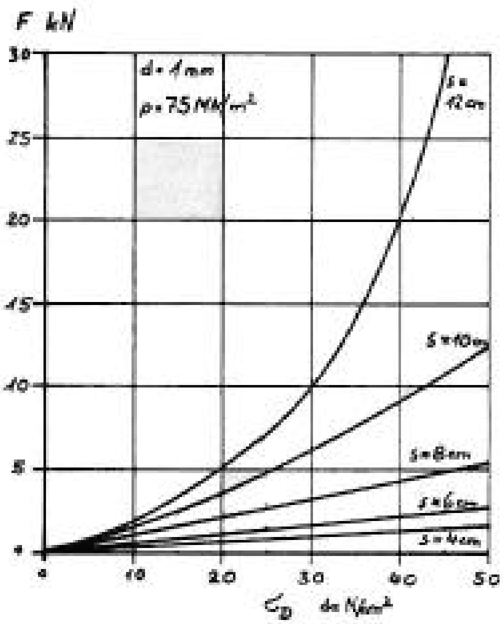

Fig. 4 Cutting force as a function of compressive strength, with web as a parameter.

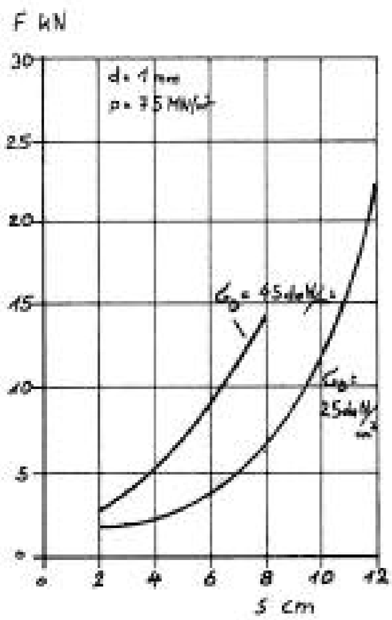

Fig. 5 Cutting force as a function of web with compressive strength as a parameter.

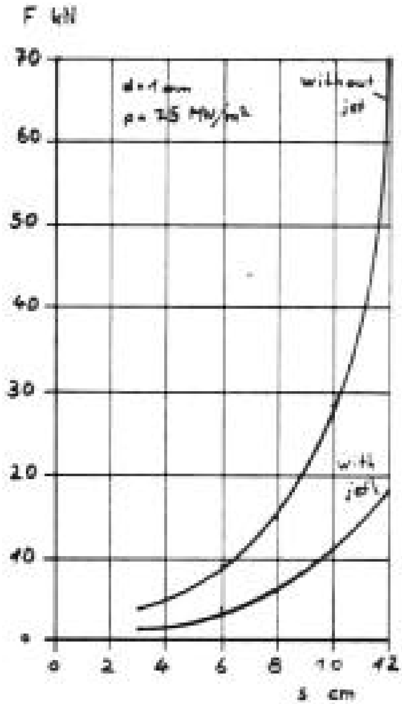

Fig 6. Cutting force as a function of web, with and without high-pressure waterjet assist

Fig. 7 Hydrohobel on mock-up coal face

Fig. 8 High-pressure water jets in action on Hydrohobel

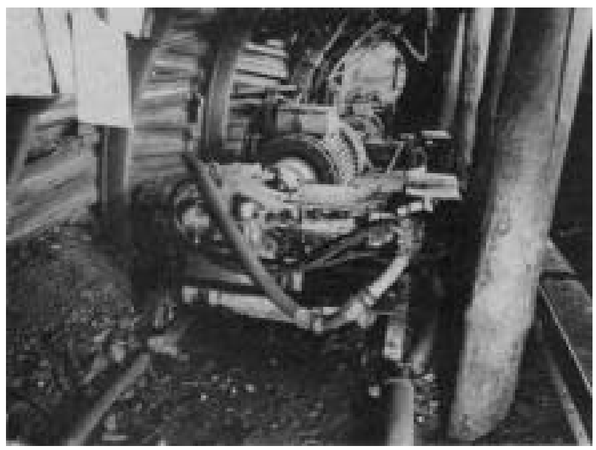

Fig. 9 Pumping station underground

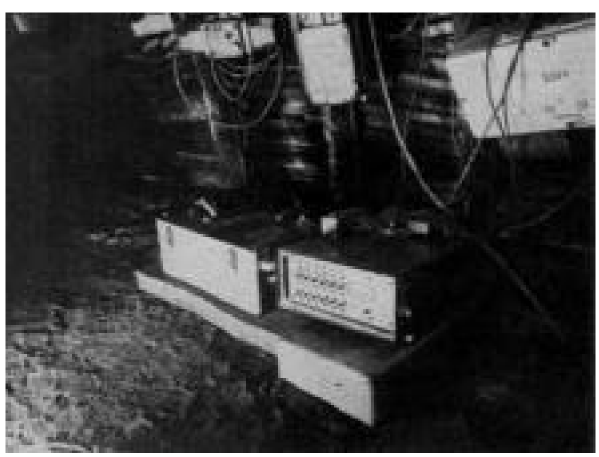

Fig. 10 Measuring equipment in the experimental coal face

Fig. 11 Hydrohobel in the coal face

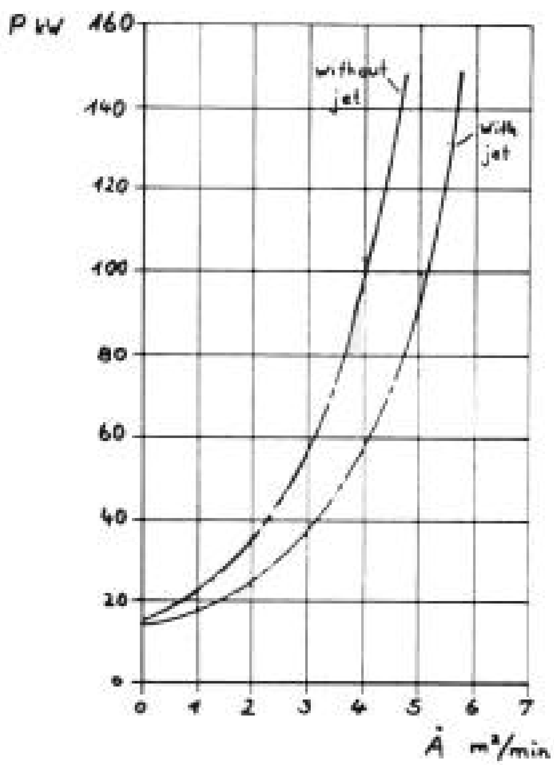

Fig. 12 Power pick-up of the motors as a function of cutting performance, with and without high-pressure waterjet assist

AN INVESTIGATION ON THE USE OF A SWING-OSCILLATION JET IN UNDERGROUND IN-SEAM DRIVAGE

Tang Xuenan
Central Coal Mining Research Institute
China

INTRODUCTION

The use of high pressure water jet is a new technique for cleaning, cutting and crushing materials. Because of its numerous advantages it has aroused great interest among the mining industry circles in various countries.

In recent years, investigation into this new technique started successively in different organizations in China. Satisfactory techno-economic results have already been obtained in the ship building and oil industries.

Some progress has also been made in its application to the coal industry. Underground experiments have been carried out on a roadheader equipped with a high-pressure continuous jet at a working pressure of 350-500 kg/cm^2. Generators for continuous jets and pulse jets at a working pressure of 3800-6000 kg/cm are being developed.

Since the seventies, further research on this technique has been carried out in many countries. As a result, new types of jets, such as the resonant jet, high-frequency impulse jet, Cavijet, swing-oscillation jet, etc., have been developed. Underground coal cutting experiments with a swing-oscillation jet are described in this paper.

I. Principles of Coal Cutting by Swing-Oscillation Jet

In order to increase the rate of motion of the jet across the coal face and find an efficient process for cutting coal in front of and perpendicular to the coal face, experiments were carried out in 1978 on the effect of cutting capacity of the swing-oscillation jet on coal drivage.

The main feature of the swing-oscillation jet is the superimposition of an oscillating motion at a given frequency perpendicular to swing motion of the swinging pistol- It is expected that with swing-oscillation it is possible to increase the cutting capability of the jet, by:

1. increasing the rate of motion of the jet across the coal face;
2. changing the loading characteristics of the jet on the solid coal, and
3. improving the cutting of solid coal by jets.

II. Experiments with a Swing-Oscillation Jet and Analysis of its Cutting Ability in In-Seam Drivage

Many mines in China experience high concentrations of air-borne dust at the heading faces. In some mines, high gas emissions accompanying driving to coal always result in gas concentrations exceeding the safety limit. It is on this basis that the attempt is being made to cut coal by a swing-oscillation jet in driving headings in coal.

It has been determined from the experiments with swing-oscillation jet in underground in-seam drivage that more efficient results, in terms of cutting intensity, could be obtained if the pistol is swinging horizontally while oscillating vertically throughout the process. The process in brief is as follows:

1. A deep fractured zone with a given width is formed by repeated scanning by the swing-oscillation jet at the bottom section of the roadway. Practice indicated that the deeper the fractured zone, the more the coal is won from the entire section, and the quicker the rate of advance.
2. Other new fractured zones will then be formed in turn by repeated scanning of coal with the swing oscillation jet at a certain spacing, thus cutting into the coal.
3. The coal left between two neighboring fractured zones and by the swing-oscillation jet, sometimes including the coal above the fractured zone, may possibly be cut down by the vertical component of the swing-oscillation jet when coal is of suitable hardness and with well bedded planes and joints.
4. In softer coals where the beddings and joints are well developed, the coal in the middle section may sometimes fall off in large pieces if the cut in the bottom fractured zone is too deep. In some cases, this calls for using the jet to trim the section to its desired profile, in the last stage of roadway drivage.

From what has been mentioned above, the total amount of coal, W. obtainable by the jet when driving an inseam roadway, is composed of four parts:

$$W = W_1 + W_2 + W_3 + W_4 \qquad (1)$$

where, W_1 - coal cut directly by the jet during undercutting

W_2 - coal spalled from the ridge between slots when the jet cutting

$W_1 + W_2$ - coal obtained from the fractured zone scanning of the jet

W_3 - coal cut by the vertical component of the jet and by the gravity of coal itself above or below the fractured zone

W_4 - coal spalled in large pieces

III. Basic Parameters Affecting the Cutting Capacity of the Swing-Oscillation Jet

From the results of coal cutting tests in driving a roadway by jets and from the preliminary analysis of formula (1), it is shown that among the four components that make up W. the key ones are W_1 and W_2 and we should endeavour to increase their proportions, such as by making the initial undercut as deep as possible. For this reason, cellular concrete blocks were used as samples in systematic laboratory studies, aimed at identifying the relationship between W_1, W_2 and the basic parameters of the swing-oscillation jet, thereby eliminating W_3 and W_4 which would otherwise be present in the use of coal.

The following is a brief account of the three functional relations obtained from the laboratory experiments related to the cutting capacity of the swing-oscillation jet.

1. Oscillation Frequency, f, versus "plume of Material Cut, V, and Rate of Cutting, V_o.

An experiment was conducted with a view to identifying if there is any increase in cutting ability by superimposing an oscillating motion normal to the swinging movement of the jet, and eventually quantifying the increase if there is any. Measurements were made at four different frequencies of oscillation, f = O. 930, 1,140 and 1,400 respectively while keeping constant other parameters such as jet pressure, standoff distance to the coal face, velocity of swing, and amplitude of oscillation. When f = 0, it means that the jet is operated with the swinging jet mode only. Fig. 1 is plotted with some of the data recorded, from which it can been seen that all the points are scattered on either side of a straight line with fair regularity.

The results shown that at a given jet pressure, frequency of oscillation and material, the volume eroded from the sample, V, and the rate of erosion, V_o , increase in direct proportion to the increase of the oscillation frequency of jet f.

2. Number of passes, n, vs Depth of Cut, d, for the Swing-oscillation Jet.

The results from a large number of tests for cutting slots with swing-only jet show that the increment decreases with each cutting pass (see curve A, Fig. 2). This, of course, is undesirable for slot-cutting operations. How then would it behave if a swing-oscillating jet is used instead of only a swing jet? From Fig. 2 it is readily seen that, within the limits of the experiment, when the swing-oscillating jet is used for cutting the sample block, the eroded depth, d, basically varies in direct proportion to the number of passes of the jet. This puts the continuous jets in a very favorable position for cutting coal. In other words, when the jet is making multiple passes, the depth of cut for each pass is basically the same. This provides a theoretical basis for obtaining a deeper fractured zone by multi-pass shooting.

Figure 3 is a photograph showing the result when a cellular concrete sample is cut by the swing-oscillating jet as well as the swing-only jet in multi-pass shooting. It can clearly be seen that the eroded depth cut by the swing-only jet approaches that of the swing-oscillation jet with increasing number of passes. It shows that the swing-oscillation jet working with repeated scanning is more effective than the swing-only jet.

3. Volume Eroded by the Swing-Oscillation Jet, V , vs Standoff Distance, s.

According to the test data, the relationship between the volume eroded by the swing-oscillation jet. V, and the different standoff distance, s, is shown in Fig. 4. Peaks in the eroded volume frequently appear when different kinds of material are cut by the swing-oscillation jet, thereby indicating that there should be an optimal standoff distance. However, no peak is observed in the sample cut by a swing-only jet at a standoff distance less than 600 mm (shown by the horizontal shaded area in the Figure 4).

In accordance with the test data obtained at different standoff distances, there is an evident peak range of cutting ability for the swing-oscillation jet. Also the cutting ability of the swing-oscillation jet varies considerably at a greater standoff distance. As shown in Fig. 4, the cutting ability is reduced almost by 50% at a standoff distance from 200 mm to 500-600 mm. Therefore, it is of great significance to determine the optimal standoff distance for swing-oscillation jet.

As shown in Fig. 4, it is evident that although the energy consumption of the swing-oscillating jet is basically the same as that of the swing-only jet, the cutting ability at the optimal standoff distance increased by 300% or so through the addition of the oscillating movement to the jet.

IV. Results of Early Trials In-Seam Drivage with the Swing-Oscillation Jet

The preliminary underground trials were made between May, 1979 and February, 1980. The swing-oscillating jet proved to be effective, and even the hard coal on the top could be cut off by the jet. It was also effective in dust-suppression, which obviously improved the working environment. For example - the dust content in the air at the face has been reduced to 1.6 mg/m^3 in the Mentougou Mine, Beijing Coal Mining Administration. Other advantages are: reduction of roadway maintenance, a saving of timber consumption and better quality of the roadway.

V. Preliminary Conclusions

The swing-oscillation jet is a new type of jet, which, by hydraulically or mechanically combining an oscillating movement with the swing movement, can increase the cutting capacity significantly. According to laboratory test results, the cutting capacity of the swing-oscillating jet can be increased by 300%, compared with that of a swing-only jet.

In developing roadways in coal, the swing-oscillating jet would be capable of getting more coal, provided the working pressure matches the hardness and bedding and joints of the coal. The pressure of this type of jet is not high and less difficulty will be encountered in its application to development work. The suppression effect on air-borne dust is remarkable. Dust content can be controlled to 8-10 mg/m^3. Water consumption is low, so that coal excavated by the jet could be transported by conventional means. In particular, a compact design of a roadheader equipped with such a jet is possible. Therefore, the swing-oscillation jet is a new and promising technique for driving roadways in coal.

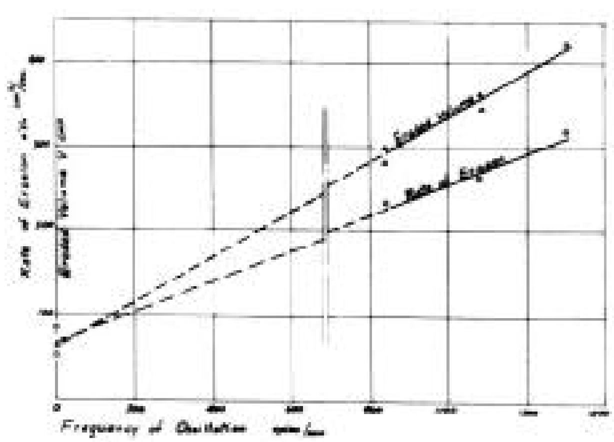

Fig. 1 Eroded volume, V, and rate of erosion, V_o, vs oscillation frequency after two passes with the swing jet.

Jet Pressure p = 250 kg/cm^2 Standoff distance s = 220 mm

Amplitude A = 44 mm Swinging velocity of jet v_n = 31.5 cm/sec

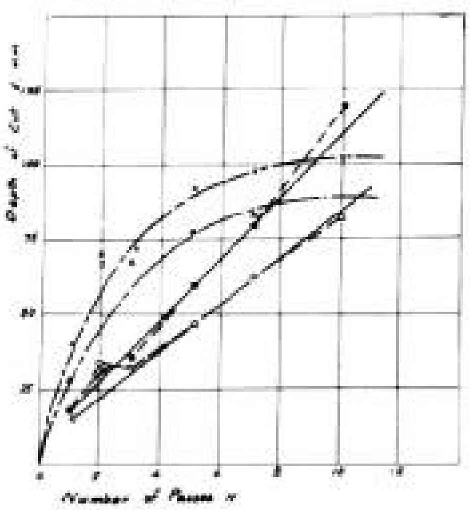

Swing Jet	Swing-Oscillation Jet	Swinging Speed
X A_1	X B_1	r=26.2 cm/sec
A_2	B_2	r=31.5 cm/sec

Fig. 2. Eroded depth, d, vs number of passes, n, for two types of jet.

Jet pressure	p = 250 kg/cm^2	Standoff distance	s = 220 mm
Oscillation frequency	f = 1400 cycles/sec	Amplitude	A = 44 mm

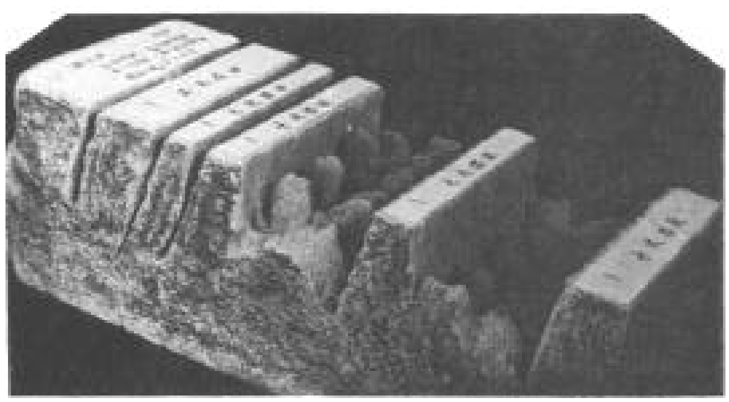

Fig. 3. Comparison of cuts made by the swing-only jet and by the swing-oscillation jet.

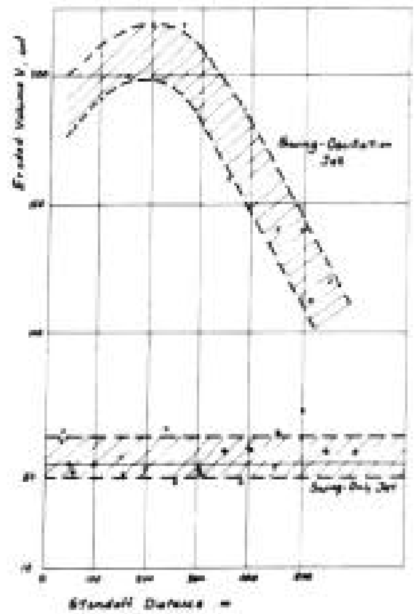

Fig. 4. Comparison of the volume of coal eroded by the swing-oscillation jet and the swing-only jet at different standoff distances.

x f = 930 v_n = 23.8 cm/sec

f = O v_n = 28.8 cm/sec

o f = O v_n = 22.5 cm/sec

DEVELOPMENT OF WATERJET-ASSISTED CABLE PLOW

M. Hashish, Ph.D., J. Reichman, Ph.D., J. Cheung, Ph.D.
Flow Industries, Inc.,
21414-68th Avenue South
Kent, WA 98031

T. Nelson
ORETEC Laboratory, Inc.
P.O. Box 64
Camas Valley, OR 97416

Notation

τ	=	shear stress
σ, σ_c	=	normal stress, compressive stress
C	=	cohesion
φ	=	angle of friction
β	=	blade angle
h	=	taper length
ℓ	=	blade length
$F_{t,l,2,3}$	=	total soil force on blade
γ_s	=	soil specific weight
w	=	blade shank length in direction of plowing
z	=	depth
F_f	=	friction forces
F_b	=	force on blunt portion of blade front
F_s	=	force on sloped portion of blade front

1. Introduction

The Electric Power Research Institute (EPRI) is assessing the feasibility of a multicapability cable-plow system. The plow will incorporate a number of new features that together will represent a significant advance in cable-plow technology. High-velocity waterjet assist is a new feature that will offer many advantages in reducing the cable-plow drawbar pull requirement. Flow Industries is currently engaged in a feasibility study of waterjet-assisted cable-plow blades. This paper presents some results of this investigation, including an analysis of the blade penetration processes, design of a waterjet-assisted blade, and results of initial field tests.

Some basic cable-plow system configurations are shown in Figure 1. Such cable-plow systems comprise the prime mover, plow point and blade shank. The prime mover pulls the point and the shank through the ground to form a void. The cable or conduit is either fed through the shank into the void or pulled behind the point through the slit made by the plow shank. A cable plow may incorporate many other features depending both on its manufacturer and specific intended use. In general, however, cable plows may be divided into either static or vibratory types. The latter type uses vibrations to reduce drawbar pull.

The waterjet-assisted plow blade concept becomes very attractive when the power consumption of a static blade engaged in the deep plowing (up to 152 cm) of hard soil is considered. As indicated in Figure 2, the exponential increase in drawbar force and power limits the use of such plows to shallow depths in relatively soft soil. While a vibrating blade will reduce required drawbar pull, it greatly increases system complexity and reduces its life time. A waterjet-assisted blade, however, both significantly reduces overall power consumption and increases blade life.

2. Objectives

The general objectives of the EPRI cable plow research program are to develop and demonstrate a complete, highly-maneuverable cable plow capable of installing primary and secondary power cables, telephone lines, TV cable, and flexible nonmetallic gas pipes at various separations simultaneously. The plow is to operate in all types of soil (e.g., frozen soils, hard dry clays, and rock) with minimum ground disturbance. It is to be designed for compactness and maneuverability so as to permit operation with a two-man crew in small subdivisions as well as commercial and rural areas. This improved plow must provide for the safety of the general public and meet all OSHA requirements.

The specific objectives of the waterjet-assisted blade program subcontracted to Flow Industries by ORETEC Laboratory, Inc. included the following:

A. Assess waterjet-assisted device state-of-the-art.
B. Produce waterjet-assisted plow blade conceptual designs.
C. Develop preliminary design specifications for the waterjet-assisted plow blade.
D. Manufacture and field test the waterjet-assisted plow blade.

3. Review of Waterjet-assisted Device Technology

The literature contains some useful information concerning waterjet-assisted devices for mining, rock cutting, and drilling. Published data ([l] through [12]) show that waterjet assist improves equipment performance an average of 30% to 45% for each such application. Although quantitative performance improvement percentages cannot be transferred from one application to another, some order-of-magnitude percentage improvement estimates for a waterjet-assisted plow blade can be made based on those of other waterjet-assisted devices. Also, system hardware arrangements can be examined for possible adaptation to the waterjet assisted plow blade program.

A sample waterjet-assisted device and some waterjet-assisted cable plow test results are shown on Figures 3, 4 and 5.

4. Penetration Analysis

The analysis presented here is a first-order study to determine plowing force in the cases of mechanical and hydromechanical soil penetration. The following cases will be considered for comparison:

A. Unassisted penetration by a smooth sharp-edged blade.
B. Unassisted penetration by a rough sharp-edged blade.
C. Unassisted penetration by a rough blunt-edged blade.

D. A single row of front jets assisting a blunt blade.
E. A double row of side jets assisting a blunt blade.
F. A combination of Cases D and E.

The parameters encountered in the blade penetration process will be realized in this analysis. Also, the effect of waterjet assist on the stress field and relevant soil parameters will aid in understanding the critical parameters and the effects of their change on drawbar pull. The effect of vibration will also be considered in order to compare the percentage of overall power reduction due to vibration assist with that due to waterjet assist. The assumptions involved in each analysis will be simplified for this first-order study as will be shown in each case. Table 1 illustrates Cases A through F above and includes a vibrating plow blade case for comparison.

4.1 Soil Penetration by an Unassisted Plow Blade

4.1.1 Case A: Unassisted Penetration by a Smooth Sharp-Edged Blade

The equations governing the penetration process of a blade in soil are the Coulomb equation

$$\tau = C + \sigma_c \tan \varphi$$

and the equilibrium equations for two-dimensional stress analysis. Figure 6 is a Mohr stress diagram for Coulomb's yield criteria and the slip-line field associated with the penetration process. Cheatham [13] expressed the solution of the penetration-governing equations as shown in Table 1 for this case. The pressure q in the Table 1 equations is the soil pressure, which simply corresponds to soil weight if the soil is loose and equals soil compressive strength if the soil is packed.

The additional frictional force F_f on the blade sides as shown in Table 1 is determined by assuming that the normal stress on the blade sides is φ_f which is again a function of the soil type. This stress will be assumed for the numerical results presented later.

4.1.2 Case B: Unassisted Penetration by a Rough Sharp-Edged Blade

The equation for the total drawbar force is shown in Table 1 to include the friction on the sloped sides of the blade front.

4.1.3 Case C: Unassisted Penetration by a Rough Blunt-Edged Blade

A place with a blunt front and rough sides represents a realistic case for plowing blades. A sharp blade front can not be maintained due to the severe wear conditions encountered in plowing. The force on the blunt front is obtained by letting β = O in Equation (4) of Table 1. The effect of the soil depth on compressive strength is neglected.

4.2 Soil Penetration by a Waterjet-Assisted Plow Blade

The mechanism by which waterjet assist reduces drawbar pull and/or increases plowing rate consists of the following:

A. Weakening soil structural resistance by introducing a number of slots that alter the slip-line field in favor of power reduction.
B. Lubricating the blade sides and front to reduce frictional forces.
C. Improving the flow characteristics of soil around the blade.
D. Facilitating penetration by moisturizing the soil.

Force reduction resulting from these effects are determined in the following simplified analysis.

4.2.1 Case D: A Single Row of Front Jets Assisting a Blunt Blade

It is assumed for this case (Table 1) that the front jet will eliminate the force on the blunt portion of the blade in the assisted region. Considering the new set of soil properties at wet conditions σ_{cl}, φ_1, μ_1, and c_1, the drawbar pull F_{t4} for this case is concluded from previous equations of unassisted plowing forces.

4.2.2 Case E: A Single Row of Side Jets Assisting a Blunt Blade

Waterjet assist for this case (Table 1) can be assumed to eliminate the forces on the sloped sides of the blade front and further reduce the frictional length of the blade shank. If we assume that the same number of jets is used for both Case D and this case, then the assisted length for this case is $\ell a/2$. The total force F_{t6} for this case is given in Table 1.

4.2.3 Case F: A Combination of Cases D and E

This case combines a row of front jets (Case D) with a row of side jets (Case E). The nozzle spacing can be made longer and consequently the equivalent assisted length will be assumed to be la/2. The plowing force F_{t7} required for this case (Table 1) is derived by utilizing previous relationships.

4.2.4 Vibratory Plows

Figure 7 illustrates the mechanism by which vibration reduces drawbar pull. As the blade vibrates, soil around the shank separates from the rest of the soil. The vibrating weight W_V becomes $W_V = W_b + W_s$ where W_b is blade weight and W_s is soil weight. The power required to vibrate the blade against the soil friction force F_f is P_V where

$$P_V = (W_V + F_f)\, u_o \sin 2\pi ft$$

where u_o is maximum velocity and f is frequency of vibrations. The frictioned force F_f is given by Equation (3) of Table 1. The force required for plowing in this case is similar to wedge penetration in soil with a perpendicular and two parallel free surfaces if the distance between the center of the blade and one of the parallel free surface is d as shown on Figure 7.

5. Criterion for Efficient Waterjet-Assist Nozzle Arrangement

This section presents the criterion for optimum waterjet-assisted plow nozzle arrangements and waterjet/vibration-assist combinations to help in selecting an optimum blade-assist design. This criterion is the ratio of reduction in plowing force to extra power required for assist, which should be as high as possible. This ratio is a convenient parameter for judging assistance efficiency because it is independent of plowing rate. If the total drag force on the blade in a certain case is F_t, then this ratio r is

$$r = \frac{F_{t3} - F_t}{HP_{extra}}$$

The additional hydraulic horsepower for waterjet assist HP_h is

$$HP_h = P * Q = Cnd_n^2 p^{3/2}$$

where n = number of nozzles. The additional power for vibrating the blade is given by the time average of $P_V (W_V + F_f) u_O \sin 2\pi ft$ (Subsection 4.2.4) over half a cycle. The ratio r is expressed in units of lbf/HP or sec/ft.

6. Analytical Results

A sample of the analytical results is shown in Table 2, which lists the forces on the blunt front, front sides, and blade sides calculated for each case from the previous equations. The percentage reduction in force relative to Case C indicates that the combined arrangement of waterjet assist in Case F is the optimum. That is, a conservative 44% reduction is obtained assuming that the jets are uniformly spaced over the lower 30 inches of the blade shank. For Cases D and E, calculations are based on reduced spacing to guarantee equal hydraulic power input. The force reduction in tons per hydraulic horsepower listed in Table 2 assumes that a 75 HP hydraulic system will be used. Values for the soil properties listed in the table were conservatively assumed to be lower for wet soil than for dry.

7. Waterjet-Assist System Design, Fabrication, and Laboratory Testing

A test bed waterjet-assist system using a 75-HP hydraulic power supply was fabricated and laboratory tested to verify the jet quality, cutting ability, durability, and safety of the design concept. The test bed system was configured to facilitate the testing of various nozzle sizes and arrangements and provided the following additional capabilities:

A. Selective blade portion assist (blade front, bottom, and bottom tooth).
B. Pressure capabilities above the normal 20,000-psi working pressure.
C. Total flow rate of between 3 and 5 gpm.
D. Ready interface with other blade components.
E. Quick nozzle changeout.
F. Ease of operation and safety.

8. Field Test Results

A prototype waterjet-assisted plow bade was fabricated and field tested subsequent to the laboratory test effort. It was noted that the average improvements in plowing speed attributable to vibration and waterjet assist were 38% and 33%, respectively. These results are close to predictions; however, waterjet assist contributed less than vibration to drawbar pull reduction. This could be due to soil properties and/or because plowing depths were not great. Combining vibration- and waterjet-assist resulted in a drawbar pull improvement of 117% for damp soil and 48% for hard soil.

Figures 8, 9, and 10 show percentage increases in plowing speeds in western Oregon clay soil at depths from 21 to ID inches and at drawbar pulls from 10,000 to 37,000 pounds. Typical plowing speeds observed were up to 30 fpm.

9. Conclusions

An analysis of waterjet-assisted plowing shows that a 44% reduction of drawbar forces can be achieved. It was determined that the optimum waterjet arrangement locates nozzles to assist both the blunt front and sloped side of the plow blade.

Field test results generally agreed with predicted percentage improvements in plowing performance due to combined waterjet and vibration-assist.

10. Acknowledgement

The work discussed in this paper was performed under ORETEK Laboratory Contract No. RP1518-1.

The authors wish to acknowledge the support given this program by the Electric Power Research Institute. Particular thanks are due to Mr. Thomas Kendrew, EPRI Project Manager, and Mr. Frank Kinnan, President of ORETEK Laboratory, Inc.

11. References

[1] Frank, H. and Lohn, P. D., "Fragmentation of Native Copper Ores with Hydraulic Jets," Second Int. Symp. on Jet Cutting, BHRA, Cambridge, England, April 1974.

[2] Moodie, K., "Coal Ploughing Assisted with High Pressure Waterjets," Third International Symp. on Jet Cutting, BHRA, Chicago, U.S.A., May 1976.

[3] Wang, F. D., Robbins, R., and Olsen, J., "Waterjet Assisted Tunnel Boring," DOT-TST-75-66.

[4] Cobb, D. E., and Sullivan, R. J., "Mechanically Actuated Water Cannon," U.S. Patent 3729137, April 1973.

[5] Hood, M., "Cutting Strong Rock with Drag Bit Assisted by High Pressure Waterjets,"South African Inst. of Mining and Metallurgy, pp. 79-90, November 1976.

[6] Summers, D. A., and Barker, C. R., "Surface Trials of the Hydrominer," Fourth Int. Symp. on Jet Cutting, BHRA, April 1978.

[7] Kuzmich, I. A., and Rutherberg, M. A., "Investigation of the Interaction Between High Speed Waterjet and Cutter During Breakage of a Rock Mass," Fourth Int. Symp. on Jet Cutting, BHRA, April 1978.

[8] Henneke, J., and Baumann, L., "Jet Assisted Tunnel Boring in Coal Measure Strata,"Fourth Int. Symp. on Jet Cutting, BHRA, April 1978.

[9] Yahiro, T. et al., "Sheet Piles Driving and H Steel Pulling by High Speed Waterjets," Fifth Int. Symp. on Jet Cutting, BHRA, Germany, 1980.

[10] Henkel, E. H., "Aims for a High Pressure Waterjet Assisted Coal Winning System," Fifth Int. Symp. on Jet Cutting, BHRA, Germany, 1980.

[11] Wang, F. D. and Wolgamott, J., "Application of Waterjet Assisted Pick Cutters for Rock Fragmentation," Fourth Int. Symp. on Jet Cutting, BHRA, April 1978.

[12] Maurer, W., "Advanced Drilling Techniques," Technical Report TR79-1, National Science Foundation.

[13] Cheatham, J. B., "An Analytical Study of Rock Penetration by a Single Point Tooth,"Eighth Annual Symp. on Drilling and Blasting, University of Miccnilri, 1958.

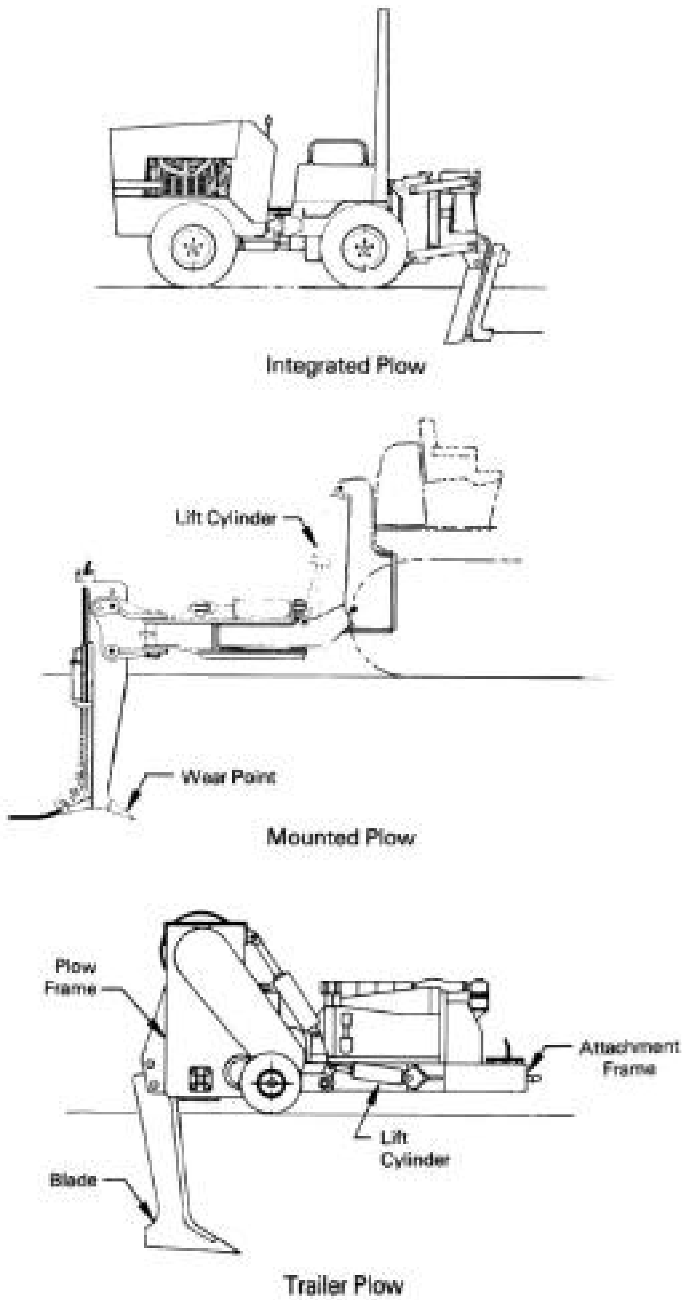

Figure 1. Basic Cable Plow Configurations

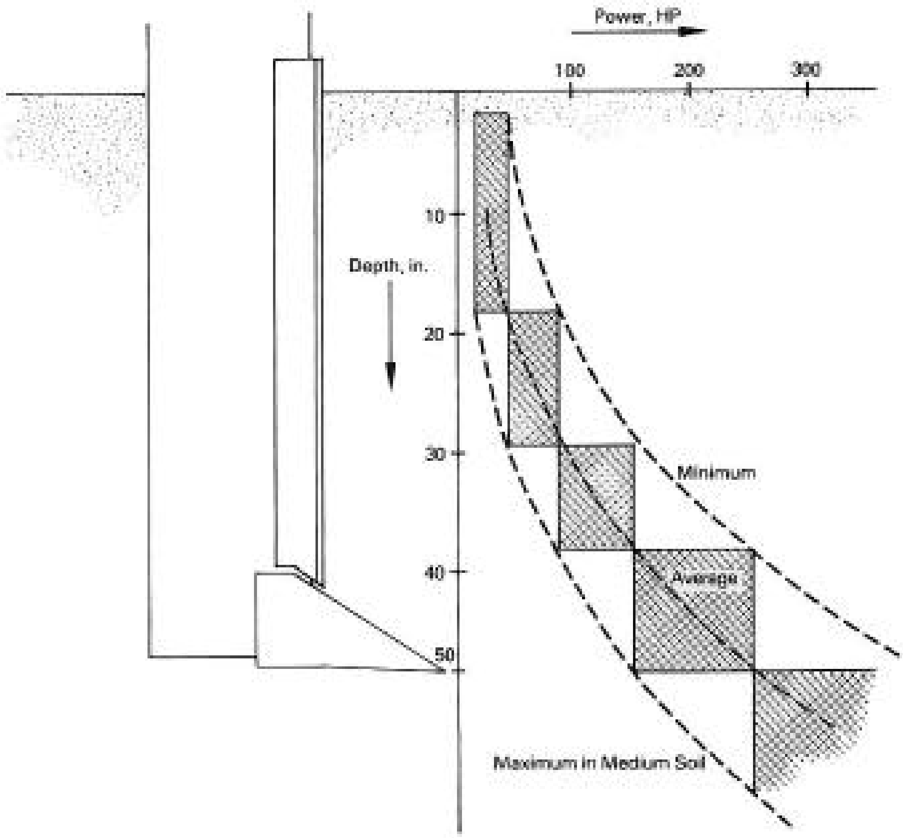

Figure 2. Plowing Power Versus Burial Depth

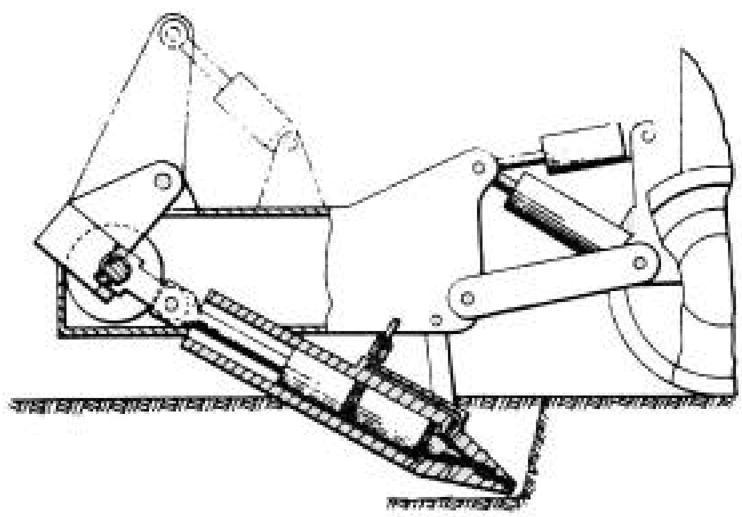

Figure 3. Pulsed Jet Rock Breaker

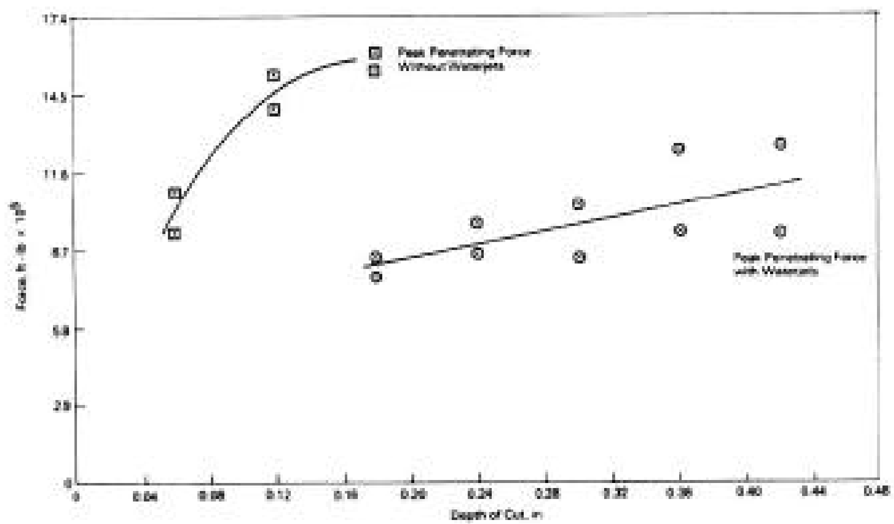

Figure 4. Peak Penetrating Force Versus Depth of Cut

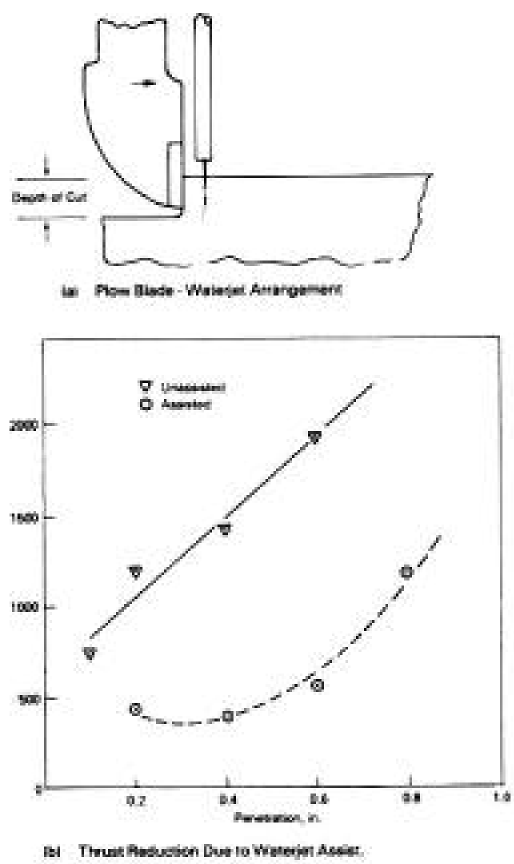

Figure 5. Waterjet-Assisted Sandstone Cuffing

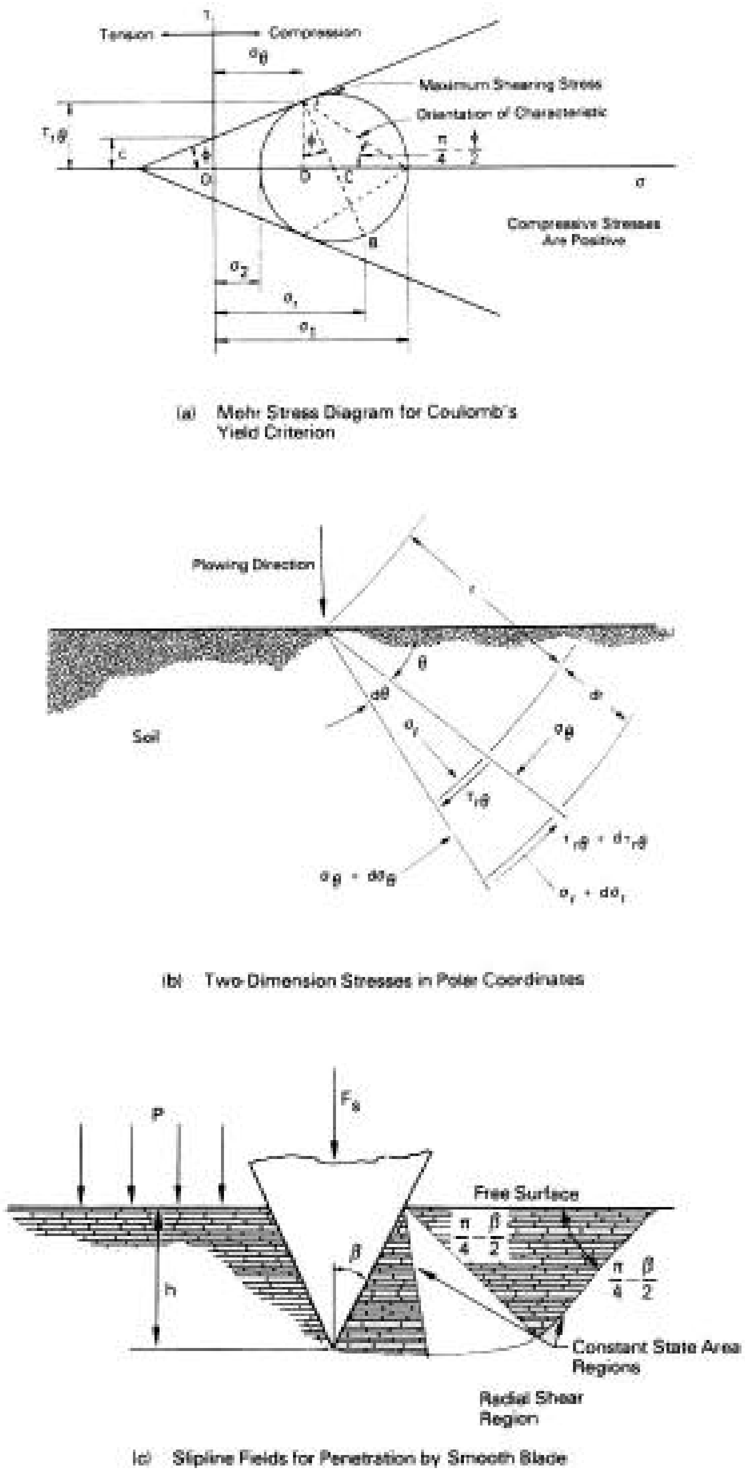

(a) Mohr Stress Diagram for Coulomb's Yield Criterion

(b) Two-Dimension Stresses in Polar Coordinates

(c) Slipline Fields for Penetration by Smooth Blade

Figure 6. Mohr Stress Diagrams for Coulomb's Yield Criteria

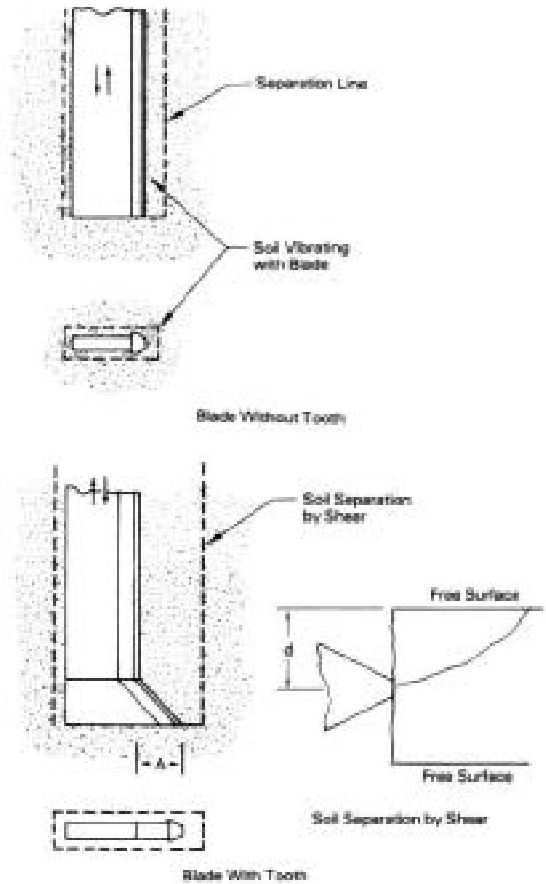

Figure 7. Mechanism by which Vibration-Assist Reduces Drawpull Requirement

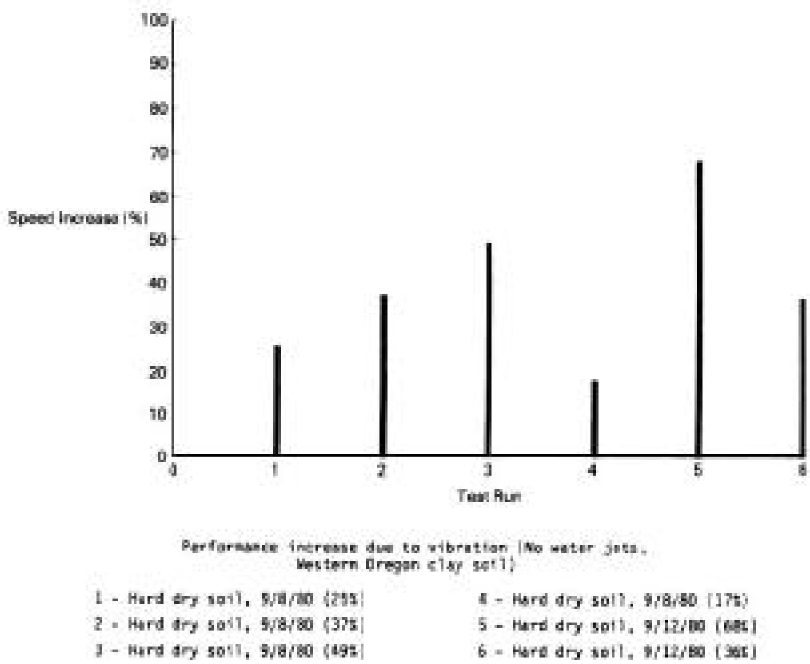

Figure 8. Plowing Speed Increase Due to Vibration Assist

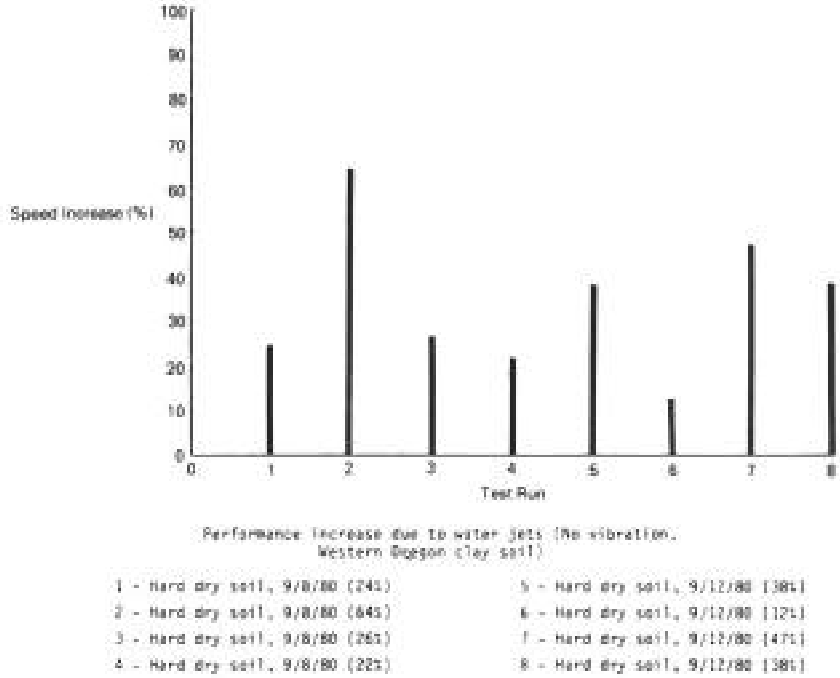

Figure 9. Plowing Speed Increase Due to Waterjet Assist

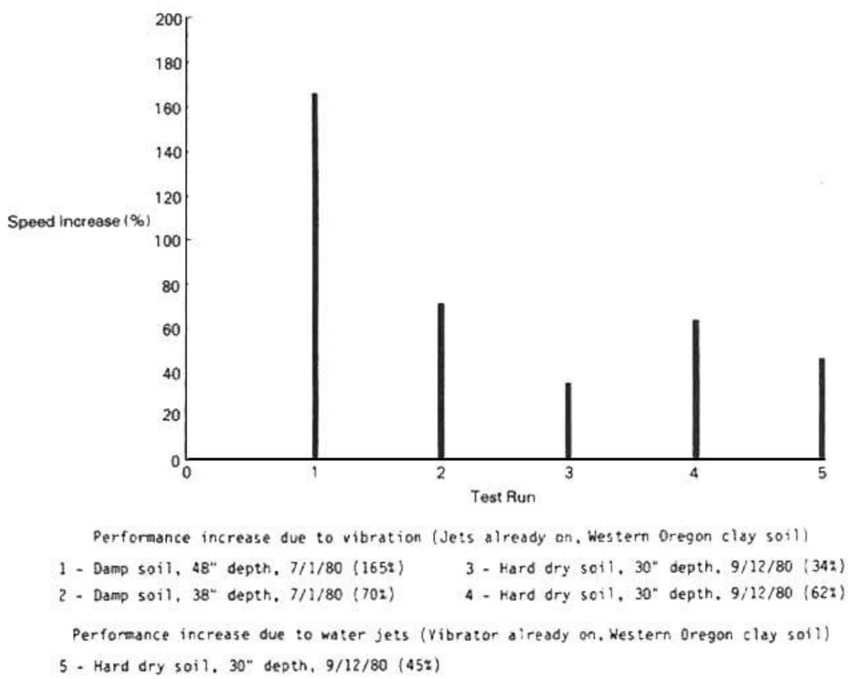

Figure 10. Plowing Speed Increase Due to Combined Waterjet Vibration Assist

Case	Total Drag	Force Component Equations	Equation No	Parameters
A. Smooth Sharp Edged 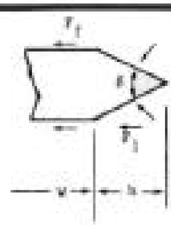	$\vec{F}_{t1} = \vec{F}_1 + \vec{F}_f$	$F_1 = \frac{b l \sigma_c}{\sin\phi}\tan\beta\,\overbrace{(1 + \frac{q\tan\phi}{c})}^{\lambda}\left[(1+\sin\phi)e^{2\beta\tan\phi} - (1-\sin\phi)\right]$ $c = \sigma_c \frac{(1-\sin\phi)}{2\cos\phi}$ $F_f = \mu\, l\, w\,(\gamma\, l + 2\sigma_f)$	1 2 3	$\sigma_c = 400 = q$ $\phi = 30°$ $\mu = 0.3$ $\sigma_f = 1$ psi $h = 1.73$ in. $\gamma = 0.1$ lb/in.^{3}
B. Rough Sharp Edged 	$\vec{F}_{t2} = \vec{F}_2 + \vec{F}_f$	$F_2 = \frac{\sigma_c h^2(1-\sin\phi)}{\cos\phi}(1 + \frac{q\tan\phi}{c})\left[(1+\frac{\tan\beta}{\tan\phi})(1+\sin\phi)e^{2(\tan\phi - \frac{\tan\beta}{\tan\phi})}\right]$ $\zeta = \beta + \frac{\pi}{4} + \frac{\phi}{2}$ $F_f = F_f$ in equ (3)	4	Same as Case A
C. Blunt Front Rough Blade 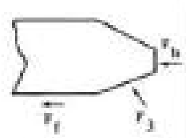	$F_{t3} = F_3 + F_b + F_f$	$F_3 = F_2$ in equ (4) with $h = 0.866''$ $F_b = K_1\, b\, \sigma_c\, l$ $K_1 = (\frac{1-\sin\phi}{2\sin\phi})(1 + \frac{q\tan\phi}{c})\left[(1+\sin\phi)e^{2\alpha\tan\phi} - 1\right]$ $\alpha = \frac{3\pi}{4} + \frac{\phi}{2}$ F_f = as in equ (3)	5 6	$b = 1$ in. Same as Case A
D. Single Row Water Jets 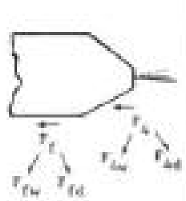	$F_{t4} = F_4 + F_f$	$F_{4d} = F_2$ in equ (4) $F_{4w} = F_2$ in equ (4) with $l = L - l_a$, $h = 0.866$ F_{fd} = as in equ (3) with $l = L - l_a = 20''$ F_{fw} = as in equ (3) with $l_a = 30''$, $\mu = 1$	 7 8	$l_a = 20$ in., $h = 0.866$ $L = 30$ in., $h = 0.866$ $\sigma_c = 1$, $\phi = 1$

Table 1. Drawbar Pull Requirement Equations

Case	Total Drag	Force Component Equations	Equation No	Parameters
E. Double Row Jets 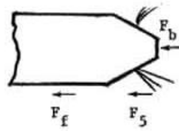	$F_{t5} =$ $F_b + F_f + F_5$ w,d w,d d	F_{bd} = as in equ (6) with $\ell = \ell - \ell a$ F_{bw} = as in equ (6) with $\ell = \ell a$, $\sigma_c = \%$, $\phi = \%$ F_{fd} = as in (2) with $\ell = \ell - \ell a$ F_{fw} = as in (2) with $\ell = \ell a$, $\mu = \%$ $F_5 = F_{5d} = F_3$ in (5) with $\ell = \ell - \ell a$		ℓa = 20 in.
F. Three Row Assist 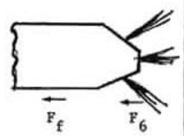	$F_{tb} =$ $F_b + F_\sigma + F_f$ dry dry w,d	$F_{bd} = F_b$ in (6) with $\ell = \ell - \ell a$ $F_{\sigma d} = F_3$ in (5) with $\ell = \ell - \ell a$ F_{fd} = as in (2) with $\ell = \ell - \ell a$ F_{fw} = as in (2) with $\ell = \ell - \ell a$, $\mu = \%$		ℓa = 15 in.
G. Vibrating Plow 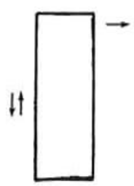	$F_{t7} = F_v + F_f$	$F_v = 2\ \sigma_t\ \ell\ \ d\ K \frac{\sin(\beta + \phi)}{1-\sin(\beta + \phi)}$ $d = \frac{h}{\cos\beta}\ (e^{\beta\tan\phi})(\tan(\frac{\pi}{4} + \frac{\phi}{2}))$ $K = 0.1 \rightarrow 0.2$ $F_f = \mu_s\ \ell\ W\ (\gamma\ell + 2\sigma_r)$, $\mu_s = 0.05$ Vibration Power P_V $P_V = (W_b + W_s)\ U_m$		σ_t = 200 psi ℓ = 50 in. $\beta = 30^o$ $\phi = 30^o$

Table 1. Drawbar Pull requirement Equations (Cont.)

Case	Parameters	F_b, lb	F_s, lb	F_f, lb	Total Drawbar Force, lb	Force Reduction	
						%	ton/HP
A. Smooth Sharp Blade 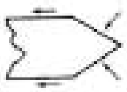	σ_c = 300, μ = 0.4 L = 50", q = σ_c ϕ = 20, σ_f = 30 psi c = 104	0.0	116,000	15,500	131,500		
B. Rough Sharp Blade 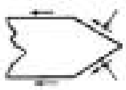	Same as in Case A	0.0	314,000	15,500	329,500		
C. Rough Blunt Blade  (reference case)	Same as in Case A	208,000	157,000	15,500	380,500		
D. Assist by Front Jets 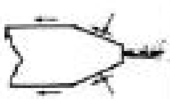	σ_c = 200, σ_f = 20 psi ϕ = 10, nozzle spacing = s μ = 0.3 q = σ_c δ_a = 30°	108	106,000	13,000	227000	40	1.02
E. Assist by Side Jets 	δ_a = 30° nozzle spacing = 25	121,000	121,000	12,000	254,000	33	0.86
F. Assist by Front and Side Jets 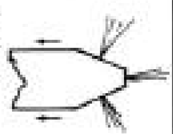	δ_a = 30° rest as C nozzle spacing = 35	91,000	110,000	10,000	211,000	44	1.13
G. Vibrating Plow 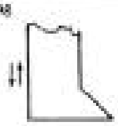					235,000	38	0.97

Table 2. Drawbar Pull Requirement Analytical Results

THE POTENTIAL ADVANTAGES OF A WATER JET REAMING DEVICE

Dr. David A. Summers
University of Missouri-Rolla
Rock Mechanics & Explosives Research Center
Rolla, Missouri 65401

ABSTRACT

One of the advantages sought for new technology, if it is to become a useful device, is that it should increase productivity while keeping the operation economical. In this regard, water jet reaming of geothermal wells for both extraction and re-injection appears to show promise. It is shown, using conventional formulae that reaming geothermal wells from 12 cm to 1 m radius will increase fluid flow to the point that 25% less wells could be required to establish a geothermal field.

With this objective, experiments are described to verify that water jets can effectively cut rock at required level, that is at a depth of 2000 m-in a fluid filled borehole. A conceptual mechanism to achieve this reaming is developed and, in simple form, the concept is demonstrated in a surface test.

INTRODUCTION

The advent of any new technology, if it is to be widely adopted, must create considerable advantage over the existing methods. This advantage must extend, in most cases, beyond that of a pure improvement in capability, and must achieve this improvement, most frequently, at a reduced cost over existing technology. Within the last decade, the advent of high pressure water jets into industry has developed, both types of advantage, for application in many widely differing circumstances. This paper addresses one such potential application.

The geothermal industry in the United States is at present a very young industry. While steam has been used, together with high temperature water as an energy resource for a number of years, it has only been since the onset and recognition of the "Energy Crisis" that major development of this resource has been undertaken. The development has not been without problems. Most particularly the high costs, both economic and environmental, in excavating through high temperature rock to obtain the hot water/steam and in treatment of the highly contaminated fluid, have slowed the use of this resource. To overcome this problem, and increase availability of the energy, the Federal Government has sought through funded research to reduce this cost with the stated objective of a 25% reduction in cost over the course of the program.
One facet of this program has been funded, through Sandia Laboratories, to the University of Missouri - Rolla, to examine the potential for enlarging the geothermal well bore.

ADVANTAGES TO REAMING

If one examines the equation for fluid flow through a permeable strata into a well, then that flow can be defined (Ref. 1) as:

$$q = \frac{2\pi k_w h(P_e - P_w)}{c\mu \ell_{10}(r_e / r_w)}$$

where

q	is the injection rate (cc/sec)
h	is the injection interval (cm)
P_w	is the well bore pressure (ctm)
r_e	is the effective reservoir radius (cm)
k_w	is the permeability (darcies)
P_e	is the reservoir pressure (ate)
μ	is the fluid viscosity (cp)
R_w	is the well bore radius
c	is a constant

If the flow is considered for a given rock horizon, where all conditions will remain the same once a well has been created; then one can examine the effect of changing the well diameter within that horizon upon the fluid flow. Simplistically this can be reduced to the ratio:

$$\frac{q_1}{q_2} = \frac{\ell_{10}(r_e / r_{w1})}{\ell_{10}(r_e / r_{w2})}$$

It has been estimated that the zone of influence for an individual well is something on the order of 300 m. The effect of changing the well radius from approximately 11.5 cm to 1 m would thus be to increase flow by 36%.

Thus if a conventional 23 cm diameter geothermal well were reamed to a diameter of 2 m, over the reservoir formation then a 36% increase in fluid flow either into or out of the rock across the well boundary (all other conditions remaining the same) could be anticipated. This can be put another way, in that were such a procedure to be adopted, three wells would be required to give the productivity achieved currently by four. This suggests a potential cost saving approaching 25% since the fourth well would no longer be required for equivalent productivity.

Such a statement of course does not consider the cost of the reaming but, neither does it examine two other problems associated with geothermal well excavation. Damage to the wellbore, during the creation of the hole may reduce the well productivity by 20%, and formation plugging by deposition of salts from the fluid may reduce well production. Both these problems may be substantially reduced by a water jet reamer. Such considerations will increase obviously, the economic advantage of the system again were the system viable. However in order to establish the viability of the system proposed it is first necessary to show that it can work. This problem was addressed in two separate phases.

PHASE I - JET CUTTING UNDER HIGH CONFINING PRESSURE

In order to maintain hole integrity while a drill is operating within a geothermal wellbore, it is necessary that the borehole be filled with a pressurized fluid. The fluid is most frequently pressurized by adding mud to increase the density of the fluid column. This, in turn, raises the fluid pressure on the liquid at the bottom of the hole. This fluid pressure is known to reduce the effectiveness of water jets in cutting through rock. The first object, therefore of the test program was to determine how great this effect was, and whether given that reduction, water jets could continue to cut into the rock to a satisfactory depth.

In order to successfully simulate conditions at the bottom of the well, which for the current test was assumed to be at a depth of approximately 2000 m, rock samples were confined in a triaxial test chamber. 15 cm diameter specimens of Berea sandstone were used for the program and were cut 30 cm long. A 5 cm diameter was drilled axially in the center of each specimen over a 25 cm increment. This would allow simulation of the preexisting wellbore. Confining pressure on the outer surface of the rock was raised to 400 bar for the test, and pressure within the simulated wellbore was raised to approximately 170 bar, by gating the fluid flow out of the triaxial chamber once the water jet had been turned on.

The water jet was raised to pressure, the nozzle was then rotated by an electric motor, located outside the chamber, while the chamber itself was slowly lowered, moving, in turn, the jet up over the inner hole surface.

In early tests, the result of this procedure was that no hole excavation occurred once the correct borehole pressure was established (Fig. 1). Analysis of the reasons for this, indicated that the major problem was with the small diameter of the jet which was being used, and the very rapid decay in jet cutting effectiveness with standoff distance. This decay is a function of the confining fluid pressure in the borehole, and to establish under what jet diameter and pressure effective cutting could be achieved, a second experiment was designed.

Rock samples were prepared, from the 15 cm diameter core with a sloping upper surface (Fig. 2). The nozzle feed pipe was bent, so that the nozzle would be located, approximately 5 cm from the sample center, with the ensuing jet pointing down. Thus, as the nozzle rotated over the sample surface, it would cut a path approximately 5 cm in radius into the rock, however standoff distance would vary over the circle perimeter.

The test procedure for this program was to locate the test sample within the test chamber, close the chamber, and, with the nozzle body oriented over the highest point of the rock, the chamber would then be raised until the rock touched the test nozzle, the chamber was then lowered 1 cm and the nozzle rotated over a half revolution so that it was at the most distant point from the rock surface. The water jet was brought up to pressure and flow from the chamber gated until the required back pressure was established in the chamber. The nozzle was then rotated through one complete revolution and the test stopped. When the sample was removed from the chamber two points could be identified from the hemispherical cut made on the rock surface (Fig. 3) indicating the distance at which the jet was no longer effectively cutting the rock. A measure of the slot depth, as a function of stand-off distance, could also be taken.

The results of this test showed that it would be necessary to go a nozzle diameter of at least 1.5 mm and to operate at a pressure in excess of 50 MPa if the jet were to effectively cut through the rock. However the results (Table 1) did not show the level of performance that had been anticipated with this system, and a subsidiary experiment was therefore carried out in which the fluid that provided the water jet was mixed with a long chain polymer to improve stability. Preliminary results from an experiment with this additive indicated an improvement in cutting performance of 70% in the best instance indicating that the addition of polymer would make the operation a much more viable one and brought the level performance up to a not unreasonable level (Table 2).

It should be mentioned, at this point, that the water jets were traversed over the sample once, and the depths measured were for a single path. The design of the reaming head which will be described below is such that the water jet will make successive, adjacent passes over the rock surface. Under such circumstances, there will be a strong interaction between adjacent jet passes. This phenomenon which has been examined in earlier work (Ref. 2) for the same agency has shown depth improvements on the order of 250% where this incremental distance is satisfactorily adjusted (Table 3). Thus performance levels indicated herein are likely to be much increased over that from the single test data developed in this part of the program. Additionally during the course of each revolution, it is anticipated that the jet will make two passes over each segment of the rock surface since the jet will be rotating over a large path and therefore each individual point will be attacked both on the forward and backward part of the jet motion around the surface.

DEVELOPMENT OF A CONCEPTUAL MODULE

Once it was established that the water jet is capable of cutting rock, at the specified strength, under the designated conditions, it was necessary to conceive a method for rotating the jet and moving it over the rock surface.

The very low levels of force generated by high pressure water systems due to the very small area of the relatively high forces involved, allows structures to be designed which do not require the high structural strength necessary with conventional mechanical bit operation.

The operational conditions required that the structure must fit down a 22 cm diameter borehole and be able to extend out to 1 m on either side of the bore axis. To achieve this, it was decided to design the reamer with two wings which would fold out to the required distance (Fig. 4). The wings would each incorporate two modules each of which would ream a 22 cm path over the rock surface. Insofar as each would be staggered relative to the other, the jets would collectively, therefore, ream out a path approximately .85 m wide which taken with the pre-existing wellbore would give us the designated 2 m final hole dimension. Configuration of each module was based on use of an existing high pressure rotating coupling which would be required to allow circular motion of the cutting nozzle and a small hydraulic motor to provide the mechanism for that motion (Fig. 5). The reamer required support between adjacent modules and this could be provided by, in the one instance, a high pressure fluid line bringing the cutting fluid to the individual module and in the second instance by the fluid line to the hydraulic motor. In the initial intent the drive motor was to have encircle the coupling, however it did not prove possible to find a commercial motor able to do this. Instead a motor was used which had been located by Dr. Barker of the Research Center in an earlier program, (Ref. 3) and which had given satisfactory performance in the field.

In order to verify that the system would work, a simplified version of the model was built incorporating the motor, the required coupling, and a single nozzle and the assembly located over a block of Berea sandstone 30 cm thick. Within a period of 3/4 of an hour, it proved possible to drill a hole some 40 cm in diameter completely through the block. Although the nozzle was rotated by the motor, the feed of the module over the surface was by hand. This is emphasized since this does not utilize optimum speed of the motor or the optimum feed rate based on the correct incremental distance. It is likely that an increase in penetration rate by an order of 2 or more could be achieved. It is further likely that, had it been possible to maintain the nozzle just above the rock surface as opposed 2 or 3 in. standoff distance which very rapidly developed as the rock was cut away, then an additional increase in the performance rate of the system could have been achieved. Combining these two factors we feel that a penetration rate on the order of between 5 and 10 ft/hr could be ultimately achieved with this reaming device, were its design optimized. Greater performance could of course be achieved were the nozzle diameter to be increased over that currently indicated since depth of cut increases at a more than linear relationship with nozzle diameter.

CONCLUSIONS

In summary the system as developed, conceptually, been shown possible to work with equipment small enough to fit within the confines of a 22 cm diameter axis bore. Further it has been shown by a simulated test in a laboratory that water jets are capable, under geothermal wellbore conditions, of cutting the rock formation and thereby potentially increasing the diameter of the wellbore from 22 cm to 2 m. It has been indicated that, were such a development to occur, that it could prove possible to reduce the number of wells at a site by a factor of 25%, for equivalent flow. Since the reamer is relatively simple and inexpensive compared with conventional methods of drilling, we feel that this indicates a potential direction for meeting the directives of the Department of Energy in the geothermal area.

ACKNOWLEDGEMENTS

This work was carried out for Sandia Laboratories, a prime contractor to the United States Department of Energy, under contract #13-3246. This submitted manuscript has been offered by a contractor of the United States Government under contract accordingly, the United States Government retains a non-exclusive, royalty free license to publish or reproduce the published form of this contribution or to allow others to do so for the United States Government purposes.

The work was under the technical supervision of Mr. David Glowka of Sandia Laboratories and the work was carried out with the assistance of Dr. Zbigniew Sebastian, Mr. J. Tyler, Mr. R. Robison, Mr. J. Blaine of the Rock Mechanics staff without their assistance this work could not have been done and we are grateful to acknowledge this support.

REFERENCES

1. Loofbouron, R.L., "Ground Water and Ground-Water Control," Ch. 26, Vol. 2, Mining Engineering Handbook, Soc. Min. Eng., 1973.
2. Summers, D.A., and Lehnhoff, T.P., "The Design of a Water Jet-Drill for Development of Geothermal Resources," Final Report on Contract DOE-E7-76-S 02 2677.M003, U.S. Dept. of Energy, September 1978.
3. Barker, C.R. and Summers, D.A., "The Development of a Water Jet Drill for In Situ Gasification of Coal," Final Report on Contract Sandia Lab 13 0214, Sandia Laboratories, December 1978.

Nozzle Diam. (mm)	Hole Fluid Pressure (MPa)					
	0	3.45	6.9	10.35	13.8	17.25
.75	28.58	15.88	15.88	7.94	--	--
1.00	47.62	22.23	22.23	11.11	--	--
1.60	69.85	--	31.75	23.81	20.63	17.46

Table 1 Effective cutting distance of a high pressure fluid jet under simulated borehole conditions.

Polymer Concen. (ppm)	Hole Back Pres. (MPa)	Jet Pres. (MPa)	Nozzle Diam. (mm)	Cutting Dist. (mm)
100	17.25	69	1.60	34.92
100	17.25	69	1.60	34.92
200	17.25	69	1.60	47.62
300	17.25	69	1.60	47.62
300	17.25	69	1.60	28.57
300	10.35	69	1.60	31.75
300	3.45	69	1.60	36.51

Table 2 The effect of adding polymer on the effective jet cutting distance.

Incremental Distance Between Successive Jet Passes over the Rock (0.001 inches).	Depth of Cut (inches) (a)	(b)
20	1.51	.58
40	1.22	.43
80	0.89	.31
160	0.65	.20

Table 3 Averaged results from a factorial experiment showing the effect of incremental distance between adjacent jet traverses with a 0.023 inch diameter jet on the depth of slot cut in a) Berea sandstone; b) Indiana limestone.

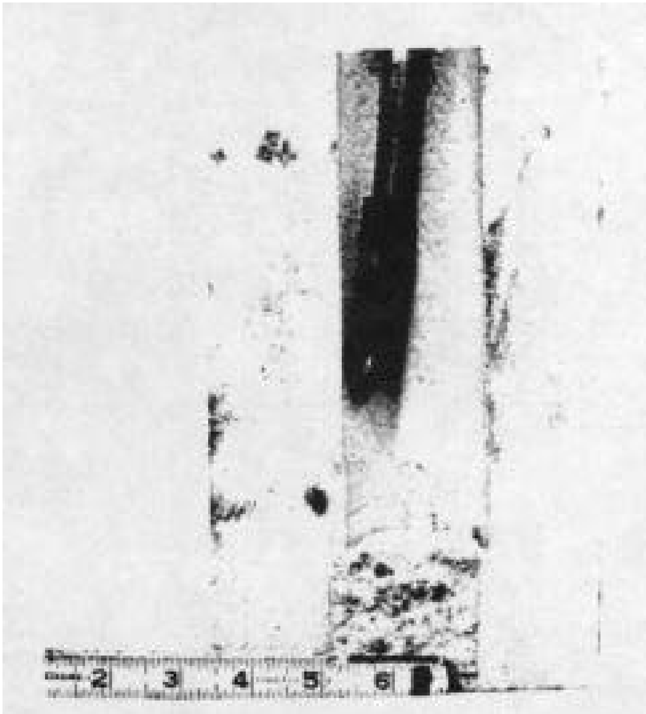

Fig. 1 Sample configuration for the first test, showing nozzle location and the undamaged sample wall.

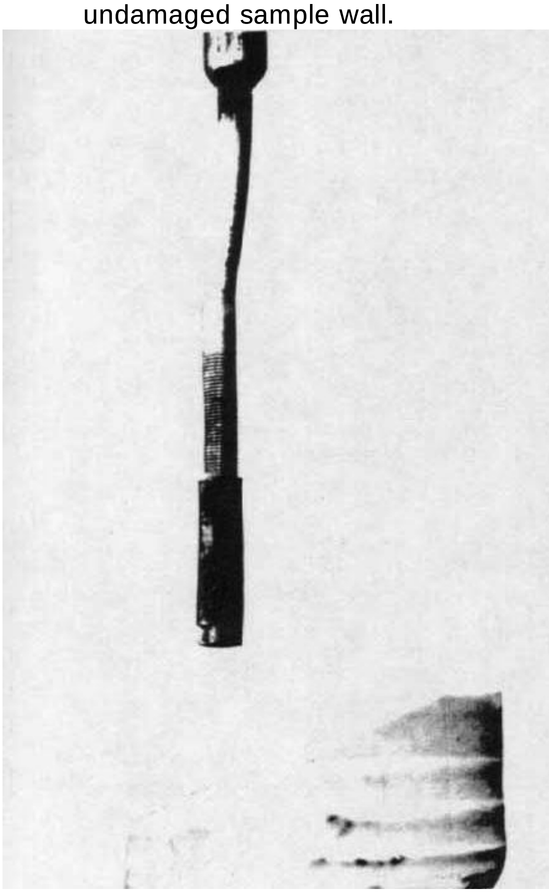

Fig. 2. Sample shape for the second test.

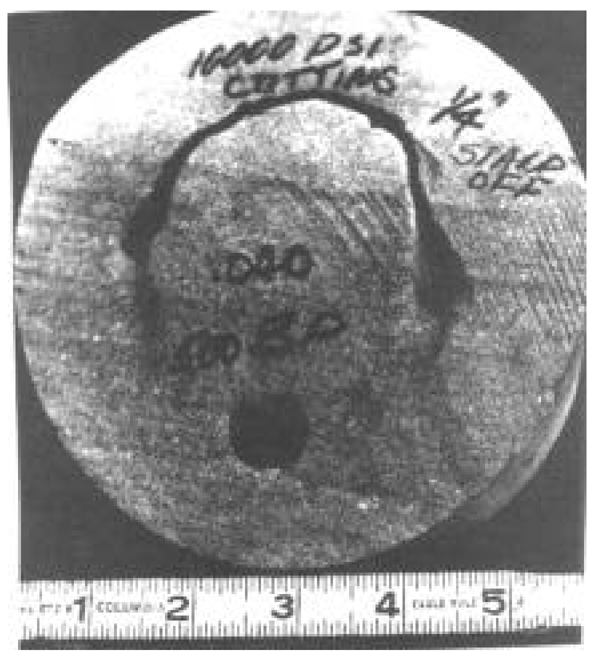

Fig. 3. Sample after "stand-off" test.

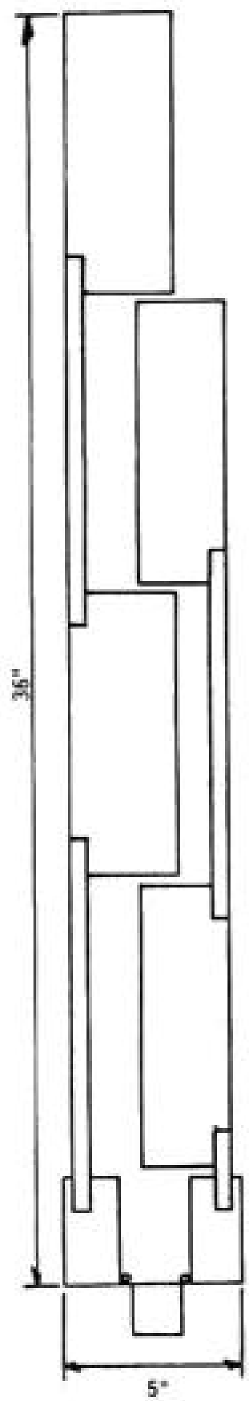

Fig. 4a. Showing the configuration of the reaming unit as it travels down the hole.

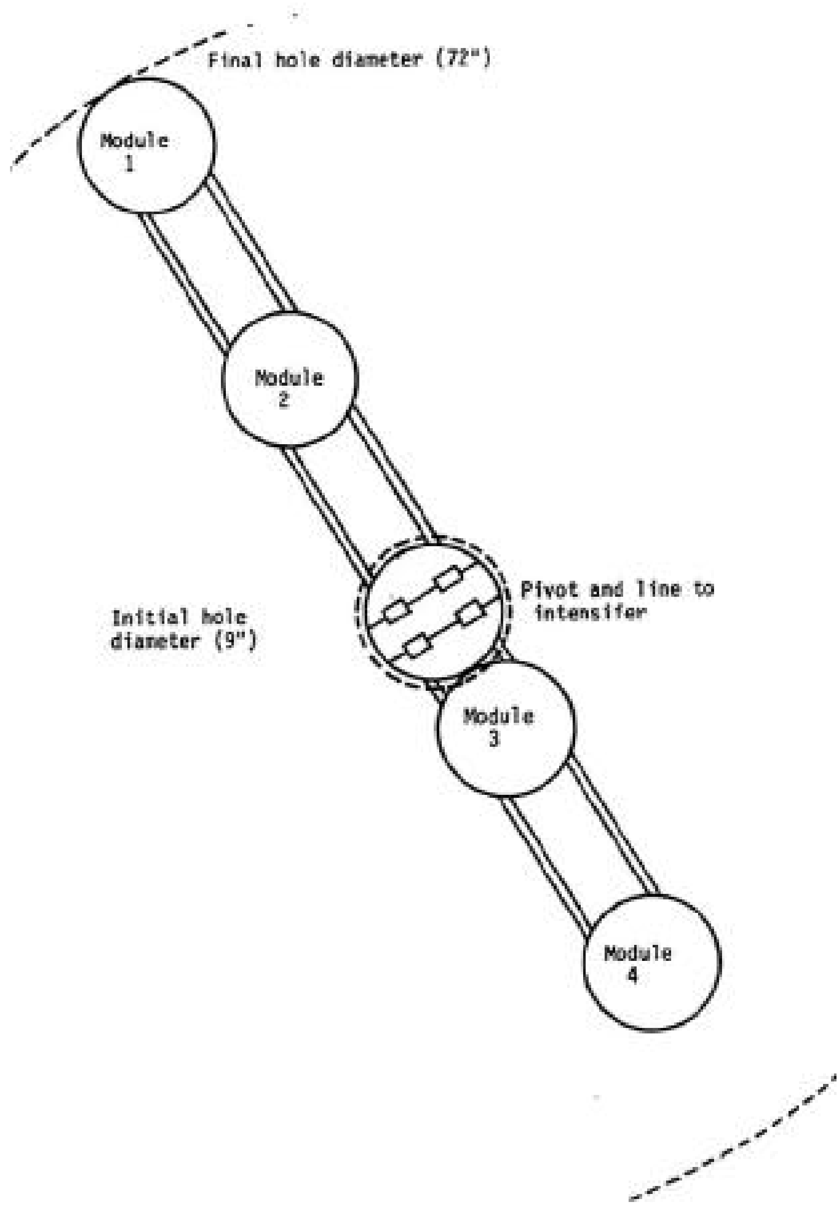

Fig. 4b. Orientation of the modulus in the hole, during the reaming operation

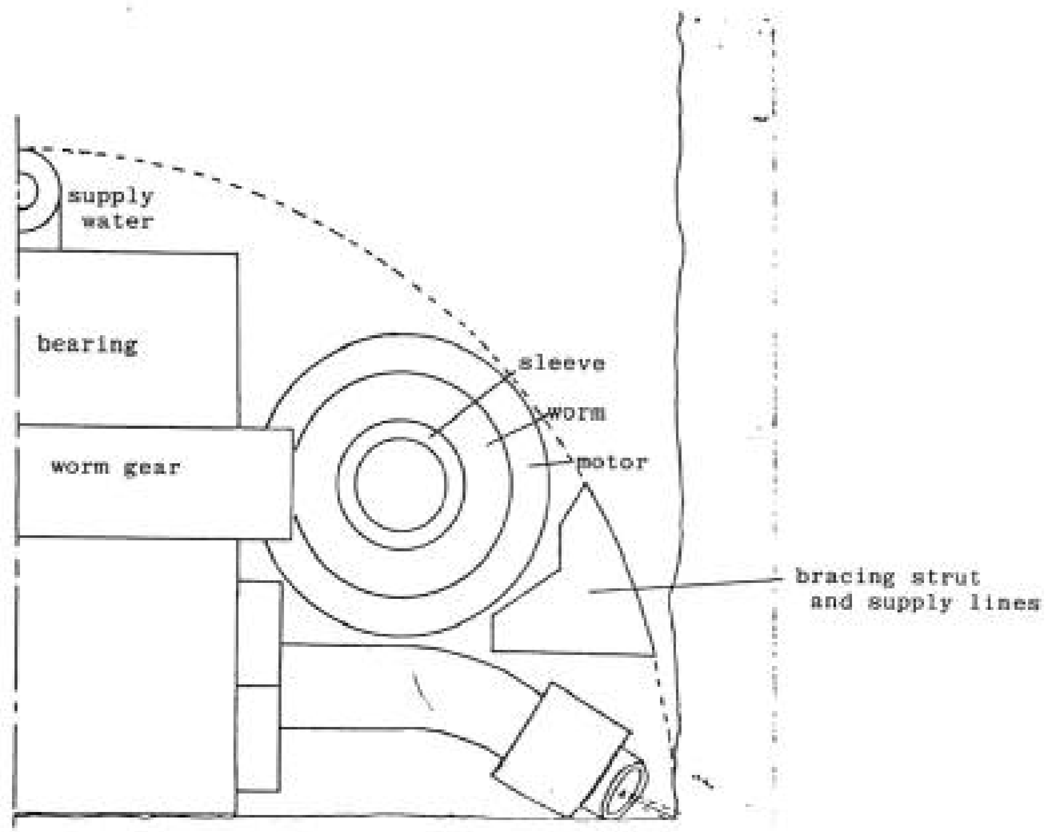

Fig. 5. Face view showing configuration of nozzle and the confinement required to fit the device down a well-bore.

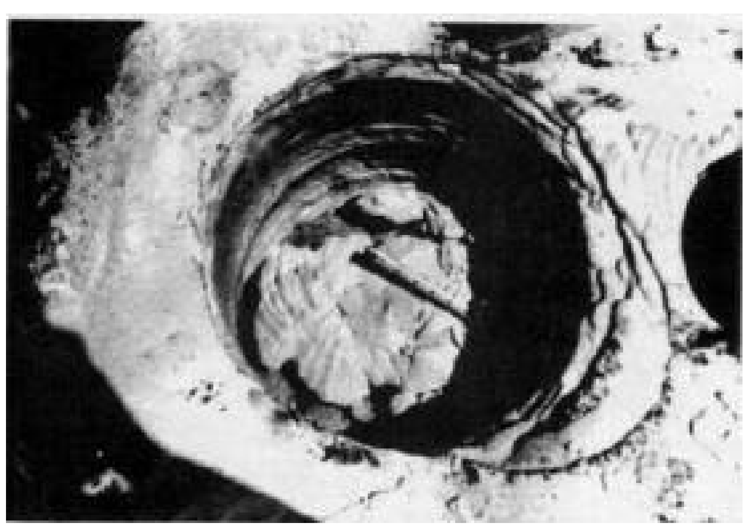

Fig. 6. Completed hole.

THE APPLICATION OF WATERJET CUTTING TO UNDERGROUND UTILITIES INSTALLATION

J. Reichman, Ph.D., G. Yie, and M. Hashish, Ph.D.
Flow Industries, Inc.
21414 - 68th Avenue South
Kent, Washington 98031

1. Introduction

A wide range of electric, telephone and television transmission and distribution cables, gas transmission and distribution pipe, and water and sewer pipe may presently be found beneath any city street. Also, new lines for special communication systems will soon be added to existing utilities installations. Therefore, there is a continuing and increasing requirement both to install new underground transmission systems and to replace existing underground distribution equipment that has failed. Utility companies must tear up streets and punch holes, dig, and plow through rock and soil to meet this requirement. The cost of such work represents a good portion of present utility company operating budgets. This is due to the high costs of concrete and asphalt cutting, traffic control, excavation, and surface restoration procedures. These costs will continue to rise very rapidly unless new, less expensive installation methods are developed. Compared to conventional methods and techniques, waterjet technology has the potential to significantly improve the speed and reduce the cost of installing underground utilities. This paper presents a variety of waterjet tools capable of effecting such improvements.

Currently, underground utilities are either plowed, trenched, or bored into place. However, each of these methods has problems associated with its use. These will be discussed briefly.

Underground utilities may be plowed into place in undeveloped areas. The specially designed blades are generally vibrated to assist their movement through the soil. Such vibratory plows work well in good soil; however, they are not adequate for plowing soils that are frozen or, for example, contain clay or scattered rock. Additionally, drawbar pull increases markedly as utilities are buried at greater depths, necessitating the use of very large prime moves to pull the blade. This sensitivity of plows to soil conditions and depth severely limits their use. It may be seen then that if the range of conditions suitable for plowing can be increased and the prime mover made smaller, plowing will be more widely used. This would be very advantageous to utility companies since plowing is an economical method for installing directly-buried underground equipment.

Trenching is an alternative to plowing. Trenching involves making an opening in the ground into which the utilities can be placed and then replacing the soil. This method is used both in undeveloped and developed areas for large utilities installation. There are a variety of tools that can be used if only soil has to be removed. The presence of concrete or rock, however, limits the number of tools available and greatly increases trenching costs. Concrete is generally removed with either jackhammers or diamond saws; rock trenches are generally blasted. In either case, the cost in equipment and labor is high. Additionally, environmental noise regulations can severely limit the utilization of these methods.

A third method of installing utilities is by boring holes in the ground. This method does not disturb the surface and thus reduces the cost of surface restoration. Such boring is generally by means of an impacting tool that punches a hole through the ground. However, commercially-available tools for this application are limited to short lengths and a narrow range of soils. Also, they cannot penetrate rocks and cannot be directionally controlled. For these reasons, the boring method is not widely used.

The application of waterjet-assist and primary waterjet-cutting technology can greatly extend the capabilities of these existing tools. Also, new waterjet tools can be developed to facilitate the replacement of failed utilities in a manner unique to this technology.

Utility companies have already funded a number of programs to explore the possibilities of various waterjet methods for underground utilities installations. These methods include waterjet assisted cable plows, boring tools, rock boring and trenching devices, and concrete cutting equipment. Both the tools developed under these programs and the power source that can be used to operate them are discussed in this paper. Power-source selection was based on providing a single power source capable of supplying the range of required pressures and flows for all waterjet tools. This would make waterjet systems analogous to compressed air tools operated by a central air compressor. Such a waterjet system will provide the most economic benefits to utility companies due to its wide range of capabilities.

2. Water jet System Descriptions

2.1 Waterjet-Assisted Cable Plow

A program has been undertaken by the Electric Power Research Institute (EPRI) to develop a waterjet-assisted cable plow. The program consisted of a study of waterjet assist and improved vibration. A prototype blade (Figure 1) was fabricated and tested. The results of an analysis performed on a waterjet-assisted blade are shown in Figure 2 and summarized as follows:

A. Waterjets reduced drawbar force requirements by 50%.
B. Waterjets eliminated ground heaving due to plowing.
C. Waterjets extended the range of soils that could be plowed.

The improvement in plow performance due to waterjet assist can be attributed to better lubrication around the blade, softening of soil by the jets, and improved migration of soil downward.

The water for the cable plow was supplied by a high-pressure intensifier pump. Water pressure was 12,000 psi and the flow rate was 4 gpm [1]. A commercial prototype system should be capable of operating at higher pressures. This could conceivably extend the acceptable performance range to frozen and rocky soils. The nozzles were located on the lower half of the blade in order to minimize the horsepower requirements. Water was supplied to the blade by a flexible high-pressure line. The nozzles were fed from high-pressure manifolds located on the blade. A commercial blade would use a similar water distribution subsystem.

The success of this prototype blade study encouraged the funding of a program to develop a complete prototype system. To date, a new prime mover has been built and is now being tested. This new crawler is especially designed for compatibility with the waterjet assisted, vibratory plow blade. It is smaller and more maneuverable than existing crawlers and will therefore be able to work in more confined areas.

2.2 Waterjet Concrete Cutting

A machine has been developed under EPRI funding for the cutting of concrete to trench transmission cable. Specifications for this system, shown on Figure 3 [2], are as follows:

A. Pump:	
Output pressure	366 MPa
Flow rate	30.3 liters per min
Displacement	0.516 liters
Dimensions	0.254 m x 483 m x 1.016 m
Weight	227 Kg
Hydraulic horsepower	187.5 KW
B. Vehicle	
Length	5.1 m
Width	2.25 m
Height	2.75 m
GVW	11,500 Kg
Turning radius	4.5 m internal

The cutting rate for the system is 0.3 to 0.6 m/min in 200-mm thick concrete.

An additional program has been undertaken to improve performance and decrease horsepower requirements. To this end, a study of abrasive waterjet concrete cutting has been initiated. A typical abrasive-waterjet nozzle is shown on Figure 4, together with a cut made in a concrete test specimen. The design goal is to decrease power and pressure requirements to under 100 KW and 200 MPa, respectively. If this reduction can be realized, then a smaller more economical cutting system can be developed.

2.3 Horizontal Boring in Soil

Horizontal soil-boring tools are effective only over limited distances and with questionable accuracy. EPRI has funded a program to develop a boring tool that can overcome these problems. The system that has been developed is self-advancing, steerable, and capable of traversing distances of more than 122 m. When this system is used in conjunction with a guidance system it can operate to within + 1 ft of a straight path. The system consists of a waterjet-assisted boring tool (Figure 5), a steering system, and an advancing system. Electronic guidance is incorporated into this design. The boring tool is a compacting device utilizing waterjet assist. The waterjet weakens and lubricates the soil and pilots the hole. This increases the tool's penetration speed 2 to 4 times over that of a non-assisted tool, enhances steering capability by weakening the soil in the desired direction of travel, and allows the tool to penetrate through small rocks by assisting the fracturing process. System water pressure is 68 MPa for average soils and can be increased for rocky soils. The water flow rate must be adjusted for soil conditions.

The boring tool is 100 mm in diameter and can advance through average soils at rates of 1 m/min or greater. The tool is also capable of penetrating frozen soil. The controls for steering and advancing the tool are located on the pump trailer. The rate of tool advance can be adjusted for various the soil conditions. The waterjet boring system has been fabricated and initial field testing is now in process. This testing will continue through 1981. At the completion of the testing, an extended test phase will be undertaken in cooperation with various electric utility companies.

2.4 Horizontal Waterjet Drilling

The tool under development for horizontal boring is not suitable for rock. However, a directionally-controlled rock drill can be developed by replacing the boring tool with a drilling head. The drilling head can be rotated downhole with either an air, hydraulic, or water motor. Depending on rock type and hole size, either complete drilling or modified coring can be performed. Both of these tool capabilities are well developed as is shown on Figure 6. This tool will have a widely varying advance rate due to the change in drilling rate for different rock types. It is estimated that most soft to medium-hard rocks can be drilled using an input power and water pressure of 75 KW and 225 MPa, respectively.

A directionally-controlled horizontal drill can be developed from knowledge already acquired from on-going drilling and boring programs. No current program, however, has yet advanced beyond a conceptual study.

2.5 Rock Trenching

It has been established that waterjets can cut slots in rock [3,4]. A trench can be formed making a slot pattern and then hydraulically breaking the rock remaining between the slots. A conceptual study to develop such a device was undertaken on behalf of Bell-Northern Research. The results of this study have previously been reported [5] and are briefly summarized here. The proposed trenching system is shown on Figure 7. The system can cut a trench 100-m wide x 150-mm deep at a rate of 5.5 m/h. This can be accomplished without blasting, which would allow the tool to be used in developed areas. Additionally, the well defined trench will protect the installed cables from damage.

2.6 Power Source

Utility companies perform a great variety of plowing, trenching, and boring activities during the course of their underground utilities installation operations. If each waterjet tool used for these activities required its own special power supply, the cost to the utility company would be high and return on investment for some tools would be low due to low equipment utilization. In order to circumvent this problem all waterjet tools should be compatible with a single modular power source. This would provide the greatest versatility to waterjet tools.

It has been determined based on testing that 100 KW hydraulic is sufficient power for all tools. This can be supplied by a 133 KW diesel engine. The required water pressure can be generated by a hydraulic intensifier. The advantage of an intensifier pump is that it can operate at desired pressures and flows without the need to bypass excess water, which wastes a great deal of power. Additionally, intensifiers can readily be cycled for a self-advancing boring tool and are inherently safe should nozzles become plugged. Such a modular power pack is shown on Figure 8. The system consists of a high-pressure module, a hydraulic module, and a power module. The high-pressure module is interchangeable to facilitate efficient operation at a variety of pressure-range requirements.

3. Conclusions

There are a variety of waterjet tools that have been developed, or are under development, to facilitate the installation of underground utilities. Some of the advantages of these tools are as follows:

1. Increased penetration rates relative to conventional tools.
2. Quieter than many conventional tools.
3. Smaller, more maneuverable equipment.
4. Extended range of applicability of each tool.
5. Permits utilities to be installed without disturbing the surrounding ground.

Waterjet tools other than those discussed in this paper are currently under development. These new products of waterjet technology will have even greater potential to reduce the complexity and costs of installing and replacing underground utilities. Both these tools, which are based on entirely new concepts, and the hybrid tools discussed in this paper will be commercially available in the near future.

4. Acknowledgment

The Authors wish to acknowledge the support given to the development of waterjet tools by the Electric Power Research Institute. Particular thanks are due to Mr. Thomas Kendrew and Mr. Thomas Rodenbaugh, EPRI Project Managers who have contributed significantly to these programs.

5. References

1. Hashish, M., Reichman, J. M., Cheung, J. B., "Development of Waterjet Assisted Cable Plow," First U.S. Waterjet Symp., Golden, CO, 1981.
2. Reichman, J. M., Kirby, M. J., Rodenbaugh, J. S., "The Development of a Waterjet Cutting System for Trenching in Concrete," BHRA Fifth Int. Symp. on Jet Cutting, Hanover, Fed Rep GR, 1980.
3. Reichman, J. M., Cheung, J. B., "An Oscillating Waterjet Deep-Kerfing Technique," Int. J. Rock Mech. Min. Sci. and Geomech. Abst., Vol. 15, pp. 135-144, 1978.
4. Reichman, J. M., and Cheung, J. B., "Waterjet Cutting of Deep Kerfs," BHRA Fourth Int. Symp. on Jet Cutting, Canterbury, G.B., 1978.
5. Huszarik, F. A., Reichman, J. M., Cheung, J. B., "Use of High-Pressure Waterjets in Utility Industry Applications," Erosion: Prevention and Useful Applications, W. F. Adler Editor, ASTM STP 664, 1979.

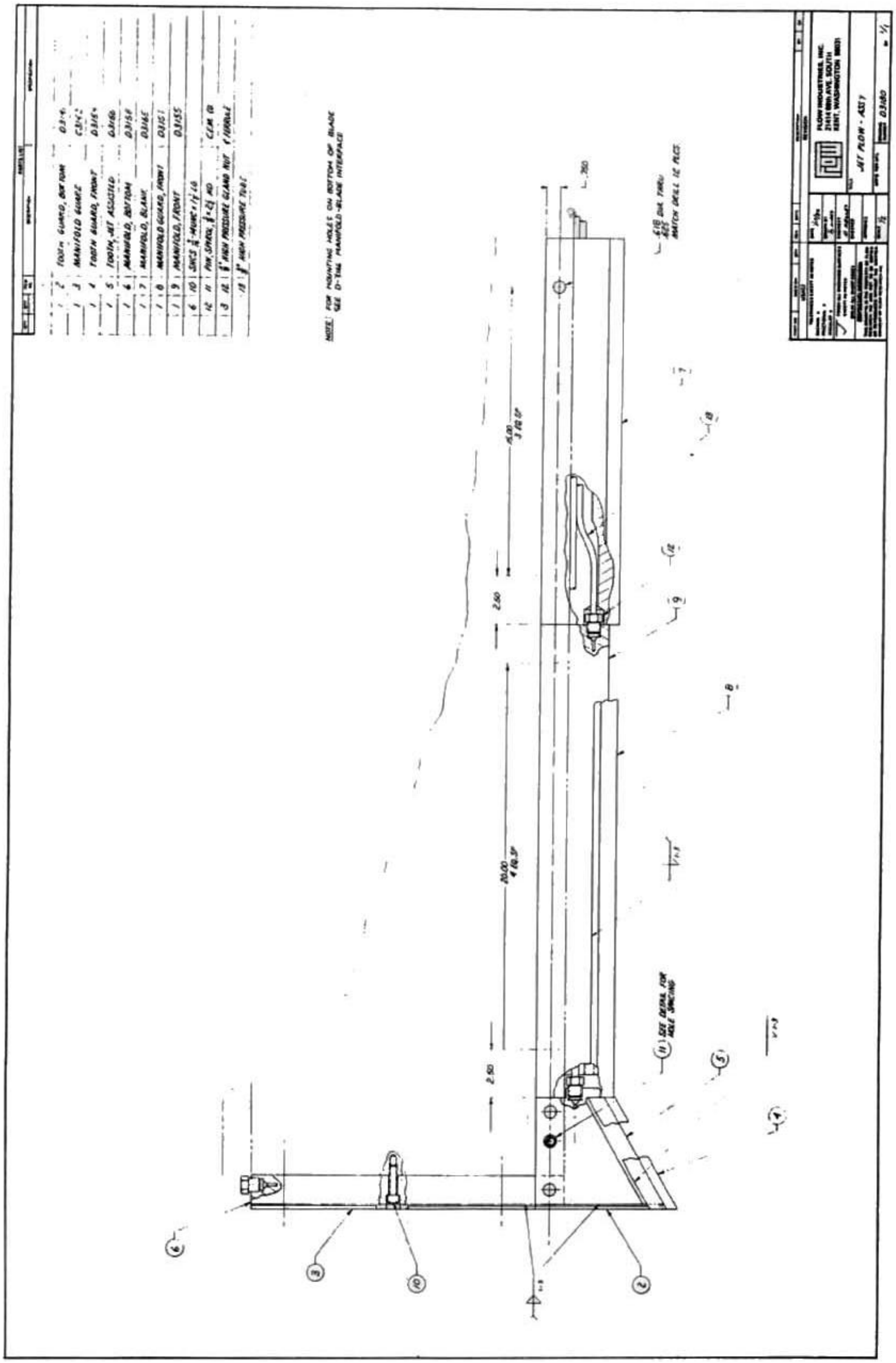

Figure 1. Prototype Waterjet-Assisted Plow Blade

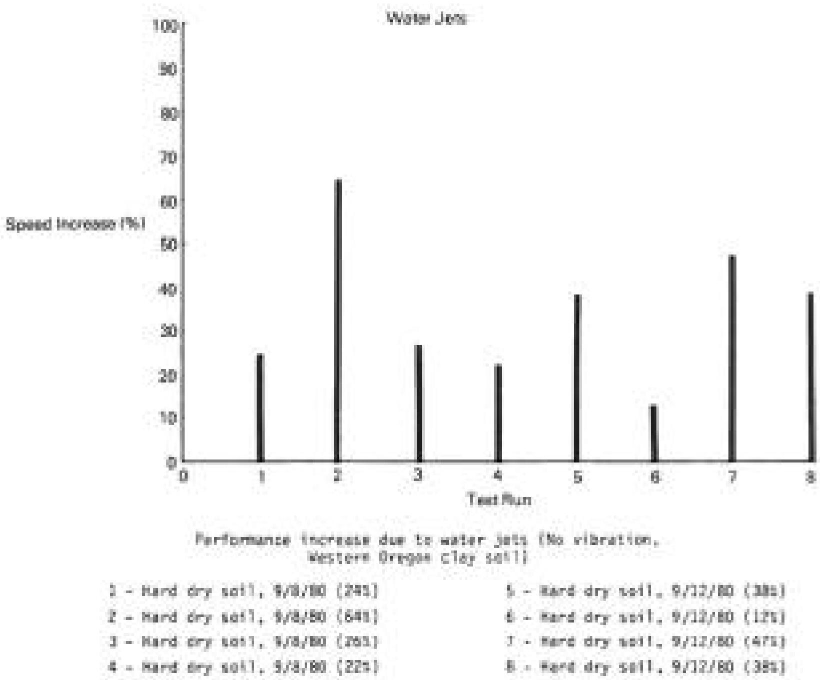

Figure 2. Waterjet-Assisted Plow Blade Analysis Results

Figure 3. Waterjet Concrete Cutting System

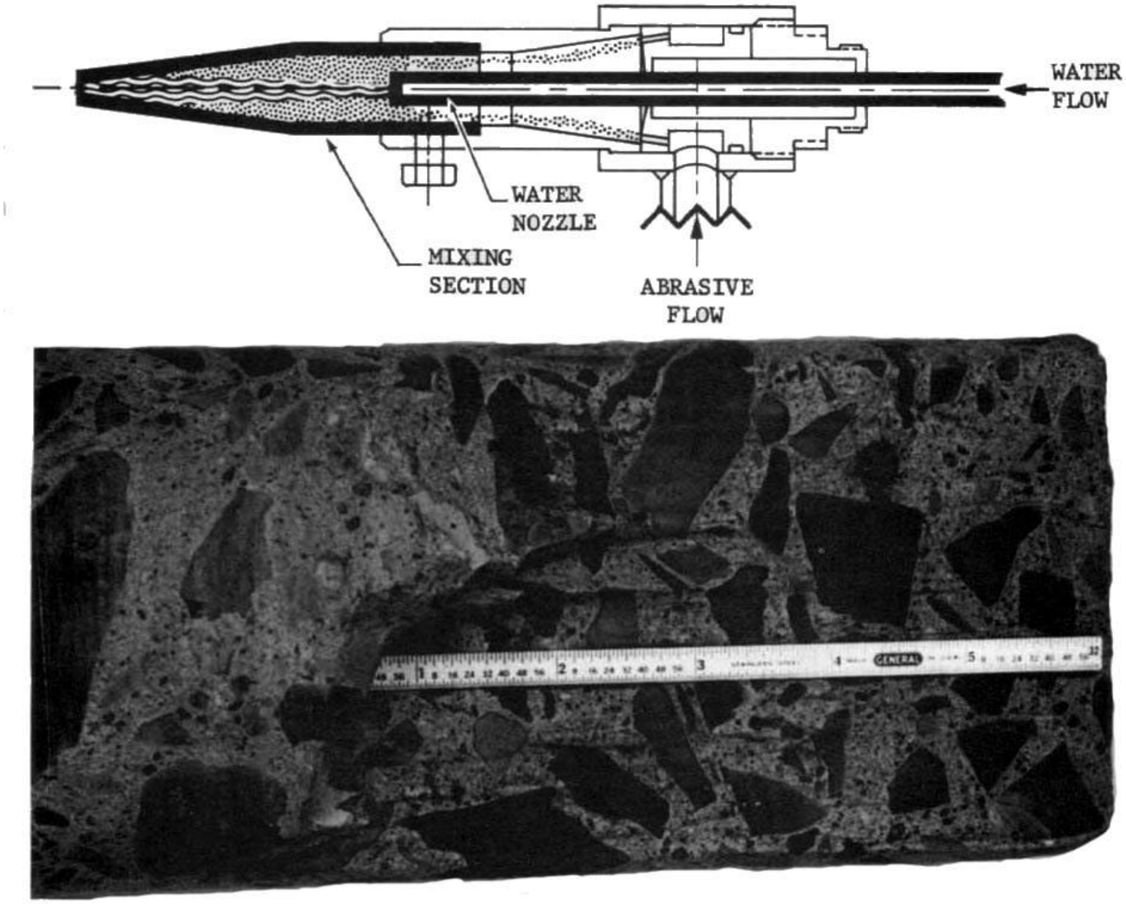

Figure 4. Abrasive Waterjet- Nozzle and Cut Concrete Test Specimen

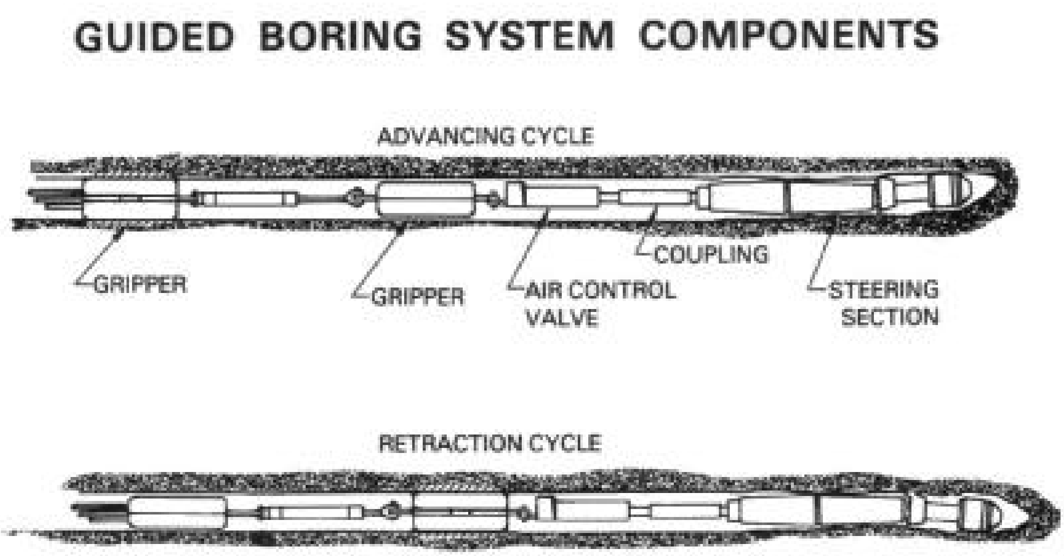

Figure 5. Waterjet Horizontal Boring Tool

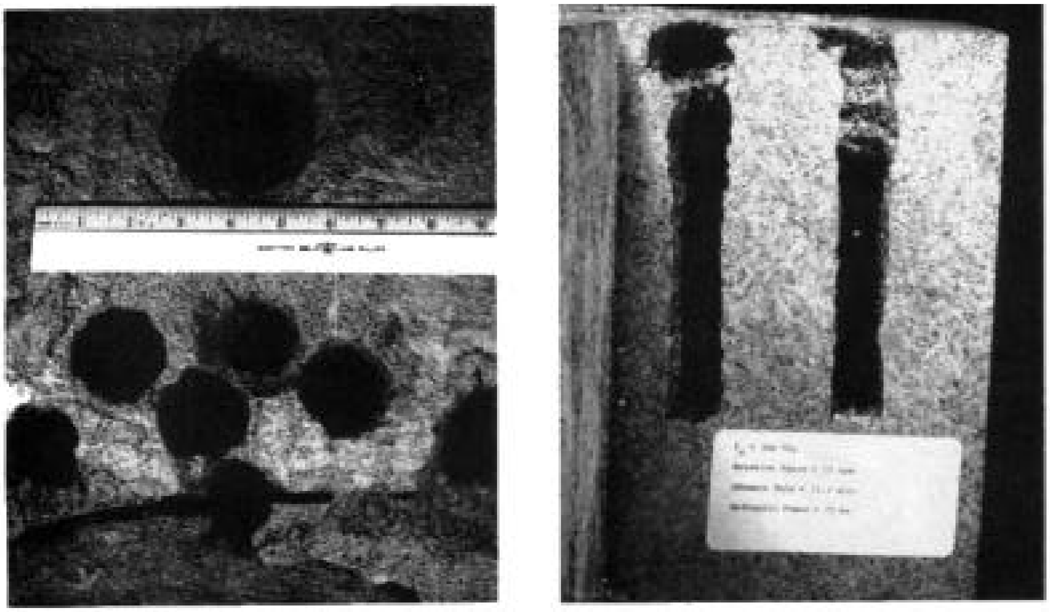

Figure 6. Waterjet Drilled and Cored Test Specimens

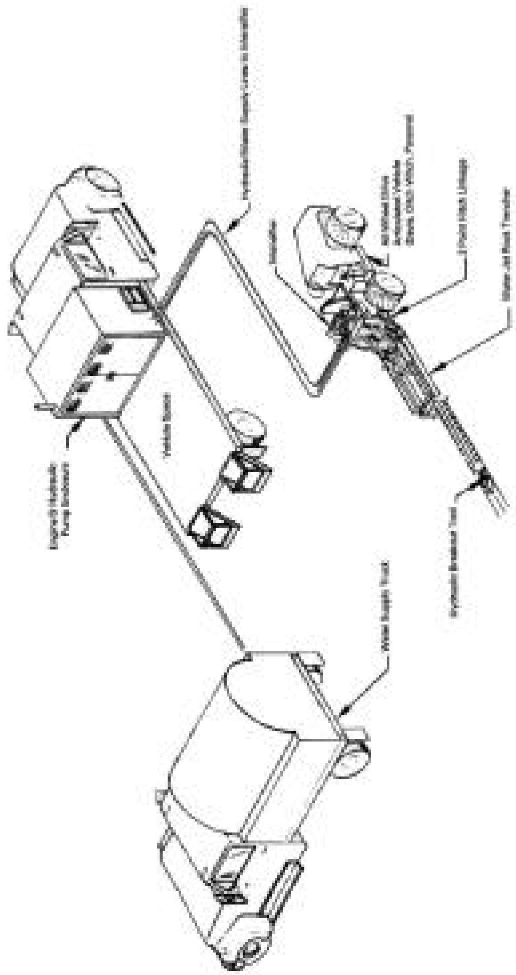

Figure 7. Waterjet Rock Trenching System

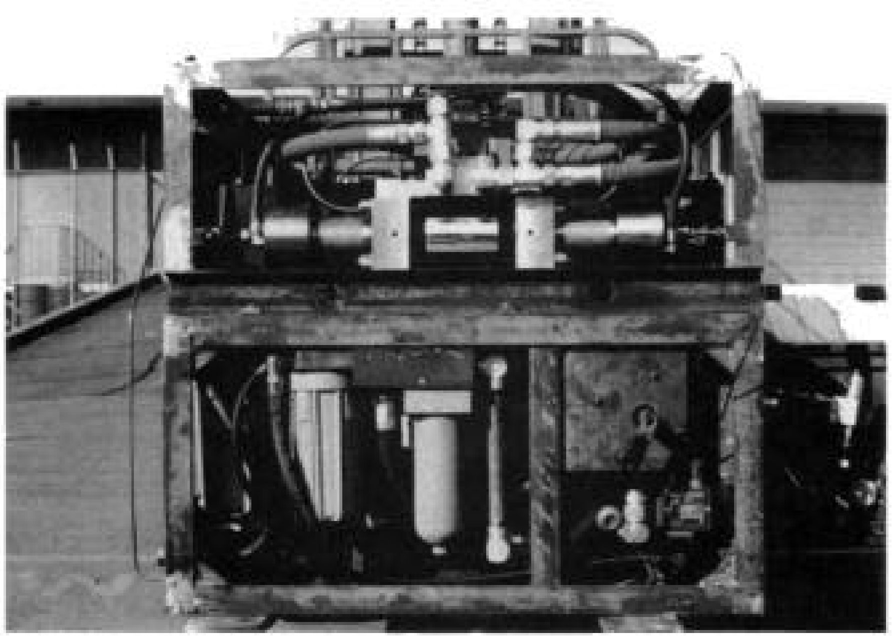

(a) High-Pressure and Hydraulic Modules

(b) Diesel Power Module

Figure 8. Modular Waterjet Power Pack

WATER JET TRENCHING IN SUBMERGED CLAYS

Philip K. Rockwell, Mechanical Engineer
Civil Engineering Laboratory
Naval Construction Battalion Center
Port Hueneme, CA 93043

ABSTRACT

Water jetting in various forms has been used in a majority of sub sea cable and pipeline burial systems as the primary means of excavating a trench for the cable or pipeline. Jet configurations have included a single nozzle used by a diver to wash in a cable, multi-nozzle configurations injecting large volumes of water into a sandy bottom to fluidize the sand, and plow-like equipment with numerous jets directed forward into the soil to break up the soil and transport it from the trench.

The Civil Engineering Laboratory (CEL), sponsored by the Naval Facilities Engineering Command, investigated the performance of a single vertical water jet nozzle for cutting a trench in submerged clay soil for burying telecommunication cables. The primary objective of the test program was to quantify the trenching capability of a single water jet nozzle as a function of the flow parameters and nozzle size.
The test program was conducted in two phases. Flow Industries Inc., Kent, Washington, under contract to CEL, performed a series of tests with 1/2-inch, 7/8-inch, and 1-1/4-inch nozzles.

The jets impinged on the surface of an artificially consolidated clay mixture. Soil shear strength, translational velocity, flow, pressure, and nozzle size were varied. Based on the results obtained by Flow Industries Inc., CEL conducted field tests in a naturally consolidated clay with water jets from 1 to 4 inches in diameter.

It was found that trenches could be cut 36 to 48 inches deep at translational speeds in excess of 100 ft/min. The Buckingham Pi Theorem was used to identify two dimensionless variables relating depth of cut, nozzle diameter, nozzle pressure, translational velocity, and soil shear strength. When these dimensionless variables were plotted against one another, an empirical design curve was established that fits the combined results of the Flow Industries Inc. and CEL tests.

INTRODUCTION

Oceanographic cables laid on the seafloor are extremely vulnerable to damage and ensuing failure from the otter boards of bottom-fishing trawlers. The most effective method for protection of these cables from damage is to bury them in the seafloor. The Civil Engineering Laboratory (CEL), sponsored by the Naval Facilities Engineering Command, investigated cable burial methods to effectively and efficiently bury these cables in the seafloor sediments. Trade-off analyses showed that mechanical trenching devices required large amounts of power at the high excavation rates desired, that they were unreliable considering their mechanical complexity and the length of trenching involved, and that they were vulnerable to damage from buried rocks and other debris. It appeared that use of a water jet trenching device would solve most of these problems. A technology validation program was initiated to evaluate water jets as the trenching subsystem by performing laboratory and full-scale field tests in soils similar to those on the floor of the ocean.

Water jetting in various forms has been used in many subsea cable and pipeline burying systems. Its use has included a simple single-nozzle jet or jet eductor used by a diver to wash in a cable, injection of large volumes of water at low pressure into a sandy bottom to fluidize the sand, and large jet-stingers with numerous medium pressure jets assisted by an airlift to excavate a large trench into which a pipeline would settle. A single, vertically impinging water jet was selected as a prime candidate for the excavation system evaluation because:

• The water jet system is extremely reliable since the pump is the only moving part.

• The water jet could create a slot with no implement in the soil.

• With the nozzle placed a few inches from the soil surface, no forces due to excavation would be imposed on the burial system.

Power requirements were estimated (Ref 1) from trench dimensions, trenching rates, and power requirements reported for other water jet trenching equipment in use. A power density function was formulated:

$$P_D = \frac{\text{Delivered Power}}{V\ A}$$

where
V = forward velocity
A = trench cross-sectional area

Using the average power density of three jetting systems, a jetting power of 256 hp was estimated to excavate a trench with a frontal area of 1 ft^2 (0.093 m^2) at a speed of 1 knot. However, no information was found that would allow prediction of jet penetration as a function of the jet parameters. A series of field tests was performed to validate the power estimate and determine the penetration capabilities of the vertical water jet.

The objectives of the vertical water jet trenching tests were to:

• Quantify the trenching capabilities of a vertically impinging water jet as a function of the flow parameters.

• Compare full-scale field results with scale model results obtained by a contractor to CEL.

• Identify characteristics that may pose operational problems with the jetting subsystem as applied to the burial system.

• Validate the power predictions made during previous trade-off analyses.

BACKGROUND

In 1977, CEL contracted with Flow Industries Inc., Kent, Washington, to investigate water jet trenching in simulated seafloor soils. In a series of 34 tests, Flow Industries evaluated the performance of water jets with three nozzle diameters (1/2 inch (1.27 cm), 7/8 inch (2.22 cm), and 1-1/4 inches (3.175 cm)) for various nozzle pressures and traverse velocities. The tests were performed with a single vertical water jet nozzle which was close to, but not touching, the soil surface. A template was used with a 12-inch-long (30.5 cm) access hole cut into it. Thus the nozzle could be accelerated to its proper traverse velocity before impinging on the soil through the access hole. The soil used in the tests was an artificially consolidated simulated ocean sediment made from commercial clay products and water, with a saturation level approaching 100%. Most resulting trench depths were less than 12 inches (30.5 cm). Flow Industries summarized their results by the empirical equations (Ref 2):

$$\frac{H}{D} = 0.13\left(\frac{V}{1.67}\right)^{-0.3}$$

and

$$P = 0.0174 p^{3/2} D^2$$

where

H = trench depth (in.)
D = nozzle diameter (in.)
p = nozzle pressure (psi)
V = traverse velocity (ft/sec)
P = power output (hydraulic) at nozzle
soil shear strength = 2 to 3 psi (13.8 to 20.7 kPa)

Figure 1 illustrates the first relationship. Flow Industries also briefly investigated the effect of standoff distance (e.g., the distance between the nozzle tip and soil surface). In general, increasing the standoff distance produced shallower trench depths (due to nozzle centerline pressure decay) as well as an increase in trench width. Flow Industries observed that the jet-cut slots were straight sided with fairly uniform widths and depths. The trench width was approximately equal to the nozzle diameter. The water jet removed soil both in chunks and fine particles and the material left in the trench was in the form of a slurry. To verify the above work and gain insight into the operation of full-scale water jet trenching, CEL conducted a series of field tests during September 1978.

FIELD TEST DESCRIPTION

Site Selection

The type and condition of the soil selected for this type of testing was one of the most important decisions made during planning of the tests. The characteristics of a dredge spoil area at the Mare Island Naval Shipyard (MINS) are presented in Table 1, but some additional comments are in order on the uniqueness of the soil with respect to the water jet trenching operations.

As the dredging operations at MINS were conducted and the basins gradually filled, the soil in different areas of the basin would dry out, then more soil would be deposited, dry out again, and so on as the months passed. This created a layered effect, with each basin having a different composite of layers than its neighbor, depending on the dredging schedule, weather conditions, evaporation, water cover, and drainage. It was desired to find a site with the most homogeneous soil possible; if any hard layer were present, it should be below the 36-inch (91-cm) anticipated trenching depth. It was also desired to test in soil with a shear strength of 2-3 psi (13.8 to 20.7 kPa). The area selected had most of the qualities desired and was diked off to retain the water level. Retaining the water was important both to prevent the soil from drying and because the water jet tests required some water cover. However, some drying did occur, resulting in a slightly firmer layer several inches thick at the surface with a myriad of cracks across the surface. The cracks extended down several inches.

<u>Test Equipment</u>

A test frame designed and built in 1977 for testing of a vibratory plow system was used as the test platform for the water jet tests. Figure 2 shows the test frame and associated hardware. The water jet was mounted on the traveling carriage, which allowed a 50-foot-long (15.25 m) trench to be cut. The width of the frame permitted two trenches to be cut in undisturbed soil before the entire frame would have to be moved to a new location. An hydraulic winch mounted on the carriage assembly pulled the carriage back and forth for these tests.

The water jet itself consisted of a vertical 4-inch-diameter (10.16-cm) pipe mounted on the carriage with a removable lower nozzle section. Three nozzles having exit diameters of 1 inch (2.54 cm), 2 inches(5.08 cm), and 2-1/2 inches (6.35 cm) were tested. All nozzles were designed to have a smooth entrance from the 4-inch-ID (10.16 cm) pipe and an inside taper of 15^{o} as shown in Figure 3.

For most of the tests, the pipe was positioned to place the nozzle tip one or two inches above the soil surface. A large, diesel-driven pump located separately from the frame supplied water to the water jet via a 6-inch-ID (15.24 cm) hose. The pump was capable of 2,000 gpm (126.2 l/sec) at 250 psi (1,720 kPa). Figure 4 shows a sketch of the water jet circuit.

<u>Instrumentation</u>

Nozzle flow and pressure were measured with a paddlewheel flowmeter and pressure transducer. The pressure measuring port was just upstream of the nozzle body; this corresponds to the manner in which Flow Industries measured nozzle pressure. A speed transducer (rolling wheel connected to a potentiometer) measured traverse velocity. All instrumentation was fed into a multichannel oscillograph recorder. Because of the cohesive properties of the soil and the high water flow rates during trenching, it was felt that any trench depth measuring device or implement placed in the trench during testing would either suffer damage during operation or give erroneous readings. It was decided that trench measurements would be taken manually upon the conclusion of each test by probing the trench with a scale to determine depth, and feeling the sides and contours of the trench to estimate width. This procedure had been successfully used by Flow Industries.

Test Plans

The range of parameters to be tested was selected using the empirical equations developed by Flow Industries. By selecting a nozzle diameter of 1 inch (2.54 cm), 2 inches (5.08 cm), or 2-1/2 inches (6.35 cm) and knowing the desired trench depth, pressure, flow, and power levels could be calculated. A diesel pump combination was selected which could produce these levels.

The water jet tests were conducted by setting the desired flow rate through the nozzle, then winching the carriage forward at a predetermined speed. Upon reaching the end of the test frame, the flow was stopped and the carriage returned to the opposite end to begin another test. The water jet was then moved sideways about 3 feet (1 m) which allowed the next trench to be cut in undisturbed soil. After cutting two trenches, the entire frame was moved sideways about 15 feet (4.6 m), again allowing testing in undisturbed soil

RESULTS

Twenty-four tests were conducted with a water cover of from 3 to 6 inches (7.6 to 15.2 cm) over the soil surface. The test results are shown in Table 2. Because the trench had irregular-shaped walls and was often partially filled with chunks of cut material, measuring the trench depth after the test was never completely satisfactory. For tests no. 8 through no. 23, the trench depth was measured by placing a probe directly behind the water jet every few feet while the test was in progress. The probe was a 5-foot (1.5-m) length of l-l/2-inch-diameter (3.8 cm) metal tubing with a scale attached. The person making the measurements rode with the carriage thrusting the probe into the trench as many times as possible and keeping a mental record of the depths measured. This method proved very satisfactory and fairly accurate for it was found that most trenches cut had a consistent and well-defined depth.

Test no. 7 was an experimental attempt to try out the new measurement technique. Depths for four of the tests were not obtained due to equipment malfunctions or trench depth measurement difficulties.

In general, most tests were to be completed at traverse velocities of either 1.0 or 2.0 ft/sec (30.5 or 6.10 cm/sec). However, due to inaccuracies in setting the flow rate on the hydraulic power source, the exact speed was not known until the test was run. This resulted in the velocities varying slightly around the nominal 1.0 or 2.0 ft/sec (30.5 or 6.10 cm/sec). Once the carriage was started, the speed stayed relatively constant and was measured both electrically and by stopwatch.

DISCUSSION

First examination of the data compared the measured trench depth and nozzle pressure with the empirical equation obtained by Flow Industries for the nozzle sizes tested at Mare Island. Figure 5 shows these comparisons. Only those tests with speeds of about 1.0 ft/sec (30.5 cm/sec) are plotted. As expected, trench depth increased with increasing pressure. Likewise, with pressure held constant, trench depth increased with larger nozzle sizes.

It can be seen that the Mare Island results do not match well with the predicted results from Flow Industries work. Also, the equation developed by Flow Industries predicts a finite cut with zero pressure (which is physically unrealistic) and does not take into account soil shear strength, which should have a substantial effect on the depth of cut. In order to include all the parameters which may affect the jet performance, and in an attempt to see if Flow Industries results with small jets were consistent with the Mare Island results with larger jets, dimensional analysis was used to derive dimensionless (n) terms which, when plotted against one another, could provide design points for various trenching requirements. The analysis (Ref 3) resulted in two dimensionless variables of interest,

$$\pi_1 = H/D$$
$$\pi_2 = \frac{p^{3/2}}{Vs_u}$$

where H = trench depth
D = nozzle diameter
p = nozzle pressure (psi)
V = translational velocity(in./sec)
s_u = soil shear strength

π_1 and π_2 were computed and plotted for the results of the Flow Industries tests and the Mare Island tests (Figure 6). Note that the depth of cut goes to zero as the pressure goes to zero or as the velocity or shear strength gets very large. Also, as the velocity tends to zero, or the pressure gets very large, it appears that a maximum depth of cut will be reached. Finally, as the soil gets weaker, the depth of cut also approaches a limit, which is consistent with the pressure decay characteristics of a nozzle as measured by Flow Industries (Ref 2). Because of the exponential nature of the curve and in an attempt to perform a regression analysis on the data, log H/D was plotted against $\log(p^{3/2}/Vs_u)$. The linear regression analysis resulted in the regression line and the 95% confidence interval lines shown in Figure 7. The equation of the regression line is

$$\log\frac{p^{3/2}}{Vs_u} = -0.42 + 1.63\log\frac{H}{D}$$

Use of these results as a design guideline requires entering the curve with a desired H/D ratio, locating the minimum, maximum, and expected values of $\log(p^{3/2}/Vs_u)$ and, knowing the desired translational speed and soil shear strength, calculating p, P_{min}, and P_{max}- Then, using the standard nozzle equation

$$Q = C_D\frac{\pi}{4}D^2\sqrt{\frac{2p}{\rho_w}}$$

where C_D = discharge coefficient
P_w = mass density of water = 9.6 x 10 5 lb-sec^2/in. ^{4}

The flow rate, and thus the power requirement, can be calculated.

Using the curve in Figure 7 as a design guide must be done with caution, since:

• The results are for clay soils only.

• The curve must be entered with a known H/D ratio and the pressure calculated. If the H/D ratio is to be predicted from known values for p, V, and s_u, Figure 8 must be used.

• The uncertainty of the results increases near the ends of the curve.

OBSERVATIONS

Several observations were made on the qualitative performance of the water jet trenching at Mare Island. As is inherent in this type of testing, these observations may be unique to the situation at that time and not necessarily a description of phenomena characteristic to water jet trenching in general. The observations are as follows:

1. The jet did not produce a trench with straight walls. In all cases the trench sides were highly irregular. In general, the trench width was equal to or larger than the nozzle diameter. The trench width at the surface varied from less than 12 inches (30.5 cm) to sometimes 24 to 30 inches (61 to 76 cm) across. At times the surface trench width was not centered but substantially offset to one side or the other of the nozzle centerline.

2. The water jet did not cut in a smooth manner but often removed material in large chunks. The actual cutting action was not nor could not be observed, and only inferences l can be made based on the material later found in the trench. The material found in the trench was a slurry containing pea gravel sized pieces of soil, and chunks of soil from a l few inches to 12 inches (30.5 cm) in size.

3. Very little material was deposited on the soil surface adjacent to the trench. The bulk of the cut material seemed to be transported backward, opposite the direction of travel. A shallow depression several inches (5 cm) deep usually remained at the surface of the trench.

4. The flow of water was generally backward with a visible small rooster tail about 4 or 5 feet (1.2 or 1.52 m) behind the nozzle.

CONCLUSIONS

Clearly, water jet trenching is a viable method to cut through clay soil of the type subjected to testing. It has the advantages of not having any components below the soil surface, having no moving parts (other than the pump), and not being subject to damage by any object already buried in the soil. Its main failing is that it does not produce a clean trench void of material. For a burial system, this is a drawback which puts severe limitations on the use of a vertical water jet as the sole trenching mechanism.

Based on the curve of Figure 7, a 24-inch-deep (61 cm) trench with a 4-inch (10.2-cm) nozzle in 4-psi (27.6 kPa) clay at a speed of 1 knot would require a nozzle pressure of 68 psi (470 kPa) at a flowrate of 3,900 gpm (246 l/sec), thus 150 hydraulic horsepower at the nozzle. The values Of P_{min} and P_{max} are 47 and 96 psi (324 and 660 kPa) and the respective power requirements are 88 and 260 hp; thus, the curve allows determining the operating point with a +70% and -40% uncertainty.

REFERENCES

1. Civil Engineering Laboratory. Technical Note N-1453: Deep ocean cable burial concept development, by P. K. Rockwell. Port Hueneme, Calif., Aug 1976.
2. Flow Industries. Report No. 115: Waterjet trenching of a simulated seafloor soil, by G. T. Hurlburt et al. Kent, Wash., Apr 1978.
3. Civil Engineering Laboratory. Technical Memorandum: Dimensional analysis of vibratory plow and water jet trenching field experiments, by P. K. Rockwell. Port Huememe, Calif. (to be published)

Liquid Limit	95-100%
Plastic Limit	45-50%
Plasticity Index	45-55%
Vane Shear Strength (s_u)	0.5 psi (3.5 kPa) to 2 psi (13.8 kPa) (top 24 inches)
Unified Soil Classification . .	MH (Inorganic Clayey Silt)
Degree of Saturation	100%

Table 1. MINS soil Characteristics

Test No.	Nozzle Diameter		Nozzle Pressure		Flow		Traverse Speed		Trench Depth	
	in.	cm	psi	kPa	gpm	l/sec	ft/sec	cm/sec	in.	cm
1[a]	1	2.54	191	1,320	425	26.8	1.37	3.48	--	--
2	1	2.54	196	1,350	430	27.1	2.30	5.84	16-24	41-61
3	1	2.54	150	1,030	380	24.0	1.76	4.47	15-24	38-61
4[b]	2	5.08	--	--	--	--	--	--	--	--
5	2	5.08	165	1,140	1,520	95.9	0.82	2.08	24-36	61-91
6[c]	2	5.08	95	660	1,220	77.0	0.91	2.31	--	--
7[d]	2	5.08	178	1,230	1,600	100.9	0.91	2.31	--	--
8	2-1/2	6.35	80	550	1,880	118.6	1.06	2.69	40-45	102-114
9	2-1/2	6.35	60	410	1,640	103.5	1.04	2.64	40	102
10	2-1/2	6.35	16	110	900	56.8	0.94	2.39	30	76
11	2-1/2	6.35	105	720	2,000	126.2	2.09	5.31	36-40	61-102
12	2	5.08	177	1,220	1,600	100.9	1.04	2.64	36-44	61-112
13	2	5.08	95	660	1,200	75.7	0.92	2.34	36-44	61-112
14	2	5.08	30	210	725	45.7	1.13	2.87	22-26	56-66
15	2	5.08	175	1,210	1,600	100.9	2.18	5.54	40-44	102-112
16	1	2.54	>250	>1,720	450	28.4	1.10	2.79	36	91
17	1	2.54	115	790	300	18.9	1.10	2.79	24	61
18	1	2.54	37	260	150	9.5	1.03	2.62	12-18	30-46
19A[e]	2	5.08	175	1,210	1,600	100.9	1.03	2.62	--	--
19B[f]	2	5.08	170	1,170	1,550	97.8	1.01	2.57	--	--
20	2	5.08	30	210	725	45.7	2.22	5.64	18-24	46-61
21	2	5.08	30	210	725	45.7	4.34	11.02	8-14	20-36
22	1	2.54	38	260	175	11.0	2.30	5.84	12-18	30-46
23	1	2.54	230	1,590	450	28.4	2.15	5.46	12-18	30-46

Table 2. Water Jet Trenching Test Data

[a]Test stopped halfway due to problem with flowmeter.

[b]Test stopped halfway due to loss of pump suction.

[c]Difficulty in trench measurement; no trench visible.

[d]Recut of trench no. 6; experimented with new depth measurement technique.

[e]Trench depth inadvertently not recorded.

[f]Recut of trench no. 19A with nozzle lowered 12 in. (30.5 cm) below soil surface.

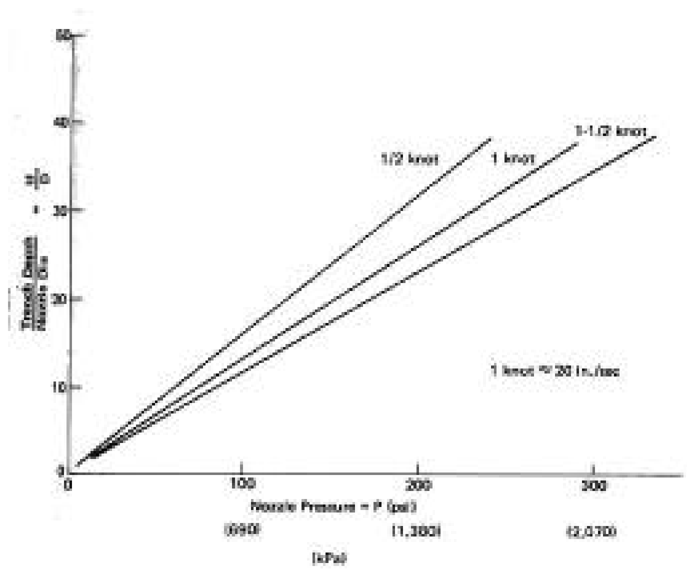

Figure 1. Water jet trenching test results (Flow Industries inc.).

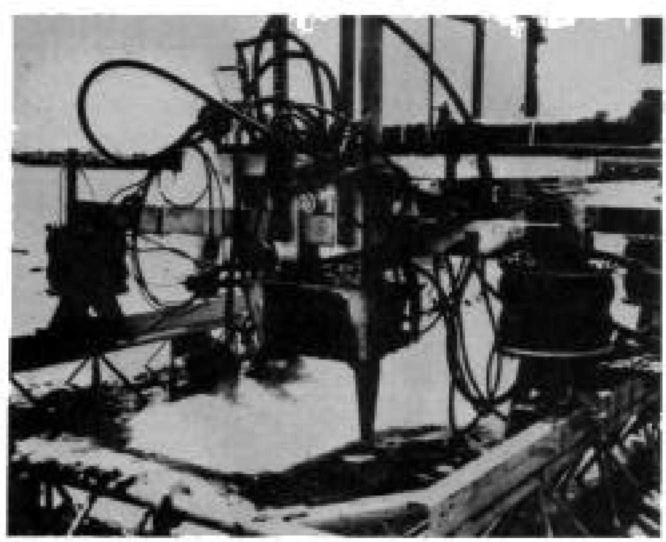

Figure 2. Water jet test equipment.

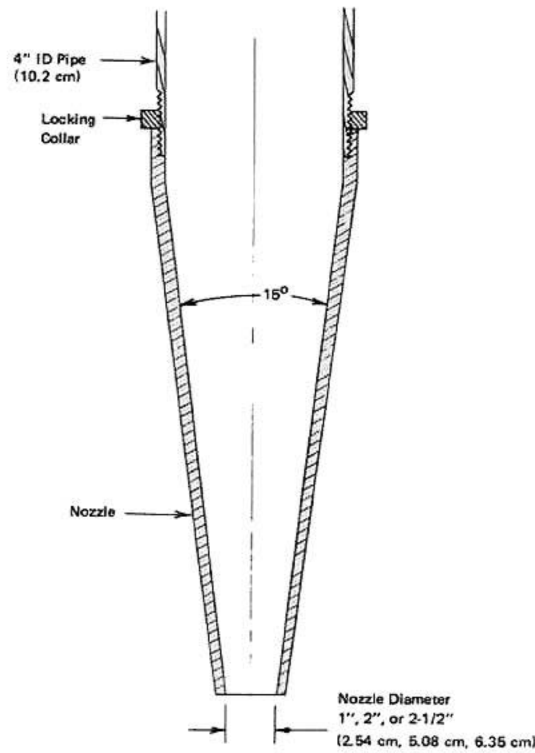

Figure 3. Nozzle configuration.

Figure 3. Nozzle configuration.

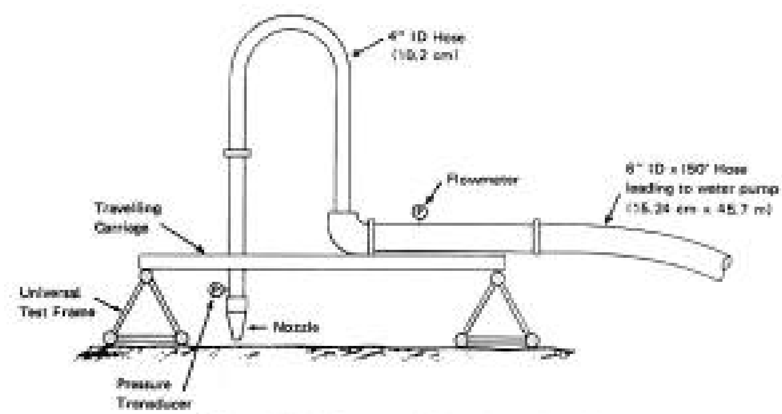

Figure 4. Water jet trenching hardware schematic.

Figure 4. Water jet trenching hardware schematic.

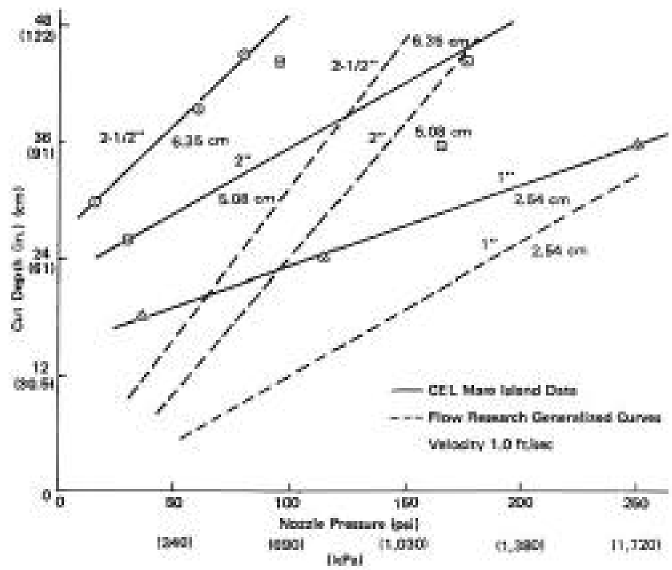

Figure 5. Water jet pressure influence on depth of cut.

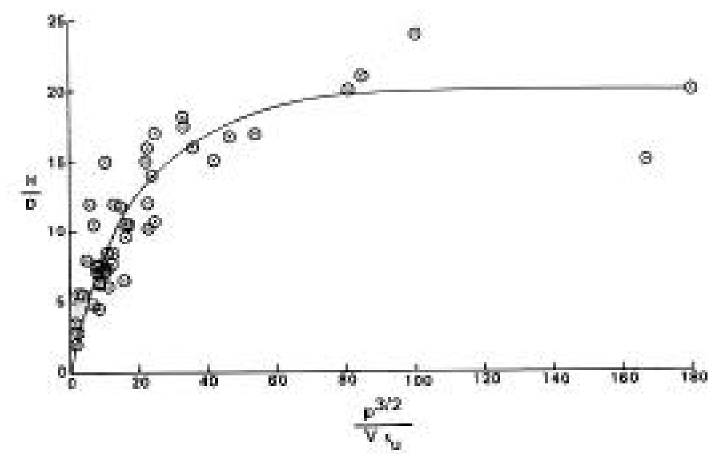

Figure 6. Water jet trenching results - normalized.

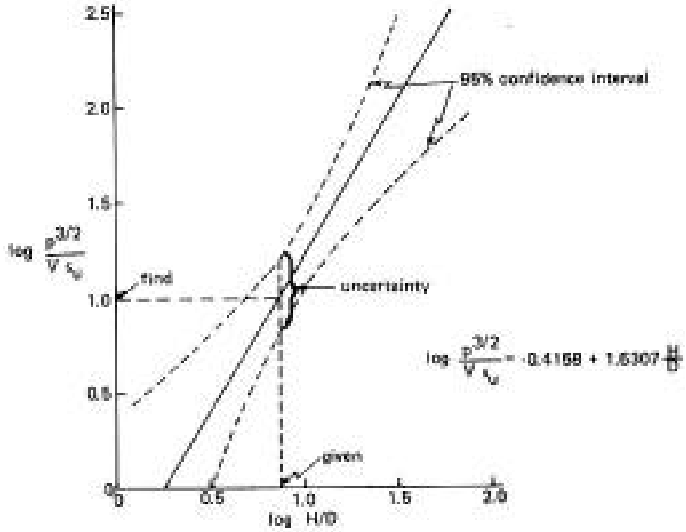

Figure 7. Log normal plot of water jet trenching results - known H/D.

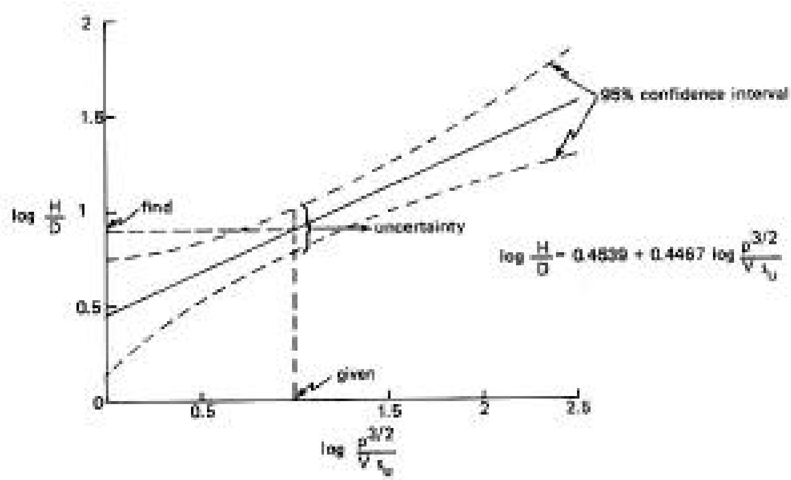

Figure 8 Log normal plot of water jet trenching results known p, v, s_u

DEVELOPMENT OF LARGE-DIAMETER PERCUSSIVE JETS

E. B. Nebeker, Ph.D.
Scientific Associates, Inc.
1639 12th Street
Santa Monica, Ca. 90404

ABSTRACT

The cutting and fracturing capabilities of high-speed water jets, along with various practical advantages of hydraulic systems, have prompted much interest in these jets for mining and other applications. The Percussive Jet is a fundamentally different free-jet form with special impact characteristics which can enhance jet effectiveness and applicability.

Percussive Jets apply force to rock as a sequence of high-frequency, short-duration impacts, rather than steadily. These Jets can be produced with a conventional, continuous flow system by modulating the discharge, i.e., cycling the discharge rate by a small amount above and below its average. With modulated discharge, the faster part of each cycle overtakes the slower in the free stream. If this process is done properly, the stream becomes bunched instead of uniform and a Percussive Jet is produced.

Earlier work has concentrated on small-diameter water jets. Results of the development and testing are summarized. Modulator frequencies (or bunches striking the rock target) have varied from 2,000 to 20,000 per second. Nozzle discharge pressures have varied from 2300 to 7200 psig using a flow rate of 9.6 gpm with relatively small nozzles (~0.060 inches diameter). Test results showed that Percussive Jets were many times more efficient than ordinary jets and sometimes over an order of magnitude more efficient. These results have been obtained with a variety of materials: coal, brick, sandstone, concrete, coal-associated shale, limestone, and granite. Even more interesting were the apparent rock fracturing or cutting mechanisms.

Current work is concerned with jet diameters in the one-half-inch range. Stream bunching could act to conserve jet velocity against air drag and thus increase the maximum range of a jet. The current activities are summarized with a discussion of the modulator, test site design, and an approach to visualizing the inner core of the jet using infrared photography.

INTRODUCTION

Scientific Associates applies the term Percussive Jet to a free stream which strikes a target as a series of high-frequency, short-duration impacts, rather than as a steady force. The percussive impact derives from the stream diameter varying periodically so that the jet actually consists of a train of bunches; Figure 1 is a photograph of a Percussive Jet. The non-uniform stream is obtained by modulating the discharge, i.e., cyclically increasing and decreasing the discharge flow rate by a small amount. With modulated discharge, the faster part of each cycle overtakes the slower in the free stream thus producing bunching and the Percussive Jet character.

Several considerations indicate that Percussive Jets should be more efficient for fracturing and excavation than conventional jets of comparable energy (Ref. 3). In brief: 1) the increased ratio of impact area to water volume obtained with Percussive Jets is generally beneficial in hydraulic excavation; 2) Percussive Jets repeatedly provide initial impact effects -waterhammer and high lateral velocities -which enhance fracturing and erosion; 3) cyclical unloading of the target material in percussive impact produces absolute tension which promotes brittle fracture; 4) the short duration of percussive impact stresses tends to reduce losses of energy within fractured material and therefore the specific energy for excavation. In addition to these impact advantages, stream bunching could act to conserve jet velocity against air drag and thus increase the maximum range of a jet. This last consideration is important for large-diameter jet applications, e.g., borehole or high-volume mining, which are economically and energetically sensitive to the effective range.

The feasibility and rock excavation potential of Percussive Jets were demonstrated in a preliminary investigation by Scientific Associates (Refs. 1, 2). Development was continued on small diameter jets (Ref. 3). Discharge modulation was obtained by means of modulator devices which produced high-frequency flow resistance variation upstream of the nozzle. Figure 2 illustrates a particularly significant result obtained in impact tests on granite. Although the granite was almost unaffected by the conventional jet, the equivalent Percussive Jet produced relatively broad and deep cavities, probably by a brittle-fracture mechanism.

SOME FUNDAMENTALS OF PERCUSSIVE JETS

The special free-stream characteristics of Percussive Jets may be obtained by modulating the discharge of water through the jet nozzle, i.e., by cycling the discharge flow above and below its average value with some particular amplitude, frequency, and waveform. Details have been discussed earlier (Refs. 1, 2, 3). The modulation amplitude would typically be small in comparison to the average flow rate.

Modulated free jet discharge has the particular property that the slow and fast portions of each discharge cycle tend to flow together or bunch in the free stream. The free stream thus becomes a train of bunches of water which eventually separate. Bunch diameter increases with downstream distance until the axial velocity becomes uniform within each bunch.

At any particular distance from the nozzle, the free flow produced by modulation is periodically thicker and thinner than the nozzle discharge. Maximum and minimum diameters depend on downstream distance according to modulation characteristics and to aerodynamic and surface tension effects. The diameter is a minimum of zero for part of the time if the stream bunches have separated.

When this varying free flow strikes a target, the momentum flux through the nozzle is not transmitted as a steady force, but as a possibly discontinuous sequence of force peaks or percussive impacts. The maximum stream impact area and force at any distance from the nozzle correspond to the maximum cross-sectional area produced by stream bunching up to that distance.

This process of discharge modulation which produces free stream bunching and Percussive Jets is very different from pulsed, intermittent, or off-and-on steady jet flow. Two distinguishing features are most important:

1. An intermittent steady jet would not produce enlargement of the stream and amplification of the impact force at a distance, i.e., force peaks. The intermittent jet would simply deliver segments of the steady-jet low-force impact.
2. The Percussive Jet flow is produced in the free stream by the action of a relatively small modulation of the flow rate, e.g., a few percent modulation. In contrast to pulsed flow, the discharge system does not suffer water hammer and extreme variations in back thrust. Modulated jet flow is therefore uniquely suited to producing high-frequency large-amplitude percussive impact while avoiding severe structural stress problems.

In spite of their potential utility for Percussive Jets and other technical applications, modulated jet flows have been hardly investigated in the past. Most research work on non-uniform free jets has involved the classical problem of stability (e.g., Ref. 4) in steady, i.e., unmodulated, jet flow. Two experimental investigations (Refs. 5, 6) dealing specifically with modulated jets were prompted by the possible relation between propellant jet modulation and combustion instability in liquid propellant rocket engines. Although this work was limited in scope, the general features of free stream bunching were verified.

However, except for the work reported here, modulated jet flow must be considered a virtually unexplored area. Two relatively recent investigations produced discontinuous jet streams by external interference. In one case (Ref. 7), an acoustic generator induced surface tension or Rayleigh instability leading to drop formation; in the other (Ref. 8), a rotating device cyclically interrupted the jet, which is of course very wasteful of energy.

Such external methods for transforming jets do not involve flow modulation and generally tend to be impractical for excavation jet applications. However, the basic modulation and bunching process is affected to various degrees by many secondary factors. The interaction of the jet with the surrounding air appears most important owing to the large jet velocities involved. One aerodynamic effect is promoting the growth of modulation bunching because air pressure deficiency or suction is produced at any jet surface protuberance, such as bunch edges, whereas increased pressure is obtained in surface depressions between bunches. This effect depends in relatively complex manner on aerodynamic pressure, air acoustic speed, and surface disturbance size and shape (Refs. 9, 10). In general, however, aerodynamic pressures should help to produce Percussive Jets. On the other hand, air drag acts to dissipate jets.

Another factor affecting jet surface behavior is surface tension which determines the so-called Rayleigh (Ref. 11) or capillary instability. Owing to surface energy changes, cylindrical liquid surfaces are unstable against sinusoidal surface disturbances having wavelengths which exceed the cylinder circumference. The fundamental wavelength or bunching length of the modulation is the ratio of jet velocity to modulation frequency. On considering the jet diameters and velocities used in mining, the minimum wavelength for surface tension instability will typically be much smaller than the modulation wavelength. Hence, expectations are that surface tension will generally promote modulation bunching. Surface tension may also be expected to be an influential factor if parting of the stream eventually occurs as the result of modulation. Surface tension will help to shape the eventual configuration of the bunch.

Many other factors can affect the modulation bunching process, e.g., fluid friction, turbulence, velocity profile, rotational flow components, etc. Fluid friction effects are probably among the least important since the jet flow is unconfined; for example, studies of surface-tension instability indicate a very weak effect of viscosity on surface disturbance growth (Ref. 12). One effect of velocity profile is to create a radial outflow as the nozzle exit profile decays in the free jet, thus reinforcing bunching outflow due to modulation. This profile effect is believed to be a factor in free jet disruption (Ref. 13) but it would be most important in fully developed laminar flow nozzles. The velocity profile is flattened by turbulence in the relatively fast jets used for mining.

MODULATOR DEVELOPMENT

An examination was made of possible modulation techniques in order to select a likely approach for development. Modulators are basically intended for producing flow rate and pressure perturbations upstream of the discharge nozzle. However, the modulator must provide a discontinuity in the oscillatory flow impedance (pressure/flow rate) because the flow channel impedances looking downstream and upstream from the modulator will generally be different (Ref. 3). Hence, an oscillatory pressure differential must obtain across the modulator. This pressure differential can be supported in two ways. One way is to have the modulator cause an oscillatory pressure drop. This varying flow-resistance modulation, implemented by varying flow area, is the approach discussed here.

A second general approach which allows for pressure differential across the modulator is "positive-displacement" modulation. In such modulators, the dynamic elements are similar to those in positive-displacement hydraulic pumps, usually pistons ox gears in various arrangements (Ref. 14). The basic characteristic of these devices is a close fit between fixed and moving elements so that upstream and downstream pressures can vary independently and any differential can be produced without affecting the volumetric displacement. Various ways of arranging positive displacement elements for producing modulation can be envisioned. In the simplest concept, though not the rendition, the modulator would merely be a small piston or gear pump interposed ahead of the nozzle and designed to produce pulsations of the desired frequency and amplitude. Whereas in conventional positive displacement pump technology flow pulsations are to be reduced or avoided, in the case of the corresponding modulators, pulsations would be deliberately sought.

The most fundamental drawback of varying flow-resistance modulators is the waste of energy associated with the pressure drop of the modulator. This waste is acceptable if outweighed by Percussive Jet benefits. Positive displacement modulators can be designed with or without a wasteful pressure drop. However, in either case and specially the latter, design and construction are much more intricate than with the simple varying area modulators. The mechanical complexities of some positive displacement modulator concepts are evident on considering that they amount to putting miniature flow-driven pumps in front of the nozzle.

Since modulator development was expected to involve many trial-and-error iterations in design, the relatively simple area modulator promised easier, faster results. The slotted rotor/stator concept is, of course, not the only approach to varying flow area. Another method considered had a valve plug oscillating within an orifice. This method had good possibilities for amplitude control, but, in common with other reciprocal motion devices, was unsuited to obtaining high modulation frequencies.

Figure 3 shows an exploded view of a modulator that was used for small-diameter (~0.006 inches) jets. The rotor fits around the stator. The rotor is made to rotate by the flow passing through tangential holes in the lucite case. The only bearing is the fluid between rotor and stator. These rotors have self-correcting axial positioning through flow dynamics.

The rotor and stator each have a set of slots or flow passages which are relatively long (axially) in comparison to their width (circumferentially). Each set is spaced uniformly along the circumference and the stator is positioned so that its slots are radially opposite to those of the rotor. However, the two sets of slots need not have equal numbers or equal slot lengths or widths.

As the rotor revolves, its slots pass periodically through various stages of alignment with the stator slots, thus producing a cyclic area variation. The amplitude of this area cycle determines the discharge modulation amplitude. As discussed in Reference 3, the modulator has to produce both a flow rate and a pressure drop oscillation. The latter is always important so that, as a first approximation, the function of the modulator is to generate a varying pressure drop. In further approximations, pressure drop is proportional to the square of the velocity, and velocity inversely proportional to the through flow area. Maximum open area and minimum pressure drop are obtained when rotor and stator slots are in alignment. Maximum area should be as large as possible in order to reduce pressure-drop energy losses, but practical limits are set by space and construction problems. Nevertheless, maximum areas were generally more than five times the nozzle discharge area giving minimum modulator pressure drops of only a few percent of the discharge pressure drop.

In these modulators, frequency is determined by the rotor speed and by the frequency multiplier or cycles per rotor revolution, which depends on the number of slots. If the stator and rotor have the same number of slots, that number is the frequency multiplier.

The desired modulation frequency is determined by considerations of standoff distance, jet velocity, and modulation amplitude. As discussed in Reference 3, the growth of bunching, or Percussive Jet character, obtained at a particular distance from discharge depends on the discharge modulation amplitude and on the number of "bunching lengths" contained within the distance. The bunching length or the ratio jet velocity/modulation frequency is simply the length of jet participating in such complete modulation cycle.

Small cutting jets typically operate at standoffs under one-hundred jet diameters because jet momentum decays rapidly beyond this distance (Refs. 15, 26). The experimental jets of interest to this work had discharge diameters of .06 - .08-inch and would presumably operate at standoffs of only a few inches. In order to produce Percussive Jets within such distances, the bunching length should be about an inch or less so that several bunches are included between discharge and target. Since the jet velocity was on the order of 1000 ft/ sec. the modulation frequency would have to be at least 10,000 hertz.

Jet bunching behavior tends to be governed by the fundamental frequency component of the modulation. Hence, the precise pattern of area variation produced by the modulator is not considered to be of major importance. The constant speed sweep of rotor slots past stator slots produces linear-in-time increases and decreases of area. Sawtooth and truncated sawtooth area waveforms can be obtained. For the truncated forms, for example, the area can be kept approximately steady at minimum by maintaining the completely "closed" condition over part of the cycle; a steady maximum or full open area can be obtained by using different slot widths in stator and rotor.

Another reason for using this design is that it leaves the upstream end of the stator available for an optional modulation bypass. With reference to Figure 3, the upstream end of the stator is holed through and threaded so it can hold screw inserts with smaller bypass holes of any chosen size. With this arrangement, some fraction, or none, of the flow goes directly to the chamber, bypassing the rotor/stator modulating action. The amount of bypass determines the modulation amplitude produced.

The flow leaving the rotor has a rotational velocity component approximately equal to the speed of the rotor. If much of this rotation gets to the discharge, it will act to widen and disrupt the jet and reduce impact effectiveness. This adverse effect of rotation can occur and must be avoided with any jet discharge. Usually, the rotational component is accidental, but, in the case of the rotor/stator modulator, strong rotation is deliberately introduced by the rotor action just upstream of the nozzle. Therefore, the modulator design must adequately provide for eliminating flow rotation between the rotor and nozzle entrance. Even with a completely empty stator chamber, much of the rotation is taken out by the rotor slots, but these are generally too short radially to provide sufficient straightening.

Figure 4 shows a complete modulator-nozzle assembly. All of the components shown in Figure 3 are attached to a typical Leach & Walker 3-D nozzle (Ref. 15).

ROCK IMPACT TESTS

Testing of small diameter jet impact effects on rock specimens was conducted with the test facility shown in Reference 3. This equipment generally consists of a triplex pump (9.6 gpm; 10,000 psi rating) connected by flexible hose to the jet discharge, a mechanism for traversing with the jet, and a structure for supporting rock targets. At the discharge the flexible hose terminates in a short steel barrel (O.9-inch ID) into which nozzles were screwed (3/4 NPT) so that attached modulators, as shown in Figure 8, were contained by the barrel. The discharge barrel is clamped to a carriage which is free to move up and down on bearings sliding over vertical shafts. The discharge carriage is driven through chains and sprockets by a variable-speed motor; vertical traversing speeds from .02 to 4 ft/sec could be selected. The fixed structure of the discharge provides for clamping typical laboratory specimens (up to about 16-inches high). In tests, the target was completely surrounded by hinged wooden panels which contained spent water and rock debris.

The primary objective of rock testing in the laboratory is, of course, to assess the potential advantage of Percussive Jets oven conventional jets. For this reason, testing largely consisted of side by side comparisons, i.e., on the same rock face, of the effects produced by a given jet with and without modulation. The unmodulated or conventional jet was obtained from the Percussive Jet by simply removing the rotor and twister, but not the stator and straightener, so that, aside from the modulation, the discharges were identical.

Reported specific energies (energy consumed/volume of rock removed) were obtained as follows. Energy was calculated as the product of power dissipation (flow rate x upstream pressure) and impact time (cut length/traverse speed). Volume was measured by the volume of fine powder required to fill the cut length. Owing to the pressure drop across the modulator, the upstream pressure for a Percussive Jet will be larger than that for the corresponding conventional jet. That is, although the two discharges are identical (modulation excepted), the Percussive Jet represents somewhat greater power consumption.

Discharge nozzles corresponded to a well-known design (Ref. 15) consisting of a straight discharge run three diameters long preceded by an accelerating section with straight walls converging at 13 degree angle. Nozzles were machined in one brass piece and polished conventionally. Three nozzles were fabricated with nominal discharge diameters of .060, .070, and .082 inch and had discharge pressures (unmodulated) of 7200, 4000, and 2300 psi respectively.

Details of the testing are reported in Reference 3. However, the Percussive Jet was more effective than the ordinary jet on all materials tested: California Black Granite, Santa Maria, Indiana & Valders Limestone, Berea 4 Santa Barbara Sandstone, coal-associated shale, concrete, coal, and ordinary brick. Differences between the two jets in cutting tests were more pronounced with the harder materials.

However, even more interesting than the apparent improvement the Percussive Jet offers over the ordinary jet was the massive type of failures seen with Percussive Jet cuts in granite, coal-associated shale and brick. Figure 2 shows a typical example. In fact, the traverse cuts illustrated in Figure 5 show a roughening of the cut, presumably a result of the same behavior. This massive failure is probably a result of the cyclical unloading of the target material in tension which promotes brittle fracture. This same mechanism may have made the concrete cuts shown in Figure 6 possible. The Percussive Jet was able to cut the aggregate as well as the softer matrix.

CURRENT WORK

Present efforts are directed at applying the Percussive Jet to large diameter water jets in the one-half-inch range. If successful, this work will help increase the standoff or effective cutting distance for jets used in high-volume coal mining and many borehole applications. Discharging large jets as Percussive Jets may increase working range because a Percussive Jet effectively simulates a discharge bigger than the actual nozzle and with correspondingly better coherence and momentum retention. Reference 17 experimentally observed that increasing jet stream diameter improves its capability for retaining momentum and impact force with increasing standoff distance, owing probably to the decreased ratio of jet surface to cross-sectional area. Hence, the spontaneous thickening of a correctly modulated Percussive Jet could help it retain momentum and increase its effectiveness at a distance.

Figure 7 shows the experimental facility used to develop one-half-inch Percussive Jets. A 125 HP multi-stage turbine pump knot shown) supplies 300 gpm at 550 psig for flow testing. For impact testing a pumping system will be rented which is capable of increasing the working pressures to 2000 psig. The oscilloscope is used to measure and record dynamic pressure transients upstream and downstream of the modulator as well as impact characteristics on a dynamic force gauge.

The modulators used for this work are conceptually similar to those discussed earlier except they are externally driven by a hydraulic system. Modulators which pass 300 gpm and operate at a frequency of 1000 Hertz have been designed and flow tested. One is shown inside the lucite case in Figure 8. This lucite case facilitates viewing the running of the modulators and is replaced with a steel case during the impact testing at 2000 psig which will come later.

In Percussive Jet development, the ability to view the bunching process as it develops is very useful. One way to study free stream bunching would be to photograph the central core of the jet. This problem is complicated because the aerodynamic drag on this high speed jet shears off the exterior surfaces of the central core to form a mist which surrounds the jet.

Naturally, the objective in photographing the core is to penetrate the mist. A number of previous investigators have attempted to photograph the central core of an ordinary jet. Unfortunately, we need to obtain a very detailed picture of the central core so that their results were considered quite marginal for our needs.

Our earlier work employed a variety of conventional photographic techniques, but the most successful employed as a light source a strobe with a flash duration of about 3 microseconds. Backlighting, in which the light passed through the jet and into the camera, produced the best results. A fresnel lens was used to create a roughly parallel beam of light coming from the strobe. A polarizing lens was positioned in front of the camera to minimize interference from reflected light from mist. Kodak EH-135-20, High Speed Ektachrome film, was used. Although some of the mist could be penetrated, sufficient resolution of the core could not be obtained to provide much information on the bunching. However, the modulation frequency could be easily confirmed because variations in the density of the jet appearing at the appropriate wavelength could be seen. In one photograph, a modulation frequency as high as 16,000 Hz could be clearly detected.

Since water absorbs light in the infrared region of the spectrum more strongly than in the visible, the same strobe was used as an infrared source and Kodak IE 135-20 Infrared Ektachrome Film was used in the camera. Wavelengths shorter than about 780 nm are excluded. Although this technique is still being developed, we feel it will be a promising way to view the central core of jets. Figure 9 shows a side-by-side comparison of the same jet photographed within the visible and infrared regions.

ACKNOWLEDGEMENTS

Current development on large-diameter Percussive Jets is being done on U.S. Department of Energy Contract DE-AC01-79ET14280. Mr. Howard Parkinson is the technical project officer and is assisted by Dr. Sedat Sami. Earlier work described above was sponsored by the U.S. Bureau of Mines and Department of Energy under Contracts HO252008 and ET-75-C-01-9094, respectively. Mr. Jack Chester and Mr. Hamilton Reese, Jr. served as technical project officers on this work.

REFERENCES

1. E. B. Nebeker and S. E. Rodriguez, "Percussive Water Jets for Rock Cutting," Third International Symposium on Jet Cutting Technology, BHRA Fluid Engineering, Paper B-1, 1976.
2. E. B. Nebeker and S. E. Rodriguez, "Percussive Water Jets for Rapid Excavation," prepared by Scientific Associates, Inc. for U. S. Army Mobility Equipment Research and Development Center under Contract DAAK02-73-C-0163, 1973.
3. E. B. Nebeker and S. E. Rodriguez, "Development of Percussive Water Jets," prepared by Scientific Associates, Inc. for U. S. Department of Energy under Contract ET-75-C-01-9094.
4. R. P. Grant and S. Middleman, "Newtonian Jet Stabklity," AIChE Journals Vol. 12, No. 4,p. 669, 1966.
5. P. D. McCormack, L. Crane, and S. Zirch, "An Experimental and Theoretical Analysis of Cylindrical Liquid Jets Subjected to Vibration," Br. J. App. Phys., Vol. 16, p. 395, 1965.
6. "Dynamics of Combustion and Flow Processes, Effects of Upstream Conditions," in Liquid Propellant Rocket Combustion Instability," D. J. Harrje and F. A. Reardon, eds., NASA SP-194, p. 117, 1972.
7. F. Danel and J. C. Guilloud, "A High Speed Concentrated Drop Stream Generator," Second International Symposium on Jet Cutting Technology, BHRA Fluid Engineering, Paper A-3, 1974.
8. A Lichtarowicz and G. Nwachukwu7 "Erosion by an Interrupted Jet," Fourth International Symposium on Jet Cutting Technology," BHRA Fluid Engineering, Paper B-2, 1978.
9. C. Weber, "Zum Zerfall eines Flussigkeitstrahles," Z. angew. Math Mech., Vol. 11, p. 136, 1931.
10. R. W. Fenn and S. Middleman, "Newtonian Jet Stability: The Rule of Air Resistance, AIChE Journal, Vol. 15, No. 3, p. 379, 1968.
11. Lord Rayleigh, "The Theory of Sound," 2nd Edition, Yol. II, p. 351, Dover Publications, New York, 1945.

12. R. J. Donnelly and W. Glaberson, "Experiments on the Capillary Instability of a Liquid Jet." Proc. Roy. Soc. London, Vol. A290, p. 547, 1966.
13. J. H. Rupe, "On the Dynamic Characteristics of Free-Liquid Jets and a Partial Correlation with Orifice Geometry," JPL Tech. Report 32-207, 1962.
14. "Fluid Power Handbook and Directory, 1976-1977," by the editors of "Hydraulics and Pneumatics," Industrial Publishing Co., Cleveland, 1975, p. All9.
15. S. J. Leach and G. L. Walker, "Some Aspects of Rock Cutting by High Speed Water Jets," Phil. Trans. Roy. Soc. London, Vol. A260, p. 295, 1966.
16. K. Yamaida, "Flow Characteristics of Water Jets," Second International Symposium on Jet Cutting Technology, Cambridge, England, 1972, Paper A2.
17. G. A. Savanick and J. N. Frank, "Force Exerted by Water Jet Impact at Long Standoff Distances," Third International Symposium on Jet Cutting Technology, BHRA Fluid Engineering, Paper B-5, 1976.

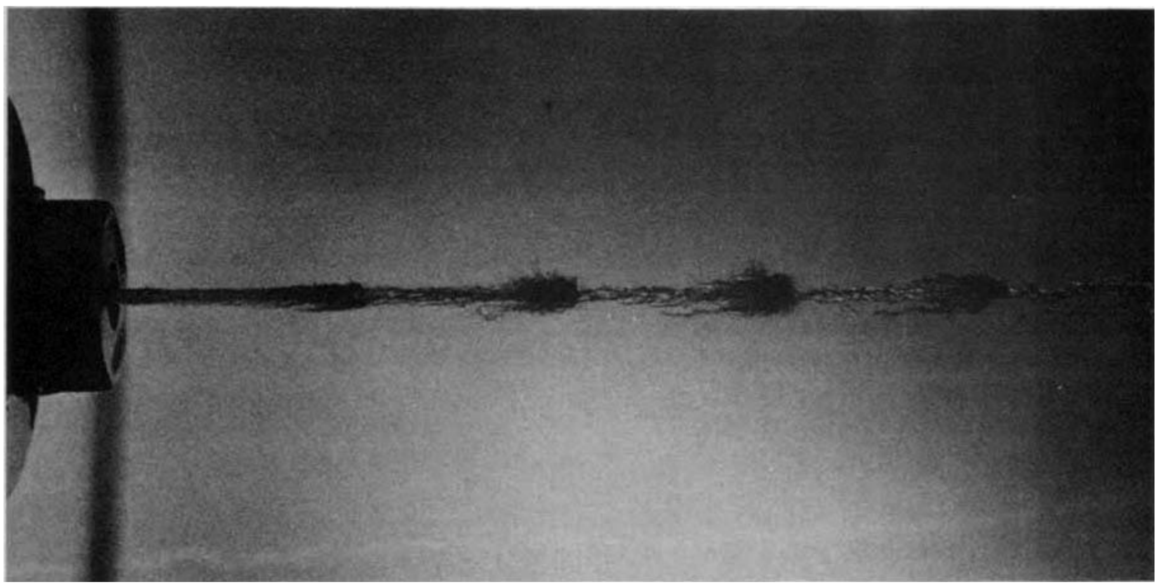

Figure 1. Example of Percussive Jets. A small cyclic variation or modulation impressed on a steady discharge of water causes the free jet to become bunched. Consequently, the jet will strike a target in a sequence of sharp impacts rather than steadily. This percussive impact makes a jet more efficient for mining and excavation. In the photograph, the Percussive Jet concept is demonstrated with a low pressure discharge (50 psig) modulated at about 900 cycles/second. Owing to the mist surrounding high-speed jets, photographs like this cannot be obtained with actual mining jets modulated at high frequency.

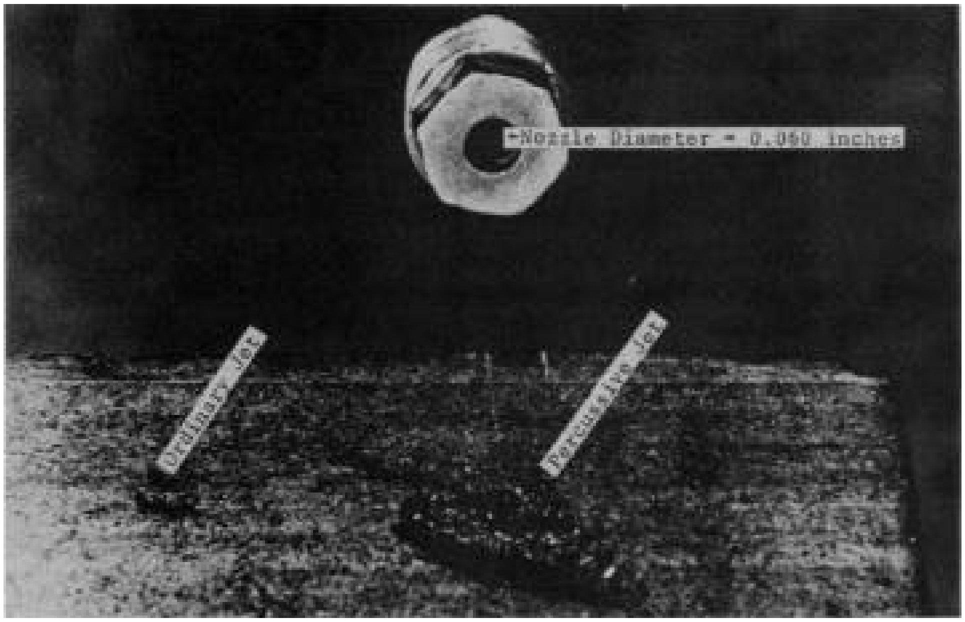

Figure 2. Illustration of Typical Massive Failure Caused by Percussive Jet. This photograph shows how a 0.06-inch diameter Percussive Jet can effect a failure over an area 300 times its own cross sectional area in granite. This test was a static burst of about 2 seconds and also shows a comparison to the impact using ordinary jets. Such failures have been observed in granite, coal-associated shale, brick, etc.

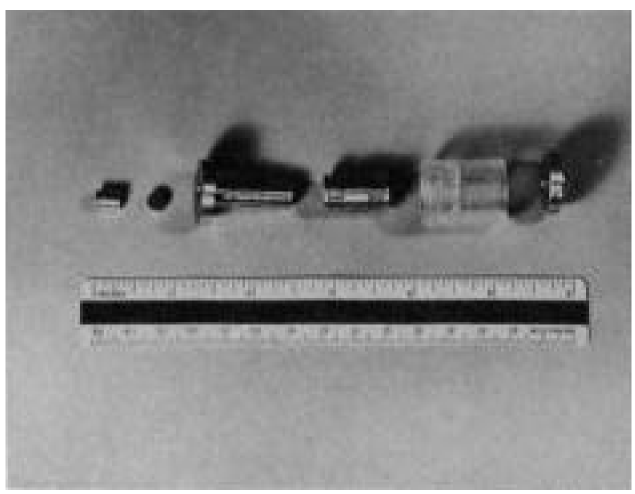

Figure 3. Disassembled Sleeve-Rotor Modulator. From left to right, Spacer, Straightener, Stator, Rotor, Lucite Case with Tangential Holes, and Back Plate with Holed Screw Insert for Amplitude Control.

Figure 4. Example of Percussive Jet Modulator Nozzle Assemblies. This hardware is relatively small, internal to the flow system, and powered by the throughflow. Therefore, conversion of an ordinary water jet system to the Percussive Jet can simply be accomplished by insertion of this assembly.

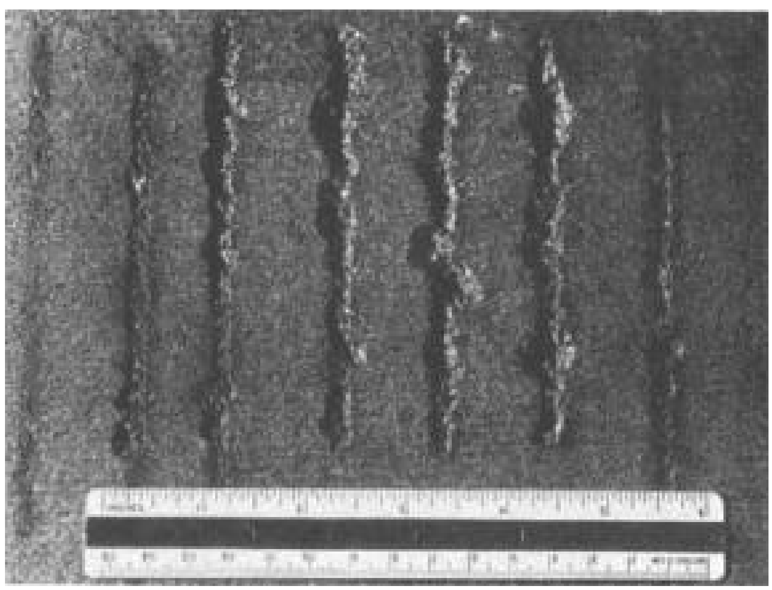

Figure 5. Percussive Jet Traverses in California Black Granite. Standoff distances varied from 2 to 8 inches (lt. to rt.) at a pressure of 7200 psi and traverse rate of 0.2 ft/sec. At best, the conventional jet would only roughen the surface.

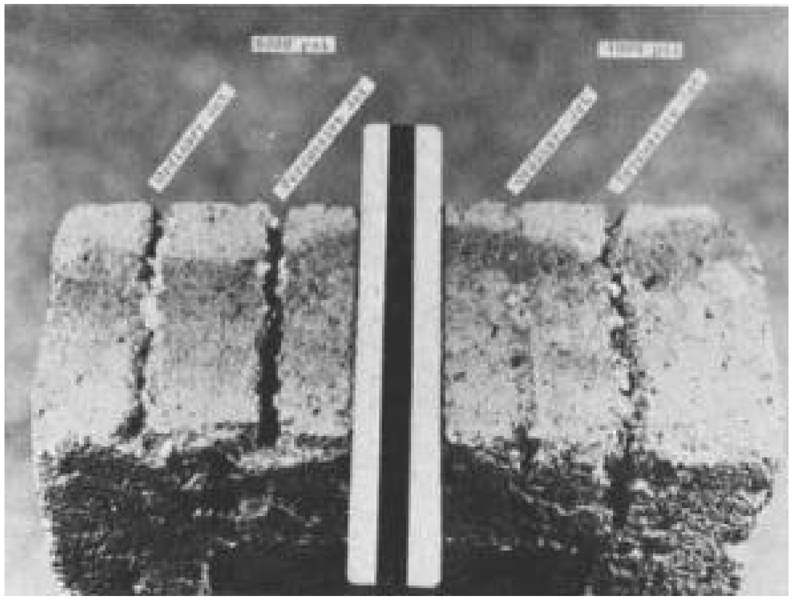

Figure 6. Concrete Cuts. This photograph illustrates the versatility of Percussive Jets. In this view, the ordinary jet could not effectively penetrate the aggregate, whereas the Percussive Jet cut the aggregate as well as the softer matrix of the concrete block.

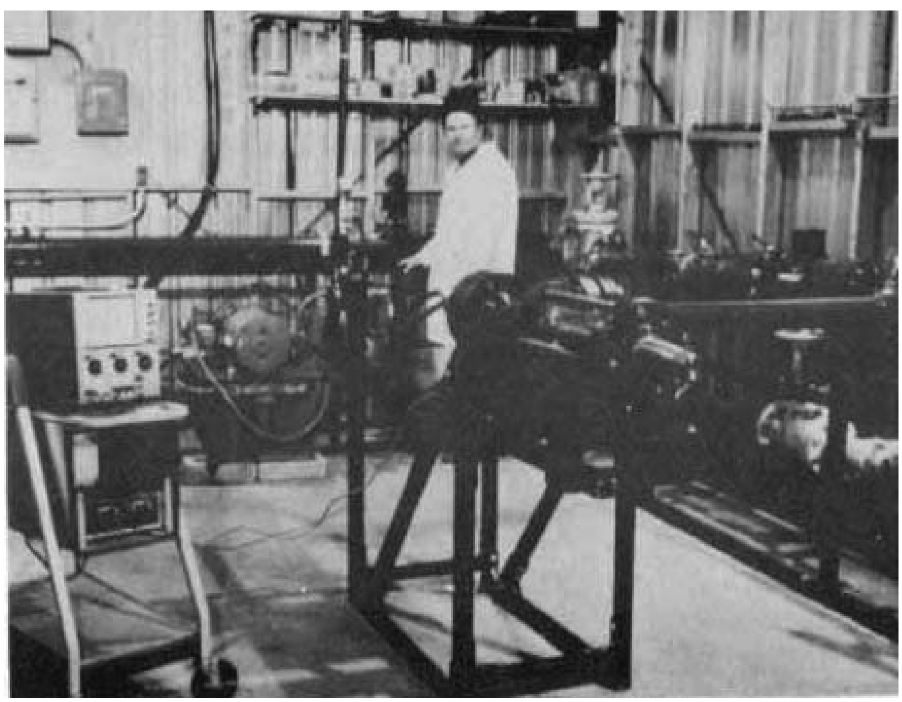

Figure 7. Overall View of Experimental Facility for Developing Large-Diameter Percussive Jets.

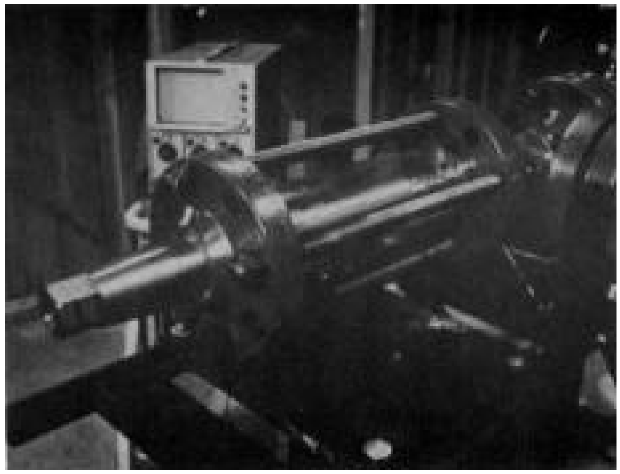

Figure 8. One-Half-Inch Diameter Percussive Jet Modulator-Nozzle Assembly.

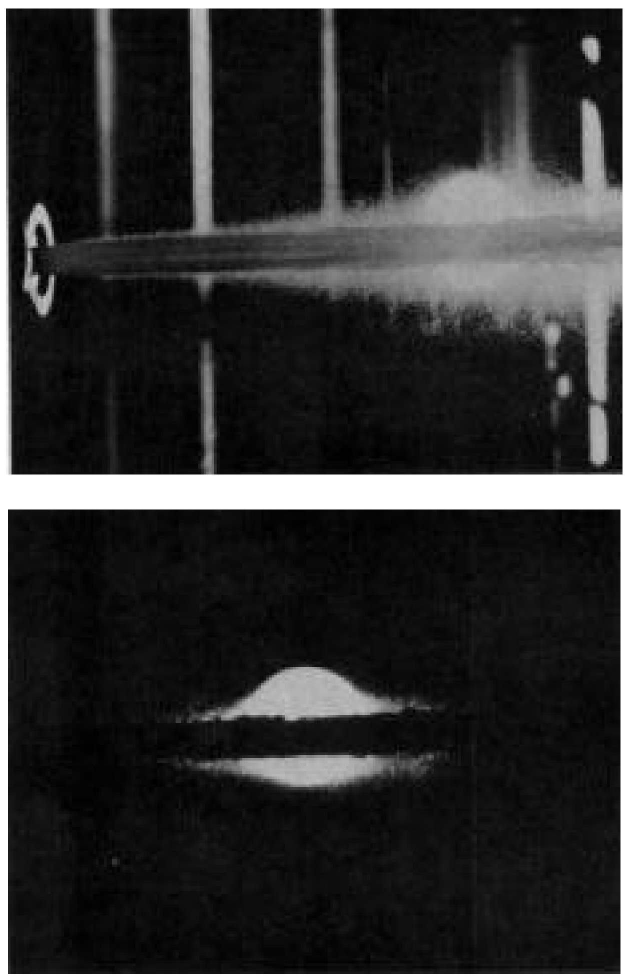

Figure 9. Example of Ordinary Jet Using Visible Spectrum (top) and Infrared (bottom) Photography.

OVERVIEW OF WATERJET APPLICATIONS IN MANUFACTURING

R. N. Draughon
Flow Systems, Inc.
Kent, Washington 98031

ABSTRACT

The purpose of this paper is to discuss the use of waterjet cutting in manufacturing and to provide an overview of several current applications.

Historically, many attempts have been made to utilize waterjet cutting technology in industrial applications. While high-pressure waterjet slitters, as compared to conventional mechanical devices, offer numerous advantages, low levels of reliability and high maintenance costs have made the equipment unacceptable for continuous run factory use.

During the period 1974 through 1980 Flow systems made significant improvements in overall high-pressure pump reliability with primary emphasis on long maintenance intervals, reduced operating costs, ease of maintenance, and improved applications engineering. Due to the substantial improvement in product performance, in excess of 250 waterjet slitters have been installed in 17 nations. High-pressure waterjet cutting equipment for manufacturing has become accepted as a reliable, standard industrial cutting tool. Economically justified applications and uses are expanding at an increasing rate.

INTRODUCTION

The first factory waterjet installation was completed in May of 1974. Wet lap mat, subsequently pressed into hardboard, is trimmed using 2 each 0.203 mm (.008") diameter nozzles. One single intensifier, 378,950 KPa (55,000) psi pump runs 24 hrs./day, 7 days/week. A backup pump is utilized during maintenance. Since this modest introduction to factory use, installations have been made on various production lines slitting materials ranging from corrugated board, paper, and disposable products to cured advanced aerospace composites, asbestos cement, and plastics. With installations numbering in the hundreds and pumping hours in the millions, the overall technology of ultra high-pressure waterjet cutting has a firm foundation from which to expand and evolve.

PRODUCT AND PRINCIPLE OF OPERATION

Waterjet cutting is defined as the severing of a material by a highly columnated fine stream of water, traveling at high speed and under extreme pressure.

Figure 1 shows corrugated fiberglass cut with a 0.152 mm (.006") diameter nozzle. The highly columnated stream is produced without additives such as ultra-high molecular weight long chain polymers.

The jet stream, traveling at speeds up to 914 mps (3000 fps), is created by pumping systems such as shown in Figure 2. Occupying an area 1690 mm (66.5") long, 965 mm (38") wide, and 2440 mm (96") high including the maintenance monitor light, the system consists of two pumps: one standard hydraulic pump and one technically advanced oil-over-water piston pump. Single or dual intensifier units are available. The piston pump intensifies low-pressure oil to high-pressure water. The hydraulic system necessary to provide oil to drive the intensifier is shown schematically in Figure 3.

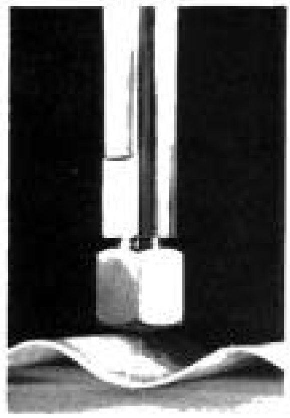

Figure 1. Nozzle Body, Nut, and Jet Stream

Figure 2. Model 106, Dual Intensifier, 55,000 psi Pumping System

Conventional hydraulic pumps with pressure ranges up to 20,670 KPa (3,000 psi) are driven by 30 HP, 50 HP and 75 HP electric motors. Oil pressure is set by standard hydraulic controls, which in turn regulate the output water pressure from the intensifier. The oil circuit also contains an oil-cooler and a filter not shown in Fig. 3.

As high-pressure water leaves the intensifier, it enters the accumulator. The purpose of the accumulator is to remove the pulses in output pressure that occur at the instant the intensifier reverses stroke direction. The accumulator contains no moving parts, serving only as a surge tank. It relies on the compressibility of water to maintain uniform discharge pressure and jet stream velocity, while the intensifier piston changes direction. The pumping system shown in Figure 2 can be located any distance from the cutting nozzle. Water is carried from the pumping system to the nozzle(s) via stainless steel high-pressure tubing. An on/off valve can be installed at the cutting nozzle, or several nozzles may be valved on and off in any combination. When a nozzle is valved off, it tends to increase the pressure in the water system, and hence in the oil system. The hydraulic controls sense the very slight increase in pressure and adjust the hydraulic pump output automatically so as to maintain a constant pressure.

The heart of the pumping system is a fluid intensifier illustrated in Figure 4. The intensifier is a hydraulically driven reciprocating plunger pump. Oil pressure acting on a large piston, balances a much higher water pressure acting on a small piston. The pressure ratio (area differential between the large oil piston and small water piston) varies depending upon the maximum pressure vs. flow rate that is desired. Current models include 20:1 and 13:1 ratio intensifiers. In operation, the piston cycles back and forth. As the piston moves toward one end, it expels water from that end and draws water in at the other end. When the piston reaches the end of its stroke, the direction is reversed, and water is expelled from the opposite end. It thus pumps on both strokes. In industrial applications where cutting pressure in excess of 275,600 KPa (40,000 psi) is required, a 20:1 ratio intensifier is specified. Applications utilizing lower pressures may use a 13:1 ratio intensifier. With a 20:1 ratio intensifier, oil pressure of 18,948 KPa (2,750) psi will produce water pressure of 378,960 KPa (55,000 psi).

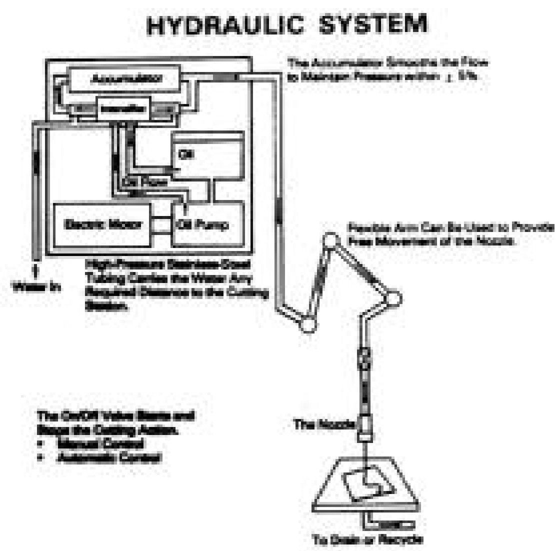

Figure 3. Hydraulic System

Each pumping station (Figure 2) is equipped with a monitor/alarm system to indicate when critical maintenance is required.

The monitor and alarm system shown in Figure 5 was designed to allow waterjet integration into continuous run production lines. Dual intensifier pumping systems as shown in Figure 3 provide electronic switching between intensifiers and are controlled as to maximum stroke rate. Misuse of the equipment is eliminated through automatic shutdown when stroke rates exceed 110 cycles per minute. In addition, one intensifier can serve as backup providing 100 percent redundancy and reliability. The combination of dual intensifiers, maintenance monitoring equipment, and electronic control systems provide minimum unscheduled maintenance and a high degree of reliability.

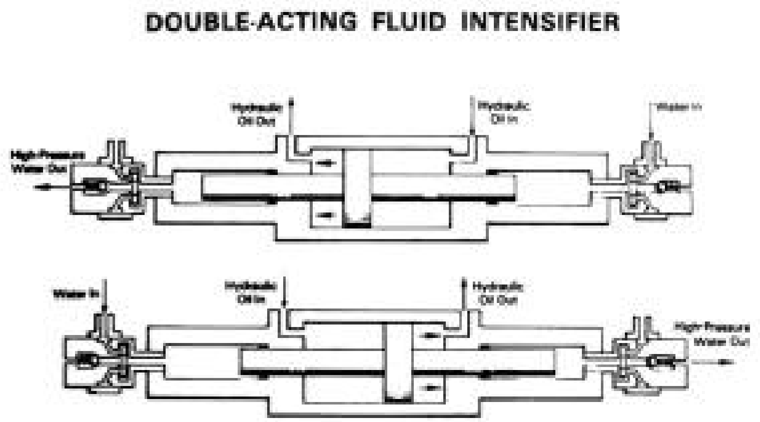

Figure 4. Double Acting Fluid Intensifier

Figure 5. Pump Monitor System

KEY FACTORS FOR INDUSTRIAL USE

The four key elements necessary to evolve high technology waterjet cutting systems into standard industrially accepted machinery are as follows:

1. Justifiable purchase price.
2. Ability to integrate with existing production lines.
3. Acceptable ongoing maintenance cost.
4. Reliability suitable for 24-hour per day operation.

I. Economic Justification: Accelerating purchase of waterjet cutting systems is testimonial that the equipment is justified. Actual justification will vary with application, depending upon the advantages attributed to waterjet slitting. Jet slitters are typically selected when mechanical devices are unusually expensive, limit productivity, or are inappropriate for the product produced. While the initial capital investment has been relatively high, the real dollar cost is declining with volume, production efficiency, reduced warranty expense, and experience. The following general trends have contributed significantly to the increasing use and justification of waterjet systems:

- Automation of Slitter Systems - Waterjet slitting nozzles are substantially simpler to reposition and/or automatically manipulate than conventional cutting devices. Most rotary knives require top and bottom slitters with critical alignment. Reciprocating knives do not have the pinpoint accuracy and omni-directional cutting capabilities of the waterjet. Conventional crosscut saws can only cut in one direction. In all of the above, close tolerances are difficult to maintain. These factors make waterjet slitters extremely attractive from the standpoint of automation. This, in turn, reduces manpower requirements, improves productivity, and increases the capability to fully automate quality control procedures.

- Escalating Raw Material Costs - As delivered prices for raw materials continue to escalate, manufacturers begin to concentrate on means to alleviate waste. Significant waste reduction can be achieved by reducing edge trim and minimizing slitter kerf (material displaced by cutting devices). Since the high velocity waterjet exerts no lateral forces on the material being cut, edge trims can be reduced to the minimum without sacrificing quality or productivity. Elimination of lateral force and material crush allows parts cut from sheet materials to be nested edge-to-edge, providing maximum material utilization. Conventional rotary slitters/saws can displace as much as 5 mm (.187") of kerf material, while the high-pressure waterjet typically displaces approximately 0.15 mm (.006"). With six to ten slitters running continuously, substantial yearly material savings are derived.

- Demand For Increased Quality - Competitive pressure is forcing manufacturers to be highly sensitive to product quality. Quality is defined by various standards, but frequently covers such areas as contamination from dust and metal particulate, crushed product from mechanical slitters, edge delamination, and appearance. Slit edges often govern product performance. In a surprisingly large number of cases, waterjets contribute substantially to product quality, performance, and appearance.

- Favorable Economics of Increasing Productivity of Existing Production Lines – In any given manufacturing situation, as product demand increases and surpasses existing capacity, manufacturers have the option of either increasing productivity levels of existing equipment through use of improved technologies, or adding more production lines. With the skyrocketing costs of energy and labor it is frequently more economical to improve existing equipment. As relates to slitting devices, this translates into cutting the existing product at higher speed. In many applications such as corrugated board, paper, disposable diapers and insulation, waterjets provide unlimited slitting speed.

- Use of Advanced Materials - Many new technically advanced materials have been introduced which cannot be successfully cut with conventional devices. The new advanced composites, typically Kevlar and graphite, as well as uncured ceramics, react poorly to the forces exerted and heat transferred by mechanical cutting devices. In these cases waterjets have successfully replaced standard slitters and routers. Typical of the problems created by mechanical cutting devices which are not present with waterjet slitters are:

1. Crushing/distorting of soft, uncured materials
2. Requirement for excessive trim.
3. Inflexibility for shape cutting
4. Inability to sever fluffy, non-woven products.
5. Hand finishing.
6. Excessive heat
7. Delamination or fracturing

2. System Integration: Most manufacturing firms are equipped solely for the purpose of producing the end product desired, e.g., diapers. Without the design and manufacturing capability necessary to produce the equipment and systems for proper use of waterjet slitting in the factory environment, it is impossible to promote volume sales. Flow Systems has developed a highly skilled engineering staff specializing in the design of systems for optimum industrial utilization of waterjet slitters.

3. Maintenance Cost/Reliability: For the most part, maintenance of waterjet cutting systems is limited to the high-pressure intensifier pump and sapphire orifice nozzles. Maintenance of waterjet slitter positioning systems is normally limited to equipment cleanliness. As an example and for the purposes of this paper, the author has selected a major corrugated board manufacturer's maintenance costs as typical of many waterjet slitting installations. The reason for this selection is: operating pressures are relatively high; multiple high-pressure pumps operate simultaneously; continuous run production environment is typical; and the product manufactured is highly price-sensitive thus ongoing maintenance costs are critical. The selected installation consists of 2 ea. single intensifier, 378,950 KPa (55,000 psi) pumping systems with a maximum slitter requirement of twelve 15 mm (.006") diameter nozzles running simultaneously. Table 1 below indicates the items required for maintenance, average life in hours, and cost per operating hour for this installation.

ITEM	AVERAGE LIFE (HOURS)	COST PER OPERATING HOUR
Nozzles	167	USD 0.239
Seals	380	0.656
Check Valves	1500	0.035
Seal Backup Rings	674	0.118
High-Pressure Cylinders	*	0.218
Pistons	*	0.218
AVERAGE HOURLY MAINTENANCE COST =USD		1.484

*No longer require normal maintenance.

TABLE 1 TYPICAL MAINTENANCE COSTS

While costs will vary at each installation depending upon operating pressure, average number of nozzles run simultaneously (flow rate), and water quality, $1.50/hr. maintenance cost is reasonably close approximation for most industrial installations, and is considered acceptable. Hourly costs will continue to decline as further product improvements are concluded and production volume increases.

In summary, Flow's waterjet cutting systems are being accepted in industry due to low maintenance costs, high levels of reliability, proper system integration, and declining prices.

INDUSTRIAL APPLICATIONS/INSTALLATIONS

High-pressure waterjets with appropriate positioning systems have been installed for slitting numerous materials. The following portion of this paper is dedicated to major industrial applications.

I. AEROSPACE -- advanced composites, plastics, gasket materials

The aerospace industry is unique in that not only must it cut newly developed materials such as Kevlar and NOMEX (DuPont's registered trademarks for aramid fibers), but it must also cut on various planes requiring multi-axis slitting systems. Waterjet slitters coupled with a variety of positioning systems are used extensively throughout the aerospace industry by both major manufacturers and subcontractors. Flow's "Composite Waterjet Cutting Facility" shown in Figure 6, encourages the use of multiple slitting devices from one central pumping station. This concept allows maximum system flexibility and return on investment.

The composite waterjet cutting facility for the aerospace industry is comprised of: 1) Waterouter™, 2) Universal WaterJet Cutting Machine, 3) Waternife™ robot, 4) Track-mounted Waterouter™, 5) Optical tracer X-Y Table, 6) Ultra-high pressure pumping system.

The primary competitive devices which waterjet slitters have replaced are high speed routers, reciprocating knives, diamond cutting tools, and lasers. The specific advantages in using waterjet slitters for applications to composite materials are:

1) zero dust; 2) no fuzzy edges; 3) no secondary finishing required; 4) no heat transfer; 5) no fiber tear-out/distortion; 6) no tool wear; 7) increased cutting speed; 8) system flexibility; 9) no tool loading; 10) use of light-weight low cost tooling; 11) omni-directional cutting capability; 12) clean bevel cuts; 13) no starting hole required for interior cuts; and 14) adaptability to multiple controllers from one central pumping system.

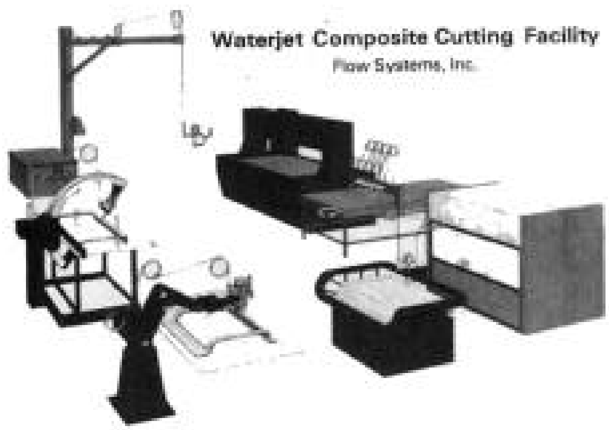

Figure 6. Composite Waterjet Cutting Facility

1. Waterouter™ Model 401. An overall view of this unique work station is shown in Figure 7 and a closeup view in Figure 8. It is used in conduction with an articulated boom manipulating system for hand-guided shape cutting and trimming applications. Free-floating and counterbalanced it is easily maneuverable in handling intricate parts. Either the cutting nozzle or waterjet catcher can be equipped with a wide range of guide pins which follow a template for shape control. The standard hand tool permits cutting of parts with up to 3.2 cm (1.25") in thickness with boom maximum reach of 4400 mm (174") and angular rotation of 195°.

2. The Universal Waterjet Cutting Machine. The Universal Waterjet Cutting Machine shown in Figure 9 is a stand-alone work station with uniquely flexible capabilities in cutting contour part shapes. The system has a removable material support table, adjustable catchers, and has capabilities for multi-axis adjustment. The entire system occupies an area 1067 mm (42") wide, 1676 mm (66") deep, and 1905 mm (75") high. The Universal Cutting Machine has the following general capabilities: 1) jet rotation +/- 65° off center positive through 130° included angle; 2) track angular pivot +/- 15°; 3) positive detent points at key dimensions. While the hand router affords slitting flexibility for large parts requiring minimum tolerance trimming, the Universal Cutting Machine offers low-cost, close tolerance slitting for smaller parts.

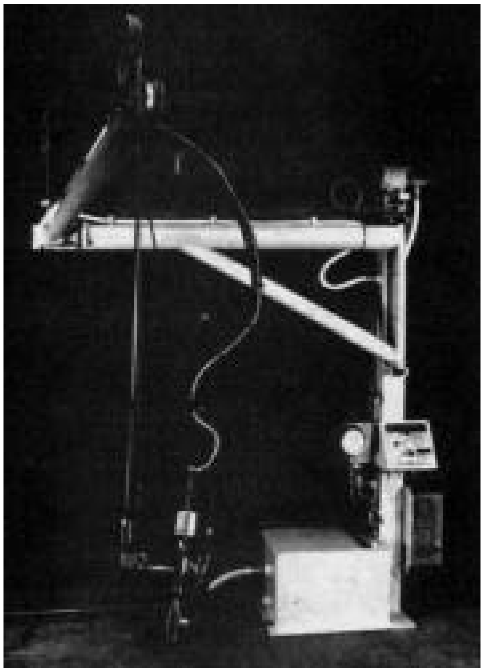

Figure 7. Articulated-800m WaterouterTM Hand Tool

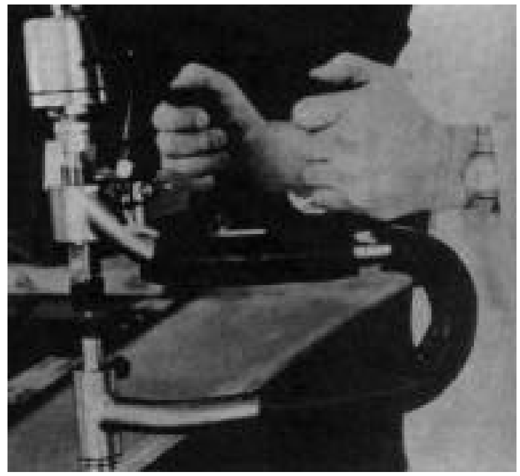

Figure 8. WaterouterTM Hand Tool

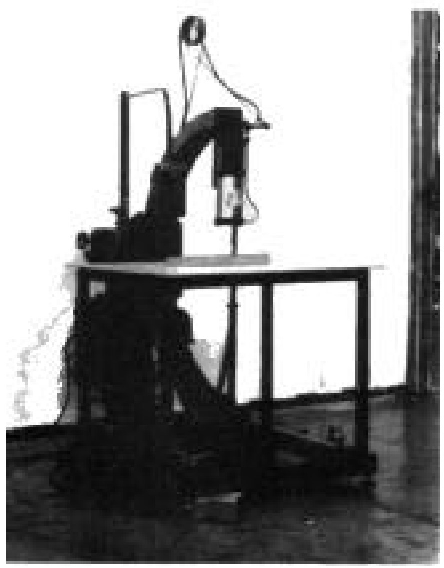

Figure 9. Universal Waterjet Cutting Machine.

3. Robotic Systems. Jetcutting equipment is readily integrated with continuous path,multi-axis robots. A combination of high-pressure stainless steel coils and swivels designed by Flow Systems provides the necessary flexibility for supplying high-pressure water to the cutting head. Robots can be used in conjunction with template guided cutting for maximum tool stability and cut quality. Compared to the WaterouterTM and Universal Cutting Machine, robotic waterjet systems are more expensive, offering close tolerance automatic cutting capability.

4. Track-Mounted Waterouter™ and Shape Cutting Systems. Track-mounted and shape cutting systems are used in the aerospace industry for cutting contour shapes--both single plane and multi-axis. While these systems are used in the aerospace industry in conjunction with waterjet slitters, they are also used in the automotive and shoe and garment industries and are explained in detail under those sections. Systems used in conjunction with waterjet slitters as described above are excellent examples of innovative design engineering directed toward proper systems integration.

II AUTOMOTIVE INDUSTRY – plastic, fiberglass, headliner material, upholstery

Most equipment developed for this industry is used for contour, multi-axis parts. As a result, automotive manufacturers primarily use the track-mounted Waterouter™ Shown in Figure 10 and computer or optical tracer controlled discussed under the industry. The track-mounted Waterouter™ is a low cost shape cutting tool for repetitive trimming of medium to large parts. It has been designed specifically for integration into automotive / truck production lines . The waterjet slitting nozzle coupled with the Instajet™ on/off valve is mounted together with an integral air motor on a pre-shaped thermoplastic tracks Track configuration and size are based on the part to be cut -- each track custom designed

The primary advantages of this system are as follows: increased slitting speeds multi axis cutting capability elimination of dusts ease of automations no material delamination system flexibility.

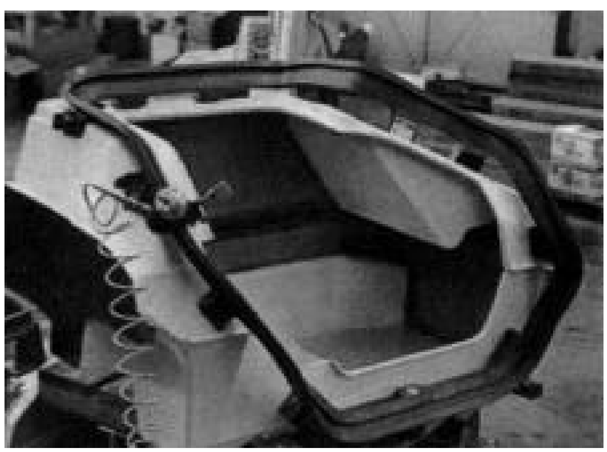

Figure 10. Track-mounted Waterouter™

III COMPOSITE PRODUCTS--multiple laminates of various materials.

Products combining multiple materials, each with unique properties present challenging cutting problems. Mechanical cutting devices are normally selected to cut a given materials. When multiple materials need to be cut simultaneously it is extremely difficult to obtain the proper tool. Waterjet slitters however have the unique capability of cutting all materials in like fashion with operating pressure and cutting speeds based on the most difficult material to be cut.

As an examples the waterjet slitter system shown in Figure 11 is for the cutting of foamy kraft paper / foil laminate. The end uses for the product are shipping containers, container dividers , appliance insulation , and automotive headliners.

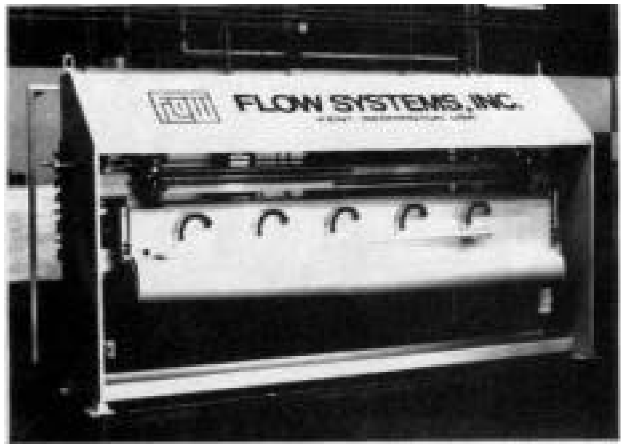

Figure 11 Composite Slitter System

The major advantages are: ability to cut multilayered laminates, no delamination, no dust, increased slitting speeds, reduced edge trim. The composite slitter system shown above is equipped for 4 waterjet slitters. Each slitter position is equipped with a backup nozzle. Maximum composite material thickness is 20.32 mm (0.8") and maximum material width 2.64 m (104"). Manually positioned slitters have setup accuracies of +/- 79 mm (+/- 0.031") slit to slit. The system has a web adjustment capability of +/- 76.2 mm (+/-3"). One single intensifier pump is required.

IV BUILDING MATERIALS—fiberglass and mineral wool insulation

Due to escalating energy costs, insulation production lines are running at maximum capacity. High productivity and minimum waste are essential prerequisites for equipment purchases. Waterjet slitters meet these objectives through:

1) elimination of material crush providing accurate dimensions;
2) reducedl kerf width, as well as;
3) elimination of air borne dust and dust collection systems.

The Model 305 fiberglass slitter system shown in Figure 12 is uniquely equipped with 2 independently adjustable catwalks on both up and down stream sides of the slitter. Two banks of slitter carriages are provided for rapid order change. While one bank of slitters is in operations the second bank is prepositioned for the next order.

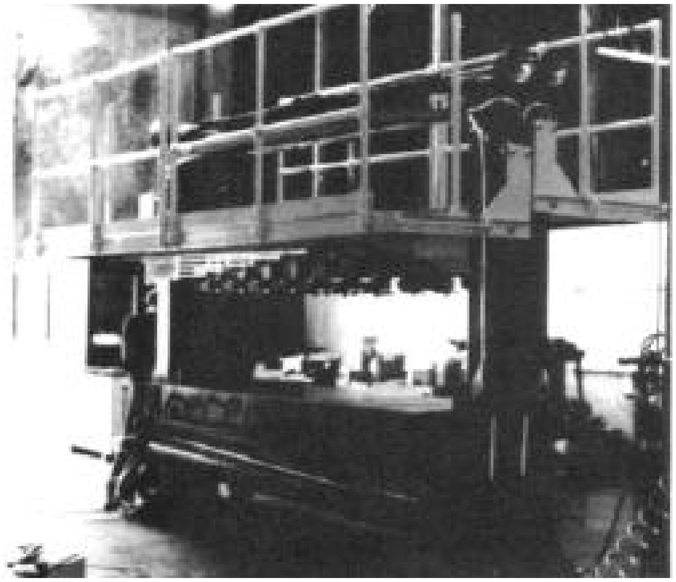

Figure 12. Model 305 Double Bank Fiberglass Slitter System

Each bank is equipped with 7 slitting stations. Positioning of the carriages is manual utilizing dial indicators with position accuracy of +/- 0.813 mm (+ 0.032"). Maximum fiberglass web width is 3048 mm (120") with pack height of 300 mm (11.82") maximum. Fiberglass insulation lines are equipped with 275,600 kpa (40,000 psi) pumps.

V. PACKAGING INDUSTRY--corrugated boxboard

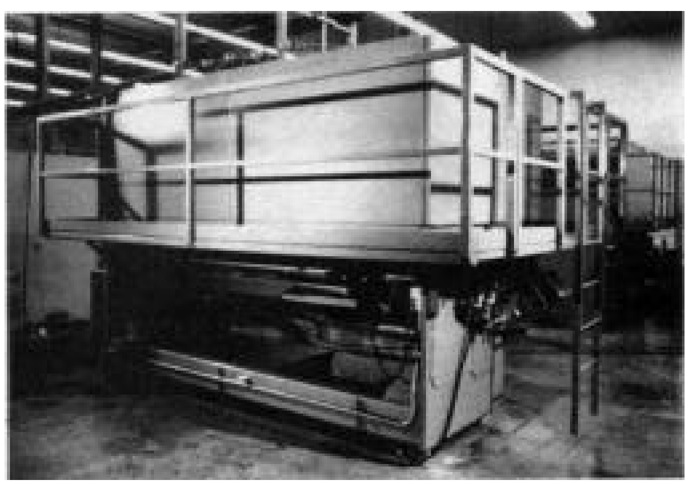

Figure 13. Computerized Slitter/Scorer

Due to the fact that a typical corrugator runs at relatively high speed and experiences frequent order changes, automatic slitter positioning or rapid order change is essential for corrugator automation. Consisting of 1 or more fluted medium materials and 2 or more liner or outside materials, the corrugated boxboard is a composite and difficult to cut with mechanical knives. Mechanical knives crush edges, and create dust detrimental to downstream printing. In addition, as line speed increases the mechanical knives begin to delaminate the product, thus limiting productivity. Waterjets offer the following benefits: elimination of edge crush resulting in high-strength board; elimination of slitter dust; improved printing quality and reduced printing roll maintenance; up to 100% increase in line speed on heavy weight corrugated board; reduced hotplate warp due to' increased line speed; reduced edge trim.

Waterjets applied to corrugated production lines have been used in 3 ways:

1) fully computerized waterjet slitter/scorers, Figure 13;
2) retrofit of automatic slitter/scorers, Figure 14;
3) slitters operating in conjunction with standard scoring equipment, similar to composite slitters.

Both slitter/scorers and slitters are equipped for up to 7 nozzles, web widths up to 246.4 cm (97") and maximum line speeds in excess of 200 m/min. (700 fpm). Two single or dual intensifier pumps are used. The number of pumps is determined by the weight of corrugated board to be cut and maximum line speeds.

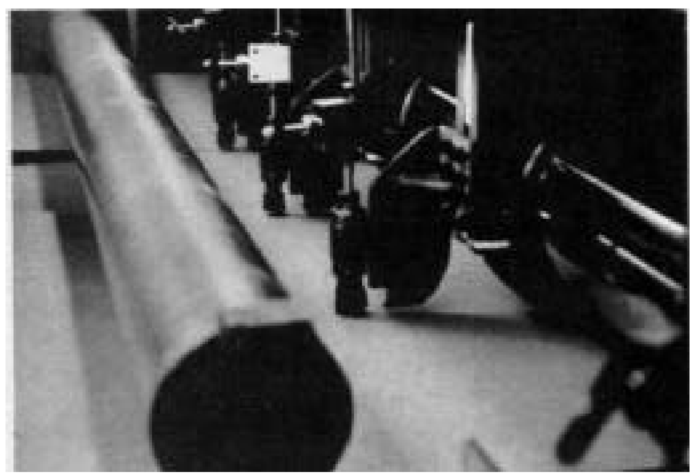

Figure 14. Retrofit Slitter / Scorer

VI. ELECTRONICS INDUSTRY--printed circuit boards, cable strippers

Several waterjet applications have been established in the electronics industry, including printed circuit cards. However, a rather interesting application is the removal of insulation from large diameter cable. Shown in Figure 15 the Cable Insulation Stripper Model 402 will accommodate cable sizes from 7.5 mm (0.295") to 46 mm (1.815"), with maximum cut length of 0-127 mm (0-5"). Electrical cable is fed through a cable guide sleeve at the front of the machine. Coupled with the Instajet™ on/off valve, the nozzle cuts the circumference of the insulation. When the cable is withdrawn, the insulation is slit lengthwise for easy manual removal. Compact in size, the Model 402 stripper measures 1220 mm (48") wide, 1245 mm (49") high, and 660 mm (26") deep. The system weighs 68 kg (150 lbs.) and is easily relocated via fork truck. The system can produce a maximum of 6 cuts per minute with a cutting speed of 4320°/minute.

The waterjet cable stripper cuts through the insulation material without damaging the conductor. Additional benefits include: 1) elimination of airborne particulate; 2) insulation remains in place as protection; 3) improved safety, and 4) increased productivity.

Figure 15. Cable Insulation Stripper (Model 402)

VII. PAPER PRODUCTS--paperboard, magazine stock, tissue, clay-coated board

As a rule of thumb, the introduction of moisture to paper in the production process is unacceptable. To alleviate fears of water absorption, production tests have been conducted slitting tissue, recycled and clay-coated paperboard, magazine stock, IBM cardstock, coffee filter media paper, and newsprint. None of the tests showed moisture absorption. The concept of using cohesive high-velocity waterjets to slit paper without moisture absorption is shown in Figure 16. In considering material thickness, material lines speed, jet diameter and velocity, it is virtually impossible for moisture to be absorbed into the paper product. Paper slitting requires small diameter nozzles and low operating pressure, thus providing a high degree of reliability and low operating costs. Waterjet slitters are applied to paper slitting in various forms. Installations vary from simple edge trim slitters to full conventional slitter retrofits (replacement of rotary slitters on conventional reminders). Full slitter retrofits closely resemble slitters used for packaging materials. The advantages in using waterjet slitters for paper products are as follows: elimination of dust; improved edge quality (see Figure 17); improved lithographic press uptime; elimination of web breaks caused by mechanical knives; elimination of slitter blade maintenance; accurate consistent positioning; ease of setup; reduced edge trim; application to fragile paper materials without product damage.

VIII. <u>SHOE AND GARMENT INDUSTRY--natural and synthentic fabrics, leather</u>

As one of the earliest major industrial categories to which waterjet slitters were applied, this application has grown steadily utilizing systems produced both by Flow and major industry OEM's. This industry uses almost exclusively Waternife™ X-Y shape cutting systems. Because of OEM involvement, at least 3 major design concepts for single plane contour cutting have evolved. For purposes of this paper the Flow system will be discussed.

The Waternife™ X-Y shape cutting system is designed to cut two-dimensional patterns in sheet materials. The system shown in Figure 18 is equipped with 3 waterjet slitting nozzles, all of which produce the same configuration part simultaneously. In operation, a pattern is placed on a stationary table aligned with the X-Y table. The photo-electric control system, which is attached to and moves longitudinally along the bridge beam, traces the pattern on the stationary table and thus directs the waterjets to cut out the same pattern in the material on the X-Y table. The waterjets are attached to the bridge of the optical tracer system. The bridge extends over the X-Y table. The bridge rides along rails to move longitudinally up and down the X-Y table (in the X direction), and the waterjets move transversely across the bridge (in the Y direction). The number of slitters which can be powered simultaneously, and the size of the X-Y cutting table is variable based on production required and purchase justification.

The major advantage associated with this system is material savings. Approximately 15% material savings is achieved due to edge to edge part nesting. Additional benefits include the ability to cut sharp inside corners and slitting quality.

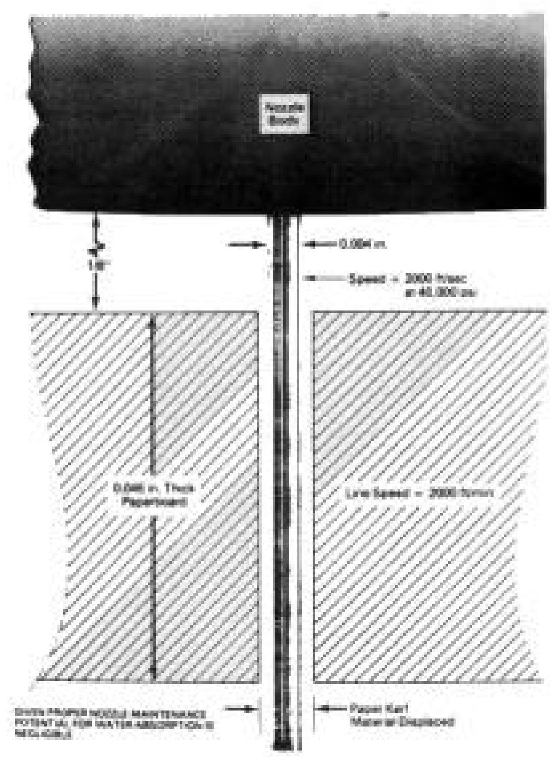

Figure 16. 1.17mm (.046”) paperboard cut with the waterjet (concept).

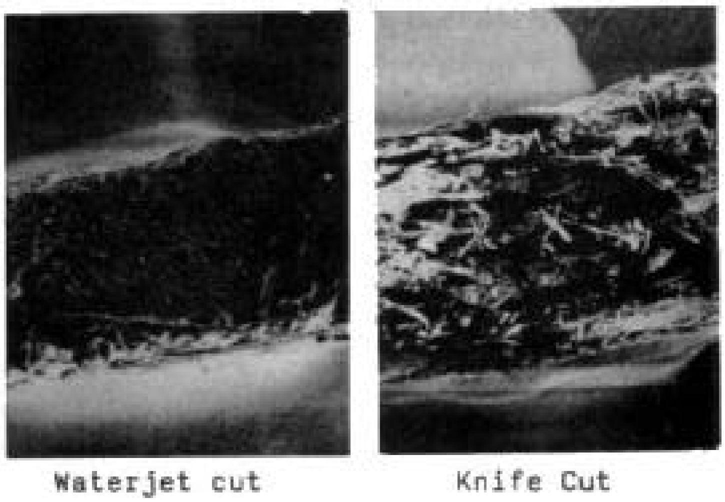

Figure 17. Exploded view of 1.17mm (.046”) paperboard

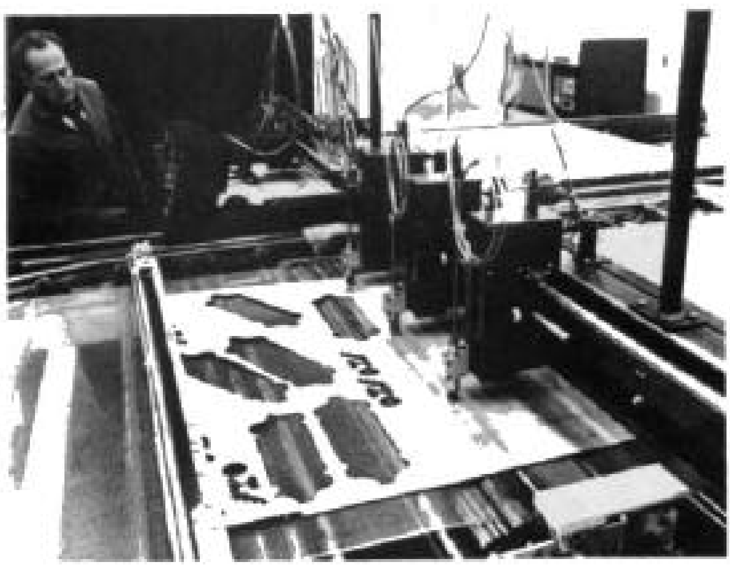

Figure 18. Flow X-Y Shape Cutting System

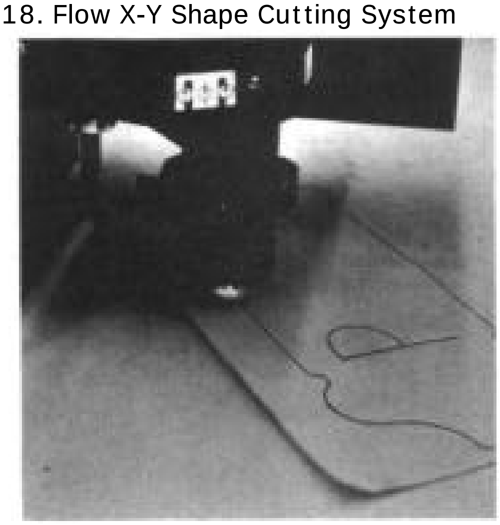

Figure 19. Photo-electric Control System

CONCLUSION

As can be seen from the wide variety of current industrial uses, waterjet slitting has been widely accepted. Meeting the stringent reliability and maintenance demands of industry has been the key to the evolution of waterjet cutting technology. It is safe to assume that only the most obvious markets for jet slitting have been penetrated. Future growth potential for the technology is outstanding.

SOME INDUSTRIAL APPLICATIONS OF CAVIJET® CAVITATING FLUID JETS

Andrew F. Conn, Virgil E. Johnson, Jr.,
William T. Lindenmuth, and Gary S. Frederick

HYDRONAUTICS, Incorporated
7210 Pindell School Road
Laurel, Maryland 20810

ABSTRACT

Over the past few years, cavitating fluid jets have received considerable attention, primarily with laboratory experiments, to understand their behavior and to determine the feasibility of using such jets in a variety of situations. Recently, these testing and evaluation efforts have proven that certain applications of the CAVIJET® cavitating fluid jet method are indeed commercially attractive.

Several of these developmental projects are described, including a brief description of the R&D effort in each case and the field trials which established the utility of cavitating jets for that purpose. Applications include: cleaning paint and rust from metal surfaces; underwater removal of marine fouling; removing high explosives from munitions; and augmenting the action of deep-hole mechanical bits used to drill for petroleum or geothermal energy resources.

INTRODUCTION

The concept of using cavitating fluid jets to enhance the erosive action of a relatively low velocity fluid stream has been given considerable exposure over the past few years (see, for instance, Refs. 1-2). Readers desiring detail beyond the following brief review are urged to explore these earlier publications.

The CAVIJET® Cavitating Fluid Jet Method

A CAVIJET cavitating fluid jet issues from one of several types of patented nozzles, each designed to stimulate the growth of undissolved gas nuclei which exist in any fluid such as water, oil, or drilling mud. Once caused to grow within and while exiting the nozzle, the cavitation bubbles are carried by the jet, until nearing the surface to be cleaned or cut. The high pressure stagnation region causes the bubbles to collapse on or near that surface, creating concentrated, extremely high stresses over many small areas. It is this very localized amplification of pressure by the mechanism of cavity implosion which provides the CAVIJET with the enhanced rates of cutting and cleaning that are observed relative to comparable jets utilizing only the stagnation pressure.

This advantage of cavitating jets is particularly seen with materials prone to cracking such as crustaceous marine-life, brittle paint, cast explosives, and rocks. In such materials, the focused and myriad attack of cavitation stress impulses causes rapid fracturing which greatly enhances the erosive process. Conversely, materials lacking such brittleness, or relatively smooth and flaw-free substances such as elastomers and wrought metals, are substantially more difficult to erode by cavitation. This natural selectivity of the cavitation erosion mechanism makes it possible to clean many surfaces without damage to an underlying substrate.

Various CAVIJET nozzle configurations have been developed to achieve optimum results in particular applications and modes of operation. For in-air cutting or cleaning, a blunt "center-body" may be inserted in the nozzle orifice to separate the flow and induce bubble growth. "Turning vanes" (actually stators) to spin the flow and induce a low-pressure vortex region are often effective for underwater applications. For some situations, a "plain" CAVIJET nozzle, utilizing only the basic nozzle geometry, is satisfactory. A new category of CAVIJETS, now under development for submerged operation, are designed to passively pulse the jet. The particular CAVIJET configuration(s) used for each of the applications described here will be cited during the discussion of that application.

The HYDRONAUTICS CAVIJET® Test and Evaluation Facilities

The various laboratory studies described below were conducted within the several facilities established at HYDRONAUTICS for both feasibility and developmental activities. The primary components of each facility include a pump, reservoirs to recover and store the working fluid, suitable filters, controls and gages for pressure and temperature, flow measuring devices, and a test chamber. Although water has been used in most of our work, studies have been performed with water-based drilling mud.

The largest chamber, 1.8 m long, 1.5 m wide, and 1.8 m high can be used for tests either in air or on submerged materials. A hydraulic translator allows the jet to be translated at any velocity up to 1.2 m/s across the material being eroded. A high pressure cell permits testing at simulated depths. Rock cubes, 15.2 cm on a side, can be eroded in either a stationary or slot-cutting mode in this cell, with ambient pressures up to 20.7 MPa (3,000 psi). The rocks can be rotated up to 66 rpm in the cell by means of a variable-speed motor and gearbox set.

The pumps used in these facilities are all of positive-displacement design. Driven by a 100 hp motor is a 303 l/m (80 gpm) capacity triplex, with a maximum pressure rating of 15.2 MPa (2,200 psi). A diesel-driven, portable quintuples, with various sets of plungers, allows a range of flow and pressure combinations in any pairing within the 112 kw (150 hp) power-envelope from 341 l/m (90 gpm) at 17.2 MPa (2,500 psi) to 76 l/m (20 gpm) at 68.9 MPa (10,000 psi). Another testing and demonstration facility, with a 3.7 kw (5 hp) triplex, delivers 19 f/m (5 gpm) at 6.9 MPa (1,000 psi) for small-scale studies and demonstrations.

CLEANING PAINT AND RUST FROM METAL SURFACES

Pollution, noise, slow rates of cleaning, and operator fatigue are factors which have caused the users of either sand-blasters or mechanical tools such as grinders or chipping hammers to seek new ways to prepare metal for repainting. Prototype CAVIJET cavitating jet hand-held tools, recently developed, have alleviated many of these problems, but new questions relating to water recycling remain to be answered before final system assessments can be made. The program described here was supported by the U.S. Navy[1], in an effort to improve upon the typically poor preparation of ship bilges for repainting. Further details are given in the report for this study (Ref. 3).

[1] Under Naval Ship Systems Engineering Station (NAVSSES) Contract No. NOO140-79-C-1751.

Laboratory Tests

A number of steel panels with the flaking paint and rust typifying a bilge surface in need of repainting were used to verify our laboratory results. However, much of this work was done on a "simulated bilge surface" consisting of spackling compound covered by an epoxy based paint. This simulant had an erosivity less than the real bilge, but had the attribute of giving reliable, reproducible results not achieved on an actual deteriorated panel.

The variables included nozzle orifice diameter, standoff, nozzle pressure, and translation rate. Tests were made in air, in our large chamber, using single, straight line passes, with jet impingement perpendicular to the panel. Typical results are shown in Figs. 1 and 2 for the three, centerbody CAVIJET nozzles used; nozzle orifices were: 1.2, 2.2, and 2.7 mm.

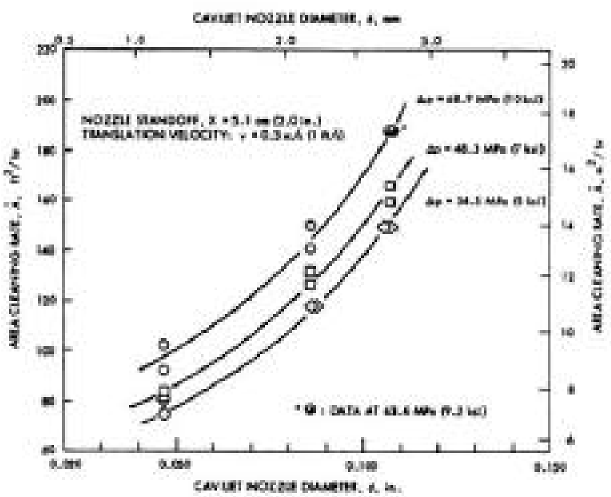

Fig. 1 – Area cleaning rate for removing laboratory simulant of bilge surface

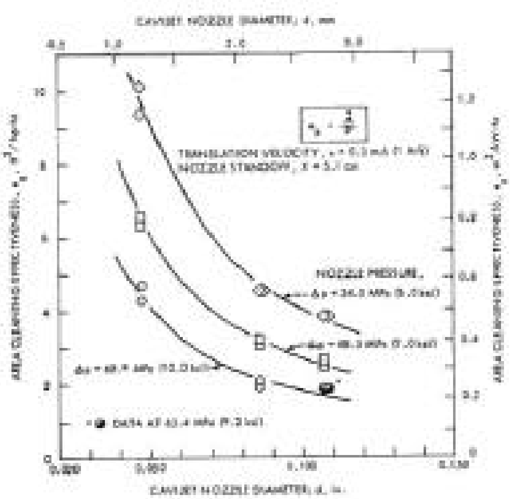

Fig. 2 - Area cleaning effectiveness for removing laboratory simulant of bilge surface

These results show that, although the largest nozzle operating at the highest pressure provided the fastest rate of cleaning, the most energy efficient cleaning (Fig. 2) was with the smallest nozzle, lowest pressure combination.

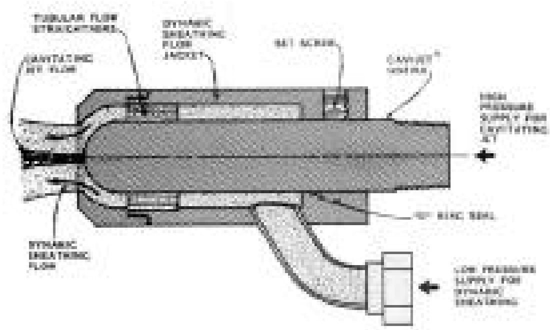

Fig. 3 - Experimental CAVIJET® dynamic sheathing design

A technique, known as "dynamic sheathing," was also used to increase the cleaning rates. Using the prototype shown in Fig. 3, a flow of low velocity water was introduced around the cavitating jet, increasing the cleaned path width by about 50 percent over the unsheathed jet in air.

Field Trials

A portion of the bilge under the No. 3 machinery space in the aircraft carrier USS AMERICA (CV-66) was used for our trials. The prototype tool for these tests is shown in Fig. 4. Quick-disconnects were used to allow easy changes of nozzles or barrel lengths. Although the field trends are comparable to those from the lab tests, substantially lower rates were achieved (Table 1).

Fig. 4 - Prototype CAVIJET® tool for paint and rust removal

Analyses of the results indicate that problems of overcoming thrust and loss of visibility due to splashback in the restricted bilge spaces were the main contributors to these differences between the automated lab device and the hand-held field tool.

Material		Laboratory: simulant	Field: actual bilge surface
Maximum Cleaning Rate	Rates	17.7 m^2/hr (190 ft^2/hr)	4.3 m^2/hr (46 ft^2/hr)
	Operating Parameters	Nozzle diameter: d = 2.7 mm (0.107 in.) Nozzle pressure: Δp = 68.9 MPa (10,000 psi)	d = 2.2 mm (0.086 in.) Δp = 68.9 MPa (10,000 psi)
Maximum Area Cleaning Effectiveness	Effectiveness	1.2 m^2/kWh (9.7 ft^2/hp-hr)	0.2 m^2/kWh (1.5 ft^2/hp-hr)
	Operating Parameters	Nozzle diameter: 1.2 mm (0.047 in.) Nozzle pressure: 34.5 MPa (5,000 psi)	

TABLE 1 CLEANING PAINT AND RUST—COMPARISON OF LABORATORY AND FIELD RESULTS

A tool, as shown in Fig. 5,perhaps affixed with splash deflectors, should provide further improvements in cleaning rates. The prototype CAVIJET tool achieved cleaning rates over ten times faster, however, than conventional means such as chipping hammers and scrapers. Tool improvements, to further compact and lighten the gun, are planned.

Fig. 5 – Artist’s concept of advanced design CAVIJET® surface preparation tool

REMOVAL OF MARINE FOULING

Increasing costs of fuel and the grit used to blast fouling organisms from hulls, propellers, and other appendages, have motivated searches for new ways to clean commercial and Naval ships - both in dry dock and underwater. Severe fouling due to long waits between missions, particularly in warmer waters, has made underwater cleaning of U.S. Navy ships a standard procedure. New CAVIJET diver-held tools, now officially "Approved for Navy Use" (ANU), are available as a consequence of an extensive laboratory and field developmental program.[2]

Laboratory Tests

Using panels heavily fouled by barnacles and other encrusting organisms, the feasibility of using CAVIJET nozzles was established (4). Cleaning rates for single and multiple nozzles were measured, using the single pass cleaning mode described above. Tests were made in air, submerged, and with "dynamic sheathing." The results showed that cavitating jets, with no additives, could achieve dry dock cleaning rates better than current dry sandsweeping, and at substantially lower costs. For instance, a single operator can achieve about 93 m^2/hr (1,000 ft^2/hr) at a grit cost of over $30 per 100 m^2 (1975-prices) (5). A six-nozzle array of 3-mm, plain CAVIJET nozzles completely removed heavy fouling from the laboratory panels at 167 m^2/hr (1,800 ft^2/hr). Operating at 13.8 MPa (2,000 psi) and 288 l/m (76 gpm), these nozzles consumed a total of 66.3 kW, for a power cost(at 5¢/kWh) of about $2.00 per 100 m^2 of cleaned area. However, the thrust from such a multi-nozzle array precludes the use of hand-held tools. A device, as suggested in Fig. 6, is needed to achieve practical dry dock hull cleaning.

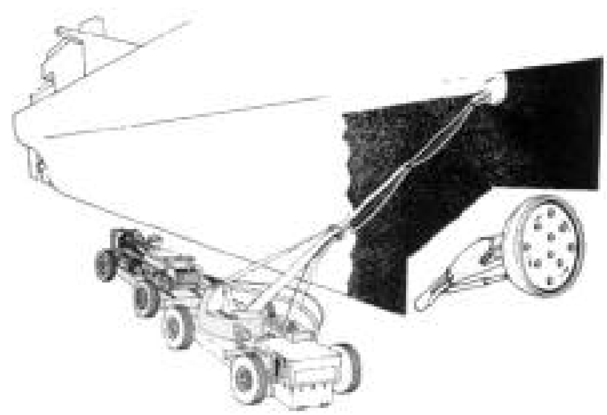

Fig. 6 - Artist's concept of CAVIJET® hull cleaner for dry dock use

Field Trials

To examine whether a multi-nozzle array could perform effectively under dry dock conditions, on actual ship hulls, a six-nozzle cleaning head (Fig. 7) was assembled, and mounted onto a hydraulically-actuated test frame (Fig. 8). This system allowed controlled rates of translation, up to 0.91 m/s, and cleaning rates up to 502 m2/hr (5,400 ft2/hr) were achieved at 13.8 MPa (2,000 psi). The field cleaning was three times faster than our laboratory results because of the difference in surfaces being cleaned. The softer "bottom paint" on the ship hulls is much easier to erode than the highly resistant epoxy paint on the lab panels. Since a few mm of paint are removed during cleaning, the higher rates could easily be achieved.

---

[2] Supported in part by the U.S. Maritime Administration under Contract No. 7-38001, and through NMRC/Todd P.O. No. RT-3700. The diver-held tools were developed by SEACO Inc., Kailua, Hawaii, under a license agreement.

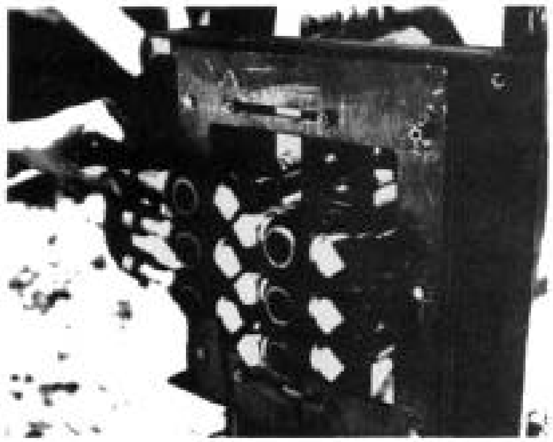

Fig. 7 - Six-nozzle CAVIJET® hull cleaning head with dynamic sheathing

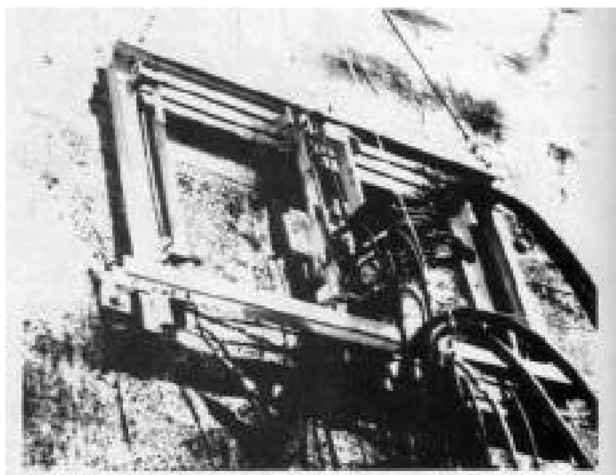

Fig. 8 - Test frame mounted on ship hull at Maryland Shipbuilding and Dry Dock Company

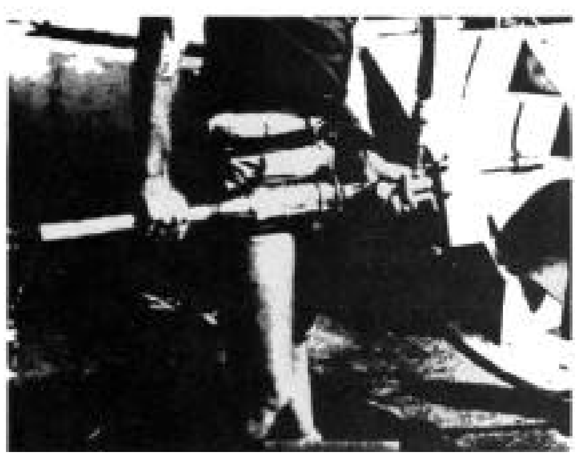

Fig. 9 - Thrust-compensated CAVIJET® tool for underwater cleaning

Fouling Category	Cleaning Rates[a] m^2/min (ft^2/min)
Light: slime, film	0.74 (8)
Moderate: grass, heavy film	0.56 (6)
Heavy: tubeworms, barnacles	0.19 (2)
Composite: all of the above	0.09 (1)

a Average times based on field experience. Factors influencing rates include diver experience, water clarity, surface condition, and degree of fouling.

TABLE 2 UNDERWATER BARE METAL CLEANING WITH CAVIJET2D DIVER-HELD TOOLS

NOZZLE: Plain CAVIJET, 2.7 mm orifice
PRESSURE: 20.7 MPa (3.000 psi)
FLOW: 83 ℓ/m (22 gym)

The development of thrust-compensated diver tools (an early version is shown in Fig. 9), was fostered by the U.S. Navy's need for more efficient cleaning of areas not reachable by the large multi-brush systems used to clean hull surfaces underwater. During a series of cleaning contracts (the propellers, sea chests, and other difficult to reach components of over 50 Navy ships and submarines have now been cleaned), SEACO divers made suggestions related to handling, controls, and safety, which eventually led to the ANU-systems now being leased for use by Navy divers. Typical cleaning rates for these CAVIJET-tools are summarized in Table 2 (Ref. 6).

REMOVING HIGH EXPLOSIVES FROM MUNITIONS

Either a finite shelf-life, obsolescence, or the inevitable rejections due to flaws in manufacture have caused large stockpiles of unwanted munitions of every shape and size to grow in virtually every industrialized nation. The solution, in the days of cheap energy, was to use steam or hot water to melt out high explosives (HE) such as TNT and Composition B (an RDX-based HE compound). With melt-out energy costs becoming prohibitive, the possibility of using high pressure water jets was explored by the U.S. Army (7).

The washout facility developed at the Iowa Army Ammunition Plant (IAAP) was found marginally capable of removing the HE, although a follow-up steam rinse was often required. Other drawbacks in their system, however, made it impractical for production operation. These included: rapid nozzle erosion (with a 68.9 MPa (10,000 psi) operating pressure); no means to recirculate the water—this severely burdened the effluent processing facility; no reclamation of explosives for reuse; and, most debilitating, a problem of foam formation which required men in hip-boots to shovel out large holding tanks—this halted the use of their facility.

<u>Laboratory Tests</u>

A feasibility study with cavitating jets was begun[3], seeking a better way to remove cast HE from munitions, hopefully using less energy than the melt-out and high-pressure jet methods, and alleviating the problems listed above. The objectives were:

[3] Supported by the U.S. Army Research & Develoment Command, under ARRADCOM Contract No DAAK10-77-C-0075. Ref. 8 is the report for this contract.

first, to see if cavitating jets could safely cut explosives and, then, whether practical rates of cutting could be achieved.

The safety tests were made in a concrete-lined bunker at the Hazards Research Corporation (HRC) in Denville, New Jersey. HRC coordinated these tests and performed hazards analyses of the results. Over 200 total runs were made, at nozzle pressures ranging from 13.8 to 68.9 MPa (2,000 to 10,000 psi). Since anticipated operating pressures were only about 27.6 MPa (4,000 psi), many tests were at substantial overpressures. The specimens were cast blocks of TNT and Composition B. each 10 by 10 by 2.5 cm, placed in a chamber that fully submerged both the HE and CAVIJET nozzle. Additional tests were run on two Composition B filled 105-mm shells. No detonations occurred in any tests. The hazards analyses provided probabilities of safety, at the 95 percent confidence level, of 95.2 percent for TNT and 97.4 percent for Composition B. These percentages are related to the number of tests; with no detonations, it requires about 200 tests with each HE to achieve the 98.5 percent probability of safety recommended by Army regulations. However, the assurance of safety was sufficient to continue the project.

To assess the system and operating parameters for a full-scale cavitating jet explosive removal system, tests were conducted in the HYDRONAUTICS facilities, using an inert material which approximated the erosive response of cast HE. This inert simulant was made by adding 60 percent sand by weight to standard inert filler E (Type II), to create a substance with the desired erosivity. In our laboratory tests with the simulant cylindrical specimens were cast, and then eroded under conditions replicating the actual IAAP mode of operation. The specimens were rotated while CAVIJET nozzles, of various sizes and angles of attack, were moved linearly into them.

The laboratory results suggested that a CAVIJET cutting head, containing three nozzles with orifice diameters in the range 2.5 to 3.8 mm, should be cost and energy effective—in comparison to the melt-out and high pressure washout methods. The first phase estimate of 1.82 minutes to clean a 155-mm shell containing 71 N (16 lb) of Composition B. at an energy consumption of 2.9 kWh per shell, was actually bettered during the later field trials with live warheads.

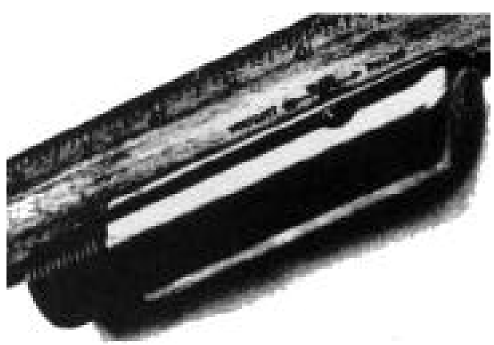

Fig. 10 - Three-nozzle CAVIJETS explosive cutting head (third nozzle not visible in this view)

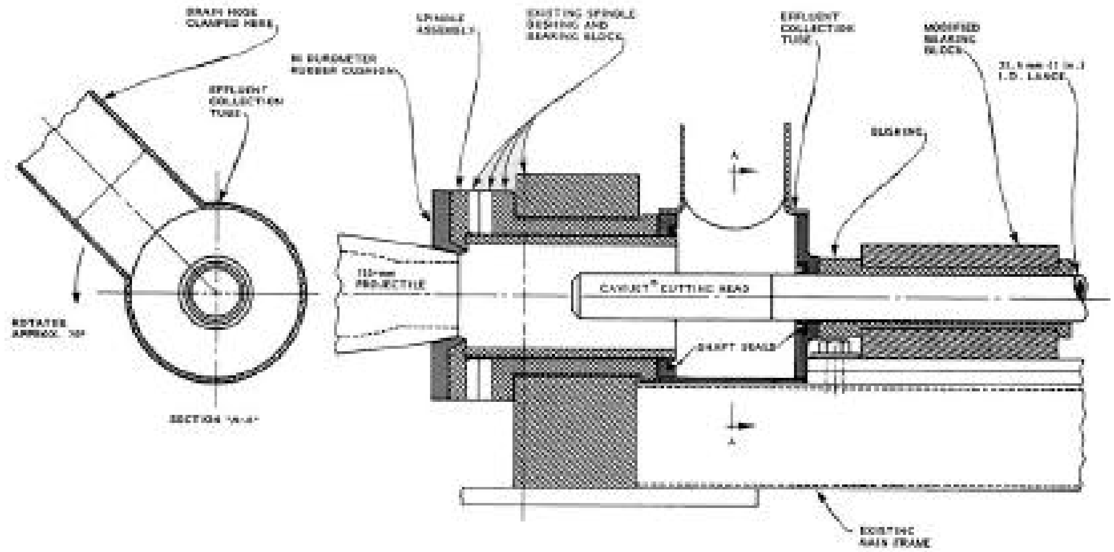

Fig. 11 - Components of prototype CAVIJET® explosive removal facility at I AAP

Field Trials

These trials were performed by retrofitting the washout facility at IAAP, making it compatible with CAVIJET cutting heads[4]. Based on the laboratory results, three preliminary, nonoptimized heads were made, containing either two, three, or four "plain" CAVIJET nozzles. The three-nozzle head, with three 3-mm nozzles, is shown in Fig. 10.

This retrofit included changing the fluid end of the IAAP pump to provide 27.6 MPa (4,000 psi) at 208 l/m (55 gpm) instead of the previous 68.9 MPa (10,000 psi) at 83 l/m (22 gpm). Other changes involved a larger hose and lance, and an improved means to route the effluent away from the shell. By redesigning the components controlling flow of the explosive-laden water (Fig. 11), it was possible to prevent air-entrainment during the erosive process. Thus, by keeping the shell fully flooded during the cleanout, the problem of durable foam generation was alleviated. Only a teaspoonful of such foam—a mixture of water, air, and very fine particles—was created per warhead.

After preliminary runs with nine inert filled shells to establish operating procedures, a total of 14 warheads, filled with either TNT or Composition B were cleaned. All HE tests were run remotely, utilizing closed-circuit TV and a duplicate set of controls. Typical operating values were 7.6 mm/s for the lance translation and 60 to 100 rpm for the shell rotation. No detonations occurred during these trials.

---

[4] Supported by ARRADCOM, through their Contract DAAA09-78-C-3008 with the Mason & Hanger—Silas Mason Co., Inc. Our work was under M&H Purchase Order No. 12606.

Operational Parameters				
Item	Hot Water Washout and Recovery	Melt and [illegible]	High Pressure Washout, plus Steam Drying	Cavitating Jet Washout, plus Steam Drying
Time to washout, minutes	7.50	7.50	2.10	1.43
Pump pressure, MPa (psi)	—	—	68.9 (10,000)	33 (4,800)
Water flow, l/m (gpm)	—	—	83 (22)	208 (55)
Pump power, kW	—	—	96	112
Washout energy per shell, kWh	19.86	19.02	3.96	2.67
HE drying energy, per shell, kWh	—	—	4.05	4.49
Total energy per shell, kWh	19.86	19.02	8.01	7.16
Unit Cost Estimation				
Steam	$0.29	$0.29	$0.37	$0.07
Electricity	0.12	—	0.18	0.13
Water and Treatment	0.02	0.09	0.21	0.05
Labor	4.40	3.79	2.33	1.80
Pump Maintenance	—	—	0.28	0.07
Nozzle Replacement	—	—	0.02	0.03
Total	$4.83	$4.17	$3.39	$2.15
Annual Cost[b]	$181,000	$156,000	$125,000	$83,000

[a] For details of these energy and cost analyses, see Refs. 8 and 9.

[b] Based on a five percent reject rate on 750,000 155-mm M549 warheads per year at IAAP.

TABLE 3 COMPARISON OF METHODS FOR REMOVING COMPOSITION B EXPLOSIVE FROM 155-mm M549 WARHEADS[a]

As summarized in Table 3, the three-nozzle CAVIJET cutting head, operating at less than one-half the pressure of the earlier high-pressure system, cleaned the Composition B from 155-mm M549 warheads in 32 percent less time (Ref. 9). This represents a cost-savings per round of over $1.00, or over $42,000 savings per year for just this one type of warhead at IAAP.

Based on these results, it has been recommended that the next phase should be initiated, wherein components necessary for recirculating the water are introduced, and means to dry the explosive are tested. With optimization of the CAVIJET cutting head, and trials to establish the best combinations of lance feed and shell rotation rates, we estimate a goal of 1.0 minute to clean Composition B from 155-mm warheads can be achieved; the TNT may require about 1.2 minutes.

AUGMENTING DEEP-HOLE DRILL BITS

Over the past several years, the feasibility of using cavitating jets to augment the cutting action of mechanical drill bits has been demonstrated (10 to 13). Some highlights of this program[5] will be described and new field trial results presented. Our objective is to utilize existing rig pressures, typically less than 27.6 MPa (4,000 psi), with available drilling mud, for cavitating jets which would be mounted in either roller cone, diamond, or "PDC" (polycrystalline diamond cutter) bits. Optimization of the design of such deep-hole bits is now underway, and we are currently examining the use of new, resonating CAVIJET nozzle designs for this application (14).

---

[5] Supported in part by the U.S. Department of Energy, Division of Geothermal Energy, under Sandia Laboratories Contracts No. 07-7067, 13-5111 and 13-5129; also by NL/Hyealog, Houston, Texas, and HYDRONAUTICS, Incorporated.

Laboratory Tests of Nozzles

The ability of CAVIJET nozzles to cut rock under the elevated ambient pressures, p , found in deep wells (over 300 m) was examined in the high pressure cell (HPC) at HYDRONAUTICS and the Well Bore Simulator at the Drilling Research Laboratory (DRL) in Salt Lake City, Utah. Results, as in Fig. 12, with both water and drilling mud, showed that "plain" CAVIJET nozzles would erode rocks at substantial depths; mud did not impair the cavitation; and the CAVIJETS outperformed conventional nozzles. Erosion rates in Berea sandstone, Indiana limestone, Georgia gray granite, and Sierra white granite have been studied.

Other techniques to examine and improve submerged cavitating jet performance have included flow studies in air; in our HPC; and in water channels at UCSD[6] and HYDRONAUTICS. High speed photography has established the importance of the ring vortex structure (idealized in Fig. 13) on the erosiveness of submerged CAVIJETS. A new category of self-resonating CAVIJETS, now being developed, strengthen these ring vortices, which enhances the erosion intensity and increases the inception cavitation number, σ_i. Larger σ_i's, (where the operating cavitation number is: $\sigma \approx P_a/\Delta p$), increase the depth to which a CAVIJET is effective for any given nozzle pressure, Δp, and for a given operating value of σ, increase the erosion intensity.

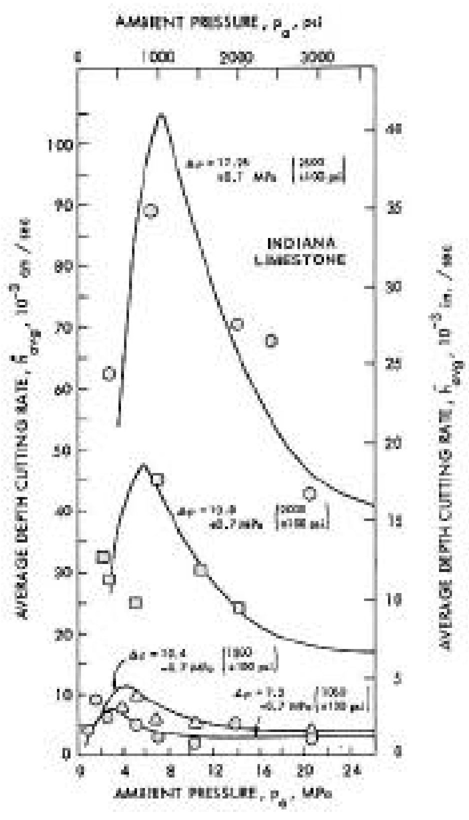

Fig. 12 - Typical results from stationary nozzle testing with mud; plain, 6.4 mm (0.25 in.) CAVIJETs nozzle; standoff: 1.6 cm (0.62 in.)

6 University of California, San Diego, by Dr. Albert T. Ellis.

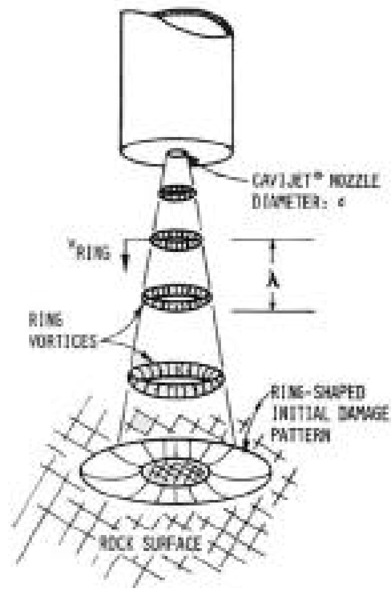

Fig. 13 - Ring vortices formed by submerged cavitating jets (based on ultra high speed photography by A. T. Ellis, UCSD)

Fig. 14 - Two-cone roller bit, 20 cm (7-7/8 in.) dia., with two, 6.4-mm CAVIJET® nozzles

Tests of CAVIJET-Augmented Bits

Preliminary drilling at DRL with a Smith two-cone bit (Fig. 14) was encouraging. Although the only tool modification involved reducing nozzle standoff from

3.8 to 1.6 cm, the CAVIJET-bits showed higher specific penetration rates (Fig. 15). The performance of roller bits has been shown to be nearly proportional to hydraulic power per unit area (15). Therefore, the abscissa in Fig. 15 is the rate of penetration (ROP) divided by the hydraulic power delivered by each pair of nozzles, to account for the 39 percent higher discharge of the conventional Smith Tool Company nozzles.

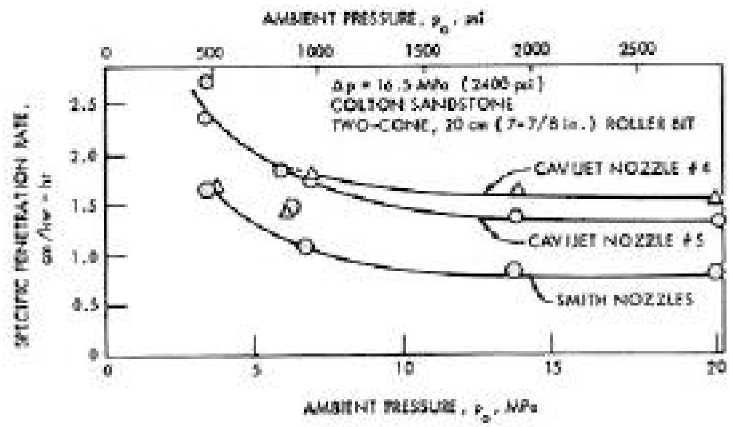

Fig. 15 - Comparison of specific penetration rates in DRL drill bit tests

The success of the laboratory tests caused our partners in this project, NL/Hyealog, to encourage a series of field trials by commercial rig operators with two-cone, extended-nozzle CAVIJET roller bits. Although proprietary, some results from these operators were recently released (16). These data (see Table 4) from wells in Canada and south Texas, show CAVIJET-augmented bits have produced ROP's from 43 to 200 percent faster than comparable, conventional bits drilling in the same holes. Although these are certainly encouraging results, much more data must be obtained before field performance can be predicted with confidence.

LOCATION: Canada; ROCK TYPE: shale; RPM: 50 to 70; WEIGHT ON BIT: 85 to 107 kN (19 to 24 x 10^3 lb)				
Bit No.	Bit Type/Nozzle Type	Distance Drilled, m	Rotating Time, hrs.	Penetration Rate (ROP), m/hr
7	Standard/Standard	101	28.5	3.5
8	Two-cone/CAVIJET	37	3.5	10.5
9	Two-cone/CAVIJET	115	11.0	10.5
10	Standard/Standard	210	36.0	5.8
LOCATION: Canada, ROCK TYPE: shale; RPM: 70 to 90; WEIGHT ON BIT: 36 to 72 kN (8 to 16 x 10^3 lb)				
19	Standard/Standard	89	34.8	2.56
20	Standard/Standard	95	35.8	2.66
21	Two-cone/CAVIJET	164	41.0	4.00
22	Two-cone/Standard	118	41.0	2.87
23	Standard/Standard	180	91.5	1.96
24	Two-cone/CAVIJET	124	35.0	3.54
25	Standard/Standard	89	33.8	2.63
26	Standard/Standard	90	30.5	2.95
LOCATION: South Texas[1]				
a	Standard/Standard	—	—	2.1[2]
b	Two-cone/CAVIJET	—	—	3.0[2]
[1] Additional data not available on this run. [2] Estimated values.				

TABLE 4 PRELIMINARY COMPARATIVE FIELD TRIALS OF CAVIJET6® AUGMENTED ROLLER CONE DRILL BITS

ACKNOWLEDGMENTS

Many individuals and organizations have contributed to the programs discussed here. The authors wish to thank the following representative few from each organization for their cooperation, assistance, and support:

ARRADCOM: E. A. Krajkowski, J. Santos; DRL: A. Black, J. Sandstrom; HRC: G. Petino, Jr.,; IAAP: J. Nemeth, J. Lestage; MARAD: W. L. Fink; Maryland Ship: R. G. Seitz; NAVSSES: R. J. DeLecce; NL/Hycalog: R. P. Radtke(now with Strata Bit Corp.), G. J. Giacchino, Jr.,; SANDIA Labs: S. G. Varnado (now with NL Petroleum Services), D. Glowka; SEACO: M. Rice, J. Harmon; SMITH Tool: W. Baker, J. Vincent; U.S. DOE/DGE: C. Carwile, M. Skalka.

REFERENCES

1. Proceedings, the 1st, 2nd, 3rd, 4th and 5th International Symposia on Jet Cutting Technology, sponsored by BHRA Fluid Engineering, Cranfield, England; held respectively: Coventry, England (April 1972), Cambridge, England (April 1974), Chicago, Illinois, USA (May 1976), Canterbury, England (April 1978), and Hannover, Germany (June 1980).
2. Proceedings, Conference on Erosion: Prevention and Useful Applications, sponsored by American Society for Testing and Materials, ASTM STP 664 (1979).
3. Conn, A. F., Cohen, S. H., and Frederick, G. S., "Evaluation of Bilge Cleaning with CAVIJETS Cavitating Jet Nozzles," HYDRONAUTICS, Incorporated Technical Report 8018-1 (December 1980).
4. Conn, A. F. and Rudy, S. L., "A Cavitating Water Jet for Fouling Removal," Proceedings of the Fourth International Congress on Marine Corrosion and Fouling, Juan-les-Pins, France (June 1976).
5. Conn, A. F. and Rudy, S. L., "Parameters for a Ship Hull Cleaning System Using the CAVIJET Cavitating Water Jet Method," HYDRONAUTICS, Incorporated Technical Report 7510-1 (July 1975).
6. Barr, M., "SEACO CAVIJET Diver Hardware Development Program, Status Report (July 1978 - June 1979)," SEACO Report No. 7907-2 (July 1979).
7. Grignon, L. R., "Development of a High Pressure Cold Water Technique for Removal of H.E. from Major Caliber Projectiles," (at the Iowa Army Ammunition Plant, Burlington, Iowa), Mason & Hanger- Silas Mason Co., Inc., Project No. 5765333 (7 July 1977).
8. Conn, A. P., Liu, H-L., Frederick, G. S., and Rudy, S. L., "Removal of Explosives from Projectiles Using CAVIJETS Cavitating Fluid Jets," HYDRONAUTICS, Incorporated Technical Report 7723-1, August 1979, (also ARRADCOM Contractor Report ARLCD-CR-79015, with E. A. Krajkowski).
9. Lindennuth, W. T., Conn, A. F., and Aymar, R. H., "Demonstration of Explosive Removal from Projectiles Using CAVIJETS Cavitating Fluid Jets," HYDRONAUTICS, Incorporated Technical Report 7984-1 (January 1981).
10. Conn, A. F. and Radtke, R. P., "Cavitating Bit Jets Promise Faster Drilling for Deep-Hole Operations," The Oil and Gas Journal pp. 129-146, (October 31, 1977), (also see: Trans. ASME, J. Pressure Vessel Tech., Vol. 100, pp. 52-59 (1978)).

11. Conn, A. F., Johnson, V. E., Jr., Liu, H-L., and Frederick, G. S., "Evaluation of CAVIJET® Cavitating Jets for Deep-Hole Rock Cutting," HYDRONAUTICS, Incorporated Technical Report 7821-1 (August 1979).
12. Conn, A. F. and Radtke, R. P., "Rock Cutting with Cavitating Jets Under Simulated Deep-Hole Conditions," Geothermal Resources Council Transactions, Proceedings 1979 Annual Meeting (September 1979).
13. Conn, A. F., "Elevated Ambient Pressure Effects on Rock Cutting by Cavitating Fluid Jets," Proceedings, Fifth Int'l. Conference on Erosion by Solid and Liquid Impact, pp. 68-1 to 68-8 (September 1979).
14. Johnson, V. E., Jr., Lindennuth, W. T., Conn, A. F., and Frederick, G. S., "Feasibility Study of TunedResonator Pulsating Cavitating Water Jet for Deep-Hole Drilling," HYDRONAUTICS, Incorporated Technical Report 8001-1 (August 1980).
15. Tibbitts, G. A., et al., "The Effects of Bit Hydraulics on Full-Scale Laboratory Drilled Shale," Society of Petroleum Engineers of AIME, Preprint No. SPE 8439, presented at the 54th Annual SPE Fall Meeting, Las Vegas, Nevada (September 23-26, 1979).
16. Giacchino, G. J., Jr., NL/Hycalog, presentation during the Sandia Laboratories Advisory Panel Meeting for Geothermal Drilling and Completion Technology Programs, Albuquerque, New Mexico (January 20, 1981).

STATE OF INVESTIGATIONS ON HIGH-PRESSURE WATER JETASSISTED ROAD PROFILE CUTTING TECHNOLOGY

Dipl.-Ing. L. Baumann
Bergbau-Forschung GmbH
4300 Essen 13
Franz-Fischer-Weg 61
Federal Republic of Germany

ABSTRACT

In order to widen the application range of mechanized tunneling in the rock for application in hard-coal mining less clumsy heading systems need to be developed. For this purpose industrial-scale tests are run on the test rigs of Bergbau-Forschung as well as on a colliery. For these tests a road profile cutting machine equipped with various sensors and with a high-pressure waterjet assist in addition to the classic hard metal tools, is used.

By systematic evaluation of test results new application possibilities for this combined heading system are found. Particular importance in this context is assigned to reduced cutting force and extension of the application range to cutting of hard rocks. Investigations also are made for finding out whether by high-pressure water jets on their own interesting heading performances can be achieved. Furthermore the use of chemical additives and new nozzle designs with consideration of their cost-effectiveness is discussed.

The summary outlines technical and ergonomical advantages as well as further development.

INTRODUCTION

Since three years Bergbau-Forschung runs tests for application of high-pressure waterjets in road profile cutting for tunneling in hard-coal mining (Fig. 1). The development work aims at function improvement of mechanical tools by means of high-pressure waterjet (Fig. 2) in order to enable less clumsy design of tunneling machinery via reduction of the necessary high cutting forces for rock crushing, and in this way to widen the application range of this technology which thus could increase its share in tunneling from approximately 20% right now to 40-50% in the years to come.

The tools used at present for rock crushing approach their performance limit set by high wear by and the limited possibility of energy transfer.

Therefore, a new technique which implies more favorable rock cutting conditions is to be developed and operationally tested. This new technology allows to cut a slot which follows the required road profile. A support element should fit into said slot so that subsequently the remaining rock mass within the profile can be removed by the classic techniques without deterioration of the strata around the road.

Research and development work is scheduled as follows:

1. Feasibility study of the technique on laboratory scale and in a sandstone quarry.
2. Experimental operation of a full-scale test array underground.
3. Planning, construction, and experimental operation of a prototype of the new tunneling system for practice of the road profile cutting principle.

The first phase was meanwhile completed successfully. At present underground tests are run on Rossenray colliery (Ruhr area). These tests are scheduled to be completed mid-1981.

EXPERIMENTAL EQUIPMENT

Profile Cutting with High-Pressure Water Jets and Hard-Metal Tools

The basic data on function principles of the combined hard-metal tool/high-pressure water jet system established on laboratory scale served as the design basis for a road profile cutting machine (Fig. 3).

The experimental version consists essentially of the base frame for housing the thrust unit which moves in the axis of heading advance. To this feed mechanism a cutting arm pivoting around a horizontal axis was fitted. Hydraulic rams are provided for both movements, i.e. the pivoting of the cutting arm and the feed in heading direction. The cutting arm pivots by 90°. Further 90° pivoting is possible by plugging the piston-rod end to another bearing provided in the cutting arm for this purpose so that a profile slot could be cut over 180°. In addition the length of the cutting arm could be adjusted by removable intermediate pieces so that for testing purposes three concentric segments could be cut.

A hydraulic power supply with adjustable pump was used for the hydraulics so that cutting speed was infinitely variable.

Cutting Tool

The cutting tool comprises three individual hard-metal bits which are equipped either with

- two leading nozzles
- two trailing nozzles
- four nozzles (two leading and two trailing ones) (see Fig. 4).
-

According to the nozzle array the forces acting on the tool can be varied dependently on the test parameters. These parameters are:

Cutting force - Fs

acting in cutting direction on the tool

Normal force - F_n

acting normally to the cutting direction (Fig. 5).

Profile Cutting by High-Pressure WaterJets Only

In parallel to the above-described joint development work of Bochumer Eisenhutte and Bergbau-Forschung, an alternative experimental equipment is developed in cooperation with the U. S. Department of Energy. This equipment comprises a guide frame which corresponds, as to its shape, to the road cross section. To this frame the tool holder is fitted (Fig. 6).

Cutting Tool

The road profile slot is cut exclusively by six high-pressure nozzles arranged at different angles thus enabling to cut a 80 mm wide slot (Fig. 7).

In addition it is tried to cut the road profile slot by two rotating nozzle heads equipped with two nozzles each (Fig. 8).

The cutting of road cross section profiles by high-pressure water jets only implies almost no reaction forces. This means considerable advantages with respect to lighter weight of the experimental equipment.

WATER-PRESSURE BOOST

The high water pressure is generated by means of so-called pressure boosters (Fig. 9) mounted to a trailer frame behind the experimental equipment and connected to the cutting arm by high-pressure mains of 6.3 mm inside diameter and 14 mm outside diameter. These crucial components were placed at our disposal by the U. S. Department of Energy and modernized to present state of technology by the supplier of these components (Messrs. Flow Industries, Inc., Seattle, U.S.A.).

The individual functional units comprise essentially the pressure booster as such which is run with a hydraulic pump. The installed power of such a unit is of 250 kW and its maximum delivery is of 30 l/min at 3000 to 4000 bar. These pressure boosters are reversible-pump systems (Fig. 10) and, up to present, unmatched with respect to capacity and efficiency; their operational reliability could be brought to a high standard in the course of the test runs so that even particularly critical parts as e.g. high-pressure seals no stand for several hours. These features, are, in addition, likely to be further improved.

GEOLOGICAL CONDITIONS

Prior to the heading trials the suitability of the rocks on site was tested by coredrilling (Fig. 11). The compression strength of the sandstone on site, the so-called Ruhr Quarzit, was determined to be of approximately 100 N/mm2, its tensile strength of approximately 8 N/mm2, and its abrasive-mineral content of 65%. Thus the rock can be regarded as a very typical sandstone as found on tunneling sites underground. However, this kind of rock is not very favorable to high-pressure water jet cutting due to the silicatic binding matter which it contains. Said acute angle results in higher normal force because the tool, while cutting, tends to "climb up" said slope.

With higher water pressure (> 1000 bar) more rock particles from the bottom underneath the plane a - a are cut off.

This break-off ahead of the tool results in hollow spaces being formed underneath the cutting edge. Since the propagation of these hollow spaces extends almost over the total cutting width, only low normal forces act on the tool while passing these "undermined" zones.

Simultaneously new application possibilities were found when cutting hard rock by high-pressure water jetassisted hard-metal tools. Rocks exhibiting compressive strengths > 80 N/mm^2 could be headed into.

At present experimental operation of the road profile cutting equipment is carried on with underground on Rossenray colliery (Fig. 16). These tests are supposed to confirm the applicability of road profile cutting technology in underground operations (Fig. 17). Here the tests are run essentially in softer rocks as well as in the transition zones rock/coal seam since there is a risk of unwanted mineral fall from stratified or fissured rock and consequently a risk of damage to the cutting arm.

The first trial series, however, gave promising results, and it is hoped to confirm by further investigations the positive effects of this new tool combination.

Road Profile Cutting by High-Pressure Water Jets Alone

Besides the use of combined hard-metal tools and high-pressure water jet arrays it was tried to cut the road profile by water jets only (Fig. 18).

Basically the feasibility of this cutting principle was confirmed by the trials run as yet. At the same time it was found that a cutting tool equipped with nozzles only still requires considerable development work.

While the water jets, due to their high impact performance, cut deep slots into the rock, rips remain between the individual slots, and these rips damage the nozzles and the cutting arm.

In order to avoid problems of this kind, the nozzles which up to present were rigidly aimed, were replaced by nozzles oscillating in a plane perpendicular to the cutting direction. Another performance improvement was obtained by using two rotating cutting heads each equipped with two nozzles.

MEASURING DATA RECORDING AND EVALUATION

For recording, processing, and evaluation of the data measured throughout the trials a computerized measuring system is used. This system is installed in a van and comprises essentially a process computer and various measuring and ancillary equipment for measuring forces, speeds, hydraulic pressures, etc. (Fig. 19). The polling of sensors and measuring-data stores is done automatically by various recording and evaluation programs.

FURTHER DEVELOPMENT

The trials run up to present on the one hand confirm the positive effects of high-pressure water jet, on the other hand, however, energy requirements are still relatively high. For this reason further investigation aim at systematic optimization of these new techniques.

RESULTS OF TRIAL RUNS

Hard-Metal Tools Combined with High-Pressure Water Jets

The design of the experimental equipment enables a wide variation range of the most relevant heading parameters (Fig. 12). For proving the feasibility of the working principle, i.e. contour cutting by high-pressure water nozzles and hard-metal tools, the following test schedule was established: Measurement of cutting force and normal force at

- various high pressure water nozzle arrays relative to the hard
- metal tool
- various water pressures
- various speeds
- various cutting webs
- small and large nozzle diameters

In addition all surrounding parameters, e.g.:

- possible cutting exactitude with respect to the contour of the cut and the resulting cross section
- space requirement of the nozzle/tool array
- longevity of the hard-metal tools, the high-pressure water nozzles, and all components of the high-pressure water system had to be recorded.

Figure 13 is to show first of all that an exactly defined slot can be cut into solid sandstone by highpressure water jets and hard-metal cutting tools.

Figure 14 is representative for a whole series of diagrams resulting from various investigations.

Figure 14 shows the cutting force components (cutting force, normal force) versus cutting web. The tool configuration comprises two (leading) nozzles aiming the rock immediately ahead of the cutting edge and two (trailing) nozzles aiming the rock immediately behind the cutting edge of the tool. This configuration yielded the best test results. The cutting force could be reduced by approximately 70% and the normal force by approximately 50%. With higher cutting speeds. This positive effect decreases, however, in those cutting speed ranges which are of interest for hard coal mining a marked reduction of the cutting force components is possible.

In the course of the investigations carried out on combined hard-metal tool/water jet array a best-suited water pressure could be determined. This value reads 1500 bar.

With water pressures below 1000 bar the high-pressure water tools do not cut yet any rock chips from the heading face. With pressures up to this value only the pulverized rock was flushed from the cut and additional rock matter was removed from above the plane a - a. Thus, the unremoved rock mass ahead of the tool forms, relative to the plane a - a an acute-angled (ε) slope (Fig. 15). A possibility for limiting the energy requirement may be found in improved nozzle geometry (Fig. 20).

The nozzles used up to present were not "made to measure," i.e. they are no optimized cutting nozzles. In cooperation with university institutes and nozzle manufacturers development work is done.

In addition it was tried to improve the efficiency of high-pressure water jets by additives. Since the generation of water pressures between 2 and 3 kbar and deliveries in the range between 50 and 60 l/min still cause problems in industrial operation, it is tried to reduce the required water pressure and to obtain a better focused jet by means of additives (Fig. 21).

Initial results confirmed that by additives to the high-pressure water a marked increase of cutting performance is possible in the investigated pressure ranges of up to 2,0 kbar. The technical and ergonomic advantages probably obtainable by use of high-pressure water jets in road profile cutting systems may be summed up as follows (Fig. 22):

1. High exactitude when cutting to profile
2. Good conditions for support setting, no deterioration of rock structure
3. Lightweight machinery
4. No reaction/restoring forces
5. Independent on rock and strata conditions
6. Low tool wear
7. Efficient dust control
8. No sparking
9.

These advantages enabled the design of an advanced heading system comprising today already the following steps: heading, loading, clearance, and support setting (Fig. 23). Subsequently full-scale technical investigations are to follow which are to support the design of a definite road-heading concept into which the profile cutting techniques will be integrated.

NB

This project is sponsored by the provincial ministry for economics and transport of Nordrhein-Westfalen.

The project is carried out in cooperation between Bergbau-Forschung GmbH, the U. S. Department of Energy, and Bochumer Eisenhutte Heintzmann GmbH & Co.

The high-pressure water system is property of the U. S. Department of Energy and was placed at the disposal of Bergbau-Forschung within the framework of a cooperation agreement.

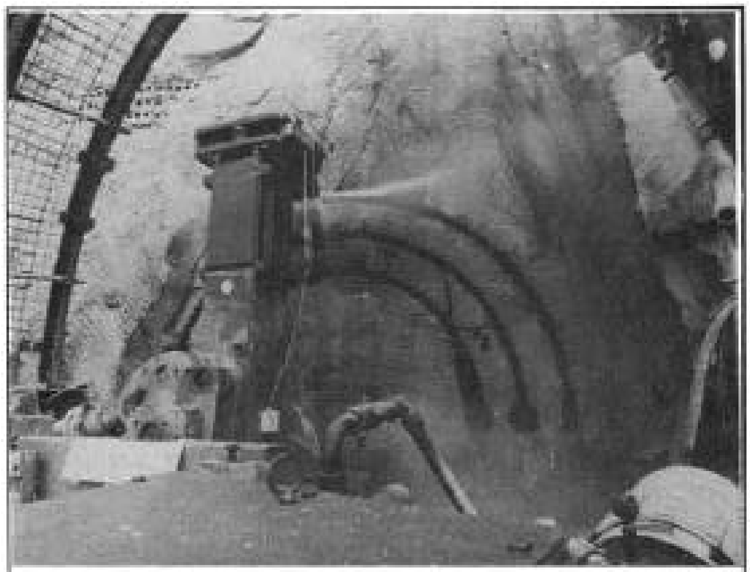

BF	High-pressure water jet assisted cutting of road profiles for optimized support setting and minimized deterioration of the strata structure	TB 12 439

Fig. 1

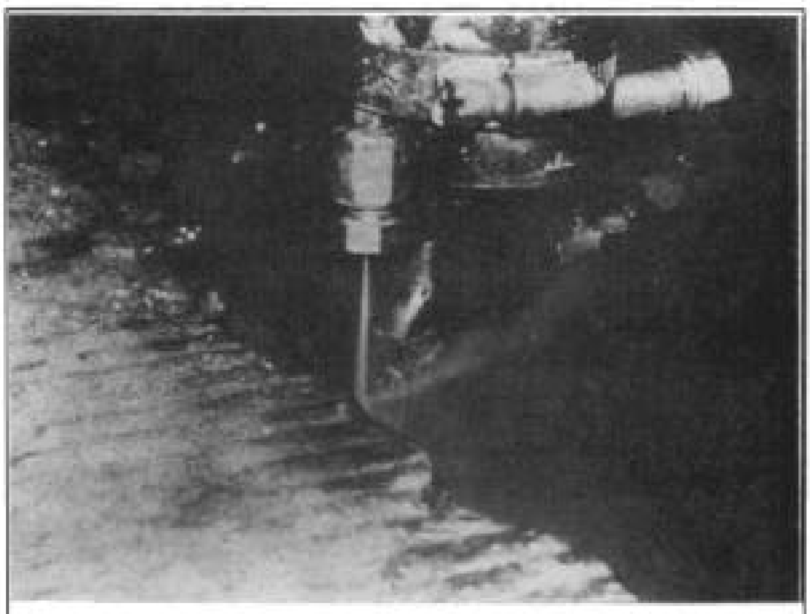

BF	Combined head-metal tool and high-pressure water jet	TB 12 440

Fig. 2

BF	Experimental installation for testing the road-profile cutter in a sandstone quarry	TB 12 441

Fig. 3

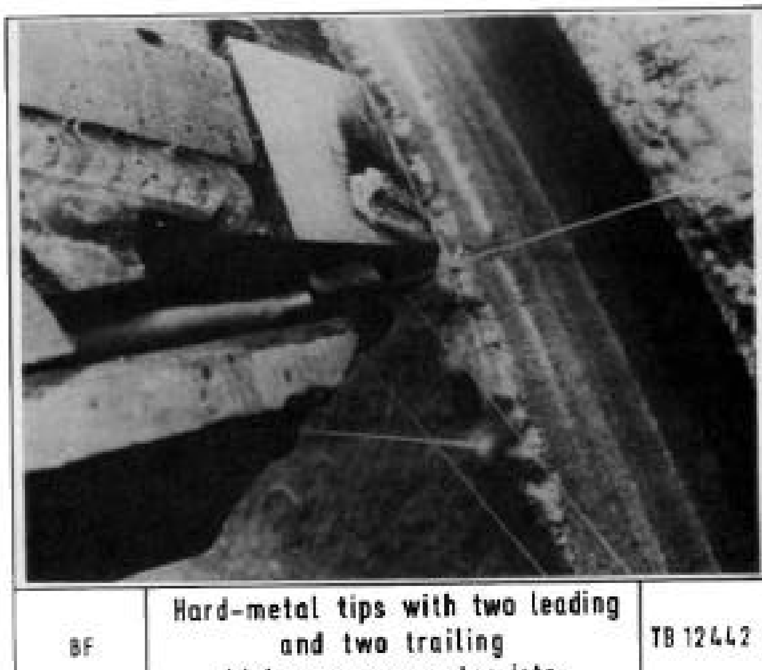

BF	Hard-metal tips with two leading and two trailing high-pressure water jets	TB 12 442

Fig. 4

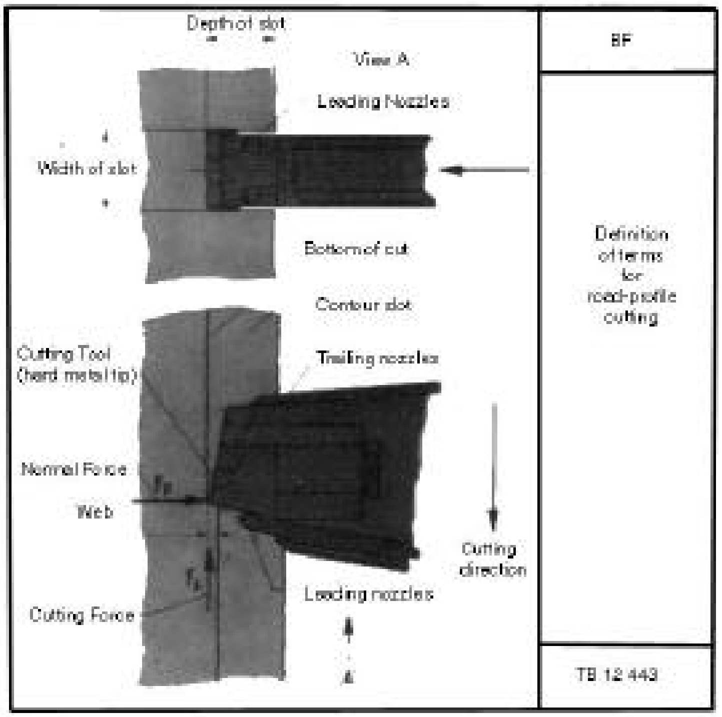
Depth of slot
View A
Leading Nozzles
Width of slot
Bottom of cut
Contour slot
Cutting Tool
(hard metal tip)
Trailing nozzles
Normal Force
Web
Cutting direction
Leading nozzles
Cutting Force
BF
Definition
of terms
for
road-profile
cutting
TB 12 443

Fig. 5

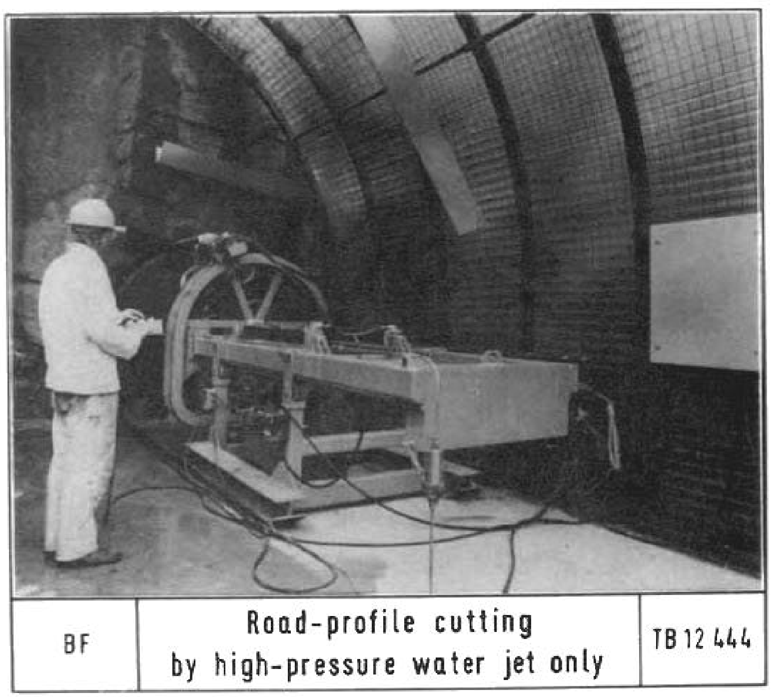
BF
Road-profile cutting
by high-pressure water jet only
TB 12 444

Fig. 6

BF	Nozzle array for road-profile cutting	TB 12 445

Fig. 7

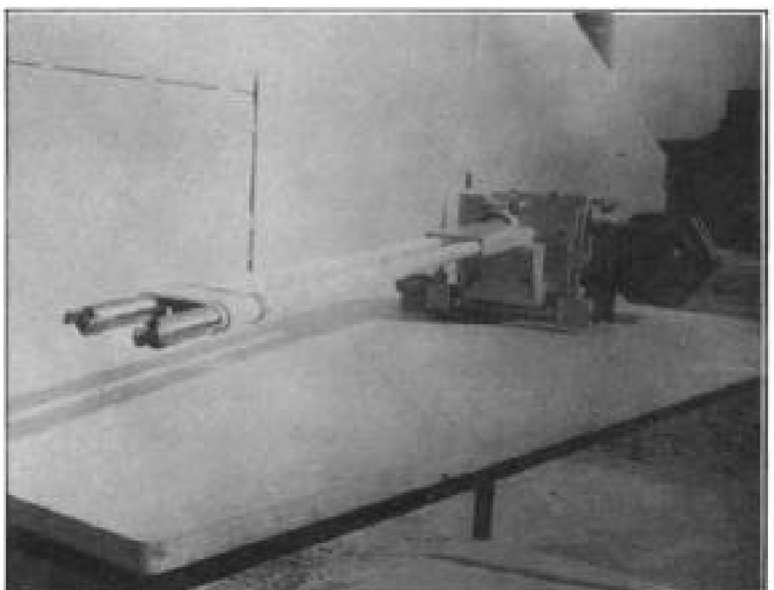

BF	Rotating nozzle-equipped cutting head for road-profile cutting	TB 12 446

Fig. 8

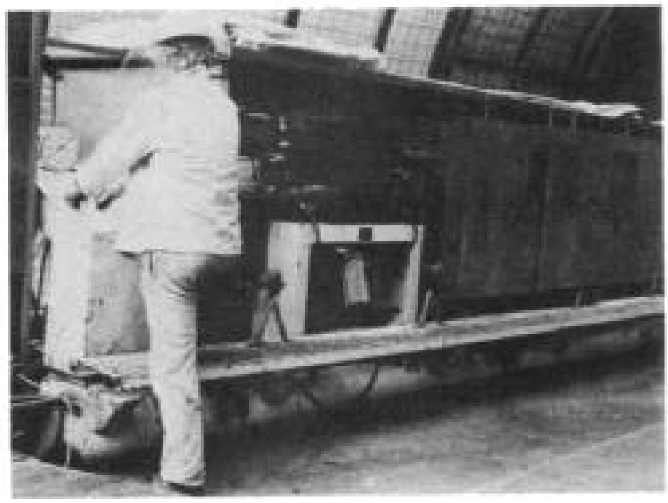

BF	High pressure equipment for tunnel boring tests	TB 12297

Fig. 9

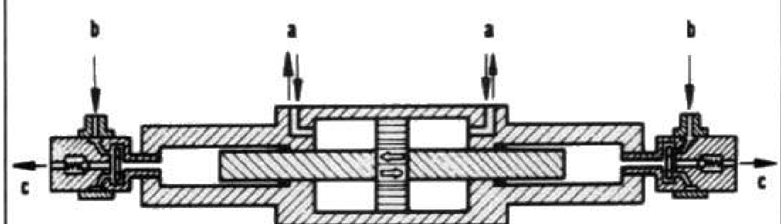

a Pressurized oil, max. 355 bar
b Water intake
c High-pressure water, max 4 000 bar

BF	Function scheme of a high-pressure booster	TB 12 448

Fig. 10

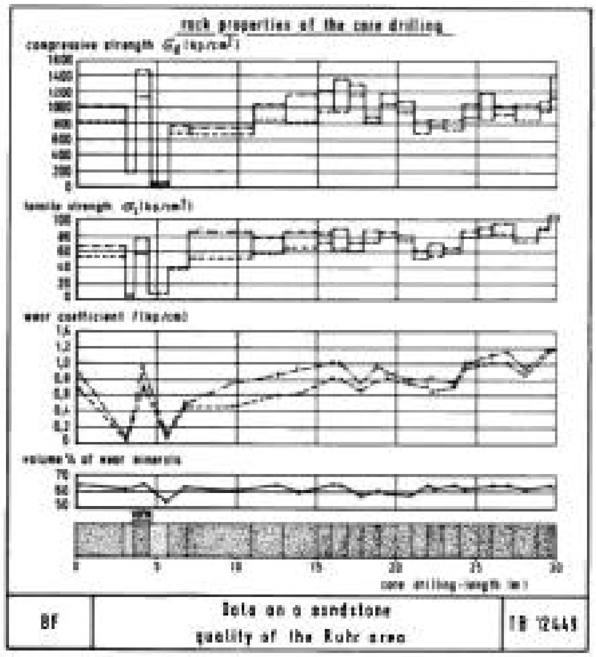
rock properties of the core drilling
compressive strength
tensile strength
wear coefficient
volume % of wear minerals
core drilling-length (m)
BF
Data on a sandstone
quality of the Ruhr area
TB 12449

Fig. 11

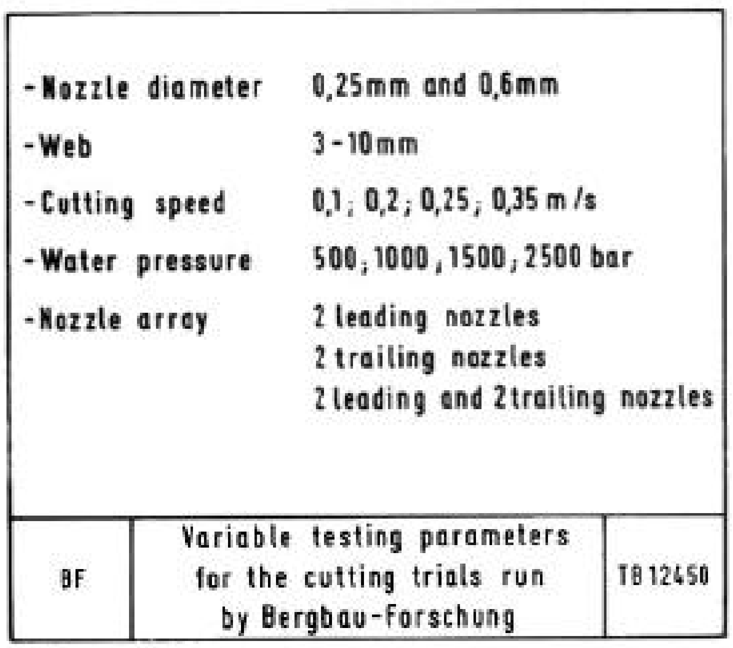
-Nozzle diameter
0,25mm and 0,6mm
-Web
3-10mm
-Cutting speed
0,1; 0,2; 0,25; 0,35 m/s
-Water pressure
500; 1000, 1500; 2500 bar
-Nozzle array
2 leading nozzles
2 trailing nozzles
2 leading and 2 trailing nozzles
BF
Variable testing parameters
for the cutting trials run
by Bergbau-Forschung
TB 12450

Fig. 12


BF
Road-profile groove,
70mm width and 400mm depth
in sandstone
TB 12 451

Fig. 13

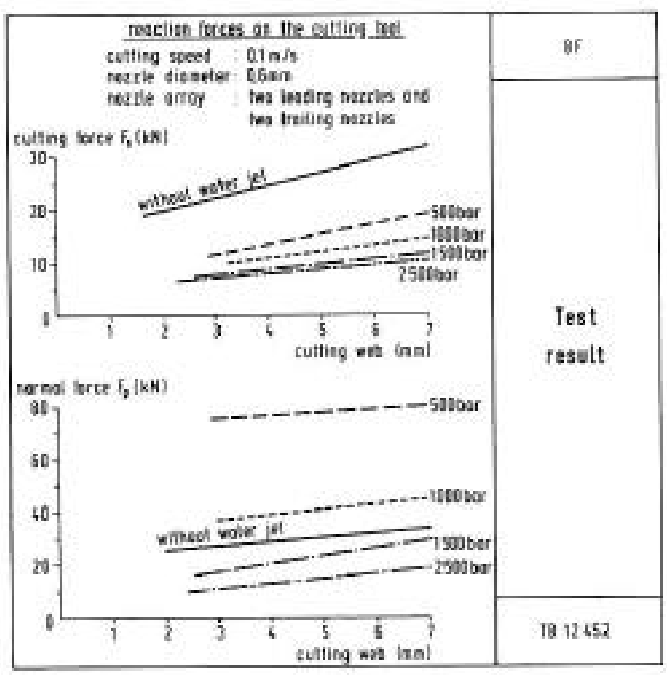
reaction forces on the cutting tool
cutting speed : 0.1 m/s
nozzle diameter : 0,6mm
nozzle array : two leading nozzles and two trailing nozzles
cutting force F (kN)
without water jet
500bar
1000bar
1500bar
2500bar
cutting web (mm)
normal force F (kN)
500bar
1000bar
without water jet
1500bar
2500bar
cutting web (mm)
BF
Test result
TB 12 452

Fig. 14

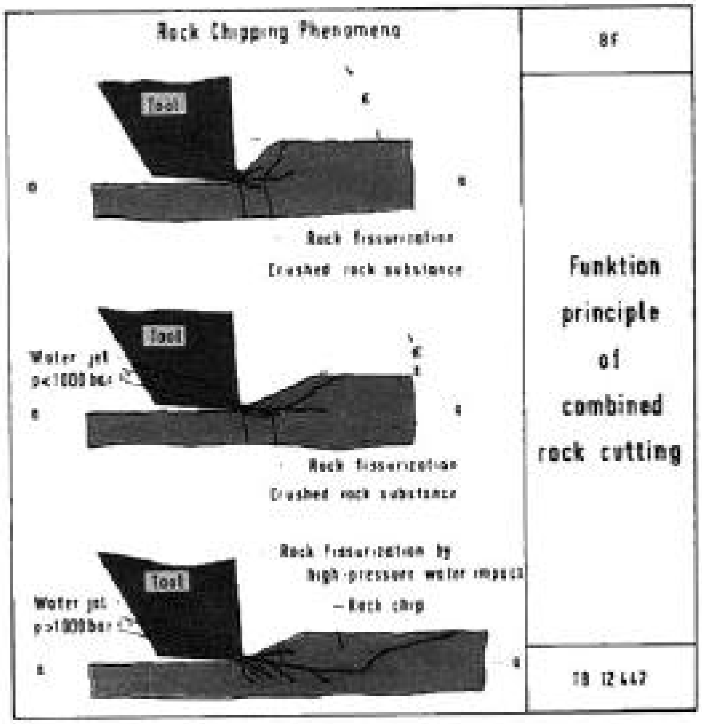

Fig. 15

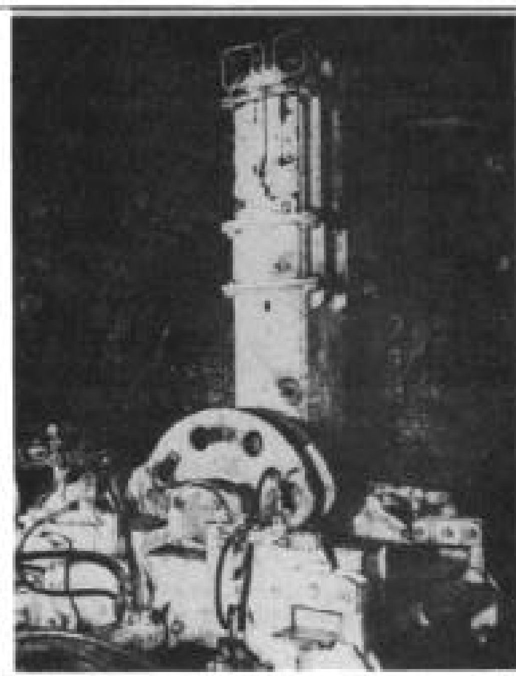

BF | Experimental operation of a road-profile cutting system in a coal seam | TB 12 454

Fig. 16

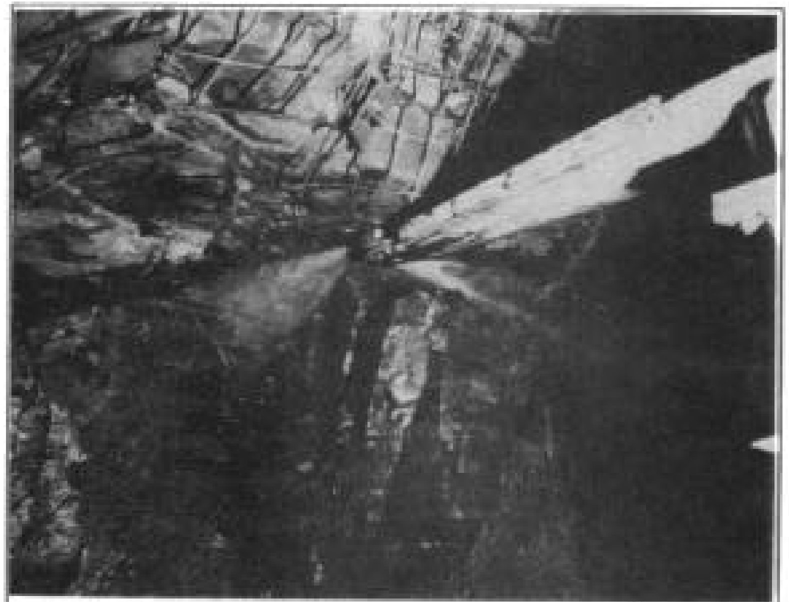

BF	Cutting arm equipped with hard-metal tools and high-pressure nozzles	TB 12455

Fig. 17

BF	Road-profile cutting with high-pressure water jets only. Slot width 80-100mm	TB 12456

Fig. 18


Stbv
CONTROL CENTER WITH COMPUTER AND TV-MONITOR
1979

Fig. 19

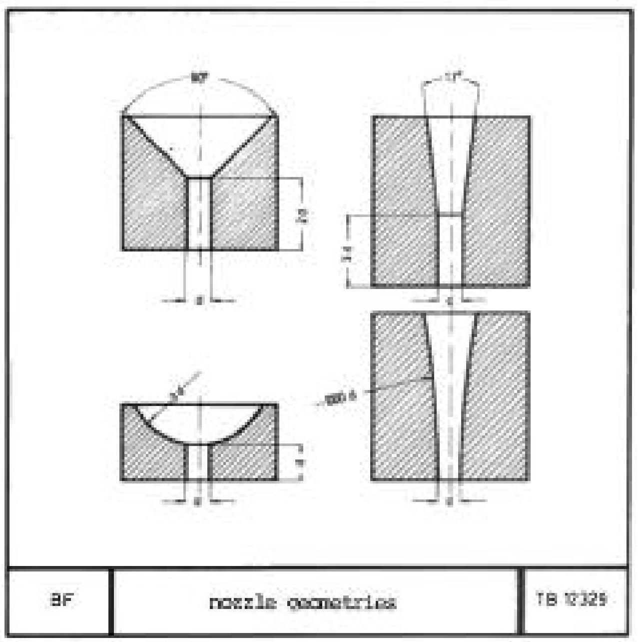
BF
nozzle geometries
TB 12329

Fig. 20

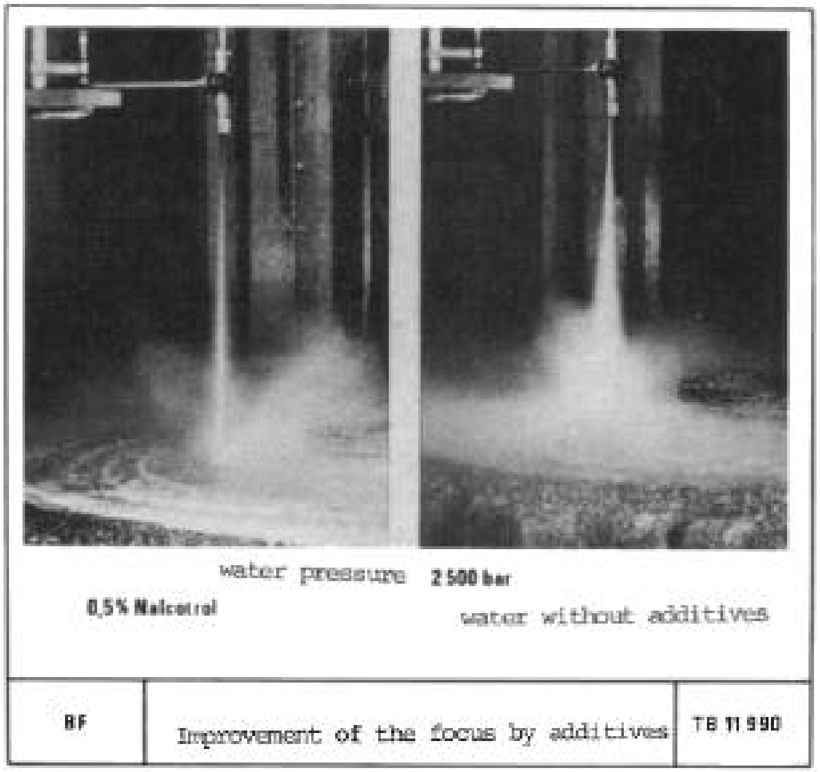

Fig. 21

(1) High exactitude when cutting to profile

(2) Good conditions for support setting, no deterioration of rock structure

(3) Lightweight machinery

(4) No reaction/restoring forces

(5) Independent on rock and strata conditions

(6) Low tool wear

(7) Efficient dust control

(8) No sparking

BF	Advantages of high-pressure waterjets assist in road profilecutting systems	TB12458

Fig. 22

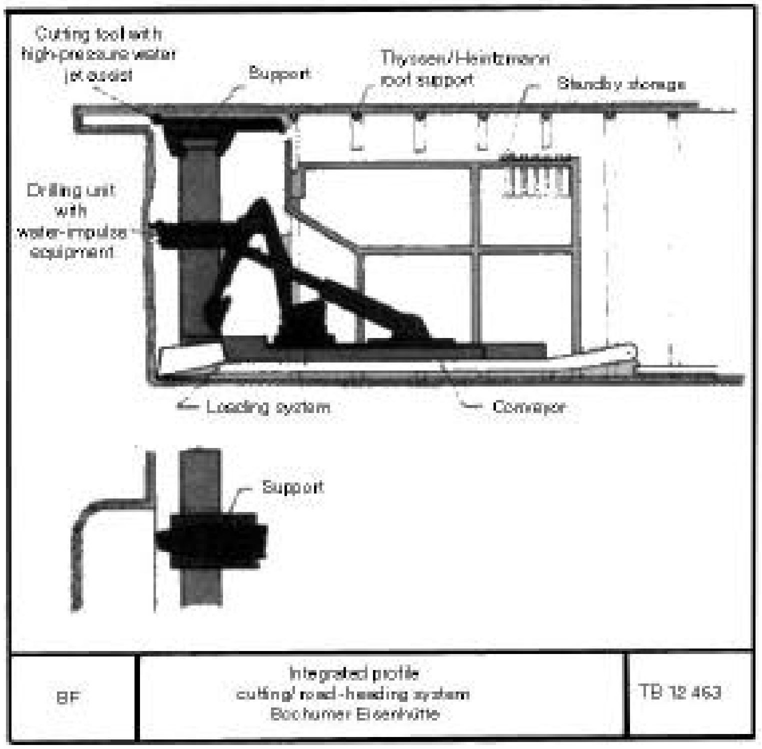
Cutting tool with high-pressure water jet assist
Support
Thyssen/Heintzmann roof support
Standby storage
Drilling unit with water-impulse equipment
Loading system
Conveyor
Support
BF
Integrated profile cutting/road-heading system Bochumer Eisenhütte
TB 12 463

Fig. 23

CUTTING CLEANING AND FRAGMENTATION OF MATERIALS WITH HIGH PRESSURE LIQUID JETS

M. M. Vijay, Ph.D.   W. H. Brierley, M.I.E.D.

Gas Dynamics Laboratory
Division of Mechanical Engineering
National Research Council of Canada
Ottawa, Ontario, Canada, K1A OR6

ABSTRACT

High pressure liquid jets can be used for cutting or fragmentation of a wide range of materials and for cleaning various process equipment. In this paper current projects and those completed during the past five years in the Gas Dynamics Laboratory of the National Research Council of Canada are described. The following topics are discussed: (i) cutting and cleaning projects undertaken in response to enquiries from firms or other organizations, (ii) cutting or breaking rocks and ice and drilling of rocks with rotating jets, and (iii) comparison of non cavitating and cavitating jets.

INTRODUCTION

A perusal of the literature (for example, Ref. 1) shows that since the inception of the high pressure water jet concept a decade or so ago, substantial progress has been made in the utilization of this new tool for various applications. The popularity of high pressure jets appears to stem from the following main advantages:

1. There is no mechanical contact between the tool and the material being processed.
2. Being a point cutter, the jet can follow any profile or shape.
3. Liquid jets are capable of delivering high power to materials. In many cases, this is a primary requirement for obtaining high penetration, cutting or fragmentation rates.
4. Dust level in the air is eliminated or reduced substantially.

Although two types of jets, viz., continuous (non cavitating and cavitating) and pulsed jets (so-called intermittent jets are similar to pulsed jets) are in common usage in jet cutting technology, the material presented here is confined essentially to the work done with continuous non cavitating and cavitating jets. Projects currently active in the laboratory and those completed during the past five years are described. The work done prior to this period has been reported in Refs. 2 and 3.

A high speed liquid jet can be used, in principle, for cutting, cleaning or fracturing any material. Whether it is practicable in any given situation depends on a number of factors which include, among others, capital and maintenance costs of the high pressure pump and accessories, safety, convenience and environmental effects. Some of these limitations will be pointed out later when the examples of applications are described in more detail.

PROJECTS CONDUCTED IN AID OF INDUSTRY OR OTHER ORGANIZATIONS

CLEANING WITH HIGH PRESSURE WATER JETS (FIG. 1, Refs. 4 & 5)

Fig. 1 shows cleaning projects undertaken in response to industrial enquiries. In Fig. 1A cleaning of a clogged gooseneck pipe with a rotating water jet device is depicted (Ref. 4). This pipe is an integral part of a coke oven in the steel manufacturing industry. When it becomes clogged, the static pressure within the oven increases, eventually causing the escape to atmosphere of noxious gases emitted during the carbonization period. Periodic cleaning of the pipe was therefore mandatory and as the existing method of mechanical scraping was unsatisfactory, a better method was required. The rotating jet device was developed in the laboratory for this purpose and was tested on site at the Stelco Steel Company of Canada. It was possible to clean the pipe completely by operating the device, for example, at 41 MPa (flow = 69.6 liters/min) and 300 RPM. A modified version of this device is now manufactured and marketed worldwide by a Canadian company.

The cleaning application shown in Fig. 1B was of a different nature (Ref. 5). Here the requirement was to wash-rip, using a minimum amount of water, the lead and zinc concentrates which gradually adhere to the conveyor belts on which they are transported. According to the company for whom the work was conducted, removal of the buildup by scraping was not satisfactory. The thickness of the buildup was stated to vary from 0.75 to 1.5 mm. Widths of the belts used ranged from 0.76 to 1.2 m. The speed of the conveyor belt ranged from 15.2 to 46 m/min for zinc and from 15.2 to 30.5 m/min for lead concentrate. Experimental results obtained in the laboratory indicated that high speed water jets could be employed to remove these concentrates from the conveyor belts with no damage to the belt. Maximum widths of approximately 7.6 cm of zinc and 1.3 cm of lead concentrates were removed from the samples of belting traversing at 46 m/min, with a single 0.254 mm jet at 69 MPa (flow = 1.14 liter/min), the standoff distance being 25.4 cm.

CUTTING WITH HIGH PRESSURE WATER JETS (Fig. 2, Refs. 6, 7 & 8)

An interesting example of cutting with high pressure water jets is depicted in Fig. 2A. The project was conducted in collaboration with a team of medical doctors from the Faculty of Medicine, University of Ottawa, Ontario, Canada. The purpose of the study was to investigate the possibilities of using high pressure water jets for cutting bones in orthopaedic surgery. A number of experiments were carried out to compare the osteotomies (bone cuttings) performed by water jet and by conventional Stryker saw. By gross tactile measurements, the heat developed at the Stryker saw osteotomy site was found to be greater than that developed at the water jet osteotomy site. This indicated that water jets might reduce or eliminate thermal injury to bone (a common problem with the Stryker saw) at the osteotomy site. However, further research work, including for example histological comparisons, was deemed to be necessary to fully evaluate the application of water jets for surgery.

Fig. 2B shows a sample of resin reinforced fiberglass sheet cut with high pressure water jets (Ref. 6). This work was carried out in aid of a small Canadian company. The experiments showed that water jets could readily be used to cut through this material. For example, a 0.254 mm jet operating at 276 MPa (flow = 2.27 liters/min and hydraulic power = 10.4 kw) could cut through a 5.9 mm thick sample at a traverse speed of 3 m/min. This speed was 5 to 10 times faster than that achieved by the diamond edged saws presently used by the company. The quality of the cut edge was judged to be satisfactory and in addition the water jets offered the possibility of cutting with relative ease different shapes of the material. However, to the firm, the cost of acquiring and operating a high pressure pump appeared to be exorbitant in comparison with the existing equipment.

A rather interesting project undertaken recently in the laboratory involved cutting scallop shells with high speed water jets (Ref. 7). As shown in Fig. 2C, the objective was to remove the edible portion of the scallop by cutting through both the top and bottom parts of the shell near the hinge (the muscle which keeps the shell closed) and the opposite edge of the shell. The existing prototype machine at Fisheries Development Branch of Fisheries and Oceans Canada, incorporates two fairly inexpensive metallic circular saws and is capable of cutting approximately 60 scallop shells per minute. Experiments with water jets were initiated with the expectation that this speed of operation could be increased. Tests conducted at pressures in the range of 69 - 310 MPa (hydraulic power = 13 - 52 kw) and with feed rate of shells as low as 3 per minute were, however, unsuccessful. It was not possible to cut through both the top and bottom parts of the shell, especially on the hinge side. The recommendation to Fisheries was therefore that although in principle their requirement could be met by increasing the jet pressure considerably beyond 310 MPa, the hydraulic system would be prohibitively expensive in comparison with the circular saws employed in their prototype machine.

Figs. 2D, 2E and 2F show some results of another Fisheries project carried out in the laboratory (Ref. 8). The purpose was to investigate the feasibility of incorporating a high pressure water jet as an incision tool in a conceptual fish gutting machine. The requirement was to cut the head or the neck (Fig. 2D) so as to reach and sever the esophagus (Fig. 2E) and then to cut open the belly (from the neck cut to the anus, Fig. 2F), without damaging the surrounding flesh. These operations were necessary to separate the edible from the inedible portions of the fish. The traverse speeds of the conveyors carrying the fish were specified to be 6.1 and 22.9 m/min for neck and belly cutting operations respectively. The production rate at these speeds was expected to be about 1800 fish/hour. The Fisheries also stated that the combined hydraulic power for both operations should not exceed 15 kw.

Experiments were conducted in the laboratory on fresh cod fish to determine the levels of pressure and power necessary to achieve these requirements. Test results indicated that while gut (belly) cuts could be made at relatively low pressures (69 MPa), the neck cuts required rather high pressures (>250 MPa), the combined hydraulic power, however, remaining well below the specified limit of 15 kw. It was felt that these high pressures could be reduced substantially (to approximately 110 MPa) by modifying the method of cutting, for instance, by increasing the flow to about 4 liter/min or by employing multiple or oscillating jets. The conclusion was that processing fish with high pressure water jets is feasible.

Finally, Fig. 2G shows a sample of semipermeable laminated PVC/leather shoe material perforated with a 0.254 mm water jet at 69 MPa. According to the shoe company for whom the work was performed, the perforations enhanced the transmission rate of sweat vapor through the material. Tests conducted in the laboratory showed that a stack of 12 samples, 3.05 cm in thickness, could be pierced in about 0.2 seconds by a single 0.127 mm jet at 207 MPa. The sapphire nozzle (Ref. 3) developed in the laboratory was quite suitable for this application due to its ability to operate at rapid high shock loads. This nozzle is now manufactured by a Canadian company. Liquid jets (water mixed with long chain polymers) have a great potential for cutting contours of shoe materials and it appears that fully automated and computer controlled prototype machines now exist in the U.S.A. and England (Ref. 1).

BASIC EXPERIMENTAL WORK WITH HIGH PRESSURE WATER JETS

The work described in the paragraphs above was carried out in aid of industry and had the sole objective of encouraging industry to consider or adopt high pressure water jet technology. In the following paragraphs the basic work done to advance the technology of water jets and to extend its area of applications is touched on. Projects currently active are the cutting or fracturing of rocks and ice, the development and design of deep penetrating nozzles for drilling or slotting of rocks and the study of cavitating jets.

FRACTURING OR CUTTING OF ROCKS AND ICE (Fig. 3, Refs.9, 10, 11, 12 &13)

Fig. 3A (Ref. 9) shows a block of Barre granite confined in a matrix of concrete to simulate the actual stress conditions in the field, fractured by a continuous stationary jet of 1.78 mm in diameter, operating at 55 MPa. A line of fracture developed in 0.5 min (No. 139 in Fig. 3A) and the rock was completely broken in 1.0 min (No. 138 in Fig. 3A). Rocks which are highly porous and include inherent weaknesses such as faults or joints are particularly easy to break into fragments with moderately high pressure (~69 MPa) continuous stationary jets While a considerable amount of work has been done on breaking rocks with extremely high pressure (~500 MPa) pulsed jets (Ref. 1), little attention has been paid to breaking rocks with continuous stationary jets. Work with stationary jets continues in the laboratory with the object of acquiring data of possible interest to mining and quarrying industries.

An extensive series of laboratory and field tests has been carried out to evaluate the potential of high pressure water jets for cutting or breaking ice (for example, in navigable channels) or for removal of ice formations from surfaces such as lock walls and concrete pavements (Refs. 10, 11, 12 & 13). Ice cutting projects cited in this paper have been conducted in collaboration with the Low Temperature Laboratory of the Division of Mechanical Engineering, National Research Council of Canada, and for more information on this topic, enquiries should be directed to that laboratory. The following paragraphs summarize the work completed to date.

During the winter of 1978-79 experiments were carried out in the field on cutting cold river ice with water jets ranging in pressure from 32 to 71 MPa (Fig. 3B, Ref. 13). The maximum depth of penetration was 0.62 m, achieved with a 3.56 mm jet at 67 MPa (hydraulic power = 243 kw) and at a traverse speed of 2.7 m/min. These tests were subsequent to earlier field experiments performed during the winter of 1977-78 using a relatively low pressure (16 MPa) but high flow (1500 liters/min., hydraulic power   250 kw) pump (Refs. 11 and 12). Based on the wide range of results obtained in all these investigations and taking into account the quality and strength of ice at the temperatures encountered, a proposal was made to establish the viability of water jets for actual commercial ice breaking operations. This would require the use of a pump capable of delivering powers up to 4000 kw.

Removing ice from surfaces poses a different kind of problem. Here the requirement is to destroy the bond between the ice and the substrate, without damage to the substrate. Preliminary laboratory experiments with high pressure angled jets (up to 310 MPa, flow=l.9 liters/min and hydraulic power = 22.4 kw) showed that it is possible to remove satisfactorily up to 6.4 mm thick ice layers formed on concrete slabs. From the standpoint of quantity of ice removed, an angle of 14° to the horizontal was found to be optimum (Ref. 10).

DRILLING OF ROCKS WITH ROTATING JETS (Fig. 4, Refs. 14, 15 &16)

A great deal of research and development work on the application of high pressure liquid jets for drilling and deep slotting of rocks is in progress in several countries (Refs. 1, 14). This interest is essentially due to the fact that high pressure liquid jets are capable of delivering up to 100 times more power to the rocks than the existing conventional systems and therefore offer the possibility of achieving penetration rates much higher than those obtained at present. In order to achieve deep penetrations it is necessary to drill holes or cut slots that are wider than the nozzle body (or drill head) itself. One method of obtaining this is to employ rotating angled jets. The nozzle body which incorporates one or more orifices (nozzles) to produce these angled jets has considerable influence on drilling performance and the study of the parameters that enter into its design is important.

In the experiments conducted in the Gas Dynamics Laboratory (Refs. 15 & 16) dual orifice nozzle bodies were employed, the objective being to study the influence of three parameters, viz., the angle of inclination of the outer jet to the axis of rotation, the distribution of total available flow area between the inner and outer orifices and the shape of the nozzle entry, conical or straight (sudden or sharp). Nozzle body configuration performance was assessed essentially on the basis of measured specific energy (energy expended per unit volume of material removed) values by drilling horizontal holes in unconfined blocks of Muskoka Pink Granite, approximately 15 nozzle body diameters in length, using a constant water jet pressure of 69 MPa (hydraulic power = 58 kw). Fig. 4A shows a general view of the experimental setup. To give some idea of the influence of the parameters investigated, the values of specific energy are plotted against the angle of inclination of the outer jet in Fig. 4B (Ref.15). The figure shows that the angle (φ_0) has a profound influence on drilling performance and an increase in its value from 10 to 20° reduced the measured specific energy by a factor of 12. The results obtained to date are encouraging and further work is in progress (Ref. 16).

STUDY OF CAVITATING JETS (Fig. 5, Refs. 1, 9, 17 & 18)

Although the phenomenon of cavitation and its deleterious effects on the performance of fluid machinery have been known for well over a century the concept of using it to augment the erosive power of a simple liquid jet originated only recently (Ref. 17). Cavitating jets are high speed liquid jets in which by some means or other cavitation bubbles (vapor bubbles) have been induced (Ref. 18). A simple method is to operate a high speed liquid jet under submerged conditions. Figs. 5A and 5B show dramatically the difference in the erosion caused by a non cavitating, that is, a simple jet issuing from a conical nozzle (Leach & Walker nozzle) in air, and a cavitating jet (the same simple jet submerged in a tank of water). Since it is not always possible to perform cutting operations under water, various other methods of generating cavitation bubbles within a jet have been considered (Ref. 18). However, the generation of vapor bubbles is governed by so many variables (the one major problem is to determine the influence of dissolved air in the liquid) that it has been difficult both to predict their presence within the jet and to obtain consistently reproducible results (Ref. 9). Research described below is in progress in the laboratory to resolve some of these difficulties.

Figs. 5C and 5D show respectively a line diagram and a general view of an experiment set up recently to visualize jets issuing from nozzles of various configurations by means of a laser, with or without the aid of other light sources. It should be stated at the outset that photographs of the jets presented here are only preliminary as the experimental program is undergoing continual modifications in order to obtain the desired results. A continuous He-Ne laser (Spectra-Physics, Model 135, 4 mw) was used in these preliminary experiments. As shown in Fig. 5C, the laser beam passes through an optical window, through the lance and the jet, illuminating the latter internally. Since a high speed jet usually appears opaque due to the fog or mist surrounding it, it was felt that this method of illumination would probably reveal more clearly the internal structure of the jet.

Figs. 5E and 5F show photographs of jets (1.78 mm, $L/d = 2$, 34.5 MPa) issuing in air from a conical and a sudden entry nozzle respectively. Although these photographs did not reveal the information sought, they are presented here to emphasize that the method could be used to examine the quality of jets issuing from different nozzles. For instance, the jet from the sudden entry nozzle (Fig. 5F) appears to have the same coherent length (25 nozzle diameters) as that from the conical entry nozzle (Fig. 5E). Such observations have raised some interesting or rather puzzling questions for which no answers have been found so far. For example, in the case of drilling experiments described earlier, the performance of a nozzle body with sudden entry orifices (nozzles) was very poor compared with the performance of an identical nozzle body incorporating conical entry nozzles (Ref. 15). On the other hand, in the study of erosion of copper plates (see Fig. 5H), the jet from a sudden entry nozzle was observed to damage the sample far more severely than the jet from a conical entry nozzle, other conditions remaining the same (Ref. 18).

The next step in the experimental program was to visualize the jets under a microscope (Wild-Heerbrugg Stereo Microscope, Model M5). Fig. 5G shows a photograph, taken at a magnification of 25, of a jet emerging at 6.9 MPa from a conical nozzle with a cylindrical body insert. Although the photograph shows more details of the jet, further refinements are deemed to be necessary before the method can be fully exploited for visualization purposes. This would require, among other things, a high frequency pulsed laser. This is currently under investigation.

Another approach, in progress at present in the laboratory, is to examine the metallic samples (copper and aluminum) eroded by cavitating and non cavitating jets at high magnification on a Leitz Metallograph (Figs. 5H and 5I). The purpose here is to try to classify the extent of the metallurgical damage in the samples, and if possible relate this to cavitation. A few samples of aluminum and steel that have been known to be eroded under purely cavitating conditions have been obtained from Dr. F. G. Hammitt of the University of Michigan, U.S.A., as reference for comparison.

Four characteristics have been chosen to describe the degree of erosion. These are:

1. The extent of grain deformation (change in shape) at the base of the crater, including an estimation of the relative number of deformed grains (Fig. 5I).
2. Surface roughness as measured by the average size and frequency of pits in the crater surface which may indicate the presence (or absence) of cavitation.
3. The extent of cracking in the crater surface, and
4. Microhardness measurements.

To date only four samples exposed to four different types of jets (jets from sudden and conical entry nozzles in air, jet from a conical nozzle under water and a high speed jet surrounded by a low speed stream, Ref. 18) have been examined and the sample (Fig. 5H) exposed to the jet from a sudden entry nozzle has been found to have suffered the most severe damage. Whether this is due to cavitation or some other phenomenon remains to be established.

CONCLUSIONS

The use of high pressure liquid jets for various applications has been described. It is believed that although high pressure water jets have potential for a number of applications, the lack of availability of a low cost high pressure pump has been a discouraging factor for adopting the technology readily in industry, particularly in small scale industries. The basic work currently active in the laboratory has also been touched on and it is hoped that the results obtained will eventually be applicable to industrial problems.

ACKNOWLEDGMENTS

The authors are grateful to Dr. R. T. Holt and Ms. M. K. Allen, Structures and Materials Laboratory of the National Aeronautical Establishment, National Research Council of Canada for the metallographic study of the eroded samples. Thanks are also due to Dr. F. G. Hammitt for readily sending the metallic samples eroded under cavitating conditions. The authors greatly appreciate the interest shown in this work by Mr. R. A. Tyler, Head, Gas Dynamics Laboratory of N.R.C.

REFERENCES

1. T. E. Brock, N. G. Coles, H. S. Stephens, et al., 1st (1972), 2nd (1974), 3rd (1976), 4th (1978) and 5th (1980) International Symposium on Jet Cutting Technology, sponsored by BHRA, Cranfield, Bedford, England.

2. H. D. Harris & W. H. Brierley, Putting Water Jets to Work, Manufacturing Developments, Vol. 4, No. 2, June 1972, Division of Mechanical Engineering, National Research Council of Canada, Ottawa, Ontario, Canada.
3. W. H. Brierley & M. M. Vijay, Research on Water Jet Cutting and Its Applications at the National Research Council of Canada - A Review, Proc. of the Workshop on the Application of High Pressure Water Jet Cutting Technology, University of Missouri-Rolla, U.S.A., November 1975.
4. W. H. Brierley & M. M. Vijay, Rotating High Pressure Water Jet Gooseneck Cleaner, Paper G3, 3rd Int. Symp. on Jet Cutting Technology, May 1976, BHRA, Cranfield, Bedford, England.
5. M. M. Vijay and W. H. Brierley, Removal of Sullivan Lead and Zinc Concentrates from Conveyor Belts with High Velocity Water Jet, Report No. LTR-GD-57, Div. of Mech. Engineering, National Research Council of Canada, Ottawa, Ontario, Canada, May 1980.
6. M. M. Vi jay and W. H. Brierley, Cutting a Fiberglass Reinforced Sheet Product with High Pressure Water Jetsaw Report No. LTR-GD-58, Div. of Mech. Engineering, National Research Council of Canada, Ottawa, Ontario, Canada, August 1980.
7. M. M. Vijay & W. H. Brierley, Cutting Scallop Shells with High Speed Water Jets, Report No. LTR-GD-60, Div. of Mech. Engineering, National Research Council of Canada, Ottawa, Ontario, Canada, October 1980.
8. M. M. Vijay & W. H. Brierley, The Utilization of High Pressure Water Jets for Processing Fish Report No. LTR-GD-61, Div. of Mech. Engineering, National Research Council of Canada, Ottawa, Ontario, Canada, April 1981.
9. M. M. Vijay & W. H. Brierley, Cutting Rocks and Other Materials by Cavitating and Non Cavitating Jets, Paper C5, 4th Int. Symp. on Jet Cutting Technology, BHRA, England, April 1978.
10. H. J. Kimberley & W. H. Brierley, Ice Removal from Concrete by High Pressure Water Jets, Report No. LTRLT-74, Div. of Mech. Engineering, National Research Council of Canada, Ottawa, Ontario, Canada, April 1977.
11. D. B. Coveney & W. H. Brierley, The Cutting of Ice with Water Jets, Report No. MD-54, Div. of Mech. Engineering National Research Council of Canada, Ottawa, Ontario, Canada, November 1977.
12. D. B. Coveney & W. H. Brierley, Cutting Cold River Ice with Water Jets During the Winter 1977-78) Report No. LTR-LT-99, Div. of Mech. Engineering, National Research Council of Canada, Ottawa, Ontario, Canada, June 1979.
13. D. B. Coveney & W. H. Brierley, Cutting Cold River Ice with Water Jets During the Winter 1978-79, Report No. LTR-LT-108, Div. of Mech. Engineering, National Research Council of Canada, Ottawa, Ontario, Canada, January 1980.
14. M. M. Vijay & W. H. Brierley, Drilling of Rocks by High Pressure Liquid Jets: A Review, ASME Paper No. 80-PET-94, American Society of Mechanical Engineers, New York, U.S.A., 1980.
15. M. M. Yijay & W. H. Brierley, Drilling of Rocks with Rotating High Pressure Water Jets: An Assessment of Nozzles, Paper G1, 5th Int. Symp. on Jet Cutting Technology, June 1980, BHRA, England.
16. M. M. Vijay & W. H. Brierley, Drilling of Rocks with Rotating High Pressure Water Jets: Progress Report No. 1, Report No. LTR-GD-59, Division of Mech.

Engineering, National Research Council of Canada, Ottawa, Ontario, Canada, Sept. 1980.
17. V. E. Johnson, Jr., A. Thiruvengadam and R. E. Kohl, Rock Tunneling with High Speed Water Jets Utilizing Cavitation Damage, ASME Paper No. 68-FE-42, U.S.A., 1968.
18. M. M. Vijay & W. H. Brierley, A Study of Erosion by High Pressure Cavitating and Non Cavitating Water Jets, Erosion: Prevention and Useful Applications, ASTM STP 664, W. F. Adler, Ed. American Society for Testing and Materials, 1979, pp. 512-529.

FIG. 1 A CLEANING A GOOSENECK PIPE WITH A ROTATING WATER JET DEVICE
P_O= Nozzle Pressure = 41MPa
Q = Flow = 69.6 liter/min
N = Rotational Speed = 300 RPM

FIG. 1B A SAMPLE OF A CONVEYOR BELT COATED WITH 0.5cm THICK ZINC ORE CLEANED WITH A HIGH SPEED WATER JET
d = Nozzle Diameter = 0.254mm
P_o = 69Mpa
S.D = Standoff Distance = 25cm
V_{tr} = Traverse Speed = 46 and 14 m/min respectively

FIG. 2A LEG BONE OF A RABBIT AMPUTATED WITH A 0.127mm WATER JET AT 172 MPa(S.D = 0.6cm)

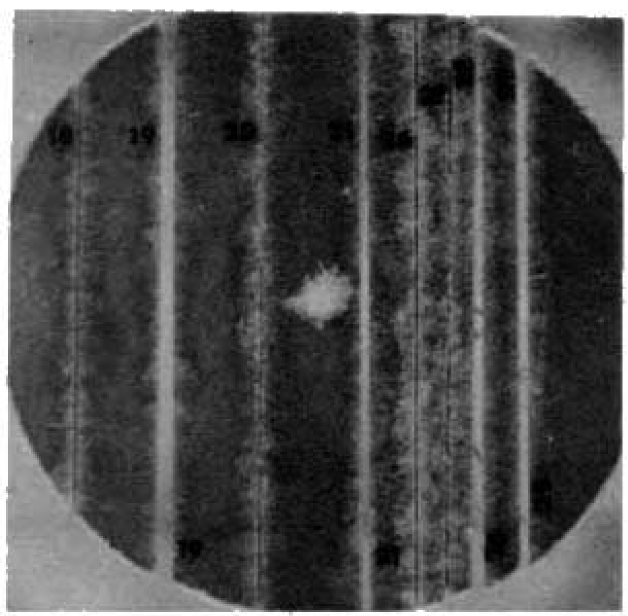

FIG. 2B A SAMPLE OF RESIN REINFORCED FIBREGLASS SHEET CUT WITH JETS FOR TEST NO. 29:
d = 0.254mm,
P = 276MPa,
V_{tr} = 3.Om/min and
S.D = 3.22mm,
Sample Thickness=5.9mm

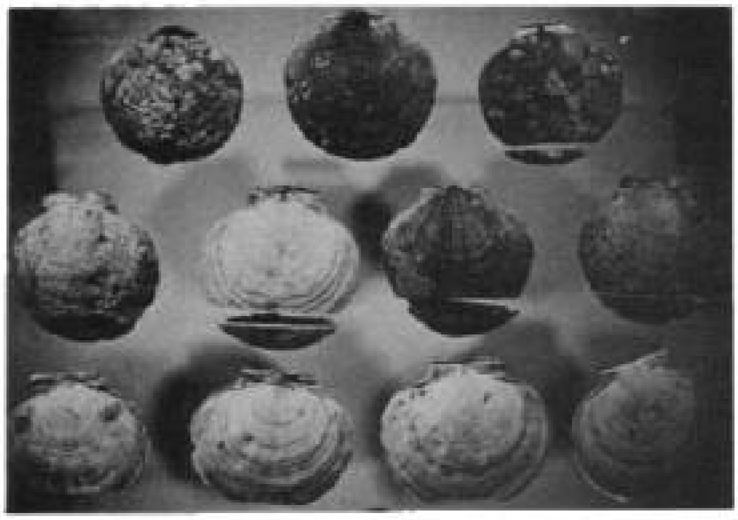

FIG. 2C SCALLOP SHELLS CUT WITH HIGH SPEED JETS

<u>Range of Variables:</u>

P_o = Nozzle Pressure = 69-310 MPa

d = Nozzle Diameter = 0.2 - 1.60mm

V_{tr}= Traverse Speed = 0.40 m/min

S.D = Standoff Distance = 0.6cm

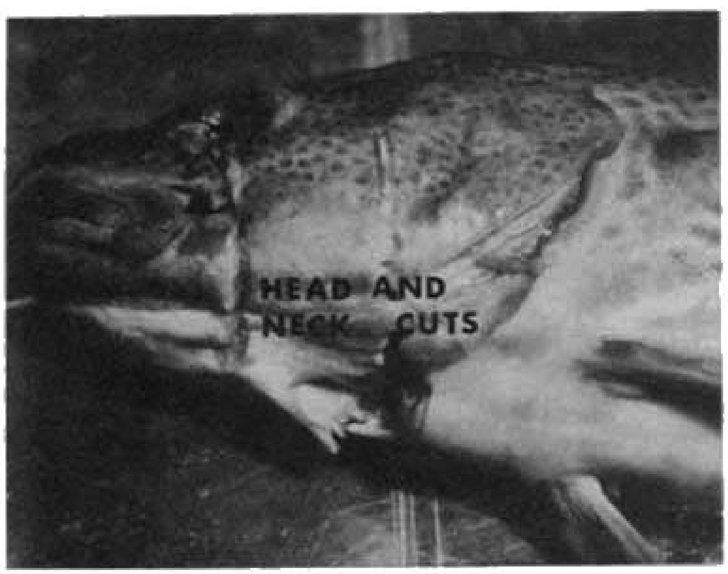

FIG. 2D WATER JET CUTTING OF COD FISH FOR APPLICATION IN THE DEVELOPMENT OF A FISH GUTTING MACHINE(CUTTING OF NECK AND BELLY, SEE FIGS. 2E and 2F)

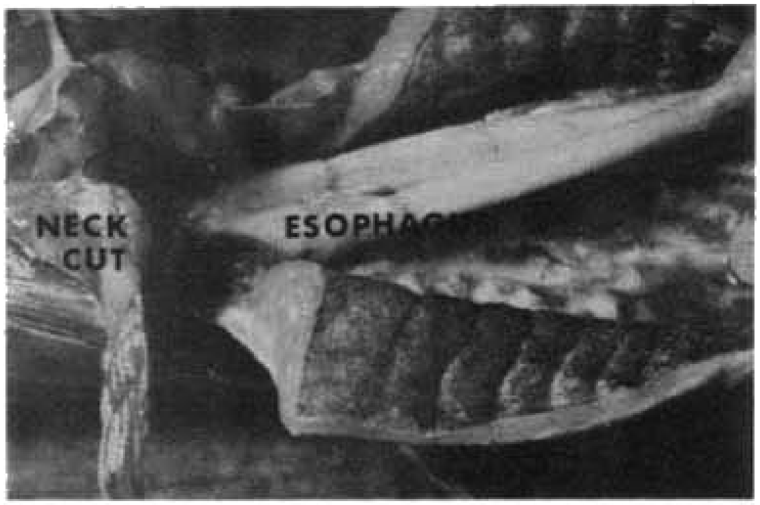

FIG. 2E A VIEW SHOWING THE CUT MADE THROUGH THE NECK TO REACH AND SEVER THE ESOPHAGUS

Range of Variables:

P_o = 62-276MPa

d = 0.10-0.381mm

V_{tr} = 6.lm/min

FIG. 2F GUT CUT(BELLY CUT)MADE WITH WATER JETS TO REMOVE THE VISCERA

Range of Variables:

P_o = Nozzle Pressure = 34-103Mpa

d = Nozzle Diameter = 0.10-0.381mm

V_{tr} = Traverse Speed = 6.1-30.5m/min

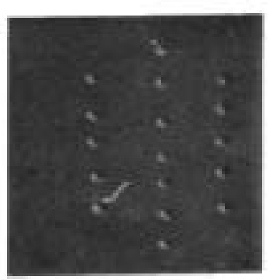

FIG. 2G HOLES PUNCHED IN A LAMINATED LEATHER SAMPLE WITH A 0.254mm JET AT 69 MPa

Thickness of Sample = 2.5mm

S.D = 1.0 mm

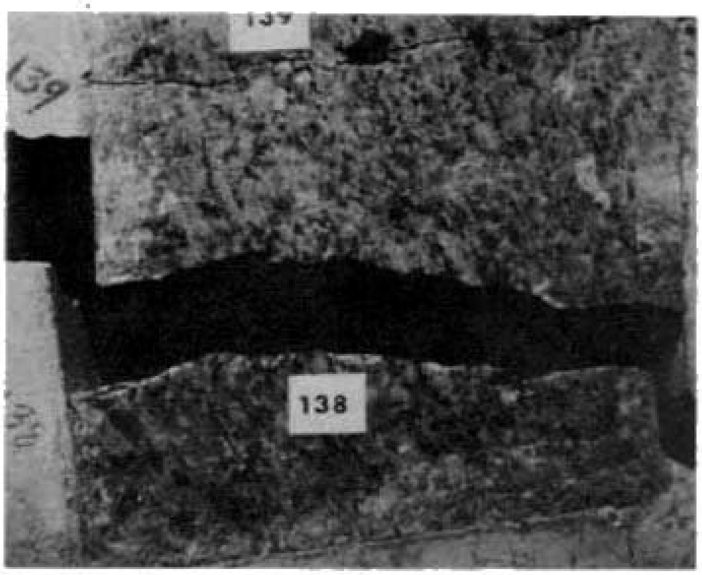

FIG. 3A A CONFINED BLOCK OF BARRE GRANITE FRACTURED BY A CONTINUOUS STATIONARY WATER JET

P_o = 55 Mpa
d = 1.78mm

DURATION OF EXPOSURE TO JET:
Test No. 138 : 1.0 min
Test No. 139 : 0.5min

FIG. 3B CUTTING OR BREAKING RIVER ICE WITH HIGH SPEED WATER JETS

<u>Range of Variables Investigated:</u>

P_o = 32-71MPa
d = 2.87-4.57mm
Flow=Q= 131-259 liter/min
Hydraulic Power = H_p = 84-262kw (Ref.13)

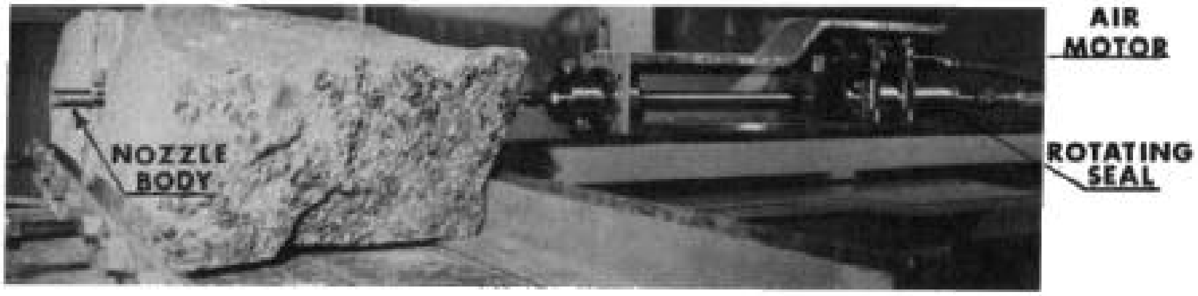

FIG. 4A A GENERAL VIEW OF THE ROTATING JET DEVICE

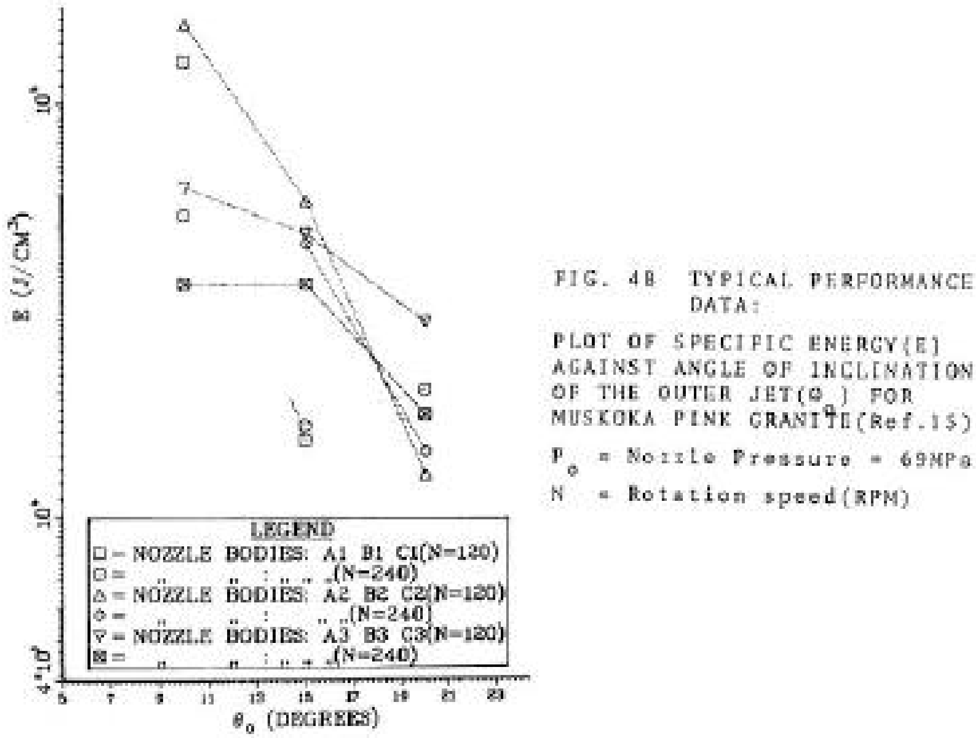

FIG. 4B TYPICAL PERFORMANCE DATA:
PLOT OF SPECIFIC ENERGY(E) AGAINST ANGLE OF INCLINATION OF THE OUTER JET(O) FOR MUSKOKA PINK GRANITE(Ref.15)

P_o = Nozzle Pressure = 69MPa

N = Rotation speed(RPM)

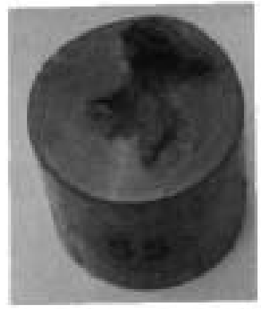

FIG. 5B EROSION DUE TO NONCAVITATING (FIG.5A) AND CAVITATING JETS(FIG,5B) OF LEAD SAMPLES

P_o =34.5MPa,

S.D = 7.6cm

Duration of Test = 4min

V-4.10

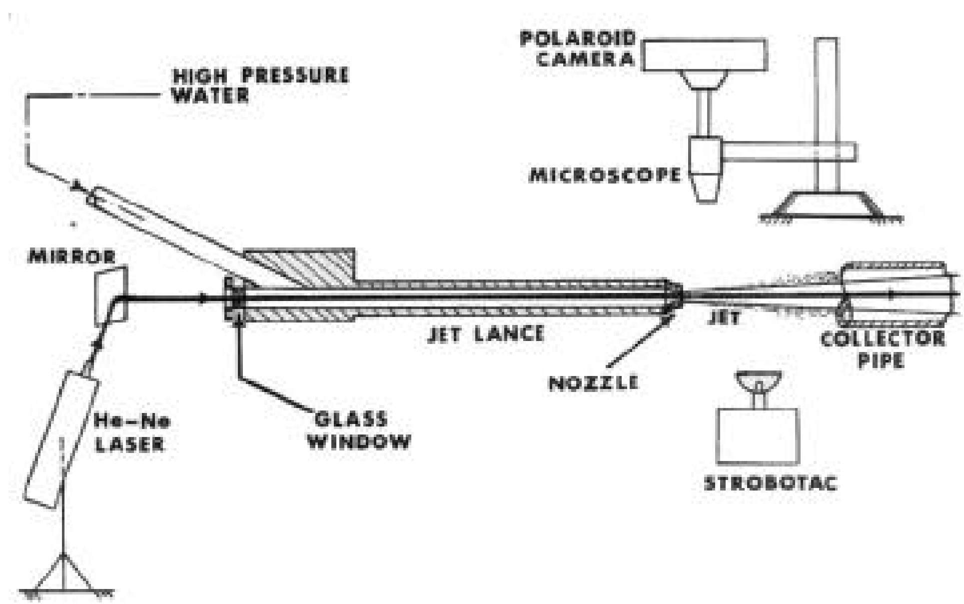

FIG. 5C A LINE DIAGRAM OF THE JET VISUALIZATION SET-UP

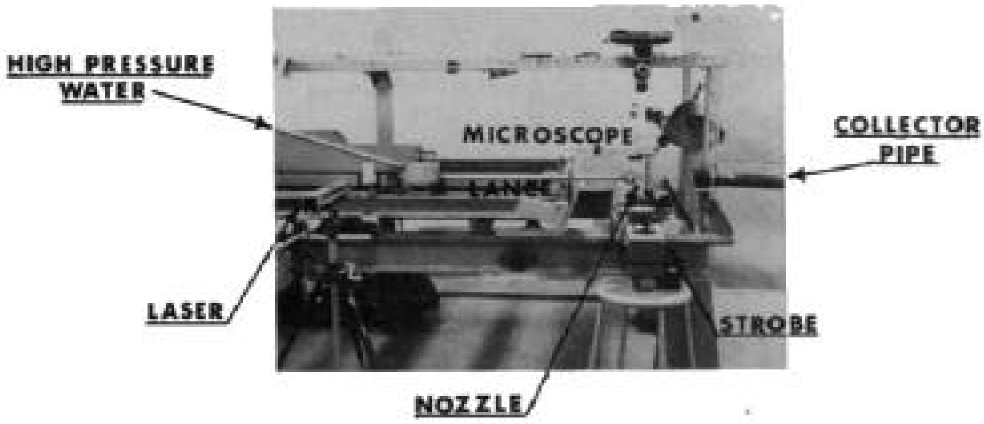

FIG. 5D A GENERAL VIEW OF THE JET VISUALIZATION SET-UP

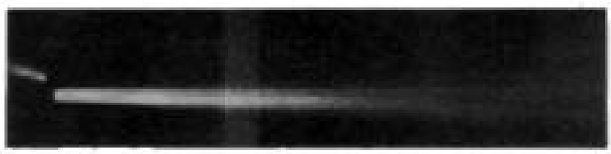

FIG. 5E JET FROM A CONICAL ENTRY NOZZLE
$d = 1.78mm$
$P_o = 34.5MPa$

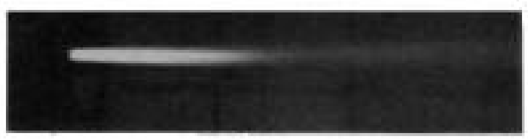

FIG. 5F JET FROM A SUDDEN ENTRY NOZZLE
$d = 1.78mm$
$P_o = 34.5MPa$

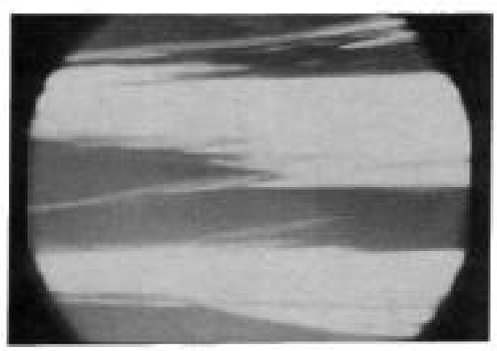

FIG. 5G A JET EMERGING FROM A CONICAL NOZZLE WITH A CYLIDRICAL BODY INSERT VIEWED UNDER A MICROSCOPE
Magnification = 25
Pressure = 6.9MPa

FIG. 5H EROSION OF AN ANNEALED COPPER SAMPLE BY A JET ISSUING FROM A SUDDEN ENTRY NOZZLE
d = 1.78mm
L/d = 5
Duration of Test = 5min
Standoff Distance = 5.1cm

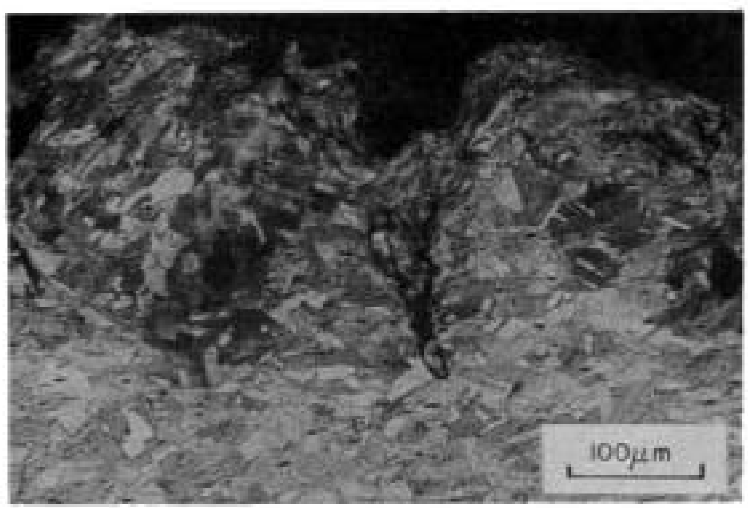

FIG. 5I SECTION THROUGH THE CRATER SURFACE OF THE SPECIMEN SHOWN IN FIG. 5H POLISHED AND ETCHED SECTION EXAMINED AT HIGH MAGNIFICATION ON A LEITZ METALLOGRAPH (Etchant: $FeCl_3$ + HCl in H_2O)